

Diss. ETH No. 31645

# **Development of an Energy-Efficient and Real-Time Data Movement Strategy for Next-Generation Heterogeneous Mixed-Criticality Systems**

A thesis submitted to attain the degree of

DOCTOR OF SCIENCES  
(Dr. sc. ETH Zurich)

presented by

THOMAS EMANUEL BENZ  
born on April 19th, 1994

accepted on the recommendation of

Prof. Dr. Luca Benini, examiner  
Prof. Dr. Alessandro Capotondi, co-examiner

2025



*The worthwhile problems are the ones you can really solve or help solve, the ones you can really contribute something to.... No problem is too small or too trivial if we can really do something about it.*

Richard Feynman

*Efficiency is doing things right; effectiveness is doing the right things.*

Peter Drucker

*Better three hours too soon than a minute too late.*

William Shakespeare

*I am Doug Dimmadome, owner of the Dimmsdale Dimmadome!*

Doug Dimmadome  
The Fairly OddParents



# Acknowledgments

Working towards my Ph.D degree has been the most intense part of my education so far. It not only provided me with a broad knowledge base and an immense set of practical and technical skills but also helped me grow personally and professionally through countless challenges. This unbelievable journey I made over the past five years would, of course, not have been possible without the support of many people I now want to thank.

First and foremost, I want to thank my supervisor, Prof. Dr. Luca Benini, for guiding and supporting me along my academic journey by constantly providing me with critical but constructive feedback. Luca, the opportunities you provided me during the last five years are truly unique; the unequaled scientific research, technical work, and teaching opportunities were fantastic for me to refine my skill set and to grow as a researcher, teacher, and person. I further want to thank you for your immense patience with me, the amount of trust issued, and the level of freedom granted while I was exploring countless side quests not directly related to my core research, but proved still invaluable to my personal development or to the advancement of the entire research group. I highly doubt that I would have found an equally supportive research group that could have provided me with the same opportunities elsewhere.

Second, I want to thank my second supervisor, Prof. Dr. Torsten Hoefler, for your support along my journey. I am especially thankful for your valuable feedback on my first journal manuscript, allowing me to submit a much more polished draft.

Third, I owe my deepest gratitude to my co-examiner, Prof. Dr. Alessandro Capotondi for his invaluable and insightful feedback, allowing me to improve and finalize my thesis and for driving an engaging discussion during my defense.

Further, I want to thank Dr. Frank Kagan Gürkaynak for leading the Microelectronics Design Center (DZ), shielding us from tedious (European) bureaucracy, and creating and supporting a fantastic work environment for us to foster. Frank, I know your role here is not easy, but this group would not exist in today's thriving form without your constant support. Thank you. Special thanks go to the entire DZ for providing us with an excellently maintained EDA environment, a broad set of cutting-edge PDKs, and an unbelievably vast knowledge in all facets of IC design. Beat Muheim, Alfonso Blanco Fontao, Zerun Jiang, and Dr. Arianna Rubino, thank you for your tireless work.

One of the fundamental pillars of our group's success is the fertile collaboration with our colleagues at the University of Bologna. I am especially grateful to Prof. Dr. Angelo Garofalo, Prof. Dr. Davide Rossi, Prof. Dr. Andrea Bartolini, Dr. Luca Valente, Simone Manoni, and Chaoqun Liang.

I am deeply indebted to Prof. em. Dr. Hubert Kaeslin for writing two such excellent books on VLSI design and for getting me into ASIC design.

A large thank you to IIS's IT team for providing such an excellent IT infrastructure for us to complete our work. Christoph Wicki, Mateo Juric, and Adam Feigin, thank you.

During my Ph.D. I was able to manufacture countless prototypes. These would not have been possible without the constructive support and tireless work of ETH's technical staff. I am deeply grateful to Hansjörg Gisler, Thomas Quanbrough, Thomas Kleier, Aldo Rossi, Michael Lerjen, and Silvio Scherr.

I want to thank Irina Rau for her many cheerful words in phases of great despair and for constantly radiating an aura of positivity.

I am very grateful to Dr. Luca Aloatti for introducing me at an early stage during my studies to the importance of free and open-source hardware and systems.

This endeavor would not have been possible without Paul Scheffler. Paul, I am deeply grateful for the last eleven years of knowing you both as a friend and as a colleague. I've enjoyed our countless academic and

recreational (and sometimes heated) discussions alongside my journey towards all my scientific qualifications to date. Your organization, excellent scientific and technical methodology and skills, and your pristine eye for detail are truly inspiring.

I was fortunate enough to spend most of my time during my studies in J85, a truly magical place with many oddities and facilities other offices could not even imagine. I am extremely grateful to my J85 colleagues, Paul Scheffler, Nils Wistoff, Matteo Perotti, and Philippe Sauter, for having many fruitful technical discussions and for making this office feel like home.

During my studies, I had the fortune to work alongside many bright minds on similar journeys. I am deeply indebted to Alessandro Ottaviano, Michael Rogemoser, Jannis Schönleber, Christopher Reinhardt, Enrico Zelioli, Sergio Mazzola, Robert Balas, Lorenzo Leone, Tim Fischer, Luca Colagrande, Luca Bertaccini, Victor Jung, Viviane Potocnik, Cyril Koenig, Cristian Cioflan, Yichao Zhang, and Chi Zhang for so many fruitful collaborations.

My thesis builds on the foundation laid by previous generations of Ph.D. students working at IIS. Many thanks to Dr. Florian Zaruba, Dr. Fabian Schiki, Dr. Andreas Kurth, Dr. Pirmin Vogel, Dr. Bjoern Forsberg, Dr. Gianna Paulin, Dr. Georg Rutishauser, Dr. Manuel Eggimann, Dr. Samuel Riedel, Dr. Matheus Cavalcante, Dr. Davide Schiavone, Dr. Moritz Scherer, Dr. Alfio Di Mauro, and Wolfgang Rönninger.

I am also grateful to Armin P. Barth, Thomas Notter, Kurt Doppler, and Ruedi Georg Vogt for awakening my interest in physics, mathematics, computer science, natural sciences and for excellently preparing me for my studies at ETH Zürich.

Many thanks to Prof. Dr. Alberto Colotti, Dr. Quentin Lohmayer, Prof. em. Dr. Elsbeth Stern, Prof. Dr. Hanspeter Hochreutener, and Dr. Beatrice Trummer for guiding me in becoming a better teacher and for strengthening my didactical skill set.

Besides oneself, the journey towards a Ph.D. degree also takes a toll on family and friends.

Words cannot express my gratitude towards my parents, Ursula Ramona Benz-Wullsleger and Peter Johann Benz, for constantly supporting me since the day I was born, for often putting my interests

above theirs, and for suffering through countless educational crises along the journey towards my degree.

My sincere thanks go to Ursula Elisabeth Trüb and Jürg Friedrich Trüb for so many joyful and happy Friday afternoons spent together. Ursula and Jürg, thank you for sparking my interest in electronics and computers and for supporting me during so many of my earlier projects.

I want to thank Edith Benz for providing me some distraction from my Ph.D. studies by posing me one or another technical challenge to solve.

I further want to thank Rolf Wullschleger for supporting me alongside my journey. I know a car workshop is not a playground, yet you have provided me with a unique place to explore and learn about cars and technical machines.

I would like to express my deepest gratitude to Karla Madžarević. Karla, thanks for all the love, unwavering support, endless encouragement, and limitless patience in the face of long working hours, countless night shifts, and many weekends spent working. This unbelievable journey would not have been possible without you. A special thanks goes to Jasmina and Karlo Madžarević for so lovingly accepting me into their family.

Thanks should also go to all my friends for helping me forget work for a couple of hours and for many therapeutic conversations far from electronics, science, and my thesis. I in particular want to thank David Perels, Lorenz Becker-Sander, Gani Aliguzhinov, Gian Marti, Thomas Kramer, Sheila Peterhans, Seline Frei, Raphael Kuhn, and Juri Nowak.

Further, I want to thank Martin Stössel for being very patient and understanding with me and my life as a Ph.D. student. I am further thankful for teaching me excellently how to keep a cool head in stressful situations, how to prioritize important tasks under stress, and the importance of always being one step ahead of the machine you are operating.

Last but by no means least, many thanks to Sherlock Olaf, Prof. Moriarty, Indira Yuna Aimé, and Cookie for providing me company during so many hours of my Ph.D. journey.





# Danksagung

Die Arbeit an meiner Doktorarbeit war der intensivste Teil meiner bisherigen Ausbildung. Sie hat mir nicht nur ein breites Wissen und eine Vielzahl praktischer und technischer Fähigkeiten vermittelt, sondern mir auch durch unzählige Herausforderungen geholfen, mich persönlich und beruflich weiterzuentwickeln. Diese unglaubliche Reise, die ich in den letzten fünf Jahren unternommen habe, wäre natürlich ohne die Unterstützung vieler Menschen, denen ich nun danken möchte, nicht möglich gewesen.

Zuallererst möchte ich meinem Betreuer, Prof. Dr. Luca Benini, dafür danken, dass er mich auf meinem akademischen Weg begleitet und unterstützt hat, indem er mir stets kritisches, aber konstruktives Feedback gegeben hat. Luca, die Möglichkeiten, die du mir in den letzten fünf Jahren geboten hast, sind wirklich einzigartig und die unvergleichlichen wissenschaftlichen Forschungs-, und Lehrmöglichkeiten waren fantastisch für mich, um meine Fähigkeiten zu verfeinern und mich als Forscher, Lehrer und Mensch weiterzuentwickeln. Außerdem möchte ich dir für deine immense Geduld mit mir, das mir entgegengebrachte Vertrauen und die Freiheit danken, die du mir gewährt hast, während ich unzählige Nebenprojekte verfolgt habe, die zwar nicht direkt mit dem Kern meiner Forschung zu tun hatten, sich aber dennoch als unschätzbar wertvoll für meine persönliche Entwicklung und den Fortschritt der gesamten Forschungsgruppe erwiesen haben. Ich bezweifle sehr, dass ich anderswo eine ebenso unterstützende Forschungsgruppe gefunden hätte, die mir die gleichen Möglichkeiten geboten hätte.

Zweitens möchte ich meinem Zweitbetreuer, Prof. Dr. Torsten Hoefler, für seine Unterstützung während meiner gesamten Laufbahn

danken. Ich bin besonders dankbar für sein wertvolles Feedback zu meinem ersten Artikel in einer Fachzeitschrift, wodurch ich einen wesentlich ausgefeilteren Entwurf einreichen konnte.

Drittens bin ich meinem Koexaminator, Prof. Dr. Alessandro Capotondi, zu tiefstem Dank verpflichtet für sein unschätzbares und aufschlussreiches Feedback, das mir half, meine Dissertation zu verbessern und fertigzustellen und für die anregende Diskussion während meiner Verteidigung.

Ausserdem möchte ich Dr. Frank Kagan Gürkaynak dafür danken, dass er das Microelectronics Design Center (DZ) leitet, uns vor mühsamer Bürokratie schützt und ein fantastisches Arbeitsumfeld für uns geschaffen und unterstützt hat. Frank, ich weiss, dass deine Aufgabe hier nicht einfach ist, aber ohne deine ständige Unterstützung würde diese Gruppe heute nicht in ihrer gedeihend Form existieren. Vielen Dank. Ein besonderer Dank geht an das gesamte DZ für die Bereitstellung einer hervorragend gepflegten EDA-Umgebung, einer breiten Palette an modernsten PDKs und einem unglaublich umfangreichen Wissen in allen Bereichen des IC-Designs. Beat Muheim, Alfonso Blanco Fontao, Zerun Jiang und Dr. Arianna Rubino, vielen Dank für eure unermüdliche Arbeit.

Eine der grundlegenden Säulen für den Erfolg unserer Gruppe ist die fruchtbare Zusammenarbeit mit unseren Kollegen an der Universität Bologna. Mein besonderer Dank gilt Prof. Dr. Angelo Garofalo, Prof. Dr. Davide Rossi, Prof. Dr. Andrea Bartolini, Dr. Luca Valente, Simone Manoni und Chaoqun Liang.

Ich bin Prof. em. Dr. Hubert Kaeslin zu tiefstem Dank verpflichtet, dass er zwei so hervorragende Bücher über VLSI-Design geschrieben und mich in das ASIC-Design eingeführt hat.

Ein grosses Dankeschön geht an das IT-Team des IIS, das uns eine hervorragende IT-Infrastruktur zur Verfügung gestellt hat, damit wir unsere Arbeit abschliessen konnten. Christoph Wicki, Mateo Juric und Adam Feigin, vielen Dank.

Während meiner Promotion konnte ich unzählige Prototypen herstellen. Ohne die konstruktive Unterstützung und die unermüdliche Arbeit der technischen Mitarbeiter der ETH wäre dies nicht möglich gewesen. Ich bin Hansjörg Gisler, Thomas Quanbrough, Thomas Kleier, Aldo Rossi, Michael Lerjen und Silvio Scherr zutiefst dankbar.

Ich möchte Irina Rau für ihre vielen aufmunternden Worte in Phasen grosser Verzweiflung und dafür danken, dass sie stets eine positive Ausstrahlung hat.

Ich bin Dr. Luca Aloatti sehr dankbar, dass er mir schon früh während meines Studiums die Bedeutung von freier und quelloffener Hardware und Systemen nähergebracht hat.

Ohne Paul Scheffler wäre dieses Unterfangen nicht möglich gewesen. Paul, ich bin zutiefst dankbar für die letzten elf Jahre, in denen ich dich sowohl als Freund als auch als Kollegen kennenlernen durfte. Ich habe unsere unzähligen akademischen und unterhaltsamen (und manchmal hitzigen) Diskussionen während meiner bisherigen wissenschaftlichen Laufbahn sehr genossen. Deine Organisation, deine exzellenten wissenschaftlichen und technischen Methoden und Fähigkeiten sowie dein unfehlbares Auge fürs Detail sind wirklich inspirierend.

Ich hatte das Glück, den grössten Teil meiner Studienzeit in J85 zu verbringen, einem wahrhaft magischen Ort mit vielen Kuriositäten und Einrichtungen, die andere Büros sich nicht einmal vorstellen können. Ich bin meinen Kollegen von J85, Paul Scheffler, Nils Wistoff, Matteo Perotti und Philippe Sauter, sehr dankbar für die vielen fruchtbaren technischen Diskussionen und dafür, dass ich mich in diesem Büro wie zu Hause gefühlt habe.

Während meines Studiums hatte ich das Glück, mit vielen klugen Köpfen zusammenzuarbeiten, die sich auf einer ähnlichen Reise befanden. Ich bin Alessandro Ottaviano, Michael Rogemoser, Jannis Schöneleber, Christopher Reinhardt, Enrico Zelioli, Sergio Mazzola, Robert Balas, Lorenzo Leone, Tim Fischer, Luca Colagrande, Luca Bertaccini, Victor Jung, Viviane Potocnik, Cyril Koenig, Cristian Cioflan, Yichao Zhang und Chi Zhang für die vielen fruchtbaren Kooperationen zu tiefstem Dank verpflichtet.

Meine Dissertation baut auf den Grundlagen auf, die von früheren Doktoranden am IIS gelegt wurden. Mein herzlicher Dank gilt Dr. Florian Zaruba, Dr. Fabian Schiki, Dr. Andreas Kurth, Dr. Pirmin Vogel, Dr. Bjoern Forsberg, Dr. Gianna Paulin, Dr. Georg Rutishauser, Dr. Manuel Eggimann, Dr. Samuel Riedel, Dr. Matheus Cavalcante, Dr. Davide Schiavone, Dr. Moritz Scherer, Dr. Alfio Di Mauro und Wolfgang Rönniger.

Ich bin auch Armin P. Barth, Thomas Notter, Kurt Doppler und Ruedi Georg Vogt dankbar dafür, dass sie mein Interesse an Physik,

Mathematik, Informatik und Naturwissenschaften geweckt und mich hervorragend auf mein Studium an der ETH Zürich vorbereitet haben.

Vielen Dank an Prof. Dr. Alberto Colotti, Dr. Quentin Lohmayer, Prof. em. Dr. Elsbeth Stern, Prof. Dr. Hanspeter Hochreutener und Dr. Beatrice Trummer, die mich dabei begleitet haben, ein besserer Lehrer zu werden, und meine didaktischen Fähigkeiten gestärkt haben.

Neben einem selbst fordert der Weg zum Doktorgrad auch von Familie und Freunden seinen Tribut.

Ich kann meine Dankbarkeit gegenüber meinen Eltern, Ursula Ramona Benz-Wullschleger und Peter Johann Benz, gar nicht in Worte fassen. Sie haben mich seit meiner Geburt stets unterstützt, oft meine Interessen über ihre eigenen gestellt und unzähligen Bildungskrisen auf meinem Weg zum Abschluss mitgemacht.

Mein aufrichtiger Dank gilt Ursula Elisabeth Trüb und Jürg Friedrich Trüb für so viele fröhliche und glückliche Freitagnachmittage, die wir gemeinsam verbracht haben. Ursula und Jürg, ich danke euch dafür, dass ihr mein Interesse an Elektronik und Computern geweckt und mich bei so vielen meiner früheren Projekte unterstützt habt.

Ich möchte Edith Benz dafür danken, dass sie mir durch die Lösung der einen oder anderen technischen Herausforderung eine willkommene Abwechslung zu meinem Doktoratsstudium geboten hat.

Ausserdem möchte ich Rolf Wullschleger dafür danken, dass er mich auf meinem Weg unterstützt hat. Ich weiss, dass eine Autowerkstatt kein Kinderspielplatz ist, aber du hast mir einen einzigartigen Ort geboten, an dem ich Autos und technische Maschinen erkunden und mehr über sie lernen konnte.

Meine tiefste Dankbarkeit gilt Karla Madžarević. Karla, danke für all die Liebe, die unerschütterliche Unterstützung, die unendliche Ermüdigung und die grenzenlose Geduld angesichts der langen Arbeitszeiten, der unzähligen Nachschichten und der vielen Wochenenden, die ich mit Arbeiten verbracht habe. Ohne dich wäre diese unglaubliche Reise nicht möglich gewesen. Ein besonderer Dank geht an Jasmina und Karlo Madžarević, die mich so liebevoll in ihre Familie aufgenommen haben.

Mein Dank gilt auch all meinen Freunden, die mir geholfen haben, die Arbeit für ein paar Stunden zu vergessen, und für viele therapeutische Gespräche fernab von Elektronik, Wissenschaft und meiner Dissertation. Insbesondere möchte ich David Perels, Lorenz

Becker-Sander, Gani Aliguzhinov, Gian Marti, Thomas Kramer, Sheila Peterhans, Seline Frei, Raphael Kuhn und Juri Nowak danken.

Ausserdem möchte ich Martin Stössel dafür danken, dass er mir und meinem Leben als Doktorand gegenüber so geduldig und verständnisvoll war. Ich bin ihm auch dankbar dafür, dass er mir auf hervorragende Weise beigebracht hat, wie man in Stresssituationen einen kühlen Kopf bewahrt, wie man unter Druck wichtige Aufgaben priorisiert und wie wichtig es ist, der Maschine, die man bedient, immer einen Schritt voraus zu sein.

Zu guter Letzt möchte ich mich ganz herzlich bei Sherlock Olaf, Prof. Moriarty, Indira Yuna Aimé und Cookie bedanken, die mir während meiner langjährigen Promotion Gesellschaft geleistet haben.



# Abstract

Industrial domains such as automotive, robotics, and aerospace are rapidly evolving to satisfy the increasing demand for machine-learning-driven Autonomy, Connectivity, Electrification, and Shared mobility (ACES). This paradigm shift inherently and significantly increases the requirement for onboard computing performance and high-performance communication infrastructure. At the same time, Moore’s Law and Dennard Scaling are grinding to a halt, in turn, driving computing systems to larger scales and higher levels of heterogeneity and specialization, through application-specific hardware accelerators, instead of relying on technological scaling only. Approaching ACES requires this substantial amount of compute at an increasingly high energy-efficiency, since most use cases are fundamentally resource-bound.

This increase in compute performance and heterogeneity goes hand in hand with a growing demand for high memory bandwidth and capacity as the driving applications grow in complexity, operating on huge and progressively irregular data sets and further requiring a steady influx of sensor data, increasing pressure both on on-chip and off-chip interconnect systems. Further, ACES combines real-time time-critical with general compute tasks on the same physical platform, sharing communication, storage, and micro-architectural resources. These heterogeneous mixed-criticality systems (MCSs) place additional pressure on the interconnect, demanding minimal contention between the different criticality levels to sustain a high degree of predictability. Fulfilling the performance and energy-efficiency requirements across a wide range of industrial applications requires a carefully co-designed process of the memory system with the use cases as well as the compute units and accelerators.

Firstly, this thesis tackles efficient, agile, and high-performance data movement in heterogeneous systems by presenting a modular and highly customizable direct memory access (DMA) architecture, *iDMA*, serving the diverse needs of today's heterogeneous platforms. Secondly, we introduce *AXI-REALM*, a modular interconnect extension, tackling the predictability problem arising in heterogeneous MCS running real-time-critical applications in the presence of DMA transfers originating from domain-specific accelerators.

In multiple case studies, we show the applicability and the benefits of *iDMA* in silicon-implemented systems and across the entire interconnect hierarchy, including an application-grade Linux-capable system-on-chip (SoC), a high-performance general-purpose compute accelerator, and an automotive-grade MCS. In the latter, we present the benefits of *AXI-REALM* restoring performance of time-critical applications running on MCSs in the presence of contention caused by domain-specific accelerator DMA engines.

# Zusammenfassung

Industrielle Bereiche wie Automobilbau, Robotik und Luft- und Raumfahrt entwickeln sich rasant weiter, um der steigenden Nachfrage nach Autonomie, Konnektivität, Elektrifizierung und gemeinsamer Mobilität (ACES), gesteuert durch maschinelles Lernen, gerecht zu werden. Dieser Paradigmenwechsel erhöht naturgemäß und erheblich die Anforderungen an die Rechenleistung an Bord und an eine leistungsstarke Kommunikationsinfrastruktur. Gleichzeitig kommen Moores Gesetz und Dennards Skalierung zum Stillstand, was wiederum dazu führt, dass Computersysteme durch anwendungsspezifische Hardwarebeschleuniger grösser und heterogener werden und sich stärker spezialisieren, anstatt sich nur auf technologische Skalierung zu verlassen. Die Umsetzung von ACES erfordert diese erhebliche Rechenleistung bei einer immer höheren Energieeffizienz, da die meisten Anwendungsfälle grundsätzlich ressourcen gebunden sind. Diese Steigerung der Rechenleistung und Heterogenität geht Hand in Hand mit einem wachsenden Bedarf an hoher Speicherbandbreite und -kapazität, da die treibenden Anwendungen immer komplexer werden, mit riesigen und zunehmend unregelmässigen Datensätzen arbeiten und darüber hinaus einen stetigen Zufluss von Sensordaten erfordern, was den Druck auf Kommunikationsnetzwerke, innerhalb desselben integrierten Schaltkreises oder bei dessen Kommunikation mit der Außenwelt, erhöht. Darüber hinaus kombiniert ACES zeitkritische Echtzeitaufgaben mit allgemeinen Rechenaufgaben auf derselben physischen Plattform und teilt sich dabei Kommunikations-, Speicher- und Mikroarchitekturressourcen. Diese heterogenen Systeme mit unterschiedlichen Kritikalitätsstufen (MCS) üben zusätzlichen

Druck auf die Verbindung aus und erfordern eine minimale Konkurrenz zwischen den verschiedenen Kritikalitätsstufen, um ein hohes Mass an Vorhersagbarkeit aufrechtzuerhalten. Um die Leistungs- und Energieeffizienzanforderungen in einem breiten Spektrum industrieller Anwendungen zu erfüllen, ist ein sorgfältig abgestimmter Prozess des Speichersystems mit den Anwendungsfällen sowie den Recheneinheiten und Beschleunigern erforderlich.

Erstens befasst sich diese Arbeit mit der effizienten, agilen und leistungsstarken Datenübertragung in heterogenen Systemen, indem sie eine modulare und hochgradig anpassbare Architektur für direkte Speicherzugriffseinheiten (DMA) namens iDMA vorstellt, die den vielfältigen Anforderungen heutiger heterogener Plattformen gerecht wird. Zweitens stellen wir AXI-REALM vor, eine modulare Kommunikationsnetzwerkserweiterung, die das Problem der Vorhersagbarkeit angeht, das in heterogenen MCS auftritt, die zeitkritische Anwendungen ausführen, wenn DMA-Übertragungen von domänenspezifischen Beschleunigern stattfinden.

In mehreren Fallstudien zeigen wir die Anwendbarkeit und die Vorteile von iDMA in siliziumimplementierten Systemen und über die gesamte Kommunikationsnetzwerkshierarchie hinweg, einschliesslich eines Linux-fähigen Ein-Chip-System (SoC), eines hochleistungsfähigen Allzwecksrechenbeschleunigers und eines MCS in Automobilqualität. Im letzten Fall präsentieren wir die Vorteile von AXI-REALM, das die Leistung zeitkritischer Anwendungen wiederherstellt, die auf MCSs laufen, wenn es zu Konflikten durch direkte Speicherzugriffseinheiten der domänenspezifischen Beschleuniger kommt.

# Zämäfassig

Industrielli Berlich wie de Automobilbau, d Robotik, und Luft- und Ruhmfahrt entwickled sich rasch wiiter um mit de steigende Nachfrog nach Autonomie, Konnektivität, Elektrifizierig und gmeinsamer Mobilität (ACES), gönüüred dur maschinells Lerne, grecht z werde. Dä Paradigmewechsel erhöht naturgmäss und au erheblich d Aforderige ad Recheleischtige an Board und ane leistigsstarchi Kommunikationsinfrastruktur. Gliichziitig chömmmed im Moores sis Gsetz und em Dennard sini Skalierig zumne Halt, was wederum dezu fürt, dass Computersystem dur awendigsspezifischi Hardwarebeschlüniger grösser und heterogener werded und sich stärcher spezialisiered, anstatt sich nur uf die technologischi Skalirig z verloh. D Umsetzig vo ACES erfordered die erheblichi Recheleischtig binere immer höchere Energieeffizienz, da die meischte Awändigsfäll grundsätzlich ressourcegebunde sind. Die Steigerig vo de Recheleischtig und de Hereogenität gohd Hand in Hand mit emne wachsende Bedarf a höher Speicherbandbreiti und -kapazität, da die tribende Awändige immer komplexer werded, mit risigne und zuhnemned unregelmässigere Datesätz schaffed und drüberhinus en stetige Zuefluss vo Sensordate erfordered, was de Druck ufd Kommunikationsnetzwerk, innerhalb vom gliche integrierte Schaltchreis oder bi desse Kommunikation mit de Ussewelt, erhöht. Drüberhinus kombiniert ACES ziitkritisch Ächtziitufgabe mit allgemeine Recheufgabe uf dergliche physische Plattform und teilt sich debie Kommunikations-, Spicher-, und Mikroproarchitekturressource. Die heterogene System mit unterschiedliche Kritikalitätsstufene (MCS) üebed zuesätzlich Druck ufd Verbindig us und erfordered nur minimali konkurrenz zwische de verschidene Kritikalitätsstufene, um es hochs Mass a Vorhersagbarkeit ufrechtserhalte. Um die Leistigs- und Energieeffizienzaforderige imne

breite Spektrum industrielle Awändige z erfülle, isch en sorgfältig abgestimmte Prozess vom Spichersystem mit de Awändigsfäll sowie de Recheeinheite und Beschlüniger erforderlich.

Zerscht befasst sich die Arbet mit de effiziente, aglie und leischtigs- starche Dateüberträgig i heterogene Systeme, indem sie e modulari und hochgradig ahpassbari Architektur für direkti Speicherzuegriffseinheite (DMA) names iDMA vorstellt, die de vielfältige Aforderige hütiger heterogene Plattformene grecht wird. Als zweits stelled mer AXI-REALM vor, e modulari Kommunikationsnetzwerkserwiiterig, die s Problem vo der Vorhersagbarkeit agohd, weles in heterogene MCS uftritt, die ziitkritisch Awändige usföhred, wenn DMA-Überträgige vo domänespezifische Beschlüniger stattfindet.

I mehrere Fallstudie zeigemer d Anwendbarkeit und d Vorteil v iDMA i siliziumimplementierte System und über die gsamt Kommunikationsnetzwerkhierarchie hinweg, einschliesslich vomne Linux-fähigen Eis-Chip-System (SoC), vomne hochleistungsfähige Allzweckrechbe- schlüniger und vomne MCS in Automobilqualität. Im letschtene Fall präsentiered mer d Vorteil vo AXI-REALM, welles d Leischting vo ziitkritischer Awendige wederherstellt, die uf MCSs laufed, wenns zu Konflikte usglöst dur direkte Speicherzuegriffseinheite vo de domänes- pezifische Beschlüniger chunnt.

In reference to IEEE copyrighted material which is used with permission in this thesis, the IEEE does not endorse any of ETH Zurich's products or services. Internal or personal use of this material is permitted. If interested in reprinting/republishing IEEE copyrighted material for advertising or promotional purposes or for creating new collective works for resale or redistribution, please go to [http://www.ieee.org/publications\\_standards/publications/rights/rights\\_link.html](http://www.ieee.org/publications_standards/publications/rights/rights_link.html) to learn how to obtain a license from RightsLink. If applicable, University Microfilms and/or ProQuest Library, or the Archives of Canada may supply single copies of the dissertation.



# Contents

<b>Acknowledgments</b>	<b>v</b>
<b>Danksagung</b>	<b>xi</b>
<b>Abstract</b>	<b>xvii</b>
<b>Zusammenfassung</b>	<b>xix</b>
<b>Zämäfassig</b>	<b>xxi</b>
<b>1 Introduction</b>	<b>1</b>
1.1 Motivation . . . . .	1
1.2 Efficient Data Movement: DMA Engines . . . . .	6
1.3 On-Chip Interconnect Protocols . . . . .	9
1.3.1 Focus: Non-Coherent Protocols . . . . .	9
1.3.2 Protocols Discussed . . . . .	9
1.4 Thesis Overview and Outline . . . . .	13
1.5 Summary of Contributions . . . . .	16
1.6 List of Publications . . . . .	17
1.6.1 Previous Publications . . . . .	17
1.6.2 Core Publications . . . . .	17
1.6.3 Related Publications . . . . .	17
1.6.4 Unrelated Publications . . . . .	19
<b>2 Modular DMA Architecture</b>	<b>23</b>
2.1 Introduction . . . . .	23
2.2 Architecture . . . . .	26

2.2.1	Back-end . . . . .	26
2.2.2	Buffer Considerations . . . . .	32
2.2.3	Multi-Protocol Customization . . . . .	35
2.2.4	Error Handling . . . . .	38
2.3	Architectural Results . . . . .	40
2.3.1	Area Model . . . . .	40
2.3.2	Timing Model . . . . .	42
2.3.3	Latency Model . . . . .	44
2.3.4	Standalone Performance . . . . .	45
2.3.5	Energy Efficiency . . . . .	47
2.4	Related Work . . . . .	48
2.5	Summary and Conclusion . . . . .	51
<b>3</b>	<b>Architectural DMA Extensions</b>	<b>53</b>
3.1	Introduction . . . . .	53
3.2	Linux Support and Extensions . . . . .	56
3.2.1	Introduction . . . . .	56
3.2.2	Architecture . . . . .	58
3.2.3	DMA Front-end Design . . . . .	58
3.2.4	DMAC Transfer Descriptor . . . . .	59
3.2.5	Speculative Descriptor Prefetching . . . . .	60
3.2.6	Cheshire integration . . . . .	61
3.2.7	Linux Driver . . . . .	62
3.2.8	Results . . . . .	63
3.3	Virtual Memory Capabilities . . . . .	71
3.3.1	Introduction . . . . .	71
3.3.2	Architecture . . . . .	72
3.3.3	Case Study: Cheshire . . . . .	74
3.4	Register Front-end and N-D Tensor Extension . . . . .	75
3.4.1	Introduction . . . . .	75
3.4.2	Architecture . . . . .	75
3.4.3	Case Study: PULP-open . . . . .	77
3.5	Multichannel Operation . . . . .	80
3.5.1	Introduction . . . . .	80
3.5.2	Architecture . . . . .	80
3.5.3	Case Study: Mempool . . . . .	81
3.6	I/O-DMA . . . . .	84
3.6.1	Introduction . . . . .	84

3.6.2	A General Template for I/O Data Movement . . . . .	84
3.6.3	Case Study: Neopixel . . . . .	85
3.7	Real-Time Sensor Scheduling . . . . .	88
3.7.1	Introduction . . . . .	88
3.7.2	Architecture . . . . .	88
3.7.3	Case Study: ControlPULP . . . . .	89
3.8	RISC-V Instruction Front-end . . . . .	92
3.9	Summary and Conclusion . . . . .	93
<b>4</b>	<b>Communication Processor</b>	<b>95</b>
4.1	Introduction . . . . .	95
4.2	Instruction-Based Front-end . . . . .	98
4.2.1	DMA Engine Architecture . . . . .	98
4.2.2	Instruction Encoding . . . . .	100
4.3	Cluster Integration . . . . .	103
4.3.1	Programming Model . . . . .	104
4.4	Case Study: Occamy . . . . .	105
4.4.1	Introduction . . . . .	105
4.4.2	Memory Architecture . . . . .	105
4.4.3	Compute Cluster . . . . .	106
4.4.4	Compute Group . . . . .	108
4.4.5	Occamy Chiplets . . . . .	109
4.4.6	Physical Design . . . . .	112
4.4.7	Occamy Chiplets . . . . .	113
4.4.8	Bringup and Silicon Measurement Setup . . . . .	121
4.5	Experimental Results . . . . .	123
4.6	Summary and Conclusion . . . . .	125
<b>5</b>	<b>Real-time Interconnect Extensions</b>	<b>127</b>
5.1	Introduction . . . . .	127
5.2	Background . . . . .	130
5.2.1	The AMBA AXI4 On-Chip Interconnect . . . . .	130
5.2.2	MCS Terminology: Essential Insights . . . . .	131
5.3	Architecture . . . . .	133
5.3.1	The irealm Unit and Architecture . . . . .	135
5.3.2	Interconnect layer . . . . .	140
5.3.3	The erealm Unit and Architecture . . . . .	141
5.3.4	Configuration Interface . . . . .	144

5.3.5	Bus Guard	144
5.4	Architectural Results	146
5.4.1	Area Model	147
5.4.2	Timing and Latency	148
5.5	Case Study: Automotive MCS	149
5.5.1	Introduction	149
5.5.2	Area Impact	150
5.5.3	Synthetic Performance Analysis of irealm	150
5.5.4	Synthetic Performance Analysis of erealm	157
5.5.5	Case Study on Carfield	158
5.6	Related Work	161
5.6.1	Real-time Extensions: irealm	161
5.6.2	Subordinate Guarding: erealm	163
5.6.3	Final Remarks: AXI-REALM	166
5.7	Conclusion and Summary	167
<b>6</b>	<b>Conclusions and Future Directions</b>	<b>169</b>
6.1	Summary and Main Results	169
6.2	Outlook	174
<b>A</b>	<b>Chip Gallery</b>	<b>175</b>
A.1	Scarabaeus	176
A.2	Thestral	178
A.3	Dogeram	182
A.4	Zest	184
A.5	Neo	186
A.6	Occamy	188
A.7	Carfield	192
A.8	Iguana	196
A.9	Basilisk	198
A.10	MLEM	200
A.11	Koopa	202
A.12	Fluffy	204
A.13	Skoll	206
A.14	Hati	208
A.15	Flamingo	210

<b>B ArtistIC</b>	<b>213</b>
B.1 Introduction . . . . .	213
B.2 Toolflow . . . . .	214
B.3 Results . . . . .	215
B.4 Case Study: RISC-V SoCs . . . . .	217
B.5 Conclusion & Outlook . . . . .	217
<b>C DUTCTL</b>	<b>219</b>
C.1 Introduction . . . . .	219
C.2 Architecture . . . . .	220
C.3 Results and Conclusion . . . . .	222
<b>D Student Theses Supervised</b>	<b>225</b>
D.1 2020 . . . . .	225
D.2 2021 . . . . .	225
D.3 2022 . . . . .	226
D.4 2023 . . . . .	226
D.5 2024 . . . . .	227
D.6 2025 . . . . .	228
<b>E Acronyms</b>	<b>229</b>
<b>List of Figures</b>	<b>231</b>
<b>List of Tables</b>	<b>237</b>
<b>Bibliography</b>	<b>239</b>
<b>Curriculum Vitae</b>	<b>267</b>



# Chapter 1

## Introduction

In this chapter, we motivate this thesis and present the fundamental problems and challenges tackled throughout the following chapters.

### 1.1 Motivation

Humankind's century-long strive for complete automation has reached an unprecedented level thanks to recent developments in the field of artificial intelligence (AI). Generative models such as OpenAI's *o3* [1] even achieved human-like results on general intelligence benchmarks [2].

With such potential in automation, the recent entry of AI into people's everyday life has become inevitable, as consumers value extensive digitization, e.g., through software-enabled features, leading to a fundamental paradigm shift in many industrial domains, including automotive, robotics, and aerospace, towards Autonomy, Connectivity, Electrification, and Shared mobility (ACES) [3–8]. To provide the customer with these needs, connected cyber-physical systems must continuously update software, engage with a wide variety of digital ecosystems, and provide high-bandwidth and low-latency access to on- and off-board data [4].

The widespread use of AI and the trend to ACES both significantly increase the desire for onboard computing performance and communication bandwidth, which in turn raises their energy demand [9], yet

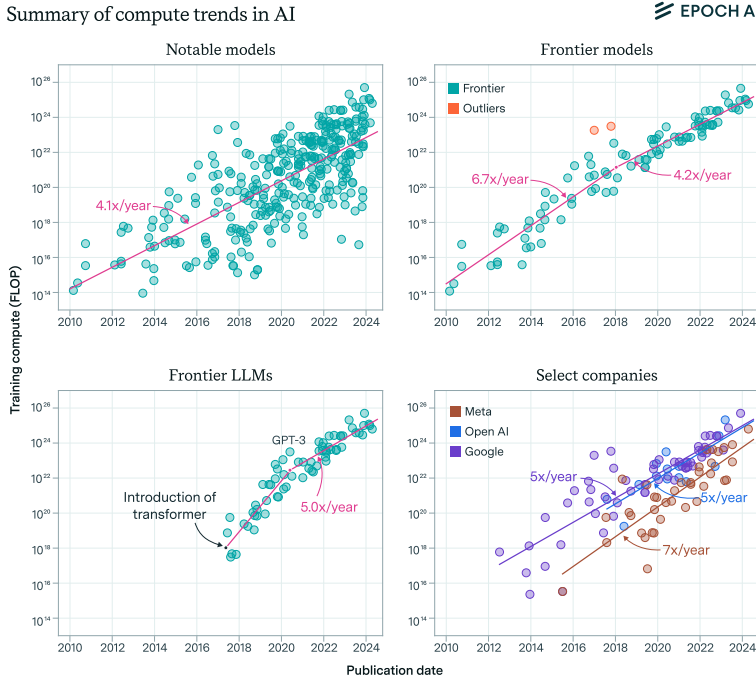


Figure 1.1: Training compute and thus number of parameters of machine learning (ML) models and their trends. Image taken from [11].

their use in automotive, robotics, and aerospace applications limits their power envelope [10] pushing architectures and systems towards an increase in energy efficiency.

The high level of automation of cyber-physical systems requires complex, more diverse, and multi-modal ML models with an ever-increasing number of parameters [3–5, 12–14]. As can be seen in Figure 1.1, recent years showed exponential growth in required training compute leading to parameter counts of hundreds of billions [11, 14]. Coupled with an increased number of sensors required to perceive the environment [15], more and more pressure is placed on both the

input/output (I/O) and the on-chip memory system [16] to fetch the required input data from the environment, to process internally, and to finally actuate the environment.

In the automotive domain, the current trend pushes towards software-defined vehicles (SDV) [5] transforming hardware-defined cars into software-defined transportation platforms, unifying classical microcontroller units (MCUs) with high-level automation functions like advanced driver-assistance system (ADAS), or AI-based self-driving capabilities and immersive on-board entertainment functionality [8, 17].

Traditionally, cars rely on hundreds of embedded real-time ECUs, distributed throughout the vehicle. This architecture cannot meet the growing compute and communication demands and complicates cable harness management, impacting space, weight, power, and cost (SWaP-C) [8, 18, 19]. Hence, integrated, interconnected *zonal* and *domain* architectures are becoming the preferred replacements for discrete ECUs [17], as they deliver the flexibility and compute capability required for ACES mobility and the SWaP-C problem by simplifying the connectivity [19, 20], see Figure 1.2.

To serve both the ever-increasing demand for core compute and memory throughput, as well as enabling *zonal* architectures, cyber-physical systems need to be adapted to embody highly heterogeneous mixed-criticality systems (MCSs) [21, 22]. These architectures usually combine general-purpose and domain-specific sub-systems with diverse real-time and specialized computing requirements coupled through a high-performance interconnect fabric, both executing workloads concurrently on the same silicon die, sharing communication, storage, and micro-architectural resources [23, 24]. Some subsystems handle hard safety- and time-critical workloads, such as engine, brake, and cruise control [8, 25, 26], while others run less time-critical but computationally demanding tasks like perception pipelines, infotainment, communication, and commodity applications [8, 27, 28]. For example, Tesla’s *Full Self-Driving Chip* [28, 29] and NVIDIA’s Jetson *Orion* platform [27] are prominent examples of heterogeneous MCSs used in automotive and robotics applications.

However, in heterogeneous MCSs, this process is complicated by the increased interference generated by multiple compute and real-time domains contending for shared memory resources on the same platform [25, 30].

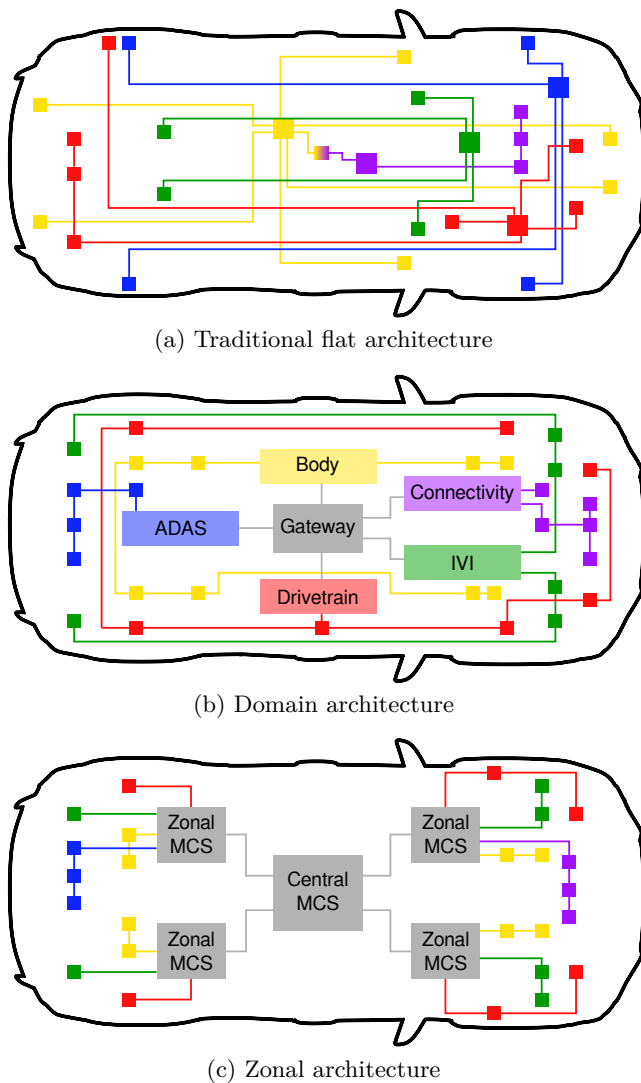


Figure 1.2: Transition from a flat or distributed electronic control unit (ECU) architecture to a structured domain and finally a zonal architecture with mixed-criticality system (MCS) nodes.

To summarize, cyber-physical systems in multiple industrial domains are forced to evolve due to an increased level of automation requested by consumers. The increased heterogeneity to meet energy-efficiency demands, the requirement to transition to MCSs to support zonal architectures, and the accelerating growth of machine-learning models increase pressure on the memory interconnect. While already causing limitations today, without novel and lightweight architectural solutions, the memory architecture will become the bottleneck for tomorrow's cyber-physical systems.

My thesis aims to tackle these memory architecture bottlenecks by developing a scalable and flexible direct memory access (DMA) architecture to maximize the efficiency of data transfers, while supporting multiple industry on-chip communication protocols tailoring it to the needs of heterogeneous platforms, and by proposing a light-weight interconnect extension enabling real-time interconnect guarantees in MCS.

In the following Section 1.2, we provide a solid background on efficient data movement. Then, we overview a selection of commonly used industry-grade non-coherent on-chip protocols in Section 1.3. Finally, we provide a detailed overview of this thesis' content in Section 1.4, provide a summary of the contributions in Section 1.5, and conclude with a list of publications acting as the base of this work in Section 1.6.

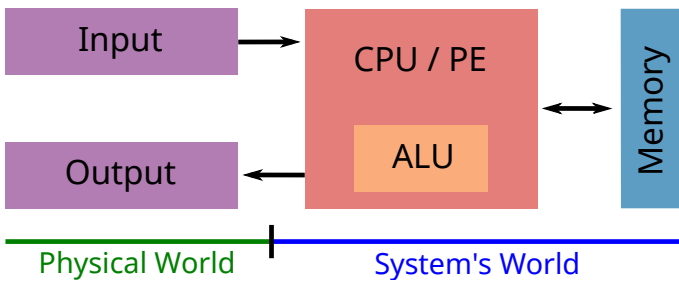


Figure 1.3: Abstract representation of a computing system; a PE including an arithmetic logic unit (ALU) sits at the center accessing both the physical world through I/O and memory.

## 1.2 Efficient Data Movement: DMA Engines

Since the advent of computing more than a century and a half ago [31], including the transition to electronic computers [32], the vast majority of digital computer architectures share the same fundamental blueprint. The data to be processed is received from the *physical world* through an *input device* and stored in *memory*. Computation on the data is done in the *central processing unit (CPU)* or *processing element (PE)* by fetching both instructions and data from memory. Results are communicated with the physical world through an *output device*. Traditionally, data is moved to and from the physical world through the I/O devices using the PE, see Figure 1.3.

Using the PE to move data either from I/Os or memory is inherently inefficient as this procedurally simple task burdens the processor unnecessarily and prevents it from performing *useful* compute. This is especially true for I/O devices as they generally run at a lower transmission speed compared to the PE's internal data access, requiring either slow accesses synchronized through polling, backpressure, or interrupts.

Linear data movement can be accelerated through a specialized DMA unit [33]. Depending on their position in the computing architecture and their primary role, we distinguish between two different

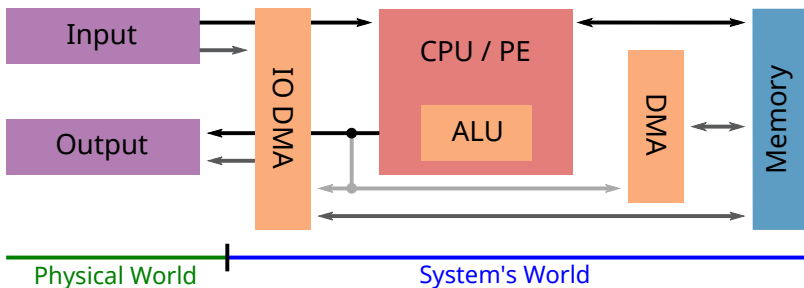


Figure 1.4: Abstract representation on a computing system extended with DMA units. A I/O DMA accelerates accesses to the physical world, whereas a memory DMA can be used to copy and reorganize data in memory.

classes of DMA units: *memory* and *I/O* units. As can be seen in Figure 1.4. The former is placed close to the system's memory and the latter between the I/O devices and the memory.

**Memory Units** They are placed close to the system's memory, allowing for fast access when initializing, moving, or reorganizing data. This class of DMA engines is particularly important in hierarchical memory systems with explicitly managed scratchpad memories and/or off-chip storage [34]; data needs to be transferred from large, but slow memories to small, but fast memories located closely to the PEs.

**IO Units** Placed between I/O and memory, they are specialized to interact with slow peripherals without stalling or slowing down either the core or the memory system. I/O units are constructed simpler and thus with a smaller resource footprint than memory units, as they do not need to be optimized for throughput nor latency [35].

Internally, DMA engines consist of two parts: the *control* and *data planes*, as presented in Figure 1.5. The control plane handles the interface with the PE, called *system binding*, and the orchestrating functions of the engine, e.g., the emission of interrupts or events once a *DMA job* is complete.

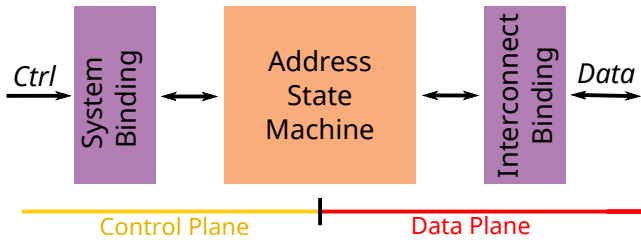


Figure 1.5: Abstract view of the internals of a DMA unit. *Control* and *data planes* can be differentiated; the former includes a system binding allowing the PE to interface the unit, the latter includes the interconnect binding over which the unit accesses memory and/or I/O. At the center, an address generator enumerates the memory region to be copied.

An internal *address generator* enumerates the individual memory transfers to be completed sequentially to perform the data movement operation commanded; basic units support linear transfers only [33]. More advanced units enable more complex transfer patterns [36, 37].

The data plane executes the data transfer using a memory interconnect binding that fits the memory architecture of the system. In traditional IBM-based system, data movement is usually done using an expansion bus protocol, e.g., Peripheral Component Interconnect Express (PCIe), whereas on-chip communication protocols, see Section 1.3, are used on systems-on-chip (SoCs).

To summarize, DMA units can be split into a control and a data plane; the former defines how the unit is interfacing the system, the latter which protocol is used to copy a deterministic stream of bytes. We work on this principle in Chapter 2, where we modularize our architecture along this split of planes.

## 1.3 On-Chip Interconnect Protocols

There are multiple commonly used non-coherent on-chip protocols currently available with an open-source specification [38–42]. Table 1.1 presents and summarizes a selection of on-chip protocols chosen for their presence in research systems or for their importance to the content presented in this thesis.

### 1.3.1 Focus: Non-Coherent Protocols

To simplify application development on multicore systems, it is assumed all PEs see the exact same state of the system’s memory [43]. This assumption holds trivially if all cores are connected to a single large memory. With the *Memory Wall* or the *Processor-Memory Gap* [44–46] increasingly growing, a fast and large unified memory becomes increasingly impossible to design and implement. Multi-level PE-coupled cache architectures promise to fill this gap but at a cost of requiring implicit synchronization of their contents to provide a unified and coherent memory view.

Specialized on-chip protocols have been developed to carry this synchronization traffic alongside the regular data stream [38, 47, 48].

This thesis focuses on explicitly managed memory architectures where data copy operations are orchestrated by the user and carried out through highly optimized DMA engines for their predictability, and high energy efficiency. While playing a significant role in application-grade systems, coherency does not play a major role in such systems, since coherency provides few benefits in explicitly managed systems, while coherent protocols impose a significant overhead in resource utilization and energy footprint, heightened latency, and a drop in bandwidth [47].

### 1.3.2 Protocols Discussed

**AMBA AXI4** This protocol supports high-performance and high-speed communication between manager and subordinate devices [38]. Its five-channel fully handshaked latency-tolerant architecture effectively decouples read and write data as well as transfer requests, data streams, and responses, maximizing pipelinability, minimizing

stalls, and facilitating a dataflow-oriented implementation. Advanced eXtensible interface 4 (AXI4) supports bursts up to 256 elements in length or 4 kB in size, enabling movement of large chunks of contiguous data with only one request and response beat. Through the use of transaction IDs (tIDs), AXI4 supports transfer reordering and multiple outstanding transactions.

Implementing the full capabilities of AXI4 requires a relatively complex manager and subordinate design. For simpler devices, e.g., configuration registers, a simplified subset of the specification, AXI4 Lite, can be selected. While still featuring the five channels, support for bursts and transfer reordering is removed to simplify the design of the interconnect and the devices.

**AMBA AXI4 Stream** This protocol targets streaming applications, where versatile, high-speed, unidirectional, point-to-point connections between transmitters and receivers are required [39]. Although primarily specified as a point-to-point protocol, interconnects can be employed to connect multiple AXI4 Stream components together. AXI4 Stream only describes the data transfer mechanism, but not the data's meaning, allowing AXI4 Stream to carry a variety of high-level protocols.

**OpenHW OBI** Featuring two double-handshaked channels targeting single-cycle, tightly coupled memory connections. Open bus interface (OBI) is optimized for low-power MCUs and can be used as the main interconnect towards fixed-latency tightly coupled data memory (TCDM) or to connect to variable-latency peripheral devices. The OBI subordinate device is very easy to implement, allowing trivial connection to static random access memory (SRAM) banks and making it a great protocol to connect configuration registers.

**SiFive TileLink Uncached** With two two double-handshaked channels, TileLink Uncached Heavyweight (TL-UH) implements a tightly coupled, scalable, pipelinable, and stateless bus protocol optimized to be used as the main interconnect in SoCs. TL-UH is considered a high-performance protocol thanks to the support of out-of-order completion, various hints, atomic operations, and burst accesses.

Table 1.1: Common non-coherent on-chip protocols and their key characteristics. All protocols share *byte addressability* and a *ready-valid* handshake.

Protocol	Request Channel	Response Channel	Key Characteristics	Applications	Burst Support
<i>AMBA AXI4+ATOP</i> [38, 49]	$AW^a, W^a, AR^b$	$B^a, R^b$	High-Performance High-Speed Fully Decoupled Max. Piplineability	HPC Interconnect	$256 \text{ beats}$ or $4 kB^c$
<i>AMBA AXI4 Lite</i> [38]	$AW^a, W^a, AR^b$	$B^a, R^b$	High-Speed Fully Decoupled Max. Piplineability	Peripheral & Configuration Interconnect	no
<i>AMBA AXI4 Stream</i> [39]	$T^d$	$T^d$	High-Speed Versatile Point-to-Point	Data Streams	unlimited
<i>OpenHW OBI</i> [40]	$D$	$R$	Tightly Coupled Low-Power	Tightly Coupled Direct Memory (TCDM) & MCSSs Interconnect	no
<i>SiFive TileLink UH</i> [41]	$A$	$R$	High-Performance Scalable Tightly Coupled Piplineable	HPC Interconnect	powers of two
<i>SiFive TileLink UL</i> [41]	$A$	$R$	Scalable Tightly Coupled Piplineable	Peripheral & Configuration Interconnect	no

<sup>a</sup> write

<sup>b</sup> read

<sup>c</sup> whichever is reached first

<sup>d</sup> symmetrical RX/TX channels

TileLink Uncached Lightweight (TL-UL) supports only read and write operations and is thus primarily used to access configuration space.

The number of used protocols clearly indicates that there is no one optimal and universal protocol to rule them all. Although these protocols differ significantly in their specifications (number of channels, signal names, capabilities), at its core, all protocols share ready-valid-handshaked interfaces and the facility to read and write data on byte-addressed granularity.

With such a zoo of protocols existing, heterogeneous SoCs will necessarily feature more than one interconnect protocol, thus requiring protocol adaptation. Although possible due to the general support for backpressure and byte-addressability, protocol adapters incur a considerable resource overhead and are likely to introduce a latency overhead and drop in utilization. In explicitly memory-managed systems, it is thus better to create a multi-protocol DMA engine directly capable of translating between different on-chip protocols, see Chapter 2.

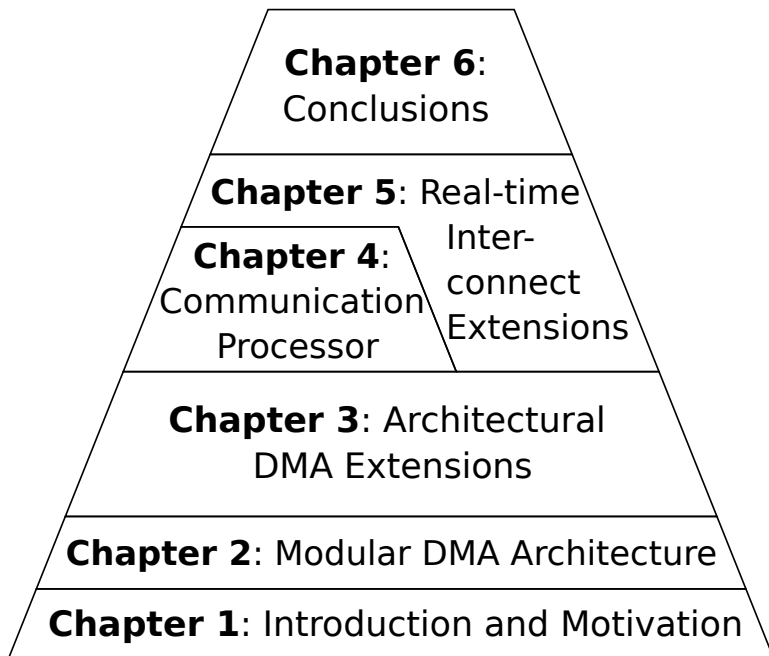


Figure 1.6: Overview of this thesis’s chapters. Chapter 2 with iDMA builds the *foundation* of this thesis. Chapter 3 defines important DMA extension which are developed into a communication processor in Chapter 4, supporting our goal of a energy-efficient real-time data movement strategy presented in Chapter 5.

## 1.4 Thesis Overview and Outline

In this section, we will summarize and motivate the structure of this thesis chapter by chapter. The overall organization is given in Figure 1.6. A substantial part of the content discussed in this thesis has been published in peer-reviewed conferences and as journal papers. A comprehensive listing of publications contributing to this thesis can be found in Section 1.6.

**Chapter 2** We first design a modular and highly versatile DMA architecture, called iDMA, which can be used in applications ranging from simple and dedicated I/O-DMAs controlling autonomous data transfer for peripherals to high-performance multi-channel engines that provide massive throughput at near-ideal bus utilization with minimal latency overheads. With the key insight in mind that most commonly used on-chip interconnect protocols share a byte-addressed data stream, iDMA is designed to support five industry-grade protocols, translating seamlessly between them, facilitating iDMA’s integration in heterogeneous SoCs.

**Chapter 3** We integrate iDMA in a wide range of systems, ranging from ultra-low-power (ULP) to high-performance computing (HPC) use cases, covering a large set of application scenarios and proving the applicability of the architecture. As part of these integration efforts, we develop three different system bindings for iDMA: a simple configuration-register-based interface, a Linux-capable transfer-descriptor-based scheme, and an agile RISC-V-compliant instruction-based front-end. To accelerate commonly occurring transfer patterns, we develop a set of DMA extensions facilitating data orchestration by handling N-dimensional (N-D) tensor transfers and scheduling of real-time transfers directly in hardware. We further include a standardized interface in iDMA’s data path to integrate in-stream operations. Finally, we develop a stream-optimized memory management unit (MMU) to be integrated into iDMA, enabling the DMA to autonomously handle virtual memory (VM) in conjunction with an application-grade host.

**Chapter 4** We combine iDMA with a tiny 20 kGE RISC-V processor tightly coupled through our instruction-based system binding, creating an agile communication processor capable of complex data scheduling and orchestration. We integrate this communication processor into a compute-cluster-based accelerator architecture with a focus on an optimal connection between the DMA engine and the cluster-local scratchpad memory. This cluster architecture is then scaled out to a 432-core dual-chiplet manycore system featuring fourteen iDMA

engines and 16 GiB of high-bandwidth memory 2E (HBM2E) connected through a hierarchical crossbar-based point-to-point interconnect.

**Chapter 5** With an efficient DMA engine developed and its integration into multiple systems studied, we shift focus towards the host by investigating real-time data transfers in heterogeneous MCSs, which become increasingly important with the advent of AI-driven applications in automotive and aeronautical use cases. We develop AXI-REALM, a lightweight and interconnect-agnostic helper-module-based architecture to module the amount of data managers can inject into the shared interconnect. This is especially important, as iDMA-equipped accelerators are tuned for maximal bandwidth efficiency through long data bursts, which can, if kept unregulated, lead to adverse performance of time-critical applications running on the host cores. We evaluate the effectiveness of AXI-REALM by integrating it into an open-source MCS research platform and evaluating using real-world workloads.

**Chapter 6** In this last chapter, we conclude the thesis, summarizing the key achievements and outlining a roadmap to continue this research and development.

## 1.5 Summary of Contributions

This thesis provides the following contributions:

1. Specifying, designing, and implementing a modular and highly parametrizable DMA architecture, called iDMA, targeting a wide range of systems from ULP to HPC systems by natively supporting multiple industry-grade on-chip protocols.
2. Developing adapted integrations for iDMA to suit multiple systems; this includes specifying a low-overhead configuration-register based programming interface for ULP system, combining a transfer-descriptor-based front-end to form an autonomous and Linux-compatible direct memory access controller (DMAC) , and extending the RISC-V instruction set with light-weight DMA extensions tightly coupling the DMA engine to the PEs.
3. Creating multiple DMA extensions to accelerate various aspects of commonly occurring transfer patterns. This includes accelerating N-D tensor transfers, a flexible VM extension, and automatically scheduling real-time memory transfers.
4. Combining iDMA with a light-weight 20 kGE RISC-V core through the developed DMA instruction extension forming a capable *communication processor* in charge of scheduling and orchestrating complex memory transfers in a compute-cluster-based HPC system. Proofing the viability and performance of the memory architecture by scaling it to an open-source 432-core RISC-V manycore system.
5. Designing and implementing a light-weight and topology-agnostic on-chip interconnect extension to provide real-time guarantees in high-performance heterogeneous MCSs by modulating the ingress of managers into the interconnect fabric. Integrating this real-time unit with a subordinate protection mechanism into an open-source MCS platform, demonstrating its performance using real-world applications.

This thesis discusses some elements developed in collaboration with Alessandro Ottaviano [50] and Paul Scheffler [51]. Their respective theses cover these elements partially with a different focus.

## 1.6 List of Publications

### 1.6.1 Previous Publications

The foundation for this thesis was laid completing my Master's Thesis.

- [52] T. Benz, "Snitch scale-out on Amazon F1 instances," Master's Thesis, ETH Zurich, 2020

### 1.6.2 Core Publications

The following publications are completely encompassed within this thesis.

- [53] T. Benz, M. Rogenmoser, P. Scheffler, S. Riedel, A. Ottaviano, A. Kurth, T. Hoefler, and L. Benini, "A high-performance, energy-efficient modular DMA engine architecture," *IEEE Transactions on Computers*, vol. 73, no. 1, pp. 263–277, 2024
- [54] T. Benz, A. Vanoni, M. Rogenmoser, and L. Benini, "A direct memory access controller (DMAC) for irregular data transfers on RISC-V Linux systems," 2025
- [55] T. Benz, A. Ottaviano, R. Balas, A. Garofalo, F. Restuccia, A. Biondi, and L. Benini, "AXI-REALM: A lightweight and modular interconnect extension for traffic regulation and monitoring of heterogeneous real-time SoCs," in *2024 Design, Automation & Test in Europe Conference & Exhibition (DATE)*, 2024, pp. 1–6
- [56] T. Benz, A. Ottaviano, C. Liang, R. Balas, A. Garofalo, F. Restuccia, A. Biondi, D. Rossi, and L. Benini, "AXI-REALM: Safe, modular and lightweight traffic monitoring and regulation for heterogeneous mixed-criticality systems," *IEEE Transactions on Computers*, vol. 74, no. 9, pp. 3072–3086, 2025

### 1.6.3 Related Publications

The following publications containing my contributions were partially covered by the content of this thesis.

- [57] S. Di Girolamo, A. Kurth, A. Calotoiu, T. Benz, T. Schneider, J. Beránek, L. Benini, and T. Hoefler, "PsPIN: A high-performance low-power architecture for flexible in-network compute," 2021

[58] ——, “A RISC-V in-network accelerator for flexible high-performance low-power packet processing,” in *2021 ACM/IEEE 48th Annual International Symposium on Computer Architecture (ISCA)*, 2021, pp. 958–971

[59] T. Benz, L. Bertaccini, F. Zaruba, F. Schuiki, F. K. Gürkaynak, and L. Benini, “A 10-core SoC with 20 fine-grain power domains for energy-proportional data-parallel processing over a wide voltage and temperature range,” in *ESSCIRC 2021 - IEEE 47th European Solid State Circuits Conference (ESSCIRC)*, 2021, pp. 263–266

[49] A. Kurth, W. Rönninger, T. Benz, M. Cavalcante, F. Schuiki, F. Zaruba, and L. Benini, “An open-source platform for high-performance non-coherent on-chip communication,” *IEEE Transactions on Computers*, vol. 71, no. 8, pp. 1794–1809, 2022

[60] A. Ottaviano, T. Benz, P. Scheffler, and L. Benini, “Cheshire: A lightweight, Linux-capable RISC-V host platform for domain-specific accelerator plug-in,” *IEEE Transactions on Circuits and Systems II: Express Briefs*, vol. 70, no. 10, pp. 3777–3781, 2023

[61] M. Rogenmoser, A. Ottaviano, T. Benz, R. Balas, M. Perotti, A. Garofalo, and L. Benini, “SentryCore: A RISC-V co-processor system for safe, real-time control applications,” *RISC-V Summit Europe*, 2024

[62] A. Ottaviano, R. Balas, T. Fischer, T. Benz, A. Bartolini, and L. Benini, “ControlPULplet: A flexible real-time multicore RISC-V controller for 2.5-D systems-in-package,” *IEEE Transactions on Very Large Scale Integration (VLSI) Systems*, vol. 33, no. 11, pp. 3057–3070, 2025

[63] M. Khalilov, M. Chrapek, S. Shen, A. Vezzu, T. Benz, S. Di Girolamo, T. Schneider, D. De Sensi, L. Benini, and T. Hoefler, “OSMOSIS: Enabling Multi-Tenancy in datacenter SmartNICs,” in *2024 USENIX Annual Technical Conference (USENIX ATC 24)*. Santa Clara, CA: USENIX Association, Jul. 2024, pp. 247–263

[64] G. Paulin, P. Scheffler, T. Benz, M. Cavalcante, T. Fischer, M. Eggimann, Y. Zhang, N. Wistoff, L. Bertaccini, L. Colagrande, G. Ottavi, F. K. Gürkaynak, D. Rossi, and L. Benini, “Occamy: A 432-core 28.1 DP-GFLOP/s/W 83% FPU utilization dual-chiplet, dual-HBM2E RISC-V-based accelerator for stencil and sparse linear algebra computations with 8-to-64-bit floating-point support in 12nm FinFET,” in *2024 IEEE Symposium on VLSI Technology and Circuits (VLSI Technology and Circuits)*, 2024, pp. 1–2

[65] C. Liang, A. Ottaviano, T. Benz, M. Sinigaglia, L. Benini, A. Garofalo, and D. Rossi, “A gigabit, DMA-enhanced open-source Ethernet controller for mixed-criticality systems,” in *Proceedings of the 21st ACM International Conference on Computing Frontiers: Workshops and Special Sessions*, ser. CF ’24 Companion. New York, NY, USA: Association for Computing Machinery, 2024, p. 55–58

- [66] C. Liang, T. Benz, A. Ottaviano, A. Garofalo, L. Benini, and D. Rossi, “Towards reliable systems: A scalable approach to AXI4 transaction monitoring,” in *2025 Design, Automation & Test in Europe Conference (DATE)*, 2025, pp. 1–7
- [67] T. Fischer, M. Rogenmoser, T. Benz, F. K. Gürkaynak, and L. Benini, “FlooNoC: A 645-Gb/s/link 0.15-pJ/B/hop open-source NoC with wide physical links and end-to-end AXI4 parallel multistream support,” *IEEE Transactions on Very Large Scale Integration (VLSI) Systems*, vol. 33, no. 4, pp. 1094–1107, 2025
- [68] A. Garofalo, A. Ottaviano, M. Perotti, T. Benz, Y. Tortorella, R. Balas, M. Rogenmoser, C. Zhang, L. Bertaccini, N. Wistoff, M. Ciani, C. Koenig, M. Sinigaglia, L. Valente, P. Scheffler, M. Eggimann, M. Cavalcante, F. Restuccia, A. Biondi, F. Conti, F. K. Gurkaynak, D. Rossi, and L. Benini, “A reliable, time-predictable heterogeneous SoC for AI-enhanced mixed-criticality edge applications,” *IEEE Transactions on Circuits and Systems II: Express Briefs*, vol. 72, no. 11, pp. 1625–1629, 2025
- [69] P. Scheffler, T. Benz, V. Potocnik, T. Fischer, L. Colagrande, N. Wistoff, Y. Zhang, L. Bertaccini, G. Ottavi, M. Eggimann *et al.*, “Occamy: A 432-core dual-chiplet dual-HBM2E 768-DP-GFLOP/s RISC-V system for 8-to-64-bit dense and sparse computing in 12-nm FinFET,” *IEEE Journal of Solid-State Circuits (JSSC)*, vol. 60, no. 4, pp. 1324–1338, 2025
- [70] Alessandro Ottaviano *et al.*, “Carfield: An open-source mixed-criticality heterogeneous RISC-V platform for next-generation autonomous systems,” 2025, unpublished

### 1.6.4 Unrelated Publications

I further contributed to the following publications while working towards my degree; while not being directly covered by the contents of this thesis, they might reveal additional insights.

- [71] S. Mazzola, T. Benz, B. Forsberg, and L. Benini, “A data-driven approach to lightweight DVFS-aware counter-based power modeling for heterogeneous platforms,” in *Embedded Computer Systems: Architectures, Modeling, and Simulation*. Cham: Springer International Publishing, 2022, pp. 346–361
- [72] V. Jain, M. Cavalcante, N. Bruschi, M. Rogenmoser, T. Benz, A. Kurth, D. Rossi, L. Benini, and M. Verhelst, “PATRONoC: Parallel AXI transport reducing overhead for networks-on-chip targeting multi-accelerator DNN platforms at the edge,” in *2023 60th ACM/IEEE Design Automation Conference (DAC)*, 2023, pp. 1–6

- [73] C. Zhang, P. Scheffler, T. Benz, M. Perotti, and L. Benini, “AXI-Pack: Near-memory bus packing for bandwidth-efficient irregular workloads,” in *2023 Design, Automation & Test in Europe Conference & Exhibition (DATE)*, 2023, pp. 1–6
- [74] T. Benz, P. Scheffler, Schöleber, and L. Benini, “Iguana: An end-to-end open-source Linux-capable RISC-V SoC in 130nm CMOS,” *RISC-V Summit Europe*, 2023
- [75] P. Sauter, T. Benz, P. Scheffler, Z. Jiang, B. Muheim, F. K. Gürkaynak, and L. Benini, “Basilisk: Achieving competitive performance with open EDA tools on an open-source Linux-capable RISC-V SoC,” *RISC-V Summit Europe*, 2024
- [76] P. Sauter, T. Benz, P. Scheffler, F. K. Gürkaynak, and L. Benini, “Insights from Basilisk: Are open-source EDA tools ready for a multi-million-gate, Linux-booting RV64 SoC design?” *33rd International Workshop on Logic & Synthesis (IWLS)*, 2024
- [77] P. Scheffler, P. Sauter, T. Benz, F. K. Gürkaynak, and L. Benini, “Basilisk: An end-to-end open-source Linux-capable RISC-V SoC in 130nm CMOS,” *2nd Safety and Security in Heterogeneous Open System-on-Chip Platforms Workshop (SSH-SoC 2024)*, 2024
- [78] C. Zhang, P. Scheffler, T. Benz, M. Perotti, and L. Benini, “Near-memory parallel indexing and coalescing: Enabling highly efficient indirect access for SpMV,” in *2024 Design, Automation & Test in Europe Conference & Exhibition (DATE)*, 2024, pp. 1–6
- [79] S. Mazzola, G. Ara, T. Benz, B. Forsberg, T. Cucinotta, and L. Benini, “Data-driven power modeling and monitoring via hardware performance counter tracking,” *Journal of Systems Architecture*, vol. 167, p. 103504, 2025
- [80] T. Benz, P. Scheffler, J. Holborn, and L. Benini, “DUTCTL: A flexible open-source framework for rapid bring-up, characterization, and remote operation of custom-silicon RISC-V SoCs,” *RISC-V Summit Europe*, 2024
- [81] T. Benz, P. Scheffler, N. Wistoff, P. Sauter, B. Muheim, and L. Benini, “ArtistIC: An open-source toolchain for top-metal IC art and ultra-high-fidelity GDSII renders,” *Free Silicon Conference (FSiC)*, 2025
- [82] P. Sauter, T. Benz, P. Scheffler, H. Pochert, L. Wüthrich, M. Povišer, B. Muheim, F. K. Gürkaynak, and L. Benini, “Croc: An end-to-end open-source extensible RISC-V MCU platform to democratize silicon,” *RISC-V Summit Europe*, 2025
- [83] P. Sauter, T. Benz, P. Scheffler, M. Povišer, F. K. Gürkaynak, and L. Benini, “Basilisk: A 34mm<sup>2</sup> end-to-end open-source 64-bit Linux-capable RISC-V SoC in 130nm BiCMOS,” in *2025 IEEE Hot Chips 37 Symposium (HCS)*. IEEE Computer Society, 2025, pp. 1–14

[84] C. Zhang, L. Colagrande, R. Andri, T. Benz, G. Islamoglu, A. Nadalini, F. Conti, Y. Li, and L. Benini, “FlatAttention: Dataflow and fabric collectives co-optimization for efficient multi-head attention on tile-based many-PE accelerators,” *2025 IEEE Computer Society Annual Symposium on VLSI (ISVLSI)*, vol. 1, pp. 1–6, 2025



# Chapter 2

# Modular DMA Architecture

## 2.1 Introduction

DMA engines form the communication backbone of many contemporary computers [33]. They concurrently move data at high throughput while hiding memory latency and minimizing processor load, freeing the latter to do useful compute. This function becomes increasingly critical with the trend towards physically larger systems [85] and ever-increasing memory bandwidths [86]. With Moore’s Law slowing, 2.5D and 3D integration are required to satisfy future applications’ computational and memory needs, leading to wider and higher-bandwidth memory systems and longer access latencies [87, 88].

Without DMA engines, PEs need to read and write data from and to remote memory, often relying on deep cache hierarchies to mitigate performance and energy overheads. In this thesis, we focus on explicitly managed memory hierarchies, where copies across the hierarchy are handled by DMA engines. We refer the interested reader to [89–92] for excellent surveys on cache-based memory systems. Caches and DMA engines often coexist in modern computing systems as they address different application needs. Dedicated DMA engines are introduced to efficiently and autonomously move data for workloads

where memory access is predictable, weakly data-dependent, and made in fairly large chunks, decoupling memory accesses from execution and helping maximize PE time spent on useful compute.

When integrating DMA engines, three main design challenges must be tackled: the control-plane interface to the PEs, the intrinsic data movement capabilities of the engine, and the on-chip protocols supported in the data plane. The sheer number of DMA engines present in literature and available as commercial products explains why these choices are usually fixed at design time. The increased heterogeneity in today’s accelerator-rich computing environments leads to even more diverse requirements for DMA engines. Different on-chip protocols, programming models, and application profiles lead to a large variety of different direct memory access (DMA) units used in modern SoCs, hindering integration and verification efforts.

In this chapter, we tackle these issues by presenting a modular and highly parametric DMA architecture called *intelligent DMA* (*iDMA*), which is composed of three distinct parts: the *front-end* handling PE interaction, the *mid-end* managing the engine’s lower-level data movement capabilities and facilitating complex data-shuffling patterns, and the *back-end* implementing one or more on-chip protocol interfaces. We call concrete implementations of our iDMA architecture *iDMA engines*. All module boundaries are standardized to facilitate the substitution of individual parts, allowing for the same DMA architecture to be used across a wide range of systems and applications, reducing management, verification, and maintenance efforts. While this chapter focuses on the general architecture of iDMA, Chapter 3 presents a wide range of system integrations, DMA extensions, and use cases served by iDMA in great detail. To foster the use of our DMA architecture, we provide the synthesizable register transfer level (RTL) description of iDMA, silicon-proven in various instances, and the system bindings are available free and open-source under a libre Apache-based license<sup>1</sup>.

In more detail, this chapter presents the following contributions to state-of-the-art (SoA) DMA research:

---

<sup>1</sup><https://github.com/pulp-platform/iDMA>

- We specify a *modular, parametric* DMA architecture composed of interchangeable parts, allowing iDMA to accommodate and benefit any system.
- We optimize iDMA to minimize hardware buffering through a highly agile, read-write decoupled, dataflow-oriented transport engine that maximizes bus utilization in any context. Our architecture incurs no idle time between transactions, even when adapting between different on-chip protocols, and incurs only *two* cycles of initial latency to launch a N-D affine transfer.
- We propose and implement a two-stage transfer acceleration scheme: the mid-ends manage (distribute, repeat, and modify) transfers while an in-stream *acceleration port* enables configurable in-flight operation on the data being transferred.
- Thanks to our modular system bindings (front-ends) and our support for multiple industry-standard on-chip protocols (back-ends), iDMA can be used in a wide range of contexts, from ULP to HPC systems. A lightweight first in, first out (FIFO) port allows easy integration into accelerators and peripherals without passing through a complex on-chip protocol. This interface can also be used to initialize memory given various data patterns.
- We thoroughly characterize our architecture in area, timing, and latency by creating area and timing models with less than 9% mean error and an analytical latency model, easing instantiation in third-party designs and accelerating system prototyping.
- We use synthetic workloads to show that iDMA achieves high bus utilization in ultra-deep memory systems with affordable area growth. Our architecture perfectly hides latency in systems with memory hierarchies hundreds of stages deep. It reaches full bus utilization on transfers as small as 16 B while occupying an area footprint of less than 25 kGE<sup>2</sup> in a 32-bit configuration.

---

<sup>2</sup>Gate equivalent (GE) is a technology-independent figure of merit measuring circuit complexity. A GE represents the area of a two-input, minimum-strength NAND gate.

## 2.2 Architecture

Unlike state-of-the-art (SoA) DMA engines, we propose a modular and highly parametric DMA engine architecture composed of three distinct parts, as shown in Figure 2.1. The *front-end* defines the interface through which the processor cores control the DMA engine, corresponding to the *control plane*. The *back-end* or *data plane* implements the on-chip network manager port(s) through which the DMA engine moves data. Complex and capable on-chip protocols like AXI4 [38], to move data through the system, and simpler core-local protocols like OBI [40] to connect to PE-local memories, are supported by the back-end. The *mid-end*, connecting the front- and back-end, slices complex transfer descriptors provided by the front-end (e.g., when transferring N-D tensors) into one or multiple simple 1-D transfer descriptors for the back-end to process. Additionally, multiple mid-ends may be chained to enable complex transfer processing steps. In a case study in Section 3.7 we show this chaining mechanism by connecting a real-time and a 3-D tensor mid-end to efficiently and autonomously gather sensor data. We discuss the available front-ends, the corresponding system bindings, and transfer acceleration through mid-ends in detail in Chapter 3.

To ensure compatibility between these three different parts, we specify their interfaces. From the front-end or the last mid-end, the back-end accepts a *1-D transfer descriptor* specifying a *source address*, a *destination address*, *transfer length*, *protocol*, and *back-end options*, as seen in Figure 2.2. Mid-ends receive bundles of mid-end configuration information and a *1-D transfer descriptor*. A mid-end will strip its configuration information while modifying the *1-D transfer descriptor*. All interfaces between front-, mid-, and back-ends feature *ready-valid* handshaking and can thus be pipelined.

### 2.2.1 Back-end

For given on-chip protocols, a back-end implements efficient *in-order 1-D arbitrary-length* transfers. *Multichannel* DMA engines featuring multiple ports into the memory system, can be built by connecting multiple back-ends to a single front- or mid-end, requiring a similar area to a true multichannel back-end but less verification and design

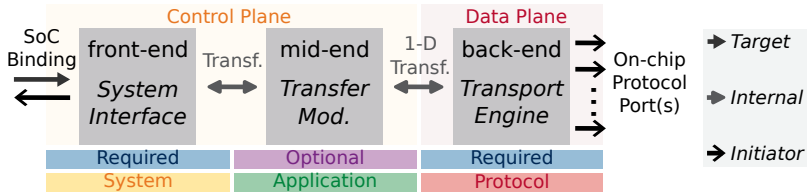


Figure 2.1: Schematic of iDMA: Our engines are split into three parts: at least one front-end, one or multiple optional mid-ends, and at least one back-end.

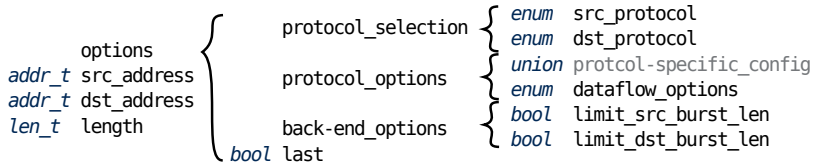


Figure 2.2: Outline of the *1-D transfer descriptor* (exchanged between mid- and back-end). The *options* field contains protocol-specific configuration independently of the chosen configuration to keep the back-end's interface interchangeable.

complexity. Arbitration between the individual back-ends can either be done explicitly by choosing the executing back-end through software or by an *arbitration* mid-end using round-robin or address-based distribution schemes. Depending on the application, explicitly managed or automatic distribution schemes might be more beneficial. In a ULP or a system with a highly non-uniform memory architecture, explicitly managed channels will deliver better results than round-robin or address-based distribution schemes. Similar hardware will be required in a true multichannel back-end to distribute transactions to available channels.

The back-end comprises three parts, see Figure 2.3. The *error handler* communicates and reacts to failing transfers, the *transfer legalizer* reshapes incoming transfers to meet protocol requirements, and the *transport layer* handles data movement and possibly in-cycle

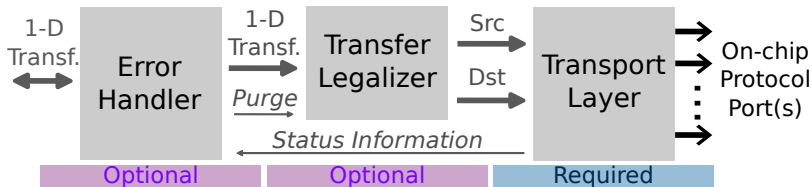


Figure 2.3: The internal architecture of the back-end. The *transport layer* handles the actual copying of the data on the on-chip protocol, supported by the optional *transfer legalizer* and the *error handler*.

switches between protocol-specific data plane ports. Of these three units, only the transport layer is mandatory.

**Error Handler** An *error handler* may be included if the system or application requires protocol error reporting or handling. Our current error handler can either *continue*, *abort*, or *replay* erroneous transfers. Replaying erroneous transfers allows complex N-D transfers to continue in case of errors in single back-end iterations without the need to abort and restart the entire transfer.

When an error occurs, the back-end pauses the transfer processing and passes the offending transfer's legalized burst base address to its front-end. The PEs can then specify through the front-end which of the three possible actions the error handler should take to resolve the situation.

We discuss the error handler in more detail in Section 2.2.4.

**Transfer Legalizer** Shown in Figure 2.4, the transfer legalizer accepts a 1-D transfer and legalizes it to be supported by the specific on-chip protocol(s) in use. Transfer information is stored internally and modular *legalizer cores* determine the transfer's maximum legal length supported given user constraints and the protocols' properties. For protocols that do not support bursts, the legalizer decomposes transfers into individual bus-sized accesses. Otherwise, splitting happens at page boundaries, the maximum burst length supported by the protocol, or user-specified burst length limitations. The source and destination protocols' requirements are considered to guarantee only legal transfers

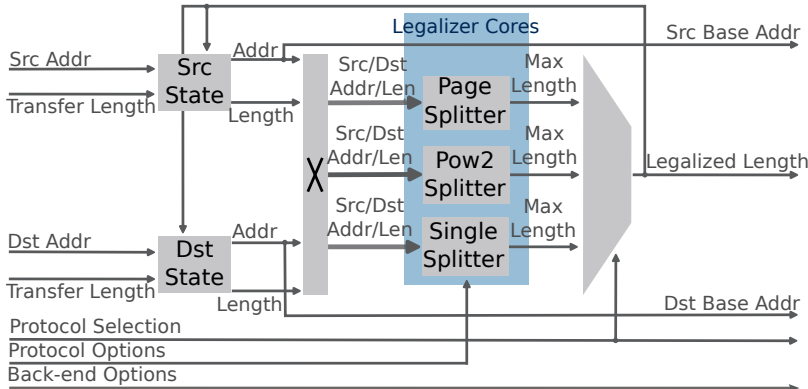


Figure 2.4: The internal architecture of the *transfer legalizer*. Any given transfer can be legalized except for zero-length transactions: They may optionally be rejected.

are emitted. In area-constrained designs, the transfer legalizer may be omitted; legal transfers must be guaranteed in software.

**Transport Layer** The parametric and modular *transport layer* implements the protocol characteristics for legalized transfers and decouples read and write operations, maximizing the bus utilization of any transfers. It uses *read* and *write managers* to handle protocol-specific operations, allowing it to internally operate only on generic byte streams, as shown in Figure 2.5. This enables our iDMA to easily support multiple on-chip protocols and multiple ports of the same protocol. The number and type of protocol ports available in the engine must be set at compile time, whereas the given protocol port a transaction uses can be selected during run-time through the front-end.

Both the *multiplexer* and *demultiplexer* within the transport layer (see Figure 2.5) can be modified to support multiple concurrent input and/or output streams to support, among others, reliable data transfers (reading/writing the same data from multiple memories) or vector operations.

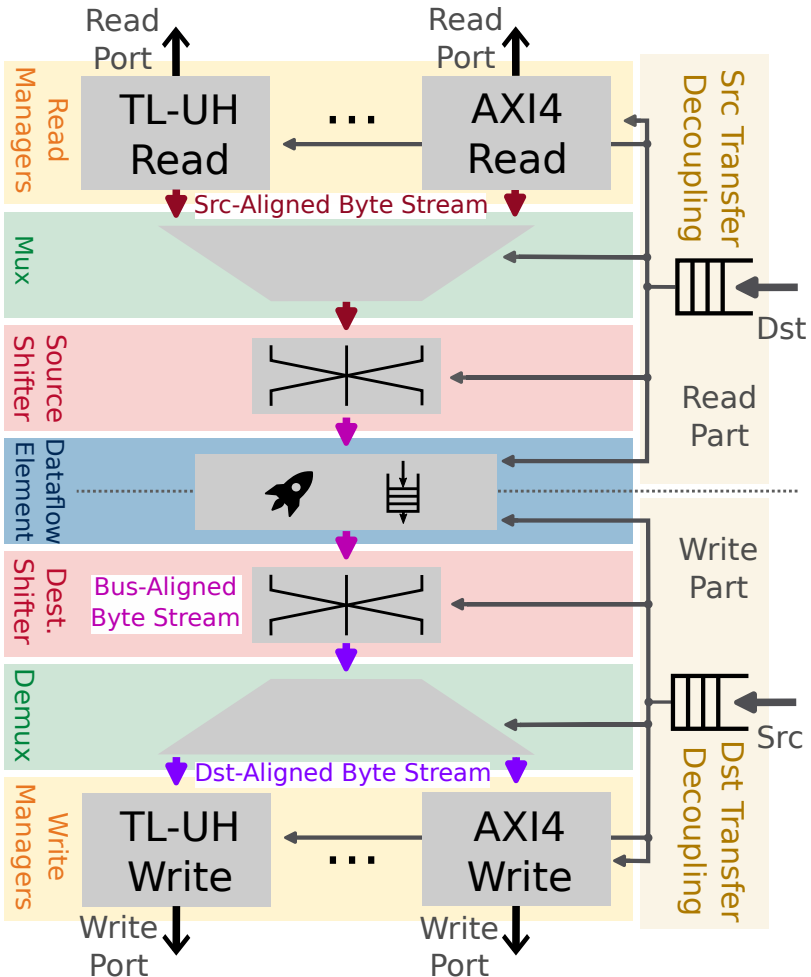


Figure 2.5: The architecture of the *transport layer*. One or multiple *read manager(s)* feed a stream of bytes into the *source shifter*, the *data flow element*, the *destination shifter*, and finally, into one or multiple *write manager(s)*.  denotes the *in-stream accelerator*.

The read and write stages of the transport layer are decoupled from the legalizer by FIFO buffers, allowing a configurable number of outstanding transfers. A *dataflow element* decouples the read and write stages, ensuring that only protocol-legal back pressure is applied to the memory system at each end, coalesces transfers, and cuts long timing paths to increase the engine’s maximum operating frequency. Fully buffered operation may be required depending on the system and the memory endpoints; in this case, the small FIFO buffer in the dataflow element may be replaced with an SRAM-based buffer, allowing entire transfers to be stored. On the other hand; if all endpoints are single-cycle memories (e.g., TCDM over OBI), the internal FIFO can be omitted to reduce the area footprint at the cost of no longer cutting the data path through the transport layer. We provide more insights regarding buffer sizing in Section 2.2.2.

Two shifters — one at each end of the dataflow element — align the byte stream to bus boundaries. To reduce the area footprint, the shifters can be merged into one single shifter at the ingress of the dataflow element at a cost of having a destination-aligned over a bus-aligned data stream in the dataflow element. *In-stream accelerators*, e.g., transposition units, allowing operations performed on the data stream during data movement, may be integrated into the dataflow element, augmenting the buffer in the transport layer. Our dataflow-oriented architecture allows us to switch between multiple read managers, write managers, and in-stream accelerators *in-cycle*, allowing our engine to asymptotically reach perfect bus utilization even when the used protocols or acceleration schemes change regularly.

**Protocol Managers** The transport layer abstracts the interfacing on-chip protocols through *read* and *write managers* with standardized interfaces, allowing for true multi-protocol capabilities. This modularization eases adapting iDMA to different on-chip protocols and verifying its proper operation as the bulk of the DMA engine does not require any changes.

*Read managers* receive the current read transfer’s base address, transfer length, and protocol-specific configuration information as inputs. They then emit a *read-aligned* stream of data bytes to the downstream transport layer. *Write managers* receive the write transfer

Table 2.1: Available on-chip protocols and their key characteristics. All protocols share *byte addressability* and a *ready-valid* handshake.

Protocol	Version	Request Channel	Response Channel	Bursts
<i>AMBA AXI4+ATOP</i> [38]	<i>H.c</i>	<i>AW</i> <sup>a</sup> , <i>W</i> <sup>a</sup> , <i>AR</i> <sup>b</sup>	<i>B</i> <sup>a</sup> , <i>R</i> <sup>b</sup>	<i>256 beats</i> or <i>4 kB</i> <sup>c</sup>
<i>AMBA AXI4 Lite</i> [38]	<i>H.c</i>	<i>AW</i> <sup>a</sup> , <i>W</i> <sup>a</sup> , <i>AR</i> <sup>b</sup>	<i>B</i> <sup>a</sup> , <i>R</i> <sup>b</sup>	no
<i>AMBA AXI4 Stream</i> [39]	<i>B</i>	<i>T</i> <sup>d</sup>	<i>T</i> <sup>d</sup>	unlimited
<i>OpenHW OBI</i> [40]	<i>v1.5.0</i>	<i>D</i>	<i>R</i>	no
<i>SiFive TileLink</i> [41] <sup>e</sup>	<i>v1.8.1</i>	<i>A</i>	<i>R</i>	UH: <i>power of two</i>
<i>Fifo/Init</i> <sup>f</sup>	N.A.	<i>REQ</i>	<i>RSP</i>	unlimited

<sup>a</sup> write    <sup>b</sup> read    <sup>c</sup> whichever is reached first    <sup>d</sup> symmetrical *RX/TX* channels

<sup>e</sup> *TL-UL & TL-UH* supported    <sup>f</sup> simple double-handshaked FIFO protocol

information and the *write-aligned* stream of data bytes from the upstream transport layer to be emitted over their on-chip protocol’s manager port.

Table 2.1 provides a complete list of implemented protocols; more details can be found in Section 1.3.

The *Fifo/Init* protocol provides a doubly handshaked streaming interface to easily connect custom hardware blocks without having to go through an on-chip communication protocol. It can be used to emit a configurable stream of either the *same repeated value*, *incrementing values*, or a *pseudorandom sequence*. This enables our engine to accelerate memory initialization.

### 2.2.2 Buffer Considerations

Buffer sizing is an elemental part of configuring our DMA architecture to achieve the full performance potential of the unit. Three distinct types of buffers are present in iDMA, each of them requiring careful tuning.

### 2.2.2.1 Job Buffer

*Job buffers* can be placed between the engine’s front-end and the back-end or first mid-end to allow the PEs to launch multiple non-blocking transfers. Operation without this buffer is possible but results in every DMA transfer being *blocking* as only one transfer can be issued by the front-end and worked on by the engine. A new transaction can only be accepted once the back-end completes the operation, which is marked by a handshake on the response channel.

Depending on the system and the application, a job buffer of two to sixteen elements is recommended.

### 2.2.2.2 Meta Buffer

*Meta buffers* are placed throughout the iDMA’s architecture to hold transfer-specific information, including addresses, transfer lengths, and configurations, among others. While not explicitly configurable through an exposed parameter, these buffers linearly scale with the number of outstanding transfers the DMA engine supports.

To achieve a high bus utilization, the number of outstanding transfers should be chosen large enough to hide the latency of the desired memory endpoint when employing the targeted burst length. In a well-designed system, expected values range from two to up to 64 outstanding transfers; to justify the latter, a deep memory system and an application issuing regularly short bursts is required.

### 2.2.2.3 Dataflow Buffer

The *dataflow buffer* within the dataflow element, see Section 2.2.1, logically and physically decouples the read and write stage of iDMA. Unlike the other two types of buffers previously discussed, incorrectly sizing the dataflow buffer not only leads to subpar performance but can result in memory interconnect deadlocks for certain combinations of systems, protocols, and endpoints.

Ideally, the dataflow buffer should just be configured for logical and physical decoupling as well as coalescing of the read and write streams, storing at most three words of the DMA transfer. This ensures maximized performance while keeping the area and resource footprint

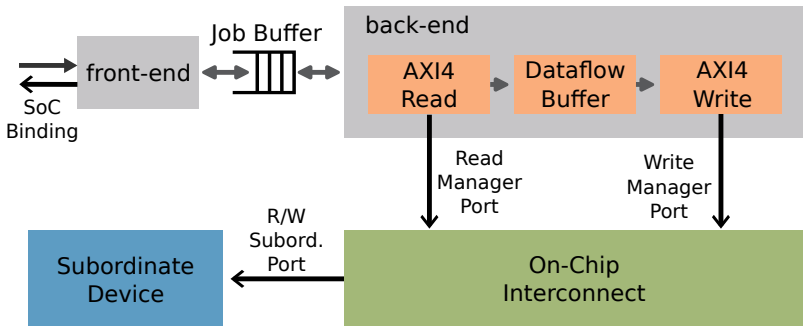


Figure 2.6: Simple system containing an iDMA; the subordinate device can either handle one read or write burst at the same time. Should the endpoint accept the write burst first and the back-end-internal dataflow buffer is not large enough to hold the full burst, a deadlock occurs as the data cannot be read from the endpoint concurrently.

minimal. For most systems, this configuration does not result in any adverse effects and should thus be used.

Burst-based protocols, like AXI4, usually arbitrate their transfers on the granularity of an individual burst [49] instead of a single data beat. Should an endpoint only support either serving reads or writes at the same time, the burst-based protocol dictates that it first complete the read or the write transaction before serving the other.

In conjunction with a minimally sized dataflow buffer, this could lead to a deadlock scenario. Let us assume a reorganization operation employing 4 kB bursts on a single endpoint is commanded to iDMA, see Figure 2.6. The DMA engine will issue both read and write operations towards the endpoint over the interconnect, which is free to reorder read and write operations freely. Should the write operation be accepted first by the endpoint, a deadlock will be inevitable as the memory endpoint will not provide any read data unless the write burst operation is complete and the DMA cannot issue any writes before receiving the read data.

As part of this thesis, we develop multiple mitigation mechanisms to prevent deadlocks from occurring.

**Serialized and Debursted Operation** The transfer legalizer supports debursting the transfers to any power-of-two granularity. Without any bursts emitted by iDMA, transfer reordering by the interconnect does allow the endpoint to handle the memory accesses interleaved.

**R-AW-Coupled Mode** In newer versions of iDMA, write requests can be stalled until the corresponding read data arrives in the dataflow element and is thus ready to be written. In conjunction with the debursted operation, this ensures deadlock-free operation.

**Leveraging AXI-REALM** As described in Chapter 5, AXI-REALM can be used to fragment a data stream and to prevent *ahead-of-time* blocking of subordinate resources. These two features together allow for the complete prevention of the deadlock scenario described above.

**R-W-Decoupled Endpoints** If we have full control over the memory endpoints in the system, they can easily be enhanced to handle reads and writes interleaved instead of blocking the read until the completion of the write burst or vice versa. We provide an enhanced *axi\_to\_mem\_interleaved* module as part of the *axi4* repository<sup>3</sup>.

**Fully Buffered Operation** As a final option, the FIFO-based buffer within the dataflow element can be replaced with a larger SRAM-based buffer designed to hold at least one maximum-sized burst. This should be considered as a last resort as buffer sizes in excess of 4 kB will be required, usually implemented through expensive and slow dual-port SRAMs.

### 2.2.3 Multi-Protocol Customization

As presented earlier in this section, one of the advantages of iDMA over SoA is its modular architecture achieved through the use of highly parameteric SystemVerilog (SV) code and the modularity of the legalizer cores and protocol managers. Although SV has well-developed capabilities of handling code parameterization, we could not identify an elegant way of handling iDMA’s multi-protocol use case with its

---

<sup>3</sup>[github.com/pulp-platform/axi](https://github.com/pulp-platform/axi)

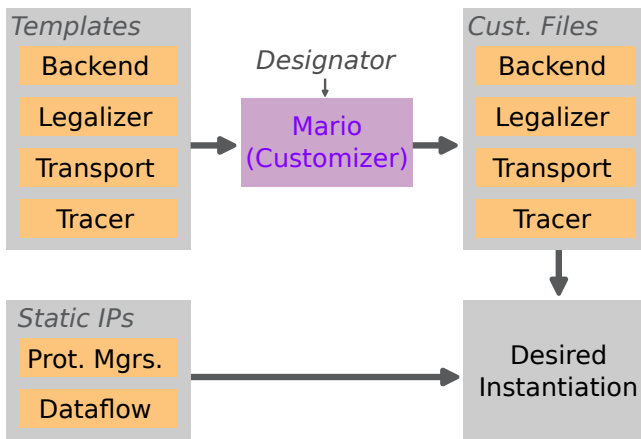


Figure 2.7: Our script, *Mario*, customizes and properly connects the SystemVerilog (SV) template files of iDMA to adapt it to specified protocol configurations.

varying interface signature. We decided to use a *Mako*-template-based configuration approach, shown in Figure 2.7, splitting the source into two parts: a static intellectual property (IP) codebase built around parameterized SV units and a their template-based wrapper files customized by a script called *Mario*, instantiating and connecting the proper IPs and creating the interface connections. Unlike other approaches, *Mario* was designed with code introspection in mind, emitting nicely formatted, human-readable and modifiable code. *Mario*<sup>4</sup> does not generate SV code, it simply connects or plumbs the fundamental IPs together using the available template code.

*Mario* assembles the desired configuration according to a unique identifier directly describing its protocol capabilities. Designators are constructed as a sequence of protocols and protocol capabilities. A capability is either described as read-only, *r*, write-only, *w*, or full-access, *rw*. Each available protocol has an identification string describing it, e.g., *axi4* for AXI4 or *axis* for AXI4 Stream. The designator is handed to *Mario* through the build environment and is used to prefix the

<sup>4</sup>Named after Super Mario, the world's best-known plumber.

customized SV code to prevent namespace conflicts of the different configurations.

As part of iDMA’s provided continuous integration (CI) framework, a fundamental set of designators is created spanning all currently available protocols. Next to the customized source code, Mario further emits a testbench for each configuration option used in CI to verify iDMA’s proper operation.

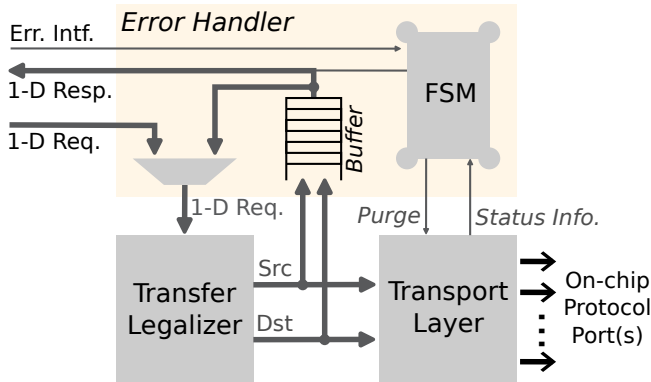


Figure 2.8: Internal architecture of iDMA’s *error handler*. A *buffer* holds the emitted transfer information to be reported or replayed in the case of an error.

### 2.2.4 Error Handling

Integrated in complex heterogeneous SoCs, it is an invalid assumption that iDMA will never encounter a failing memory transfer. Such errors can occur should the user or the operating system access an invalid memory region or if a subordinate device encounters an unexpected failure. Although uncommon, such errors need to be handled efficiently.

As can be seen in Figure 2.8 and previously outlined in Section 2.2.1, the error handler is an optional part of the back-end. It introduces two additional doubly handshaked signals to the back-end facing towards the front-end: the *response* and the *error handler* interfaces. The response interface informs the front-end whether a transfer completed successfully or resulted in an internal, e.g., zero-length transfer, or an external error, e.g., decode or subordinate error. The error handler interface is used to communicate the intent of how to handle the issue. It further intersects the request channel carrying the 1-D transfer information from the front-end to the legalize within the back-end to relaunch previously failed transfers.

### 2.2.4.1 Error Operation

Once an error is detected through one of the protocol ports, the transport layer informs the error handler that the current transfer failed. The entire back-end halts operation, and a failing response is issued. It is ample for the software running on the PE to understand the exact location of the error that occurred; this is especially true for N-D tensor transfers. The error handler thus has a *transfer buffer* holding the address of the legalized transfers currently in-flight. This address information, bundled with the type of error, is then handed to front-end.

Depending on the application's or platform's needs, one of three possible options can be selected to handle the error at runtime.

**Abort** The internal finite state machine (FSM) of the error handler allows the failed transfer in the dataflow element to finish, setting the write strobe to all zeros through the *poison* signal to save energy by omitting writing wrong data. The current transfer is finished, as many protocols do not allow terminating a burst prematurely. The state of the legalizer is flushed, bringing the DMA engine into an idle state. After completion, new transfers are allowed to be started again.

**Continue** Like in the *abort* case, the current transfer is completed without effects through issuing the poison signals. Following this, normal operation is just resumed, effectively ignoring the error. After completing the rest of the transfer successfully, the software may relaunch the failed part of the transfer manually.

**Replay** It is the most complex handling mode currently implemented in iDMA. Like before, the currently failing transfer is completed without an effect, followed by a completion of all the outstanding transfers in the transport layer. Once the transport layer becomes idle, the failed transfer is fetched from the transfer buffer and automatically relaunched. It is assumed that the relaunched transfers are now complete and successful; if not, a new error handling operation can be launched, this time only allowing abort and continue.

## 2.3 Architectural Results

To deepen the insight into iDMA and highlight its versatility, we provide IP-level implementation results in this section. We first present area and timing models characterizing the influence of parametrization on our architecture, enabling quick and accurate estimations when integrating engines into new systems. We then use these models to show that iDMA’s area and timing scale well for any reasonable parameterization. Finally, we present latency results for our back-end and discuss our engine’s performance in three sample memory systems. For implementation experiments, we use GlobalFoundries’ *GF12LP+* technology with a 13-metal stack and 7.5-track standard cell library in the typical process corner. We synthesize our designs using Synopsys Design Compiler NXT 2023.12 in topological mode to account for place-and-route constraints, congestion, and physical phenomena.

### 2.3.1 Area Model

We focus our evaluation and modeling effort on our iDMA back-end, as both the front-end and mid-end are very application- and platform-specific and can only be properly evaluated in-system. Our area model was evaluated at 1 GHz using the typical process corner in GF12LP+.

For each of the back-end’s major area contributors listed in Table 2.2, we fit a set of linear models using *non-negative least squares*. For each parametrization, our models take a vector containing the number of ports of each protocol as an input. This set of models allows us to estimate the area decomposition of the base hardware of the back-end and the area contributions of any additional protocol port, given a particular parameterization, with an average error of less than 4%. For example, Table 2.2 shows the modeled area decomposition for our *base* configuration of 32-bit address width, 32-bit data width, and two outstanding transfers.

A second step is required to estimate area contributions to the back-end depending on the parameterization, the number, and the type of ports. We created a second *param* model estimating the influence of the three main parameters, *area width (AW)*, *data width (DW)*, and the *number of outstanding transactions (NAx)*, on the back-end’s area contributions. We can estimate the area composition of the back-end

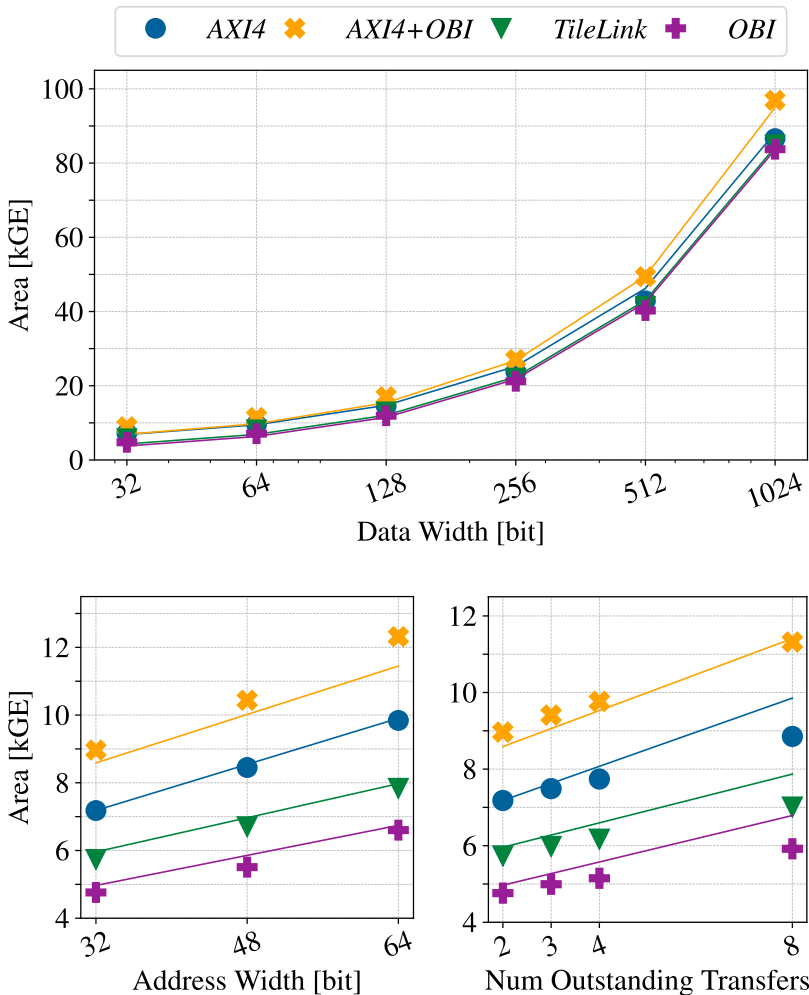


Figure 2.9: Area scaling of a back-end base configuration (*32-bit* address and data width, *two* outstanding transactions). Markers represent the measurement points and lines the fitted model.

with an average error of less than 9%, given both the parameterization and the used read/write protocol ports as input.

We provide a qualitative understanding of the influence of parameterization on area by listing the parameter with the strongest correlation using *big-O* notation in Table 2.2.

To outline the accuracy of our modeling approach, we show the area scaling of four of our iDMA engines for different protocol configurations, depending on the three main parameters, starting from the *base* configuration. The subplots of Figure 2.9 present the change in area when one of the three main parameters is modified and the output of our two linear models combined. The combined area model tracks the parameter-dependent area development with an average error of less than 9%. In those cases where the model deviates, the modeled area is overestimated, providing a safe upper bound for the back-end area.

### 2.3.2 Timing Model

We again focus our timing analysis on the back-end, as the front-end should be analyzed in-system and mid-ends may be isolated from the iDMA engine's timing by cutting timing paths between front-, mid-, and back-ends. Our investigation shows a *multiplicative inverse* dependency between the longest path in *ns* and our main parameters. We use the *base* configuration of the back-end to evaluate our timing model by sweeping our three main parameters. The tracking of our model is presented in Figure 2.10 for six representative configurations ranging from simple OBI to complex multi-protocol configurations involving AXI4. Our timing model achieves an average error of less than 4%.

The results divide our back-ends into two groups: simpler protocols, *OBI* and *AXI Lite*, run faster as they require less complex legalization logic, whereas more complex protocols require deeper logic and thus run slower. Engines supporting multiple protocols and ports also run slower due to additional arbitration logic in their data path. *Data width* has a powerful impact on iDMA engine's speed, mainly due to wider shifters required to align the data. The additional slowdown at larger data widths can be explained by physical routing and placement congestion of the increasingly large buffer in the dataflow element.

Table 2.2: Area decomposition of the DMA engine configuration used in the PULL-open cluster, see Section 3.4.3. The *base* area is always required, the contribution of each protocol added is shown. If the area contribution is non-zero, the parameter influencing the value is provided using the *big-O* notation. The area contribution scales linearly with the data width (*DW*) if no scaling is provided.

Units	Base	AXI4 read	AXI4 write	AXI4 Lite read	AXI4 Lite write	AXI4 Stream read	AXI4 Stream write	OBI read	OBI write	TL-UH read	TL-UH write	Init/FIFO
Decoupling	-	3.71kGE <sup>a</sup> $\mathcal{O}(NAr)$	1.4kGE $\mathcal{O}(NAr)$	1.4kGE $\mathcal{O}(NAr)$	310GE $\mathcal{O}(NAr)$	0						
Backend	Legelizer	State $\mathcal{O}(AW)$	1.51kGE <sup>b</sup> $\mathcal{O}(AW)$	710GE <sup>c</sup> $\mathcal{O}(AW)$	200GE <sup>c</sup> $\mathcal{O}(AW)$	180GE <sup>c</sup> $\mathcal{O}(AW)$	180GE <sup>c</sup> $\mathcal{O}(AW)$	180GE <sup>c</sup> $\mathcal{O}(AW)$	180GE <sup>c</sup> $\mathcal{O}(AW)$	215GE <sup>c</sup> $\mathcal{O}(AW)$	215GE <sup>c</sup> $\mathcal{O}(AW)$	21GE $\mathcal{O}(AW)$
Page Split	0	95 GE $\mathcal{O}(I)$	105 GE $\mathcal{O}(I)$	7 GE $\mathcal{O}(I)$	8 GE $\mathcal{O}(I)$	0	0	5 GE $\mathcal{O}(I)$	5 GE $\mathcal{O}(I)$	0	0	0
Pow2 Split	0	0	0	0	0	0	0	0	0	20 GE $\mathcal{O}(I)$	20 GE $\mathcal{O}(I)$	0
Transport Layer	Dataflow Element Contribution of Each Read/ Write Manager Respectively	1.31kGE <sup>d</sup> 0	0	0	0	0	0	0	0	0	0	0
Shifter/Muxing	120 GE	250 GE c 0	250 GE c 0	75 GE c 0	75 GE c 0	180 GE c 0	180 GE c 0	170 GE c 0	170 GE c 0	65 GE c 0	65 GE c 0	0

<sup>a</sup> *NAr*: Number of outstanding transfers supported. Used configuration: **16**.

<sup>b</sup> *AW*: Address width. Used configuration: **32-bit**.

<sup>c</sup> If multiple protocols are used, only the maximum is taken.

<sup>d</sup> *DW*: Data Width. Used configuration: **32-bit**.

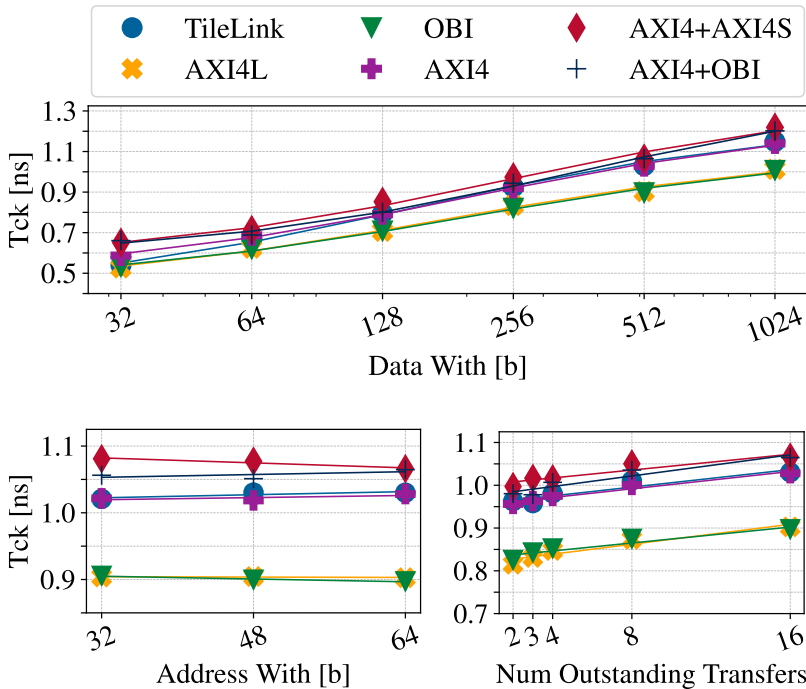


Figure 2.10: Clock period scaling of a back-end base configuration (32-bit address and data width, two outstanding transactions). Lower is better. *AXI4L* denotes AXI4 Lite, *AXI4S*, AXI4 Stream.

*Address width* has little effect on the critical path as it does not pass through the legalizer cores, whose timing is most notably affected by address width. Increasing the number of *outstanding transactions* sub-linearly degrades timing due to more complex FIFO management logic required to orchestrate them.

### 2.3.3 Latency Model

Our iDMA back-ends have a fixed latency of *two* cycles from receiving a 1-D transfer from the front-end or the last mid-end to the read request

at a protocol port. Notably, this is *independent* of the protocol selection, the number of protocol ports, and the three main iDMA parameters. This rule only has one exception: in a back-end without hardware legalization support, the latency reduces to *one* cycle. Generally, each mid-end presented in Chapter 3 requires *one* additional cycle of latency. We note, however, that the *tensor\_ND* mid-end (Section 3.4) can be configured to have *zero* cycles of latency, meaning that even for an N-D transfer, we can ensure that the first read request is issued *two* cycles after the transfer arrives at the mid-end from the front-end.

### 2.3.4 Standalone Performance

We evaluated the out-of-context performance of an iDMA engine in the *base* configuration copying a *64 KiB* transfer fragmented in individual transfer sizes between 1 B and 1 KiB in three different memory system models. The analysis is protocol-agnostic as all implemented protocols support a similar outstanding transaction mechanism; we thus use *AXI4* in this subsection without loss of generality. The three memory systems used in our evaluation differ in access cycle latency and number of outstanding transfers.

*SRAM* represents the level-two (L2) memory found in the PULP-open system (Section 3.4.3) with three cycles of latency and eight outstanding transfers. *RPC-DRAM* uses the characteristics of an open-source AXI4 controller for the reduced pin count (RPC) DRAM technology [93, 95] run at 933 MHz, around thirteen cycles of latency and support for sixteen outstanding transactions. *HBM* models an industry-grade high-bandwidth memory (HBM) [94] interface with a latency in the order of 100 cycles and supporting the tracking of more than 64 outstanding transfers.

In shallow memory systems, the iDMA engine reaches almost perfect bus utilization, copying single bus-sized data transfers required to track as low as eight outstanding transactions. More outstanding requests are required in deeper memory systems to sustain this perfect utilization. Any transfers smaller than the bus width will inevitably lead to a *substantial* drop in utilization, meaning that unaligned transfers inherently limit the maximum possible bus utilization our

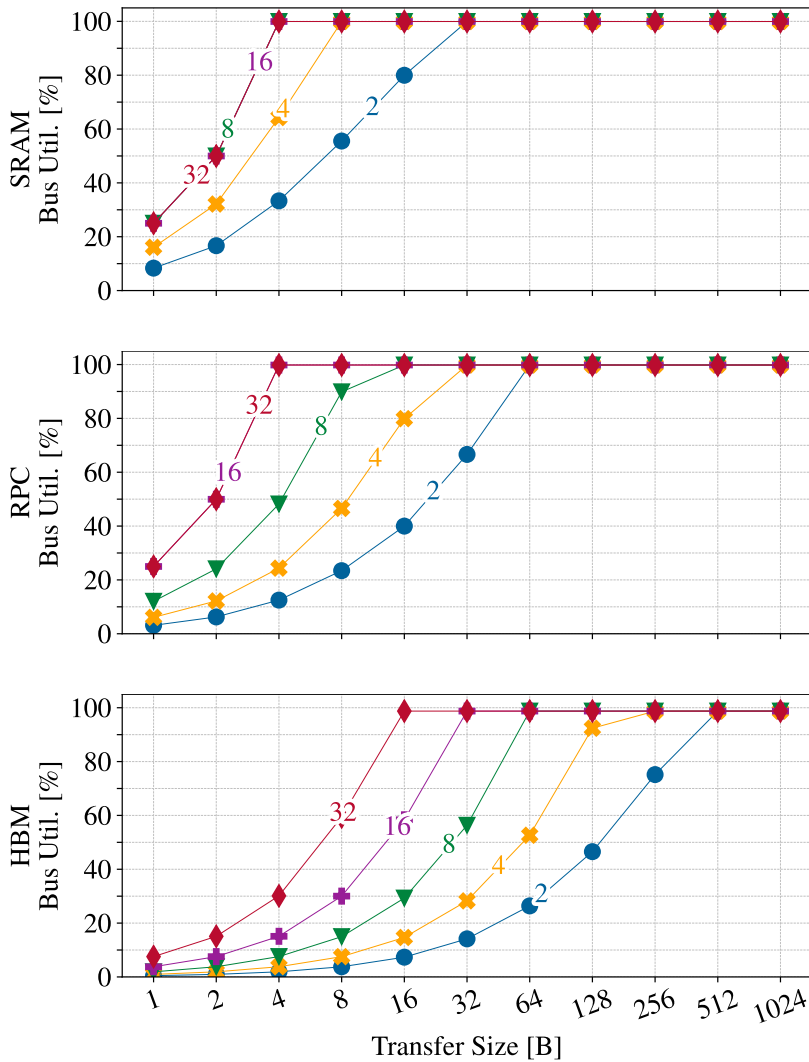


Figure 2.11: Bus utilization of our iDMA engine in the base configuration (32-bit address and data width) with varying amounts of outstanding transactions in three different memory systems; *SRAM*, *RPC DRAM* [93], *HBM* [94].

engines can achieve. Nevertheless, our fully decoupled data-flow-oriented architecture *maximizes the utilization of the bus* even in these scenarios.

Figure 2.11 shows that even in very deep systems with hundreds of cycles of latency, our engine can achieve almost perfect utilization for a relatively small transfer granularity of four times the bus width. This agility in handling transfers allows us to copy N-D tensors with a narrow inner dimension efficiently.

The cost of supporting such fine-granular transfers is an increased architectural size of the engines’ decoupling buffers. As shown in Section 2.3.1, these scale linearly in the number of outstanding transactions to be supported, growing by roughly 400 GE for each added buffer stage. In our base configuration, supporting 32 outstanding transfers keeps the engine area below 25 kGE.

### 2.3.5 Energy Efficiency

With iDMA’s area-optimized design, the capability of selecting the simplest on-chip protocol, and the effort to minimize buffer area, we can curtail the area footprint and thus the static power consumption of our iDMA engines.

iDMA’s decoupled, agile, data-flow-oriented architecture is explicitly designed to handle transfers efficiently while maximizing bus utilization, limiting the unit’s active time to a minimum. Coupled with our minimal area footprint and low-buffer design, this directly minimizes energy consumption. Furthermore, the engine’s efficiency allows *run-to-completion* operating modes where we maximize the interconnect’s periods of inactivity between transfers, allowing efficient clock gating of the iDMA engine and the interconnect, further increasing energy efficiency.

## 2.4 Related Work

We compare iDMA to an extensive selection of commercial DMA solutions and DMA engines used in research platforms; an overview is shown in Table 2.3.

In contrast to this work, existing DMA engines are designed for a given system, a family of systems, or even a specific application on a system. These engines lack modularity and cannot be readily retargeted to a different system. To the best of our knowledge, our work is the first fully modular and universal DMA architecture. Moreover, most of the DMA engines in our comparison are closed-source designs and thus not accessible to the research community, hindering or even preventing benchmarking and quantitative comparisons.

We identify two general categories of DMA engines: large high-bandwidth engines specialized in efficient memory transfers and low-footprint engines designed for accessing peripherals efficiently. Ma *et al.* [33], Paraskivas *et al.* [96], and Rossi *et al.* [36] present high-performance DMA engines ranging in size from 82 kGE to over 1.5 MGE. On the contrary, DMA engines designed for accelerating accesses to chip peripherals, as shown in the works of Pullini *et al.* [35] and Morales *et al.* [97] trade off performance for area efficiency by minimizing buffer space [35] and supporting only simpler on-chip protocols like AHB [97] or OBI [35]. Our iDMA can be parameterized to achieve peak performance as a high-bandwidth engine in HPC systems, see Chapter 4 and Chapter 4, as well as to require less area (<2 kGE) than the ultra-lightweight design of Pullini *et al.*'s  $\mu$ DMA [35].

SoC DMA engines, e.g., Fjeldtvedt *et al.* [37], Rossi *et al.* [36], and Morales *et al.* [97] feature a fixed configuration of on-chip protocol(s). Some controllers allow selectively adding a simple interface to connect to peripherals. The DMA IPs from Synopsys [98] and ARM [99] are two examples. We identify one exception to this rule: *FastVDMA* from Antmicro [100] can be configured to select one read- and one write-only port from a selection of three protocols. *FastVDMA* only supports unidirectional data flow from one read to the other write port. *Inter-port* operation, meaning copying data from one port and storing it using the same port, is not supported, which can limit its usability. iDMA allows the selective addition of one or multiple read

or write interface ports from a list of currently five industry-standard on-chip protocols. If configured, our engines allow bidirectional data movement in *inter-port* and *intra-port* operations. Thanks to the standardization of interfaces and the separation of data movement from protocol handling, new on-chip protocols can be added quickly by implementing *at most* three modules, each only a couple of hundred GEs of complexity.

*FastVDMA* [100] shows basic modularity by allowing users to select one read and one write protocol from a list of three on-chip protocols. Its modularity is thus limited to the back-end, and there is neither any facility to change between different programming interfaces nor a way of easily adding more complex N-D affine stream movement support. As presented in this work, our approach tackles these limitations by specifying and implementing the first fully modular, parametric, universal DMA architecture.

Table 2.3: Comparison of iDMA to the SoA.

DMA Engine	Application	Technology	Supported Protocols	Transfer Type	Programming	Stream Cap.	Modularity	Configurability	Area
CuteDMA [37] Feldkraet et al.	Hyperspectral Imaging	FPGA	AXI4 Stream <sup>a</sup>	3-D	Register File	None	Limited	Configurability	2162 LUTs 1796 FFs
RDMA [96] Paraskerous et al.	HPC	FPGA	AXI4	Linear	Transfer Descriptors	None	None	None	N.A.
cDMA [101] Rita et al.	DNN	ASIC <sup>c</sup>	N.A.	Linear	None	Compression & Decompression	No	0.21 mm <sup>2</sup> <sup>d</sup> 420 kGE <sup>e</sup>	
Rossi et al. [36] MT-DMA [33] Ma et al.	ULP	Tech. - Indep.	STBus <sup>f</sup> OBI <sup>g</sup>	Linear	Per-PE Register File	None	Limited Configurability	≈ 0.04 mm <sup>2</sup> ≈ 82 kGE	
FastVDMA [100] Antonero	Scientific Computing	ASIC	Custom	2-D	Transfer Descriptors	Block Transp.	None	1.07 mm <sup>2</sup> 1.5 MGE <sup>h</sup>	
DMA-330 [99] ARM	General-Purpose	Tech. - Indep.	AXI4 Stream <sup>i</sup>	Linear	Register File	None	Protocol Selectable	455 Shires <sup>j</sup>	
AXI DMA v7.1 [102] Xilinx	General-Purpose	Tech. - Indep.	AXI4 Stream <sup>i</sup>	Wishbone <sup>k</sup>	None	Yes, But Non-Modular	N.A.	N.A.	
xDMA AXI [103] RA MBUS	General-Purpose	Tech. - Indep.	AXI3 <sup>l</sup>	2-D	Custom Instructions	None	Yes, But Non-Modular	2745 LUTs <sup>m</sup> 4738 BRAM <sup>m</sup>	
DW - ext. DMAc [98] Synopsis	General-Purpose	Tech. - Indep.	AXI3/4	Scatter-Gather	Optional 2-D Scatter-Gather	None	Yes, But Non-Modular	216 kbit BRAM <sup>m</sup>	
Dynamengine [104] STMicroelectronics	MCU	FPGA	AXI4 <sup>f</sup>	Scatter-Gather	Transfer Descriptors	None	Yes, But Non-Modular	N.A.	
DDMA [105] DC2-SEMI	MCU	STM32	Xilinx-only	AXI4-Stream <sup>f</sup>	Scatter-Gather	None	Yes, But Non-Modular	N.A.	
iDMA [35] Paldani et al.	MCU	Tech. - Indep. <sup>n</sup>	AXI3/4	2-D Scatter-Gather	Transfer Descriptors	None	Yes, But Non-Modular	N.A.	
Monroes et al. [97]	IoT	Tech. - Indep.	OBII <sup>o</sup>	2-D Scatter-Gather	Transfer Descriptors	None	Yes, But Non-Modular	N.A.	
Su et al. [106]	General-Purpose	Tech. - Indep. <sup>n</sup>	RX/TX Channel <sup>p</sup>	Linear	Custom Instructions	None	Yes, But Non-Modular	15.4 kGE 3.2 kGE	
VDMA [107] Nanure et al.	Video	AXI4	AHB <sup>f</sup> ; Perif. Intf. <sup>f</sup>	Linear	Register File	None	Yes, But Non-Modular	N.A.	
Comisig et al. [108]	MCU	Custom	N.A.	Linear <sup>n</sup>	Register File	None	No	N.A.	
Extreme-Edge ULP, Datacenter HPC, Application-Grade	Tech. - Indep.	AXI4 AXI4 Lite, AXI4-Stream, TL-UL, TL-ABH, OBII	Optional N-D Arb. Strides Scatter-Gather	Register File, Transfer Descriptors, RISC-V ISA Ext., Custom	Memory Int., In-Stream Accelerator	Configurable and Modular	≥ 2 kGE		

<sup>a</sup> read-only      <sup>b</sup> write-only      <sup>c</sup> TrueFDDK45      <sup>d</sup> 28 mm node      <sup>e</sup> assuming 0.5 μm<sup>2</sup> per 1 GE      <sup>f</sup> cross-protocol operation only      <sup>g</sup> 32bit AXI4 read, AXI4-Stream write      <sup>h</sup> one manager port, main interface optional in UltraScale\_mm2s\_64DPW\_1\_100 (zecku09, ffuu156, 1)

<sup>i</sup> write-only per GE      <sup>j</sup> one read-only and one write-only selectable      <sup>k</sup> wrapper for APB, AHB, AXI4 Lite available      <sup>l</sup> very similar to OBI

## 2.5 Summary and Conclusion

We present iDMA, a modular, highly parametric DMA architecture composed of three parts (front-end, mid-end, and back-end), allowing our engines to be customized to suit a wide range of systems, platforms, and applications.

We evaluate the area, timing, latency, and performance of iDMA, resulting in area and timing models that allow us to estimate the synthesized area and timing characteristics of any parameterization within 9% of the actual result.

Our architecture enables the creation of both ultra-small iDMA engines incurring less than 2 kGE, as well as large high-performance iDMA engines running at over 1 GHz on a 12 nm node. Our back-ends incur only two cycles of latency from accepting an 1-D transfer descriptor to the first read request being issued on the engine's protocol port. They show high agility, even in ultra-deep memory systems. Flexibility and parameterization allow us to create configurations that achieve asymptotically full bus utilization and can fully hide latency in arbitrary deep memory systems while incurring less than 400 GE per trackable outstanding transfer. In a 32 bit system, our iDMA engines achieve almost perfect bus utilization for 16 B-long transfers when accessing an endpoint with 100 cycles of latency. The synthesizable RTL description of iDMA is available free and open-source.



# Chapter 3

# Architectural DMA Extensions

## 3.1 Introduction

In Chapter 2, we discussed the importance of efficiently moving linear streams of data in today’s high-performance heterogeneous SoCs [33], and we proposed iDMA, a modular and parameterized DMA architecture to fill this need. This chapter presents iDMA integrated in a wide range of systems and enhanced with multiple extensions, further accelerating DMA transfers and increasing their efficiency.

To enable efficient DMA transfers integrated in a system, an efficient and low-latency connection between the PEs and the DMA engines is of essential importance. DMA engines can be grouped according to their system binding: register, transfer-descriptor, and instruction-based. Engines requiring a high degree of agility [36, 37] or featuring a small footprint [35, 97, 100] tend to use a register-based interface. PEs write the transfer information in a dedicated register space and use a read or write operation to a special register location to launch the transfer. In more memory-compute-decoupled systems [96] or manycore environments [33, 96] transfer descriptors prevail. In some MCU platforms [99, 104] DMA engines are programmed using a

Table 3.1: Identifiers and descriptions of front-ends employed in the use cases. Front-ends in gray are available but not further discussed in this thesis.

Front-end	Description	Conf.
<i>reg_32</i>		32-bit, 1-D
<i>reg_32_2d</i>		32-bit, 2-D
<i>reg_32_3d</i>	Core-private register-based configuration interface for ULP-systems	32-bit, 3-D
<i>reg_64</i>		64-bit, 1-D
<i>reg_64_2d</i>		64-bit, 2-D
<i>reg_32_rt_3d</i>	Core-private register-based system binding supporting our real-time mid-end	32-bit, 3-D
<i>desc_64</i>	Transfer-descriptor-based interface designed for 64-bit systems compatible with the Linux DMA interface	64-bit, 1-D
<i>inst_64</i>	Interface decoding a custom iDMA <i>RISC-V</i> instructions used in HPC systems	64-bit, 2-D

custom instruction stream. Generally, DMA engines only feature one programming interface with some exceptions: both Xilinx’s *AXI DMA v7.1* and Synopsys’ *DW\_axi\_dmac* support, next to their primary transfer-descriptors-based interface, a register-based interface usable with only a reduced subset of the engines’ features [98, 102]. This chapter will combine these three system bindings with iDMA, showing its capabilities as a universal DMA architecture. With our standardized interfaces, any custom binding can be implemented, fully tailoring the engine to the system it is attached to. We provide an overview of the available bindings for iDMA in Table 3.1.

Many DMA engines support transfers with more than one addressing dimension. 2-D transfers are commonly accelerated in hardware [33, 99, 102]. Fjeldtvedt *et al.*’s *CubeDMA* can even handle 3-D transfers. Any higher-dimensional transfer is handled in software either by repetitively launching simpler transfers [37] [36] or by employing transfer descriptor chaining [33, 102]. In Section 3.4, we present our *tensor\_ND* mid-end, which can execute arbitrary high-dimensional transfers in hardware. Our *desc\_64* front-end, presented in Section 3.2,

supports descriptor chaining to handle arbitrarily shaped transfers without putting any load on the PE. Our flexible architecture can easily accelerate special transfer patterns required by a specific application: once programmed, we present our novel *rt\_3D* mid-end in Section 3.7, which can autonomously fetch strided sensor data without involving any PE. Rhu *et al.* [101] and Ma *et al.* [33] present DMA engines able to modify the data while it is copied. Although their work proposes a solution for their respective application space, none of these engines present a standardized interface to exchange *stream acceleration modules* between platforms easily. Additionally, both engines, especially *MT-DMA* [33], impose substantial area overhead, limiting their applicability in ULP designs. Our engines feature a well-defined interface accessing the byte stream while data is copied, allowing us to e.g., include both buffered and buffer-less matrix transposition units as well as ALUs in iDMA.

In heterogeneous systems, physically addressed accelerators are combined with host systems running operating systems (OSs) employing virtual memory [68, 70]. Thanks to the modularity of iDMA, we can present a stream-optimized MMU, called *sMMU* in Section 3.3, allowing the accelerator to do the address translation directly within the DMA engine.

To summarize this chapter. Section 3.2 introduces a Linux-capable transfer-descriptor-based front-end which we combine with an iDMA back-end, creating a direct memory access controller (DMAC). Section 3.3 introduces virtual memory support. In Section 3.4 we introduce a low-overhead configuration-register-based front-end and our N-D tensor extension accelerating edge-ML inference workloads. Section 3.5 introduces how we coordinate multiple iDMA back-ends in a manycore system. Section 3.6 presents a generalized methodology on how to combine peripherals with iDMA. In Section 3.7 we presents an extension, allowing us to efficiently schedule sensor data accesses. Finally, Section 3.8 gives a peek into Chapter 4 and in Section 3.9 we conclude the current chapter.

## 3.2 Linux Support and Extensions

### 3.2.1 Introduction

Modern computing systems are rapidly increasing in complexity and scale to combat the slowdown of Dennard scaling and to satisfy the ever-increasing need for more computing performance and memory, driven by ML and big data workloads [109]. Kumar *et al.* highlight the importance of irregular memory accesses in sparse data structures when dealing with large-scale graph applications [110]. Today’s systems require high-performance interconnects with components that efficiently move the data required to supply their compute units. Using such specialized direct memory access controllers (DMACs)<sup>1</sup> is a well-established method to transfer data independently of processors, thereby promising to achieve high throughput while the processor is free to perform computationally useful work [98, 102, 106, 108, 111, 112]. With a shift towards more heterogeneous architectures, as well as smaller datatypes [109, 113], more diverse transfers are emerging, requiring greater flexibility and less overhead in the programmability of DMACs.

Highly flexible programming hardware interfaces and hardware abstraction layers (HALs) for DMACs are usually based on *descriptors*, data structures stored in shared memory that hold the information of a transfer. Descriptors have multiple advantages compared to simpler register-based programming interfaces, which are widely used in embedded and MCU applications [36]. Descriptors massively reduce the requirement for dedicated configuration memory space by storing the transfer specification in general-purpose memory segments, thus eliminating the need for configuration space replication in multicore applications to enforce atomic transfer launching [36]. Descriptors can be chained as a linked list, enabling the automatic launch of subsequent transfers. This allows N-D affine and fully arbitrary and irregular workloads to be processed [37]. A concrete example of a DMAC is the *LogiCORE IP DMA*, an AXI4 DMA soft IP by *Xilinx* [102]. It is a high-bandwidth DMAC with a descriptor-based programming interface and is designed to transfer data between a memory-mapped AXI4 interface and an AXI4-Stream target device.

---

<sup>1</sup>We explicitly use DMAC for Linux-capable DMA units. This includes an iDMA back-end and our transfer-descriptor-based front-end (*desc\_64*).

Applying this descriptor configuration model to fine-grained, irregular transfers leads to long chains of individual descriptors, requiring the DMAC unit to handle a large amount of data when executing the transfer. Excessive descriptor size degrades the throughput of such fine-grained transfers, as the DMAC may require multiple cycles to fetch the descriptors. Furthermore, larger descriptor sizes result in more significant resource utilization and power overhead required by buffering logic. *Synopsys' DesignWare AXI4 DMA controller* presents a parametrizable and high-performance DMAC solution, using 64-byte-long descriptors in *scatter-gather mode* [98]. Paraskevas *et al.* describe an efficient 32-byte-long descriptor format without prefetching capabilities [96]. In their work, descriptors are stored in dedicated pages of the core's on-chip scratchpad memory. Ma *et al.* describe a five-entry-long descriptor format supporting chaining for N-D data transfers [114]. To ensure efficient fetching of the descriptors, they are stored in a dedicated DMAC-internal *parameter RAM*. As descriptors are usually handled in sequence [38], requesting the next descriptor once the prior is read, full DMAC utilization is only reached if the described transfer is long enough to hide the latency of fetching a descriptor. This can no longer be guaranteed for fine-grained transfers in a non-ideal memory system, limiting the maximum achievable DMAC utilization for such transfers. We tackle these issues by introducing a DMAC with a minimal descriptor format, as well as a low-overhead prefetching mechanism; our contributions are:

- A lightweight, minimal, and efficient descriptor format holding only the essential information required to describe a transfer. Our format supports chaining and provides a mechanism to track transfer completion, increasing DMAC utilization by  $3.9 \times$  for 64-B transfers compared to the *LogiCORE IP DMA* [102].
- Implementing our descriptor format, as well as speculative descriptor prefetching, together with iDMA presented in Chapter 2, creates a fully parametrizable, synthesizable, and technology-independent DMAC.

- Evaluating our DMAC out-of-context (OOC) regarding its performance, area requirements, and timing in a 12 nm node. Our AXI4-compliant DMAC can achieve near-ideal performance while exceeding clock frequencies of 1.5 GHz and requiring only 49.5 kGE.
- Integrating the resulting DMAC into Cheshire [60], our 64-bit Linux-capable SoC platform, we achieve an improvement in terms of latency by  $1.66 \times$  compared to the *LogiCORE IP DMA AXI4 DMA* [102], while requiring 11% fewer lookup tables, 23% fewer flip-flops, and no block RAMs.

### 3.2.2 Architecture

With efficient data transfer being an essential requirement for ML workloads, we make use of our iDMA architecture presented in Chapter 2. This fully open-source DMA engine directly interfaces with our AMBA AXI4 memory system and is capable of asymptotically utilizing the available bandwidth. Furthermore, iDMA is optimized for low area utilization, low transfer launch latencies, and high clock frequencies. The iDMA architecture does not directly provide a programming interface to the system. In the following section, we describe a descriptor-based programming interface implemented as an iDMA front-end, called *desc\_64*. The *desc\_64* front-end and iDMA back-end together form the DMAC, as shown in Figure 3.1.

### 3.2.3 DMA Front-end Design

To configure a DMA transfer, the *desc\_64* front-end exposes a memory-mapped configuration and status register (CSR), which accepts an address pointing to a DMA transfer descriptor in shared memory, described in Section 3.2.4. Once this pointer is written into the CSR, the front-end requests the descriptor from memory through the read channel of an AXI4 manager port, shown as the request logic in Figure 3.1. This manager port is configurable in both AXI4 address width, allowing descriptors to be located in any memory location, and AXI4 data width, ranging from 16 to 512 bits. Using this port, *desc\_64* retrieves the necessary information for a generic linear memory transfer: source address pointer, destination address pointer, transfer length, and

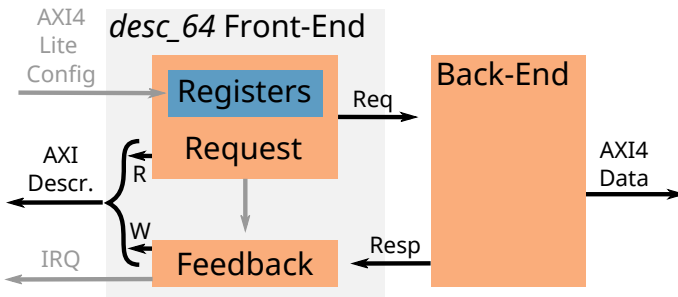


Figure 3.1: Overview of the DMAC, containing request logic with internal registers for configuration and read logic to fetch the descriptor, and feedback logic to update the system once the iDMA back-end completes the transfer.

configuration. Once fetched, `desc_64` forwards the information to the back-end, which executes the transfer. To improve performance, both the CSR and the connection to the back-end implement a queue. This allows multiple transfers to be enqueued, maximizing the utilization of the back-end.

Once the back-end has completed a transfer, `desc_64` reports completion back to the system, shown as the feedback logic in Figure 3.1. For each transfer, the corresponding descriptor is modified to indicate its completion, and an interrupt is signaled if configured.

### 3.2.4 DMAC Transfer Descriptor

Our DMAC descriptor contains the information necessary to fully describe a linear memory transfer: a 64-bit source and destination address, and the length of the transfer. The transfer length is stored in an unsigned 32-bit field, allowing individual transfers of up to 4 GiB in size. Longer transfers can easily be achieved by chaining together multiple descriptors.

A *config* field in the descriptor holds configuration information for both the iDMA front- and back-end. For the former, different interrupt request (IRQ) options can be set, while for the latter, various AXI4-related parameters are configurable. A complete descriptor structure

can be found in Listing 3.1. Apart from information describing the transfer, the descriptor contains a pointer to the next descriptor to be processed, enabling *descriptor chaining*. This allows our DMA to process a *linked list* or *chain of descriptors* in memory without involving the CPU. The last descriptor in a chain carries all ones (equals to -1) in the *next* field; we call this value *end-of-chain*. This value was chosen as no descriptor can fit at the corresponding address. Descriptor chaining allows the construction of arbitrary and irregular transfers from simple linear transfers. When designing the descriptor format, we minimized its size while keeping it a multiple of the AXI4 bus width. The former has two benefits; it not only reduces the required bandwidth of the memory subsystem when storing and fetching descriptors, but also the overall memory footprint to describe a given transfer. The latter allows us to fetch the 256-bit descriptors and chains thereof without losing utilization in memory systems with widths up to 256 bit. In systems featuring a 512-bit infrastructure, such as a wide range of *Xilinx Zynq UltraScale+ MPSoCs*, two full descriptors could be fetched in one cycle.

Listing 3.1: Descriptor Layout

```
struct descriptor {
    u32 length;
    u32 config;
    u64 next;
    u64 source;
    u64 destination;
}
```

To compare, the *LogiCORE IP DMA* [102] uses a descriptor format of thirteen 32-bit words or 416 bit, of which usually only 256 bit are read. Its AXI4 manager interface used to fetch descriptors is limited to a data width of 32 bit, leading to a descriptor read latency of at least eight to thirteen cycles. In contrast, our DMA may read a descriptor in four cycles in a comparable 64-bit system.

### 3.2.5 Speculative Descriptor Prefetching

To compensate for memory latency, we employ *speculative descriptor prefetching*. Once a descriptor address is written to the CSR, we not

only request the first descriptor over `desc_64`'s manager interface but send up to a configurable amount of requests with sequential addresses. The number of descriptors speculatively requested is configured using the *prefetching* compile-time parameter, zero deactivating the prefetching logic, as can be seen in Table 3.2. Once a descriptor arrives at the DMA front-end, we compare the *next* field of this descriptor with the speculatively requested address. On a match, the speculative address is committed and one speculation slot is freed up. Transfers are only forwarded to the back-end once the speculatively fetched descriptor is confirmed through a positive match ensuring data integrity. Should a misprediction occur, we discard all descriptor addresses in the *speculation slots* and start to fetch from the correct *next* address while ignoring the incoming data that was mispredicted. Care was taken not to introduce any latency in the case of mispredictions compared to prefetching disabled. Assuming there is space in the *speculation slots*, the proper request is issued over the AXI4 manager interface in the same cycle the DMA front-end receives the *next* field. This is the same latency we observe in the case of prefetching disabled. Thus, the only performance degradation that may occur is caused by minimal additional contention in the memory system due to fetching data that is directly discarded.

### 3.2.6 Cheshire integration

Heterogeneous systems often rely on a high-performance 64-bit memory system due to compatibility with the central host processor. While parametrizable, our implementation configures the DMAC for such a memory system, using 64 bit both for address and data width of the AXI4 bus in accordance with Cheshire [60], we integrate our DMAC into. An overview of the resulting system can be seen in Figure 3.2: The two manager interfaces of our DMAC, as well as the subordinate configuration interface, are connected to the memory system of the SoC. We occupy one new IRQ channel at the systems' platform-level interrupt controller (PLIC), which is used to signal transfer completion when configured. For lightweight in-system progress reporting, we repurpose a transfer descriptor by overwriting its first 8 bytes with *all ones* after the transfer is completed. This allows us to forego raising an

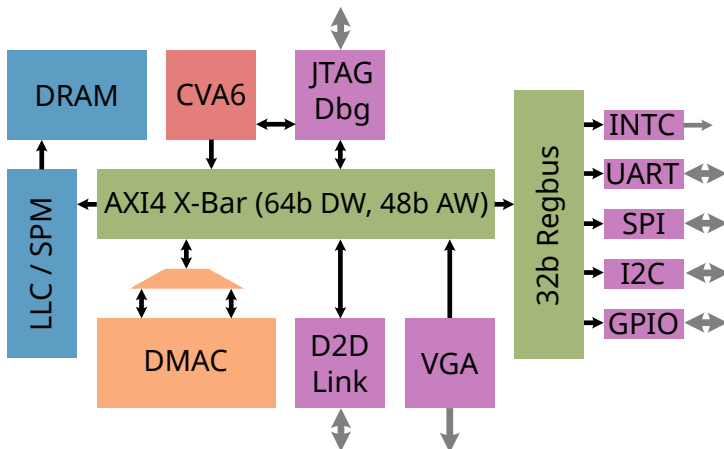


Figure 3.2: Integration of our DMAC into the Cheshire [60]. The two manager interfaces, after arbitration, as well as the subordinate configuration port of the DMAC, are connected to the SoC’s interconnect. The IRQ line is connected to the platform’s PLIC.

interrupt after each linear transfer is completed, thus making interrupt notification optional.

### 3.2.7 Linux Driver

To ensure simple integration into existing environments, we provide a sample *Linux* driver with an accompanying device-tree file. The DMA subsystem of the Linux kernel exposes a broad application programming interface (API) [115], of which we implement the *memcpy* interface.

For a DMA client to request a data transfer, the application requests the driver to prepare the *memcpy* transfer. This is done by allocating one or more chained descriptors and populating *source*, *destination*, *length*, and *config* fields. For more complex transfers, multiple descriptors are allocated and chained. Transfer completion notifications are only needed after a (possibly multi-descriptor) transfer is completed. Therefore, IRQ signaling is only enabled in the last

Table 3.2: The compile-time parameters used in our OOC experiments.

Configuration	Descriptors In-flight	Prefetching
<i>LogiCORE IP DMA</i> [102]	4	<i>N.A.</i>
<i>base</i>	4	Disabled (0)
<i>speculation</i>	4	4
<i>scaled</i>	24	24

descriptor of a transfer. Should a transfer consist of more than one descriptor, then only the last has IRQ signaling enabled. As a second step, the client commits to specific transfers, which results in the driver chaining them in a FIFO fashion to a new chain. It is checked if any transfers are already in progress; if so, the driver attempts to commit the transfers to the end of the running chain. Otherwise, they are queued for submission. Third, the client requests to submit all committed transfers to the hardware. The driver checks whether fewer than the maximum number of allowed chains are already running on the DMAC; if so, it schedules the new chain with a write to the DMAC’s CSR, otherwise, the transfers are stored to be scheduled later. Finally, on transfer completion, the DMAC raises an IRQ. This leads to a call of the *interrupt handler*, which schedules any completion callbacks the client has registered, updates the number of active chains if the transfer was the last of a chain, and schedules stored transfers.

### 3.2.8 Results

#### 3.2.8.1 OOC Results

We evaluate our DMAC with our optimized descriptor format OOC and integrated into Cheshire. For the OOC evaluation, we attach our DMAC to a configurable memory system to assess its performance, as can be seen in Figure 3.3. We then present area and timing results from synthesizing our controller out-of-context using GlobalFoundries’ GF12LP+ node. We then show both performance and implementation

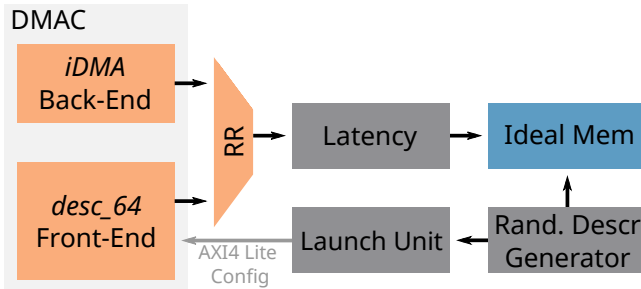


Figure 3.3: The OOC testbench setup; the DMAC has its two AXI4 manager interfaces connected to a fair round-robin arbiter (RR), which in turn is connected to a latency-configurable memory system. Contention between DMA data transfers and reading descriptors is thus modeled. Descriptors are loaded into the memory using backdoor access and are launched via the DMAC’s subordinate configuration interface.

results of our DMAC integrated into Cheshire [60] implemented on a *Diligent Genesys 2* field-programmable gate array (FPGA) [116].

To evaluate the standalone performance of our DMAC, we created a testbench environment consisting of a *latency-configurable* memory system and a *launch unit* to set up and execute random streams of descriptors. To simulate a real system, both of our DMAC’s AXI4 manager ports are connected to the same memory system using a fair round-robin arbiter (RR), as shown in Figure 3.3. To stay aligned with Cheshire, we set the address and data width of our OOC testbench to 64 bit. The randomness of the descriptions can be closely controlled, allowing us to emulate different transfer characteristics. The corresponding descriptors are immediately preloaded into our simulation memory using a backdoor, while the actual launch of the transfers is controlled using our DMAC’s CSR interface. The bus utilization is measured at the back-end’s AXI4 *manager* interface; only *useful* payload traffic contributes to utilization. We only report *steady state* bus utilization, suppressing any possible cold-start phenomena.

In our analysis, we assessed three distinct memory system configurations reflecting different use cases:

Table 3.3: Area requirements at the maximum clock frequency of the DMAC and its main sub-components; desc\_64 and the iDMA back-end. Clock frequencies are achieved in typical conditions.

Config.	desc_64 front-end	Back-end	DMAC	Achievable Freq.
<i>base</i>	25.8 kGE	15.4 kGE	41.2 kGE	1.71 GHz
<i>speculation</i>	34.8 kGE	14.7 kGE	49.5 kGE	1.44 GHz
<i>scaled</i>	151.1 kGE	37.3 kGE	188.4 kGE	1.23 GHz

1. *Ideal Memory*: We configure our simulation memory to have one cycle latency, emulating an SRAM-based main memory.
2. *DDR3 Main Memory*: Replicating the conditions found on the *Diligent Genesys 2* FPGA [116] when accessing DDR3 off-chip memory, we include a configuration with *thirteen* cycles latency.
3. *Ultra-deep Memory*: Representing a large network-on-chip (NoC) system found in a modern SoC, we include a configuration with a latency of *one hundred* cycles.

To ensure a fair comparison against the *LogiCORE IP DMA*, we include a *base* configuration closely matching the *LogiCORE IP DMA*'s default configuration. In our evaluation, we included two additional configurations; one enabling *speculation* while closely resembling the *base* configuration, and a *scaled* configuration setting both the number of *descriptors* outstanding and the *prefetching* to 24. We summarize the respective parameter configurations in Table 3.2.

As access to main memory is shared between the iDMA front- and back-end, the bus utilization, as defined above, cannot reach 100%. The transfer of the payload will be interrupted by descriptor transfers, limiting the *ideal bus utilization*,  $\bar{u}$  – see Equation (3.1) – where  $n$  is the transfer size in byte.

$$\bar{u} = \frac{n}{n + 32} \quad (3.1)$$

Descriptor misprediction, in the case of speculative prefetching enabled, further limits the ideal utilization, as it inflates the number

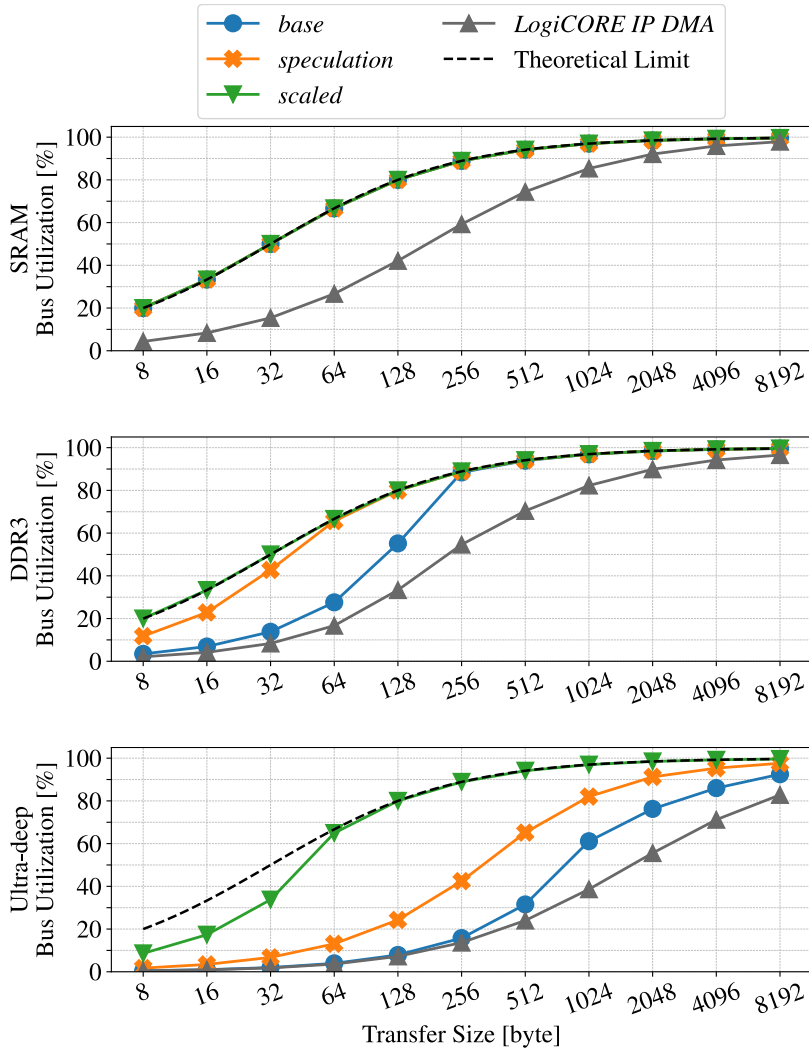


Figure 3.4: DMA *steady-state* bus utilization given a prefetch hit rate of 100% in memory systems featuring various latencies. *Ideal*, DDR3, Ultra-deep memory systems featuring 1, 13, 100 cycles of latency, respectively.

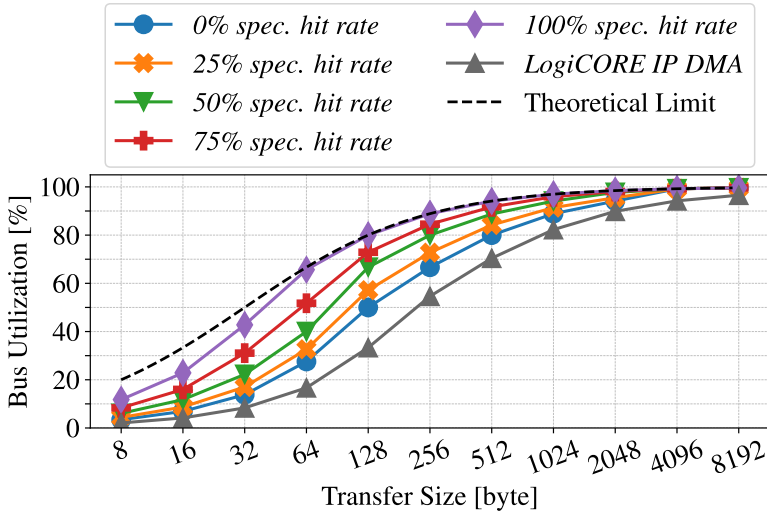


Figure 3.5: DMAC steady-state bus utilization in the case of the DDR3 main memory with speculation misses; *speculation* configuration.

of additional bytes fetched by the iDMA front-end per transfer. In this case, the *ideal bus utilization*  $\bar{u}$  is given by:

$$\bar{u} = \frac{n}{n + 32(1 + m)} \quad (3.2)$$

In Equation (3.2)  $n$  denotes the transfer size and  $m$  the average number of wrongfully fetched descriptors for each transfer. In very shallow or ideal memory systems, our *base* configuration already achieves ideal steady-state utilization for any bus-aligned transfer size, as shown in Section 3.2.8.1. At transfer sizes of 64 B – a typical cache line size in many memory architectures – we improve the utilization by  $2.5 \times$  compared to the *LogiCORE IP DMA*. When using the *Genesys 2 DDR3* latency configuration, we achieve ideal steady-state utilization at 256 B without and 64 B with prefetching enabled, as can be seen in Section 3.2.8.1. This increases the utilization by up to  $1.7 \times$  and  $3.9 \times$ , respectively, compared to the *LogiCORE IP DMA*. Finally, we show that our DMAC can be configured to still achieve

Table 3.4: FPGA resource requirements of the DMAC at 200 MHz.

Configuration	LUTs	FFs
<i>base</i>	2610	3090
<i>speculation</i>	2480	3935
<i>scaled</i>	6764	11353
<i>LogiCORE IP DMA</i> [102]	2784	5133

near-ideal steady state utilization even in ultra-deep memory systems. As can be seen in Section 3.2.8.1, the *scaled* configuration achieves ideal utilization starting from 128 B. Varying prefetching hit rates of 75 to 0%, our achievable increase in bus utilization compared to the *LogiCORE IP DMA* still ranges from  $1.65 \times$  to  $3.1 \times$  at 64 B, see Figure 3.5.

We evaluate the timing and resource requirements of our DMAC in the various configurations presented in Table 3.2 by synthesizing our work in *GlobalFoundries’ GF12LP+ FinFET* technology using *Synopsys’ Design Compiler NXT* in *topological* mode. All results are presented in the typical corner of the library at 25 °C at 0.8 V, in Table 3.3. Our *base* configuration requires an area of 41.2 kGE, achieving a maximum clock frequency of 1.71 GHz. Enabling prefetching adds 8.3 kGE while reducing the achievable maximum clock frequency to 1.44 GHz. We synthesized our design in numerous configurations, creating a model of the circuit area as a function of the parameters in Table 3.2. The design’s area in *kGE* is described by:  $A = 20.30 + 5.28d + 1.94s$ , where  $d$  denotes the number of descriptors in flight and  $s$  the number of speculatively launched descriptors. The total area is linear in  $d$  and  $s$ , allowing the hardware to be easily scaled to larger sizes. The *scaled* configuration requires a total of 188.4 kGE achieving 1.23 GHz. Comparing these numbers to CVA6 [60], we find the DMAC area to be less than 10% of the core’s area while achieving similar clock speeds, confirming the scalability of our controller.

### 3.2.8.2 In-System Results

To evaluate the required resources on a FPGA, we synthesized Cheshire with the various configurations of our DMAC integrated. Synthesis

Table 3.5: DMAC latencies between various events and memory systems for the *scaled* configuration

Metric	<i>LogiCORE IP DMA</i> [102]	<i>scaled</i>
<b>i-rf</b>	10	3
<b>rf-rb</b>	22	8
1 cycle latency	48	32
13 cycles latency	222	206
100 cycles latency	1	1
<b>r-w</b>		

was done using *Vivado 2019.2* targeting the *Genesys 2* board, which features a *Kintex 7* FPGA from *Xilinx*. In the *base* configuration, the footprint of the DMAC is 2610 LUT<sup>2</sup> and 3090 FF<sup>3</sup>, while the entire SoC occupies 79 142 LUT and 58 086 FF, see Table 3.4. This puts the base configuration at 3.3% of total LUT usage and 5.3% of total FF usage, and is a reduction of 6.25% LUT and 39.8% FF utilization compared to the *LogiCORE IP DMA*. Compared to the *base* configuration, the *speculation* configuration uses 27% more FF, but reduces the number of LUT by 5%. The scaled configuration increases resource utilization further, requiring 2.59  $\times$  as many LUT and 3.67  $\times$  as many FF as the *base* configuration.

We use our latency-configurable memory system presented in Section 3.2.8.1, which we integrate into the upstream CVA6-SoC to measure the following three different latencies:

- *i-rf*: the CPU issuing a write to the iDMA front-end issuing a read request
- *rf-rb*: between the issue of the read request from iDMA front- and back-end
- *r-w*: the latency between our DMAC reading and writing the same data

As can be seen in Table 3.5, we achieve three cycles of latency for *i-rf*, an improvement of 3.33  $\times$  over the *LogiCORE IP DMA*. For *rf-rb*,

<sup>2</sup>LUT: lookup table

<sup>3</sup>FF: flip-flop

we achieve a latency of eight cycles in ideal memory, 32 cycles with a memory latency of 13, and 206 cycles in the case of 100 cycles of latency. This results in an improvement of  $2.75 \times$ ,  $1.5 \times$ , and  $1.08 \times$ , respectively. Latencies for  $r-w$  are equal at one cycle for both our DMAC and the *LogiCORE IP DMA*.

## 3.3 Virtual Memory Capabilities

### 3.3.1 Introduction

With the advent of multi-user- and multi-application-capable computing systems in the second half of the last century, the necessity of an elegant and efficient way to implement address space isolation, program modularity, resource sharing, and machine independence has become an undeniable truth [117]. Virtual memory (VM) has established itself as the solution to achieve these objectives by distinguishing the *virtual* address regions an application uses to refer to its information and the *physical* addresses used by the memory system to identify hardware storage devices.

With all the benefits introduced, VM also incurs challenges to be solved when designing a system's memory architecture. This is especially true in heterogeneous systems, where VM-enabled hosts are paired with physically addressed accelerator subsystems [68, 118–121]. If designed improperly, the required translation layer between the accelerator and the host, leads to a substantial loss in performance transferring data between the regions [122].

Traditional approaches handle physically addressed accelerators coupled to VM-enabled application-class hosts either by placing an IO translation lookaside buffer (IOTLB) [120, 122] or a full IO memory management unit (IOMMU) [118, 119] between the domains.

Having a dedicated unit handling the translation process higher up in the memory hierarchy leads to both a programming overhead and a slow reaction to unexpected situations. Setting up a dedicated IOTLB or IOMMU requires configuration setup through dedicated memory-mapped registers. Depending on the exact implementation, periodic reconfiguration is required to ensure all of the accelerator's memory accesses are mapped and can be properly translated. In the case of a non-mapped access, a *page table fault*, either an interrupt is raised, requiring around one hundred cycles of latency to be communicated to the application-class core [123], or an error response is propagated through the interconnect back to the initiator device, where it is then handled (e.g. Section 2.2.4). Both communication methods, in the case of these loosely coupled translation devices, introduce a substantial

latency to even communicate the fault to the core in charge of defining the translation table.

Currently used industry-grade on-chip interconnects, see Section 1.3, do not feature a mechanism for communicating streaming intent, and thus specifying its access patterns. An upstream translation unit thus can only reactively handle memory transfers [119]. Ahead-of-arrival translation can thus be only accomplished by employing predictive schemes identifying access patterns and preparing the required page table entries (PTEs) to be present in the unit once the memory access arrives. With AXI-Pack [73], we tackled the challenge of transferring a streaming intent over AXI4 interconnects by introducing additional signals. Whilst communicating the nature and shape of the stream, the latency between the stream initiator and the MMU still prevails, limiting the agility of such an approach.

We thus propose our streaming memory management unit (sMMU); specifically designed to translate memory streams at high efficiency. Placed close to the stream initiator, e.g., an iDMA engine, sMMU can use the stream source to perfectly fetch page table PTEs into its internal translation lookaside buffer (TLB) unit, hiding translation latency and achieving a high bus utilization, achieving over 95% of the ideal bandwidth at a transaction granularity of 256 B.

### 3.3.2 Architecture

We present an overview of the architecture in Figure 3.6. The stream request enters the sMMU, where it is legalized into 4-kB-sized and page-aligned fragments. The fragments are then enumerated and sent to the translation unit, consisting of the TLB and the page table walker (PTW). Fragments hitting in the TLB will directly be translated in-cycle, whereas misses are handed to the PTW to be fetched from the page table. The translation latency of the PTW depends on the system’s memory system and the number of levels on non-leaf PTEs stored in the TLB. To increase throughput, the individual 4-kB-sized fragments get translated and forwarded out-of-order (OoO).

OoO-completion of individual fragments of a memory stream is not an issue, as most API abstractions, e.g., *memcpy*, only operate on the granularity of an individual transfer. To keep consistency, we just need to ensure that a transfer response, marking the transfer as completed,

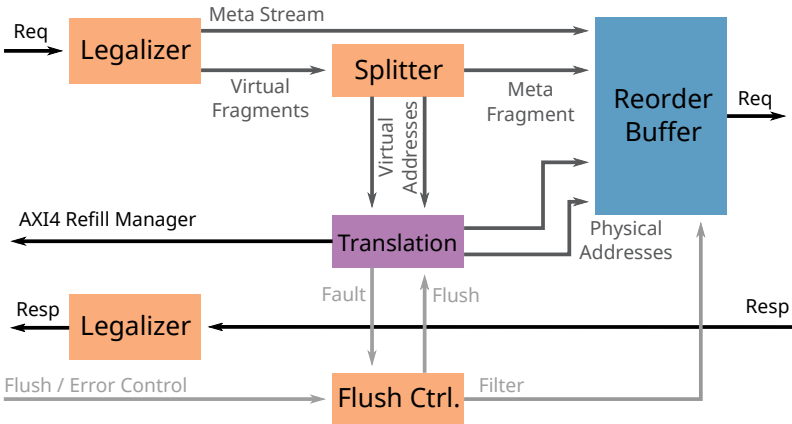


Figure 3.6: Architecture of our sMMU implemented as a mid-end. It is placed between a 1-D front-end and an iDMA back-end.

is only issued once all fragments of a transfer are completed, and that fragments of different transfers are not mixed. A small reorder buffer (ROB) is used to ensure this consistency.

Our sMMU checks the TLB access permissions and prevents the corresponding transfer fragments from being forwarded should an access violation be detected. Should a transfer violate access permissions, a fault is issued. In this case, the sMMU waits for the outstanding (and valid) fragments of the transaction to complete and then flushes all metadata information of the transfer that caused the violation. The violating transfer is then terminated and an error response is issued. A similar abort mechanism is employed should a page table fault be detected. In this case, one or multiple fragments of the transfer are not properly mapped in the translation table, making them impossible to complete. Thanks to the tight coupling between our sMMU and the device initializing the stream, these error responses can be forwarded to the issuing manager within a few cycles, rendering this approach very agile.

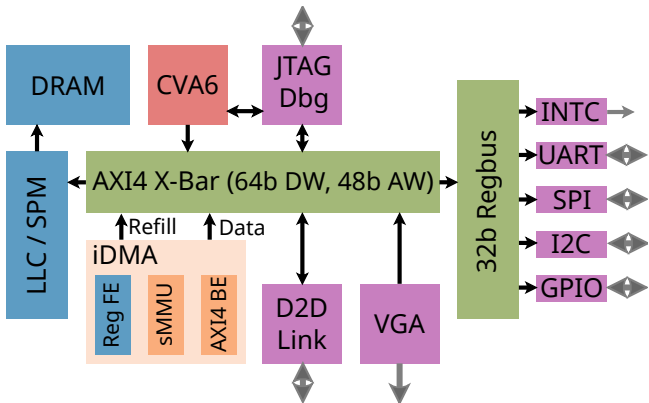


Figure 3.7: Our sMMU integrated into Cheshire’s SoC-level iDMA engine.

### 3.3.3 Case Study: Cheshire

We integrated our sMMU into Cheshire’s SoC-level iDMA engine, see Figure 3.7 and implemented the system on a *Diligent Genesys 2* FPGA [116]. Our sMMU is implemented as an iDMA mid-end translating both source and destination addresses using *SV48* [124]. The PTW accesses Cheshire’s memory system through an additional AXI4 manager port, giving the system’s DMA now one subordinate port for configuration and two manager ports for fetching PTEs and for transferring the data.

Implemented on the *Diligent Genesys 2*, sMMU requires 8.1 kFF and 9.0 kLUT whilst not impacting the critical path of the SoC. Copying transfers of varying length, sMMU can achieve in excess of 99% of the non-translated performance when issuing 4-kB-sized transfers. At a transfer size of 256 B and 64 B, a performance of over 95% and over 80%, respectively can be achieved allowing sMMU to achieve good performance even for fine-granular transfer accesses.

## 3.4 Register Front-end and N-D Tensor Extension

### 3.4.1 Introduction

Operations on matrices or N-D tensors are the fundamentals of scientific computing [125] and machine learning [126]. Basic Linear Algebra Subprograms (BLAS) [127] implements the fundamental set of both matrix and vector operations and is one of the most optimized and widespread libraries to date. BLAS-based benchmark suits, *LINPACK/LAPACK*, are an integral part of the *Top500* workload sets.

With such a widespread use of matrix operations, many DMA engines feature support for 2-D data transfers [36, 37]. However, SoA units only implement two or three dimensions. Higher-level transfers are either implemented via descriptor chaining (Section 3.2.4) or by programmatically launching multiple lower-dimensional transfers.

### 3.4.2 Architecture

**Register-Based Front-end** Core-private register-based configuration interfaces are the simplest class of front-ends, their core architecture is shown in Figure 3.8. Each PE uses its own dedicated configuration space to eliminate race conditions and ensure transfer-atomicity while programming the attached DMA engines [36]. We employ different memory-mapped register layouts depending on the host system’s word width and whether our *N-D tensor mid-end* is present. The *src\_address*, *dst\_address*, *transfer\_length*, *status*, *configuration*, and *transfer\_id* registers are shared between all variants. In the case of a N-D configuration, every tensor dimension introduces three additional fields: *src\_stride*, *dst\_stride*, and *num\_repetitions*. After configuring the shape of a transfer, it is launched by reading from *transfer\_id*, which returns an incrementing unique job ID (jID). The last completed jID may be read from the *status* register, enabling agile transfer-level synchronization.

**N-D Tensor Mid-end** The tensor mid-end consists of a compile-time-configurable number of stage counters, which handle the number of times each dimension is repeated. On transfer launch, each stage is

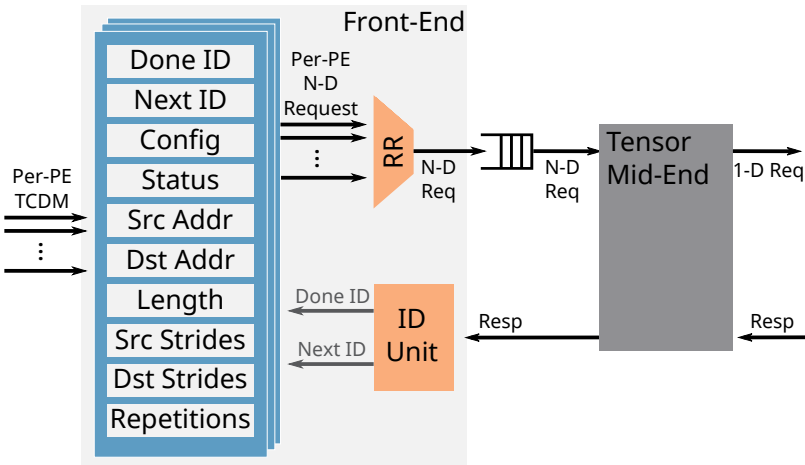


Figure 3.8: Architecture of the register-based front-end and its connection to our tensor mid-end. Each PE has its private register file containing the transfer shape.

loaded with its corresponding number of repetitions (*num\_repetitions*). Once the lower-dimensional transfer completes, this could be the linear transfer executed by the backend, or when the lower stage counter arrives at zero, the stage counter is decremented. While the transfer is still active, once a stage counter is at zero, it is reloaded with its respective *num\_repetitions* register value. The N-D transfer is completed once the highest-stage counter is at zero.

Once stage counters expire, their corresponding stride has to be added to the transfer's base address. Should more than one stage conclude in one cycle, only the highest stage's stride is added, simplifying the hardware substantially by ensuring each cycle at most one stride is added to the base address. As a direct consequence of this hardware simplification, the first two dimensions of transfers feature inclusive, whereas higher dimensions feature exclusive strides. This mix of stride definitions does not complicate software and thus is a valid hardware optimization.

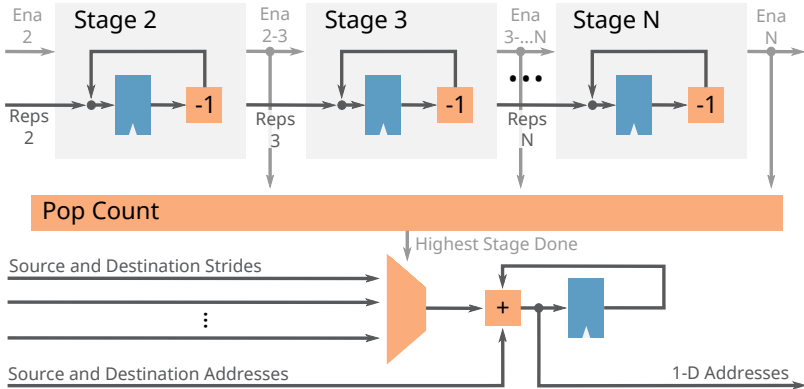


Figure 3.9: Architecture of our tensor mid-end. Each stage is activated by the previous; the strides of the highest stage are added to the base address.

### 3.4.3 Case Study: PULP-open

PULP-open is a ULP edge compute platform consisting of a 32-bit RISC-V microcontroller host and a parallel compute cluster [34]. The compute cluster comprises eight 32-bit RISC-V cores with custom instruction set architecture (ISA) extensions to accelerate digital signal processing (DSP) and ML workloads, enabling energy-efficient ML inference in extreme-edge AI nodes. These cores are connected to an SRAM-based TCDM with single-cycle access latency, providing the processing cores with fast access to shared data. While the TCDM is fast, it is very limited in size; the platform thus features a L2 on-chip and level-three (L3) off-chip HyperBus RAM [128]. To allow the cluster fast access to these larger memories, a DMA unit is embedded, specialized for transferring data from and to the level-one (L1) memory.

**iDMA Engine Integration** In the PULP-open system, our iDMA engine is integrated into the processing cluster with a 64-bit *AXI4* interface to the host platform and an *OBI* connection to the TCDM, see Figure 3.10. The multi-protocol back-end is fed by a *tensor\_ND* mid-end, configured to support three dimensions, allowing for fast

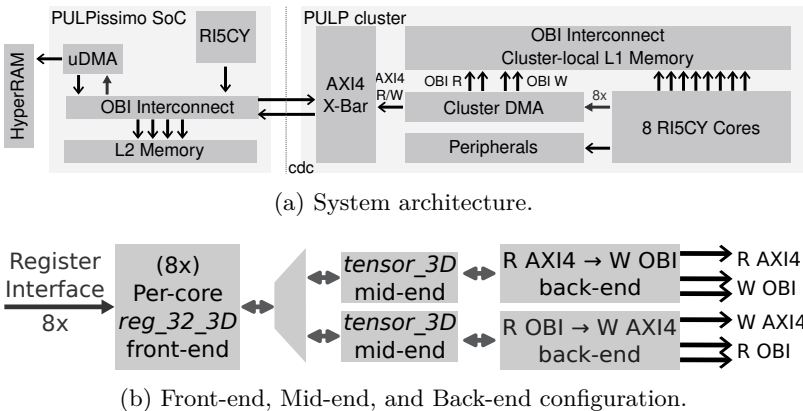


Figure 3.10: (a) Block diagram of the PULP-open system. (b) Configuration of the cluster iDMA engine.

transfer of 3-D data structures common in ML workloads. At the same time, higher-dimensional transfers are handled in software. The back- and mid-end are configured through per-core *reg\_32\_3D* front-ends and two additional front-ends, allowing the host processor to configure the iDMA engine. Round-robin arbitration is implemented through a round-robin arbitration mid-end connecting the front-ends to the *tensor\_3D* mid-end. Multiple per-core front-ends ensure atomic DMA access and prevent interference between the cores launching transactions.

**Benchmarks** To evaluate iDMA engine performance in a realistic application, we use Dory [129] to implement MobileNetV1 inference on PULP-open. This workload relies heavily on the iDMA engine to transfer the data for each layer stored in L2 or off-chip in L3 into the cluster’s TCDM in parallel with cluster core computation. 2-D, 3-D, and very small transfers are frequently required for this workload.

In previous versions of PULP-open, MCHAN [36] was used to transfer data between the host L2 and the cluster’s TCDM. We assume this as a baseline for our evaluation.

**Results** In PULP-open, iDMA engine can almost fully utilize the bandwidth to the L2 and TCDM in both directions: measuring with the on-board timer, a transfer of 8 KiB from the cluster’s TCDM to L2 requires 1107 cycles, of which 1024 cycles are required to transfer the data using a 64-bit data bus. The minimal overhead is caused by configuration, system latency, and contention with other ongoing memory accesses. During MobileNetV1 inference, individual cores frequently require short transfers, incurring a potentially high configuration overhead. With its improved *tensor\_3D* mid-end, iDMA improves the cores’ utilization and throughput for the network over MCHAN, achieving an average of 8.3 MAC/cycle compared to the previously measured 7.9 MAC/cycle. Furthermore, configured with similar queue depths as MCHAN, iDMA engine with its *reg\_32\_3d* achieves a 10% reduction in the utilized area within a parallel ultra-low power (PULP) cluster.

## 3.5 Multichannel Operation

### 3.5.1 Introduction

As mentioned in Section 2.2.1, we design our iDMA back-end to handle one data stream as efficiently as possible. Should an architecture be capable of handling multiple data streams at once, either because it features multiple compute units working on different threads or data sets [69, 130], a compute unit accesses multiple non-uniform memory architecture (NUMA) endpoints, or a mixture of both.

Multiple channels, or iDMA back-ends, can easily be integrated into a system’s memory architecture, as each back-end features a doubly handshaked request and response port. The true challenge arises in coordinating the different channels, minimizing interference of the channels in the process, and providing a simple programming abstraction for the user to launch and synchronize on transfers.

To facilitate transfer scheduling in a single-cluster manycore architecture, we device two mid-ends dividing and distributing transfers over multiple channels or back-ends, efficiently transferring data from/into physically separated cluster-local memory endpoints, while giving the user a single-DMA memory abstraction supporting a regular *memcpy* abstraction.

### 3.5.2 Architecture

To distribute work among back-ends, we create two specialized mid-ends called *mp\_split* and *mp\_dist*. Our *mp\_split*, seen in Figure 3.11a, splits a single linear transfer into multiple transfers aligned to a parametric address boundary, guaranteeing that no resulting transfer crosses specific address boundaries. This is required when sending distributed transfers to multiple back-ends. When accepting a transfer, the length of the transfer is checked against a maximum support transfer length. Larger transfers will be split and emitted as multiple shorter transfers. Responses are coalesced to keep this action transparent to the front-end.

*Mp\_dist*, presented in Figure 3.11b, then distributes the split transfers over  $N$  parallel downstream mid- or back-ends. Transfers are

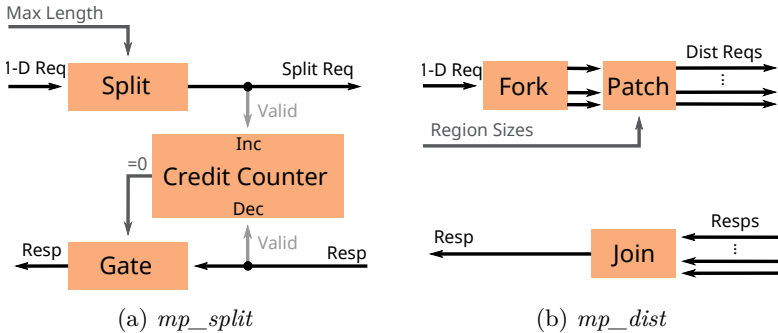


Figure 3.11: The architecture of our multichannel *MemPool* (*mp*) mid-ends.

distributed with their addresses modified, so that the  $N$  parallel back-ends each complete a non-overlapping interleaved block. Responses are collected, and the transfer will be marked as completed if all back-ends working on an interleaved block range are completed.

### 3.5.3 Case Study: Mempool

MemPool [130] is a flexible and scalable single-cluster manycore architecture featuring 256 32-bit RISC-V cores that share 1 MiB of low-latency L1 scratchpad memory (SPM) distributed over 1024 banks. All cores are individually programmable, making MemPool well-suited for massively parallel regular workloads like computer vision, deep learning, and machine learning and irregular workloads like graph processing. The large shared L1 memory simplifies the programming model as all cores can directly communicate via shared memory without explicit dataflow management. The L1 banks are connected to the cores via a pipelined, hierarchical interconnect. Cores can access banks close to them within a single cycle, while banks further away have a latency of three or five cycles. In addition to the L1 interconnect, the cores have access to a hierarchical AXI4 [38] interconnect connecting to the SoC.

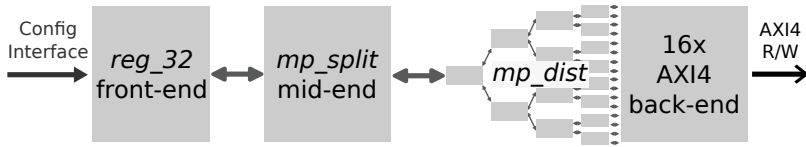


Figure 3.12: Our distributed iDMA engine is implemented in MemPool. *Mp\_split* splits the transfers along their L1 boundaries, and a tree of *mp\_dist* mid-ends distribute the transfer.

**iDMA Engine Integration** MemPool’s large scale and distributed L1 memory make a monolithic DMA engine incredibly expensive, as it would require a dedicated interconnect, spanning the whole MemPool architecture, connecting all 1024 memory banks. The existing interconnect between cores and L1 memory is built for narrow, single-word accesses; thus unsuitable for wide, burst-based transfers.

To minimize interconnect overhead to L1 memory, multiple back-ends are introduced into MemPool placed close to a group of banks. To connect to the SoC, it can share the existing AXI4 interconnect used to fetch instructions.

These distributed iDMA engine back-ends, each controlling exclusive regions of the L1 memory, greatly facilitate physical implementation. However, individually controlling all back-ends would burden the programmer and massively increase overhead due to transfer synchronization of the individual DMA engines. Instead, our iDMA engine’s modular design allows for hiding this complexity in hardware by using a single front-end to program all the distributed back-ends.

As seen in Figure 3.12, the *mp\_split* mid-end splits a single DMA request along lines of MemPool’s L1 memory’s address boundaries, and a binary tree of *mp\_dist* mid-ends distributes the resulting requests to all back-ends.

**Benchmarks** We evaluate MemPool’s iDMA engine by comparing the performance of various kernels compared to a baseline without DMA. Since MemPool requires our modular iDMA engine to implement a distributed DMA, a comparison with another DMA unit is not feasible here. First, we compare the performance copying 512 KiB from L2 to L1 memory. Without a DMA, the cores can only utilize one-sixteenth

of the wide AXI4 interconnect. The iDMA engine utilizes 99% and speeds up memory transfers by a factor of  $15.8 \times$  while incurring an area overhead of less than 1%.

The performance improvement for kernels is evaluated by comparing a double-buffered implementation supported by our iDMA engine to the cores copying data in and out before and after the computation. Even for heavily compute-bound kernels like matrix multiplication, iDMA engine provides a speedup of  $1.4 \times$ . Less compute-intensive kernels like the convolution or discrete cosine transformation benefit even more from the iDMA engine with speedups of  $9.5 \times$  and  $7.2 \times$ , respectively. Finally, memory-bound kernels like vector addition and the dot product are dominated by the data transfers and reach speedups of  $15.7 \times$  and  $15.8 \times$ .

## 3.6 I/O-DMA

### 3.6.1 Introduction

SoC MCUs and general-purpose systems feature a wide range of peripherals, including UART, SPI, I2C, I2S, among many [35, 83]. Although different in their exact operation, these peripherals share a common trait; they are low-bandwidth and feature a high latency compared to on-chip communications and memories. It is further common to connect the different peripheral devices over a low-performance on-chip interconnect to reduce the area overhead [35]. These factors combined make accessing peripheral data an intensive task requiring a high number of cycles if done exclusively through the CPU.

Most systems feature dedicated and complex peripheral subsystems to autonomously move data [34, 35]. While effective, having a monolithic peripheral subsystem combining both data movement and peripheral configuration through a single subsystem, complicates the design of MCUs, limits its extendability, and complicates place and route (P&R) [131]. This is especially true if the interfaces between the individual peripherals and the I/O subsystems are not pipelinable [131].

It is overall simpler and more flexible to couple individual peripherals with highly area-optimized DMA engines. Such engines can be instantiated using our iDMA architecture [131]; see Chapter 2.

### 3.6.2 A General Template for I/O Data Movement

Thanks to iDMA’s multi-protocol capabilities and its flexible system-binding interface, integrating iDMA engines into a peripheral device is facilitated and straightforward. An integration overview can be seen in Figure 3.13. The iDMA back-end first needs to be customized to the peripherals’ and the system’s needs. This includes selecting between unidirectional and bidirectional operation, deciding on the manager interface towards the system, and parameterizing it for the targeted use case.

For most architectures, AXI4-Lite is the preferred protocol to select for the system-facing manager interface as it is latency-tolerant and pipelinable. Peripherals usually deliver data at a low rate compared to the throughput of the on-chip interconnect; thus, one outstanding

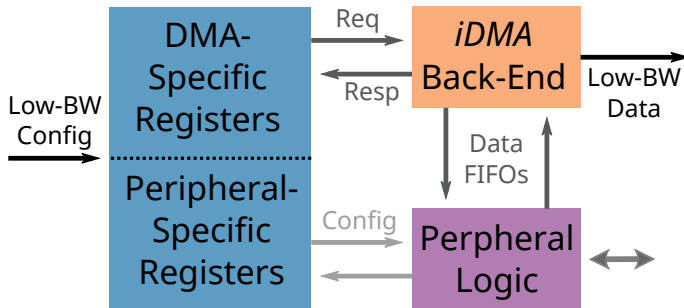


Figure 3.13: I/O-DMA template.

transfer is sufficient to meet the peak bandwidth requirements. Scaled-down, a minimal iDMA engine only incurs an area overhead of less than 2 kGE.

To configure the I/O-DMA, an extension of the peripheral's registers can be used and directly connected to the back-end using the request and response interfaces.

The preferred way of interaction between the back-end and the peripheral is done using the *Fifo/Init* protocol, see Section 2.2.1, for its simplicity. The back-end exposes one stream FIFO containing valid read data and one where data to be written is placed, behaving like a memory-mapped FIFO device.

### 3.6.3 Case Study: Neopixel

Neopixel [132] describes both a type of light-emitting diode modules and a protocol to control them. Neopixel modules are chainable to up to 5050 pixels, whilst still remaining individually RGB-addressable.

We implemented a Neopixel host controller as part of MLEM [82, 133], a pipecleaner application-specific integrated circuit (ASIC) to silicon-harden *Croc*, our educational SoC platform [82, 134].

It is connected to MLEM through an OBI subordinate device exposing its configuration registers as well as a read-only manager port to fetch data from the SoC's memory system. We provide a block diagram of MLEM in Figure 3.14.

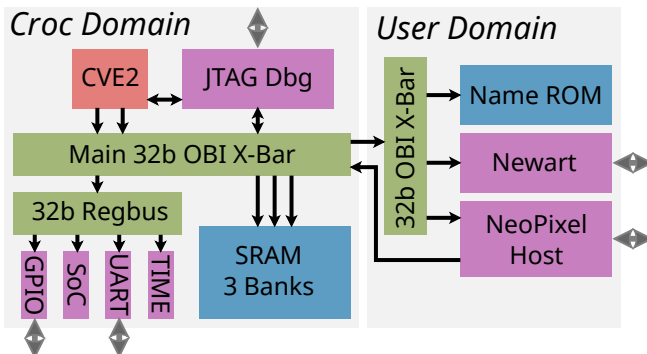


Figure 3.14: Top-level architecture of MLEM, including our Neopixel host controller.

Internally, the Neopixel host controller consists of a configuration register controlling both the I/O-DMA and the configuration of the Neopixel protocol FSM, a pixel FIFO, and the I/O-DMA engine; as can be seen in Figure 3.15. The pixel FIFO can be filled both through explicit OBI writes of individual pixel values, called *direct mode*, or by configuring the iDMA to fetch a stream of pixels from main memory, called *DMA mode*.

**Direct Mode** Direct mode is ideal to supply a huge amount of procedurally generated pixel data to the device without storing it into SRAM beforehand. It needs to be ensured that the CPU provides the data fast enough for the Neopixel protocol FSM to only emit valid pixel data to the devices.

**DMA Mode** Once configured, our iDMA engine fetches the pixel stream over the host controllers OBI manager port and delivers it over its *Fifo/Init* interface to the pixel FIFO without requiring any external protocol conversion, facilitating the integration. The DMA engine can be configured to fetch as many pixel values as Neopixel devices in the chain, updating the entire array in one operation. Repeated DMA transaction allows the MLEM to display animations stored in SRAM over Neopixel.

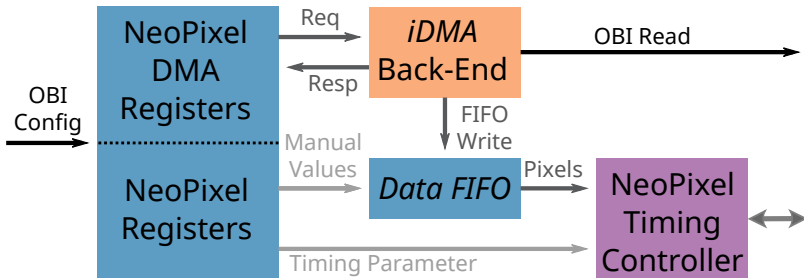


Figure 3.15: Architecture of our Neopixel host controller including an iDMA back-end.

Our Neopixel host controller was implemented on MLEM [82, 134] using IHP’s 130 nm open process design kit (PDK). The entire Neopixel host controller requires 16.4 kGE, with the I/O-DMA occupying 5.0 kGE. The I/O-DMA instantiation is around  $2 \times$  larger than expected (see Table 2.3) due to an OBI *rready* converter required by croc. This converter adds a two-deep stream FIFO between the DMA and the interconnect. The I/O-DMA can achieve asymptotically 100% bus utilization, requiring four cycles of latency until the first data arrives at the output FIFO ports, ensuring agile and efficient data transport to our Neopixel host controller.

## 3.7 Real-Time Sensor Scheduling

### 3.7.1 Introduction

Cyber-physical systems must continuously sense and actuate their environment with a high degree of predictability and meeting all deadlines imposed by their real-time schedule. This, in particular, includes reading a multitude of sensor values from memory-mapped I/O devices [62].

I/O devices are usually attached over a slow, low-bandwidth, and high-latency interface, keeping the initiator waiting until the sensor data has been retrieved. To complicate things, distributed sensor arrays usually feature complex address maps [62, 135, 136]. To keep the CPU free to complete useful workloads, we introduce our, *sensor DMA (sDMA) engine*, specialized to retrieve sensor data autonomously on a schedule, ensuring critical information of the outside world is always present on time and the real-time core is freed of this data movement burden. We configure our sDMA unit to be light-weight, only supporting one outstanding transaction in line with the sensor interfaces, keeping the area overhead minimal.

### 3.7.2 Architecture

Our real-time extension adds additional fields to the front-end specifying the length, shape, and periodicity of the sensor accesses. A compile-time SV parameter specifies the maximum number of events supported. A bypass mechanism allows the core to dispatch unrelated transfers using the same front- and back-end.

We present a block diagram of our real-time mid-end in Figure 3.16. It introduces a counter for each event tracked. Once the corresponding event is enabled, the counter decrements from the specified cycle count. An event is triggered once the counter reaches zero. A stream arbiter selects between all triggered events and the bypass port and relays the selected transfer through a N-D mid-end to the back-end to execute the transfer and gather the sensor data.

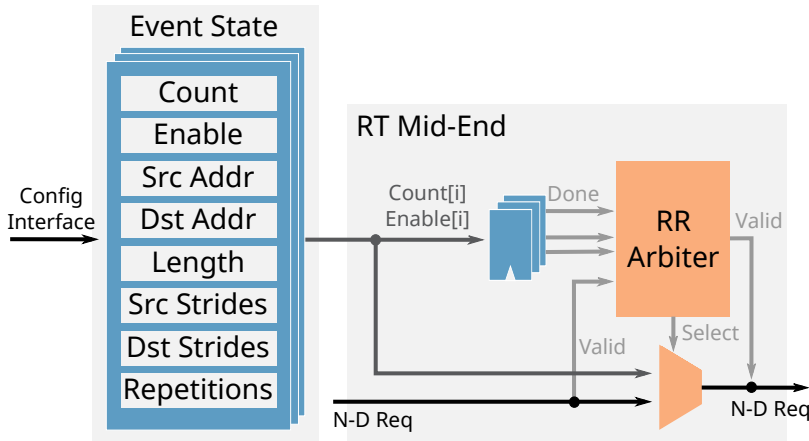


Figure 3.16: Architecture of the real-time mid-end. The event state, holding the frequency and the shape of the transfer, can be part of the front-end.

### 3.7.3 Case Study: ControlPULP

ControlPULP [62, 135, 136] is an on-chip parallel MCU employed as a power controller system (PCS) for manycore HPC processors. It comprises a single 32-bit RISC-V *manager domain* with 512 KiB of L2 scratchpad memory and a programmable accelerator (*cluster domain*) hosting eight 32-bit RISC-V cores and 128 KiB of TCDM.

A power control firmware (PCF) running on FreeRTOS implements a reactive power management policy. ControlPULP receives (i) dynamic voltage and frequency scaling (DVFS) directives such as frequency target and power budget from high-level controllers and (ii) temperature from process-voltage-temperature (PVT) sensors and power consumption from voltage regulator modules (VRMs), and is tasked to meet its constraints. The PCF consists of two periodic tasks, periodic frequency control task (PFCT) (low priority) and periodic voltage control task (PVCT) (high priority) that handle the power management policy.

ControlPULP requires an efficient scheme to collect sensor data at each periodic step without adding overhead to the computation part of the power management algorithm.

**iDMA Engine Integration** As presented by Ottaviano *et al.* [135, 136], the *manager domain* offloads the computation of the control action to the *cluster domain*, which independently collects the relevant data from PVT sensors and VRMs. We redesign ControlPULP’s data movement paradigm by integrating a second dedicated iDMA engine, called *sDMA engine*, in the *manager domain* to simplify the programming model and redirect non-computational, high-latency data movement functions to the *manager domain*, similar to IBM’s *Pstate* and *Stop* engines [137]. Our sDMA engine is enhanced with *rt\_3D*, a mid-end capable of autonomously launching repeated 3-D transactions. ControlPULP’s architecture is heavily inspired by PULP-open; iDMA engine integration can thus be seen in Figure 3.10. The goal of the extension is on one hand to further reduce software overhead for the data movement phase, which is beneficial to the controller’s *slack* within the control hyperperiod [138], and to ensure sensor data is always present on time. The sDMA engine supports several interface protocols, thus allowing the same underlying hardware to handle multiple scenarios.

**Benchmarks and Results** We evaluate the performance of the enhanced sDMA engine by executing the PCF on top of FreeRTOS within an FPGA-based (Xilinx Zynq UltraScale+) hardware-in-the-loop framework that couples the programmable logic implementing the PCS with a power, thermal, and performance model of the plant running on top of the ARM-based Processing System [135, 136].

Data movement handled by *rt\_3D*, which allows repeated 3-D transactions to be launched, brings several benefits to the application scenario under analysis. First, it decouples the main core in the *processing domain* from the sDMA engine in the *I/O domain*. The sDMA engine autonomously realizes periodic external data accesses in hardware, minimizing the context switching and response latency suffered by the manager core in a pure software-centric approach. We consider a PFCT running at 500  $\mu$ s and the PVCT at 50  $\mu$ s, meaning

at least ten task preemptions during one PFCT step with FreeRTOS preemptive scheduling policy. The measured task context switch time in FreeRTOS for ControlPULP is about 120 clock cycles [135, 136], while iDMA engine programming overhead for reading and applying the computed voltages is about 100 clock cycles. From FPGA profiling runs we find that the use of sDMA engine saves about 2200 execution cycles every scheduling period, thus increasing the slack of the PVCT task. As it is no longer the core’s burden to fetch the data, it reduces the variability of the PVCT task by isolating computation from data retrieval over slow and unpredictable peripheral interconnects. Further, sensor data of physical qualities usually are continuous in values, thus most control algorithms are robust against spuriously outdated sensor data. Autonomous and intelligent data access from the *I/O domain* is beneficial as it allows the two subsystems to reside in independent power and clock domains that could be put to sleep and woken up when needed, reducing the *uncore* domain’s power consumption.

Our changes add minimal area overhead to the system. In the case of eight events and sixteen outstanding transactions, the sDMA engine is about 11 kGE in size, accounting for an area increase of only 0.001% of to the original ControlPULP’s area. The overhead imposed by sDMA engine is negligible when ControlPULP is used as an on-chip power manager for a large HPC processors. It has been shown [135, 136] that the entire ControlPULP only occupies a small area of around 0.1% on a modern HPC CPU dies.

### 3.8 RISC-V Instruction Front-end

To enable closer coupling between the core and the iDMA engine, we design and implement a front-end, called *inst\_64*, encoding transfers directly as RISC-V-compliant instructions. Our *inst\_64* allows connected cores to launch 1-D DMA transactions within only three cycles, enabling highly agile transfers and reducing the setup cost to a minimum.

The architecture of *inst\_64*, its integration into the Snitch cluster [139], and a scale-out study will be detailed in Chapter 4.

## 3.9 Summary and Conclusion

In this chapter, we present how iDMA is integrated in a wide range of systems and how we enhance our architecture with multiple extension further accelerating DMA transfers and increasing their efficiency.

In Section 3.2 we present a scalable, platform-independent, synthesizable, transfer-descriptor-based DMAC for fast and efficient data transfers in Linux-capable AXI4-based systems. Integrated in Cheshire, our Linux-capable SoC platform [60], we achieve  $1.66 \times$  less latency, increasing bus utilization by up to  $2.5 \times$  in an ideal memory system with 64-B transfers, overall requiring 11% fewer LUT and 23% fewer FF without requiring any block RAMs compared to Arm’s LogiCore DMA IP [102]. In deep memory systems, we show an even more significant increase in the utilization of  $3.6 \times$  with 64-B transfers.

Section 3.3 presents our very capable sMMU architecture and its integration into iDMA enhancing our DMA architecture with VM support. Implemented on the *Diligent Genesys 2*, sMMU requires 8.1 kFF and 9.0 kLUT whilst not impacting the critical path of the SoC. Copying transfers of varying length, sMMU can achieve in excess of 99% of the non-translated performance when issuing 4-kB-sized transfers.

Equipped with our N-D tensor mid-end and our light-weight register-based front-end presented in Section 3.4, iDMA engine almost fully utilizes the bandwidth to the L2 and TCDM in both directions in PULP-open: measuring with the on-board timer, a transfer of 8 KiB from the cluster’s TCDM to L2 requires 1107 cycles, of which 1024 cycles are required to transfer the data using a 64-bit data bus. During MobileNetV1 inference, with its improved *tensor\_3D* mid-end, iDMA improves the cores’ utilization and throughput for the network over MCHAN, achieving an average of 8.3 MAC/cycle compared to the previously measured 7.9 MAC/cycle. Configured with similar queue depths as MCHAN, iDMA engine with its *reg\_32\_3d* achieves a 10% reduction in the utilized area within a PULP cluster.

Our multi-channel extensions presented in Section 3.5, show performance improvements in MemPool. Even for heavily compute-bound kernels like matrix multiplication, iDMA engine provides a speedup of  $1.4 \times$ . Less compute-intensive kernels like the convolution or discrete cosine transformation benefit even more from the iDMA engine with

speedups of  $9.5 \times$  and  $7.2 \times$ , respectively. Finally, memory-bound kernels like vector addition and the dot product are dominated by the data transfers and reach speedups of  $15.7 \times$  and  $15.8 \times$ .

We show in Section 3.6, how small configurations of iDMA can be used to enhance peripherals with fast and standalone memory accesses. On the example of our Neopixel host controller, we show that integrating an I/O-DMA incurs only an area overhead of around 5.0 kGE. With an even more efficient memory system implementation, I/O-DMAs requiring less than 2.0 kGE can be configured whilst still achieving near-ideal bus utilization.

Finally, we present our real-time mid-end extension and the corresponding integration into ControlPULP in Section 3.7. From FPGA profiling runs we find that the use of our sDMA unit saves about 2200 execution cycles every scheduling period, thus increasing the slack of the PVCT task. Our changes add minimal area overhead to the system. In the case of eight events and sixteen outstanding transactions, the sDMA engine is about 11 kGE in size, accounting for an area increase of only 0.001% of to the original ControlPULP's area.

To summarize; iDMA brings clear benefits in systems spanning the entire compute continuum, thus proofing the versatility and flexibility of our architecture.

# Chapter 4

# Communication Processor

## 4.1 Introduction

With the *Memory Wall* or the *Processor-Memory Gap* still prevailing [44–46] and with the advent of AI further demanding ever more compute [14], pressure on the memory system is tightening. Classical computing architectures employ a tiered cache architecture trying to mitigate the performance loss when accessing slow and low-bandwidth off-chip memory at the cost of a high area and power consumption [46]. An other approach is to use explicitly managed and tightly coupled scratchpad memory, called TCDM, located close to the PEs. DMA engines are used to copy data from and to TCDM traditionally employing long bursts to hide the latency into last-level storage [34]. With PULP, and thus with this thesis, we use the latter approach and thus focus our discussion on explicitly managed storage architectures.

High-bandwidth memory (HBM) is the dominating dynamic random access memory (DRAM) organization for low-latency and high-bandwidth applications. Its immense bandwidth is provided through a combination of a massively parallel I/O connection into the DRAM array and 3D-stacked multi-channel packages [140]. Recently, systems have evolved to use multi-site HBM configurations [141–143] to further

increase the available bandwidth into main memory. Using such multi-site configurations with systems employing explicitly managed TCDM leads to a set of challenges; to get the prospective bandwidth advantage, DMA transfers need to be optimized to access multiple sites concurrently, as datasets might be interleaved over the channels, at the same time, long bursts need to be split to equalize the access intensity of the sites and channels, and the DMA engines need to be tolerant towards non-uniform site access latencies.

Compressing the data set size is another way of overcoming the *Memory Wall* [144]. Leveraging data sparsity poses a very elegant compression strategy, especially as data sets from a wide range of fields, like image and signal processing, computer vision, and pattern recognition, are inherently sparse [145]. Moving and processing these sparse data sets fundamentally incurs indirect data accesses and data-dependent program flows [144, 146], which are incompatible with traditionally employed coarse-grained data transfers used to hide last-level memory access latencies [146].

DMA engines need to evolve to suit these application scenarios by designing them to be latency-tolerant, capable of handling short and irregular transfers. In Chapter 2, with iDMA, we propose exactly such a configurable, agile, and latency-tolerant DMA architecture. Chapter 3 extends the architecture’s capabilities with regular strided tensor accesses and describes loosely coupled register- and transfer-descriptor-based programming models.

To maximize agility, we tightly couple our iDMA engine directly to a core inside of our compute cluster, allowing it to launch DMA transactions in as little as three instructions and have the first data moved in as little as four cycles. Compared to the prevailing approach of using custom ISAs [99, 104], our instruction-based front-end extends the RISC-V ISA, allowing data-dependent and irregular DMA movement patterns to be easily calculated alongside the program execution with minimal synchronization and communication overhead.

We present the general architecture of the instruction-based front-end, *inst\_64*, in Section 4.2.1, followed by our RISC-V DMA instruction extension in Section 4.2.2, and its programming model in Section 4.3.1. We then present the integration of our front-end into the Snitch cluster [139] in Section 4.3 and a case study of a scaled-out system based on our instruction-based iDMA integration in Section 4.4.

Tightly coupling our `inst_64` and our iDMA back-end with a Snitch core creates a *communication processor* in-charge of orchestrating data transfers and synchronizing with other PEs doing useful compute. Finally, we end the chapter with a summary and conclusion.

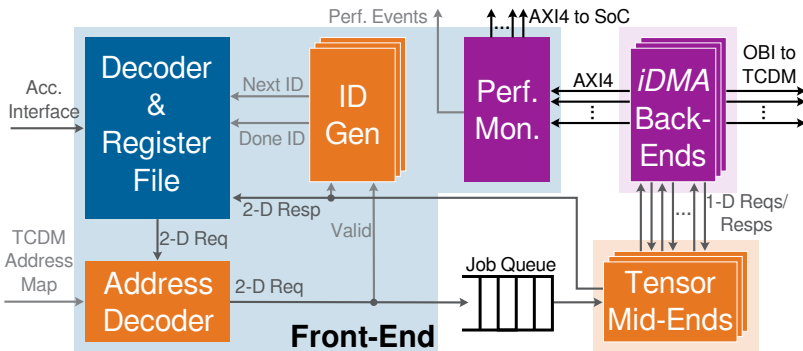


Figure 4.1: Architecture of the tightly coupled *Snitch* DMA engine. It combines the *inst\_64* front-end with a configurable number of *tensor\_ND* mid-ends and iDMA back-ends.

## 4.2 Instruction-Based Front-end

In the following, we will describe the architecture, the instruction encoding, and the programming model of the tightly coupled instruction-based *inst\_64* iDMA front-end.

### 4.2.1 DMA Engine Architecture

Figure 4.1 shows the architecture of our *inst\_64* front-end coupled with a configurable number of *tensor\_ND* mid-ends and iDMA back-ends.

Our *inst\_64* front-end is connected to a core through its *accelerator offloading interface* [139], allowing our front-end to receive and decode the *dm* subset, see Section 4.2.2, of the core’s issued RISC-V instructions. A *decoder* handles the *dm* subset and interfaces the DMA engine by either returning status information, updating the internal register file holding the job currently being constructed to be dispatched, or launching a job.

Transfers are identified through the software via *job IDs* (*jIDs*). On launch, the front-end returns a monotonically increasing *jID* identifying the job just launched. As each back-end handles transfers strictly in-order, see Section 2.2.1, the *jID* are marked as completed in the same monotonically increasing order as they were launched. If the last

Table 4.1: Events emitted by the tightly coupled Snitch DMA.

Event	Description
AW	<i>done</i> $AW$ handshake successfully completed
	<i>stall</i> iDMA back-end has a valid $AW$ beat, but memory is not ready
	<i>issued</i> Number of bytes <sup>a</sup> requested during successful $AW$ handshake
W	<i>done</i> $W$ handshake successfully completed
	<i>stall</i> iDMA back-end has a valid $W$ beat, but memory is not ready
	<i>bytes</i> Number of bytes <sup>b</sup> transferred during successful write operation
B	<i>done</i> $B$ handshake successfully completed
	<i>stall</i> iDMA back-end can accept $B$ beat, but memory is not providing it
Buffer	<i>in stall</i> Buffer is full, put back-pressure on read transfers
	<i>out stall</i> Buffer is empty, cannot write
AR	<i>done</i> $AR$ handshake successfully completed
	<i>stall</i> iDMA back-end has a valid $AR$ beat, but memory is not ready
	<i>issued</i> Number of bytes <sup>a</sup> requested during successful $AR$ handshake
R	<i>done</i> $R$ handshake successfully completed
	<i>stall</i> iDMA back-end can accept $R$ beat, but memory is not providing read data

<sup>a</sup>according to  $(AX_{len} + 1) << AX_{size}$     <sup>b</sup>only *strobed* bytes are counted

completed jID is larger than or equal to the jID of a job previously launched, the DMA engine has successfully completed said job.

In multi-channel DMA engine configurations, we currently select the active channel through the configuration instruction. Automatic channel assignment can be implemented if required; our *in-network accelerator* works [57, 58, 63] employ multi-channel-selection using round-robin (RR) arbitration. As the channels are independent of each other, we have one *jID generator* for each channel present in the system.

The back-ends used are configured to have both AXI4, connecting to the SoC, and OBI, for efficiently accessing TCDM, read and write ports. An *address decoder* determines the port combination used for the current job.

A *job queue* is used to allow the core to launch multiple jobs while the DMA engine is busy; once the queue is full, the *dmcpy* instruction will be blocking until the queue can accept a next job.

Finally, all AXI4 interfaces are channeled through a *performance event unit*, which emits the DMA events described in Table 4.1.

### 4.2.2 Instruction Encoding

We extend the RISC-V ISA with our ten *dm* instructions presented in Table 4.2. Our instructions use *0x2b* as *opcode*, partially occupying one of four custom blocks, *0x0A* of quadrant 3.

Our *dmsrc*, *dmdst*, *dmstr*, and *dmrep* are used to configure the *shape* of the transfer. They specify the source and destination addresses as well as the strides and number of repetitions in the case of a 2-D transfer. The status instructions, *dmstat* and *dmstati*, can be used to retrieve the current state of the DMA, including the last completed jID, the next jID, and the busy signals of the mid- and back-ends. Jobs are launched using *dmcpy* and *dmcpyi*, as well as *dminiti*; the former two launch regular DMA transfers where data is copied according to the defined shape, the latter initializes a memory region located at *dmdst* with a specified byte in *dmsrc*. The length of the transfer, as well as the back-end configuration and the chosen DMA channel, are given by the launching instruction, while the jID is placed in the specified destination register.

The *dmuser* instruction populates AXI4 user signals with a value specified in the source registers. This functionality is currently used to issue multicast operations through iDMA [147].

Table 4.2: Our RISC-V *dm* instructions introduced by *inst\_64*.

Type	Mnemonic	Immediate	Funct 7	Source 2	Source 1	Funct 3	Destination	Opcode
<i>R</i>	<i>dmsrc</i>	–	0	<i>address_high</i>	<i>address_low</i>	0	–	0x2b
<i>R</i>	<i>dndst</i>	–	1	<i>address_high</i>	<i>address_low</i>	0	–	0x2b
<i>I</i>	<i>dmcpyi<sup>a</sup></i>	<i>config<sup>b</sup></i>	–	–	<i>num_bytes</i>	1	<i>jID</i>	0x2b
<i>R</i>	<i>dmcpy<sup>a</sup></i>	–	2	<i>config<sup>b</sup></i>	<i>num_bytes</i>	0	<i>jID</i>	0x2b
<i>I</i>	<i>dmstati</i>	<i>metric</i>	–	–	–	2	<i>information</i>	0x2b
<i>R</i>	<i>dmstat</i>	–	3	–	<i>metric</i>	0	<i>information</i>	0x2b
<i>R</i>	<i>dmstr</i>	–	4	<i>dst_stride</i>	<i>src_stride</i>	0	–	0x2b
<i>R</i>	<i>dmrep</i>	–	5	–	<i>num_repetitions</i>	0	–	0x2b
<i>R</i>	<i>dmuser<sup>c</sup></i>	–	6	<i>user_high</i>	<i>user_low</i>	0	–	0x2b
<i>I</i>	<i>dminiti<sup>a,d</sup></i>	<i>config<sup>b</sup></i>	–	–	<i>num_bytes</i>	3	<i>jID</i>	0x2b

<sup>a</sup> launches DMA job on execution<sup>b</sup> up to eight channels selectable<sup>c</sup> primarily used as *dmcast* for multi-cast operations [147]<sup>d</sup> byte to be written is specified using *dmsrc*

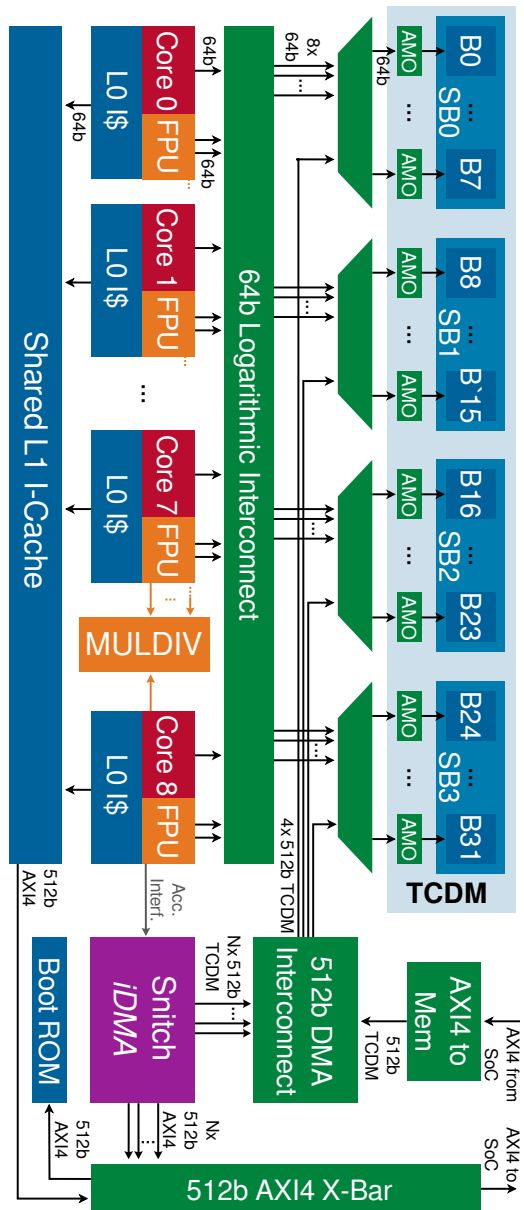


Figure 4.2: Our iDMA integration into a Snitch compute cluster.

## 4.3 Cluster Integration

We present the integration of our tightly coupled DMA engine into the Snitch cluster [139] in Figure 4.2. Compared to the original architecture [139], we introduce an  $(N+1)$ th Snitch core, dedicated to orchestration and data movement operations, we add a 512-bit-wide DMA interconnect dedicated to move data, and we group the TCDM into *superbanks (SBs)*, each 512 bit wide.

We present a case study integrating iDMA into *Occamy*, a scaled-out Snitch system in Section 4.4.2.

**Data Movement Core** Our tightly coupled DMA engine is connected to a ninth Snitch core, constituting our system’s communication processor, purposefully introduced to perform initialization, synchronization, orchestration, and data management operations, hence we call it *data movement core*. The eight regular *worker cores* constitute the *worker team*.

To allow the data movement core to compute *more complex* data movement patterns for N-D tensor transfers, it has access to the clusters’ shared *mul/div* unit over its *accelerator offloading interface*. The data movement core can be coupled to a *simplified* floating point unit (FPU) subsystem, should all nine cores be required to execute floating-point workloads, but for most control and *data* scheduling operations, this is not required.

**Superbanks** We group the 32 64-bit-wide TCDM banks into four 512-bit-wide superbanks. Each superbank has a priority-arbitrated multiplexer which connects either the eight individual banks to the cluster’s logarithmic interconnect or as one superbank to the 512-bit-wide DMA interconnect. The DMA connection has priority over fine-grained TCDM accesses by the cores and accelerator subsystems. This increased priority of the DMA accesses reduces back-pressure in the global SoC interconnect. In the default configuration with one DMA channel present in the system, having four superbanks gives the Snitch cores 75% and 50% of the undisturbed TCDM bandwidth with only iDMA and iDMA and an external manager being active, respectively.

A minimum of four superbanks is required to provide the Snitch cores and their tightly coupled accelerator subsystems enough bandwidth into TCDM, whilst still maintaining the priority-based arbitration mechanism.

**Wide DMA Interconnect** To move data between the cluster and the SoC, we introduce a second, 512-bit-wide AXI4 interconnect next to the already existing 64-bit-wide bus. After our modifications, the *narrow* interconnect handles only synchronization traffic between the clusters and the host, with all the bulk data transfers and instruction traffic being moved to the wide interconnect. A width of 512 bit directly corresponds to the size of a cache line in most host systems, and it is the default bus width of HBM memory controllers, see Section 4.4.5.

As mentioned in Section 4.2.1, the iDMA engine included into the Snitch cluster is configured to feature both AXI4 and OBI ports, allowing it to be a bridge between the wide AXI4 interconnect towards the SoC and the 512 bit DMA interconnect. External accesses are directly connected to the 512 bit DMA interconnect through an *axi\_to\_mem* adapter. Having both an iDMA engine connected to and an external path into the the cluster-local TCDM, allows two clusters to bidirectionally exchange data among themselves while all involved Snitch cores are still executing useful workloads.

### 4.3.1 Programming Model

For primarily data-oblivious [148] and tileable workloads, we use the data movement core to double-buffer the tiled workload data into the cluster-local TCDM scratchpad. Once the data is ready, the worker team can then be launched to do the computation on the tiles present in TCDM. Communicating through semaphores in TCDM, the data movement core can then relaunch the team on the next tiles. So far, we have not observed significant interference in the instruction cache between the worker team and the data movement core.

For data-depended workloads running on Snitch systems [69, 149, 150], the split between data movement core and worker team has been proven to be a fruitful architectural decision [149].

## 4.4 Case Study: Occamy

### 4.4.1 Introduction

Sparse ML and high-performance computing applications in fields like multiphysics simulation and graph analytics often rely on sparse linear algebra (LA), stencil codes, and graph pattern matching [145]. These workloads achieve low FPU utilization on modern CPUs and GPUs because of their sparse, irregular memory accesses and complex, indirection-based address computation [151–153].

This section presents the integration of iDMA into Occamy, a flexible, general-purpose, dual-chiplet system with two 16 GiB HBM2E stacks optimized for a wide range of irregular-memory-access workloads. We present Occamy as an industry-scale use case study for our tightly coupled instruction-based Snitch iDMA engine introduced in Section 4.3.

Occamy demonstrates in silicon three innovations: **(A)** efficient multi-precision compute cores with sparse streaming units (SUs) supporting indirection, intersection, and union operations to accelerate general sparse computations, **(B)** a scalable, latency-tolerant, hierarchical architecture with separate data and control interconnects and distributed DMA engines for agile on-die and die-to-die (D2D) traffic, and **(C)** an innovative system-in-package 2.5D integration for two compute chiplets with two 16 GiB HBM2E stacks.

### 4.4.2 Memory Architecture

Occamy combines two 216-core compute chiplets on a passive interposer, each paired with an eight-device, 16 GiB HBM2E stack and connected through a fully digital, fault-tolerant D2D link. Figure 4.3 and Figure 4.5 show the hierarchical compute chiplet architecture: at the lowest level, nine RISC-V Snitch cores are organized into clusters (Section 4.4.3, four such clusters form a group (Section 4.4.4), and each chiplet contains six such groups (Section 4.4.5) , which we describe in a bottom-up fashion in the following sections.

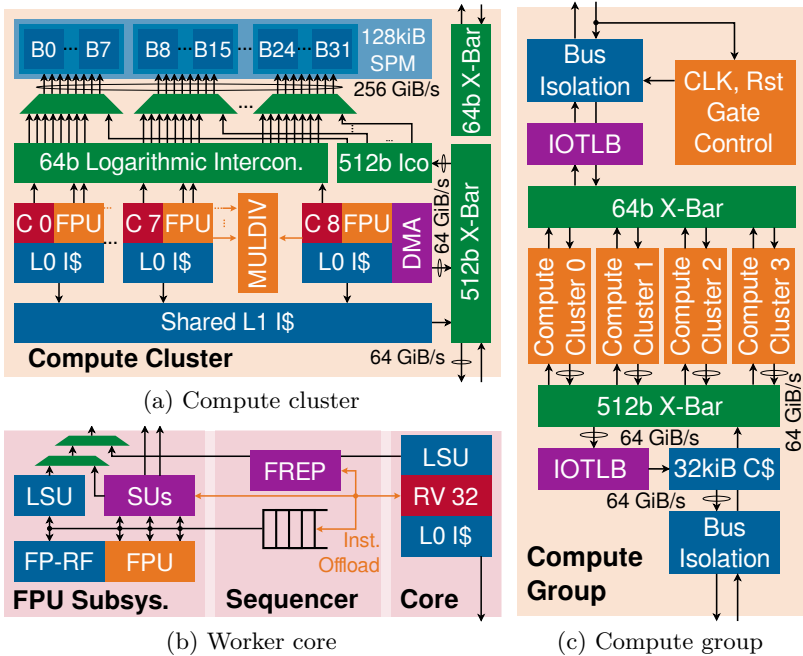


Figure 4.3: Architecture of the Occamy compute cluster, the worker core, and the compute group.

#### 4.4.3 Compute Cluster

Occamy's compute cores are based on the RV32G ISA and are organized into compute *clusters* [139] shown in Figure 4.3a. Within each cluster, eight worker cores and one *communication processor* share a 128 KiB 32-bank SPM through a single-cycle logarithmic interconnect with double-word interleaving. The clusters also feature 8 KiB of shared L1 instruction cache, a shared integer multiply-divide unit, *mul/div*, a local hardware synchronization barrier, and sixteen retargetable performance counters capable of tracking various per-core and cluster-wide events.

Each worker core, shown in Figure 4.3b, features a 64-bit-wide SIMD FPU supporting FP64, FP32, FP16, FP16alt (8,7), FP8, and FP8alt (4,3) formats. In addition to fused multiply-add (FMA)

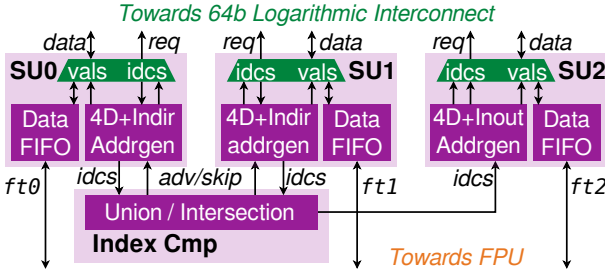


Figure 4.4: Architecture and interconnection of the three cooperating sparsity-capable SUs in each worker core.

instructions, the FPU supports widening sum-dot-product and three-addend summation instructions for all FP8 and FP16 formats [154]. Two worker-core ISA extensions maximize the FPU utilization for both regular and irregular workloads: a hardware loop buffer [139] and three sparsity-capable SUs [150].

The SUs, shown in Figure 4.4, map buffered streams of SPM accesses directly to floating-point registers, generating the necessary addresses in hardware. All three SUs in each core support up to 4-D strided accesses to accelerate dense tensor workloads; for instance, a regular general matrix multiply (GEMM) utilizes all four SU loop levels to cover the algorithm’s three nested loops and an inner unroll for performance. Two SUs additionally support indirect streams with 8-, 16-, or 32-bit indices to accelerate the scatter-gather accesses underlying irregular-access applications such as sparse-dense LA and stencil codes. Finally, these indirect SUs can also compare their indices to accelerate the sparse tensor intersection and union underlying sparse-sparse LA or graph matching; the third SU can optionally write out the joint indices for sparse result tensors. Our SUs can handle any sparse tensor format whose major axis is given by a value-index array pair, which includes the widespread and scalable CSR, CSC, CSF, and many of their variations, without restrictive assumptions on operand structure or density. In general, our SUs enable a sustained per-core bandwidth of up to three double-words per cycle into the shared SPM.

The cluster SPM is dimensioned to balance throughput, interconnect complexity, and area. 32 banks are chosen to reduce the

probability of banking conflicts between SUs (24 per cluster) and the DMA while keeping the logarithmic interconnect physically implementable. A capacity of 128 KiB achieves a reasonable SRAM bit density (avoiding significant drops that would appear for  $\leq 4$  KiB banks) while keeping area prevalently allocated to compute logic.

The communication processor in each cluster features a tightly coupled 512-bit iDMA engine, described in Chapter 2, programmed through *inst\_64* (Section 4.2), enabling asynchronous  $\leq 2$ -D transfers between external memory (other clusters, HBM2E, or other chiplet) and the local SPM. This core coordinates the computation of worker cores and their fine-grained, low-latency accesses to the SPM with the latency-tolerant DMA transfers of large, double-buffered data tiles to and from the SPM, as presented in Section 4.3.1. The iDMA engine accesses blocks of eight SPM banks (*superbanks*, see Section 4.3) at once through a secondary interconnect, transferring up to 64 B per cycle or 64 GiB/s; this way, it maximizes throughput without significantly slowing down ongoing memory-intensive computations, which can access up to 24 SPM banks at once using all SUs. To reduce backpressure in the group- and chiplet-level interconnect, the DMA has priority accessing the SPM through the secondary interconnect over the cores and SUs.

#### 4.4.4 Compute Group

Four clusters together form the next compute hierarchy level, a *group*, shown in Figure 4.3c. Clusters within a group have full-bandwidth access to each other through two fully connected AXI4 crossbars: a 512-bit crossbar used by DMA engines and instruction caches for bulk transfers and an atomics-capable 64-bit crossbar used by cores for global synchronization and message passing. Thus, groups allow their clusters to locally share data at higher bandwidths than at the global level and constitute a replicable multi-cluster design that significantly simplifies top-level chiplet implementation.

On each crossbar, a group has one outgoing and one incoming port, providing a shared bandwidth to and from the chiplet interconnect of 64 GiB/s for bulk transfers and 8 GiB/s for message passing. Providing one outgoing port per group best matches the HBM2E bandwidth available at the chiplet level and keeps the chiplet-level interconnect

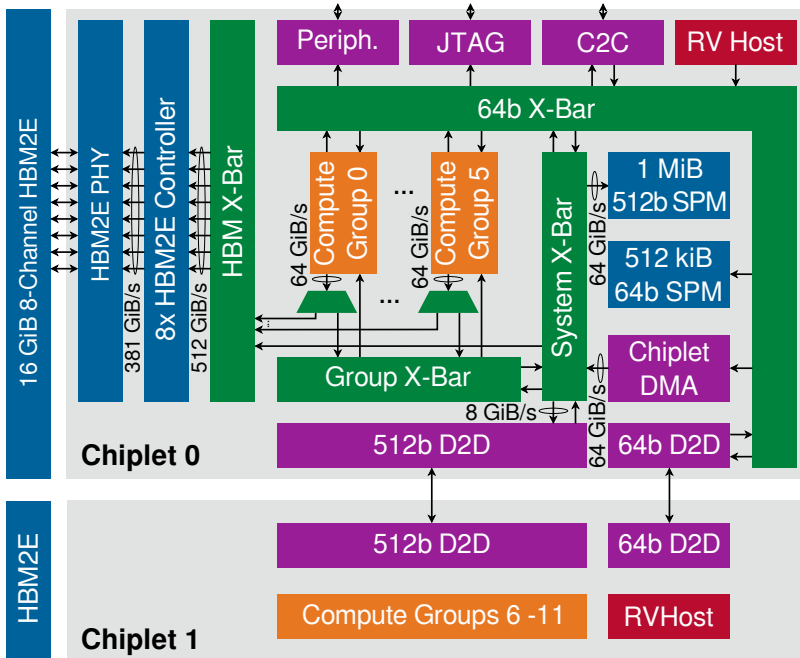


Figure 4.5: Architecture of the two Occamy chiplets. Occamy features only one address region; narrow managers can access wide subordinates and vice versa through the *system* crossbar.

implementable. IOTLBs on the outgoing ports allow for per-group address remapping and access control at page granularity. A remappable 32 KiB constant cache on the outgoing 512-bit port can be used to cache program code and other immutable data. Finally, the groups can be individually clock-gated, reset, and isolated from their interconnect ports to the chiplet level through memory-mapped registers for online power management.

#### 4.4.5 Occamy Chiplets

Figure 4.5 shows Occamy's top-level chiplet architecture. Each chiplet features six groups, totaling 216 cores, and a single Linux-capable 64-bit

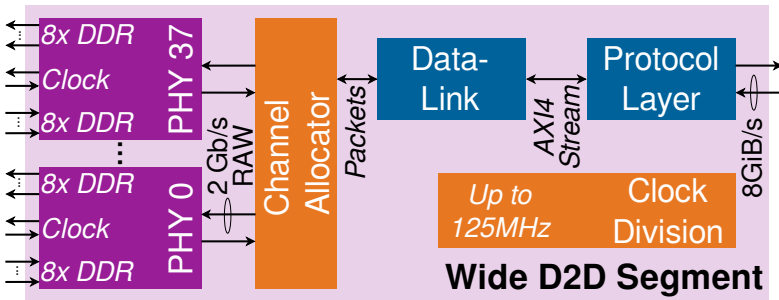


Figure 4.6: Architecture of the wide D2D segment with its 38 source-synchronous double-data-rate PHYs, carrying up to 2 GiB/s of raw data at a clock speed of 125 MHz.

RISC-V host processor managing the groups and all other on-chip resources. Like the groups, the chiplets feature a hierarchical 512-bit AXI4 network for bulk data transfers and an atomics-capable 64-bit AXI4 network for synchronization, message passing, and management. The D2D link, which serializes cross-chiplet transactions, comprises a *narrow* and a *wide* segment carrying 64-bit and 512-bit transactions, respectively.

The 512-bit network is composed of three fully connected crossbars. Each group's 64 GiB/s outgoing port provides access to an *HBM* crossbar and a *group* crossbar, interconnecting the six on-chip groups. The *HBM* crossbar provides access to the eight on-chip 47.68 GiB/s HBM2E controllers (381.47 GiB/s in total). It can be configured at runtime to interleave the HBM2E channels at page granularity, facilitating load balancing and data reuse. A *system* crossbar connects the group and HBM crossbars to the wide D2D segment and 64-bit network, providing all actors across both chiplets access to the entire memory space. It also connects to a 1 MiB SPM used for low-latency on-chip storage of shared data and a chiplet-level DMA engine used by the host for fast, explicit data movement and memory initialization. As a chiplet-level memory, the 1 MiB SPM was dimensioned to be significantly larger than the 128 KiB cluster SPMs, but small enough to fit into the area available to chiplet-level logic and routing.

The 64-bit network consists of a single crossbar. It connects the Linux-capable host and the 64-bit ports of the groups to the narrow D2D segment, the 512-bit network, and various peripherals. It also features a 512KiB SPM used by the host for management tasks. The peripherals include UART, I2C, QSPI, GPIOs, a 1.33 Gbit/s off-interposer chip-to-chip (C2C) link, and a JTAG test access point for live host processor debugging. They also include RISC-V-compliant timers and platform-level interrupt controllers providing interrupts for both the host processor and all on-chip compute cores.

The main benefit of our hierarchical crossbar-based interconnect over a ring or mesh topology is its *symmetry*: the memory topology looks identical to all compute cores and clusters, meaning that the architectural bandwidth and latency of accesses to each hierarchy level (cluster, group, chiplet) are *constant*. This greatly simplifies programming, as network performance is homogeneous and code can be written in a *cluster-agnostic* way without sacrificing performance. However, crossbars pose challenges in physical implementation, requiring effort to provision sufficient bandwidth while managing area costs. While this was feasible for our design, larger systems may face scalability limitations. In this case, alternative NoC topologies such as mesh and torus could be more suitable.

The D2D link enables seamless communication across chiplets, allowing the system to scale to 432 cores and two HBM2E stacks. This approach improves overall performance while avoiding the yield challenges and high manufacturing costs associated with large monolithic dies [155]. The D2D link consists of a narrow segment, optimized for synchronization and message passing, and a wide segment, designed for high-throughput bulk data transfers.

The wide segment is a scaled-up version of the narrow segment with 38 physical layers (PHYs) to increase bandwidth; its architecture is shown in Figure 4.6. The *protocol layer*, shown in Figure 4.6, arbitrates between AXI4 requests and responses and converts them to AXI4-Stream payloads. It handles the five independent channels of the AXI4 protocol (AW, AR, W, R, B) and applies backpressure to the AXI4 interface to prevent protocol-level deadlocks. Each AXI4-Stream payload includes a header that contains information about the packet type and credits required for flow control. The *data-link* layer further packetizes the payloads based on the available number

of off-chip lanes; it also handles credit-based flow-control to ensure that no packets are lost, as well as synchronization and alignment of packets if multiple PHYs are configured. Additionally, the data-link layer features debugging capabilities, including a *Raw Mode* that allows the link to operate independently of the AXI4 interface by sending patterns over specific PHY channels for fault detection. Each PHY features an all-digital and source-synchronous interface with eight double data rate (DDR) lanes in each direction. On the transmitter side, the PHY operates with a forwarded clock derived from the system clock. On the receiver side, the transmitted packets are synchronized with the system clock and reassembled into the original payload. The narrow and wide segments can achieve effective duplex bandwidths of up to 1.33 Gbit/s and 64 Gbit/s, respectively. The wide segment additionally features a *channel allocator* to enable fault tolerance. An initial calibration detects faulty PHYs, which can individually be disabled; the channel allocator then reshuffles packets among the functional PHYs with only linear bandwidth degradation. This fault tolerance mechanism ensures reliable communication across chiplets, even in the presence of manufacturing defects.

The Occamy chiplet relies on frequency locked loops (FLLs) to generate on-chip clocks for each of its three clock domains: the *compute* domain, the *peripheral* domain, and the *HBM2E PHY* domain. The *compute* domain includes the compute groups, the 64-bit host, the chiplet-level interconnect, the D2D link, and the HBM2E controller. Like the groups, the D2D link and the HBM2E subsystem can be clock-gated through memory-mapped configuration registers.

#### 4.4.6 Physical Design

The full Occamy 2.5D system was implemented and fabricated along with a dedicated carrier board, resulting in the compute module shown in Figure 4.10. The 73 mm<sup>2</sup> chiplets were fabricated in GlobalFoundries' 12 nm LP+ FinFET node using a 13-metal stack. The two compute dies with their respective Micron *MT54A16G808A00AC-32* HBM2E stacks were mounted on *Hedwig*, a passive, 4-metal-stack 65 nm PKG-25SI interposer from GlobalFoundries, shown in Figure 4.11.

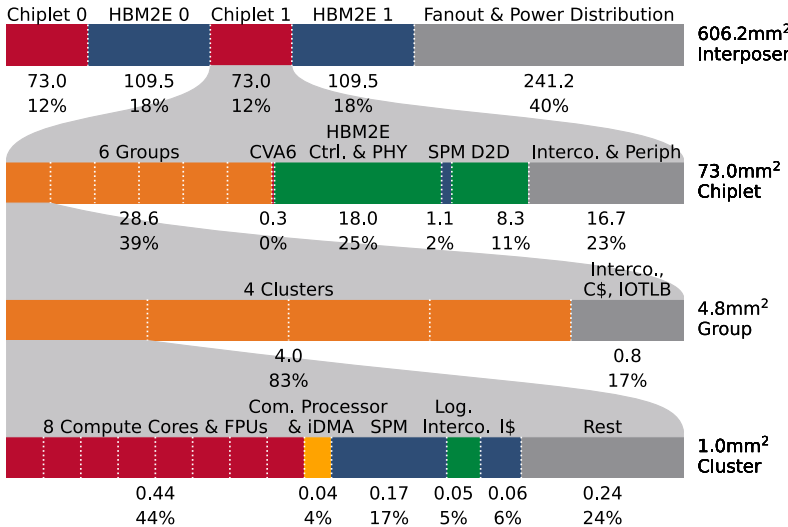


Figure 4.7: Hierarchical area breakdown of the Occamy system.

#### 4.4.7 Occamy Chiplets

The compute chiplets were synthesized, placed, and routed hierarchically using Synopsys' *Fusion Compiler* 2022.3. We used 7.5-track standard cell libraries from Arm and HBM2E IPs (controller and PHY) provided by Rambus. We targeted a nominal compute domain clock of 1 GHz under typical conditions (0.8 V, 25 °C) with a worst-case (0.72 V, 125 °C) constraint of 950 MHz. The peripheral domain was constrained to 500 MHz under worst-case conditions. The HBM2E controllers and PHY were constrained as specified to match the DRAM's peak 3.2 Gbit/s/pin throughput.

Figure 4.7 presents a hierarchical area breakdown of an entire Occamy assembly. Figure 4.8 and Figure 4.9 show the resulting hierarchical chiplet layout; we describe our implementation in a bottom-up fashion. In accordance with our findings in [156], we arranged the compute cluster's IO ports and L1 instruction cache on one side and its SPM SRAMs in a U shape on the opposite side, resulting

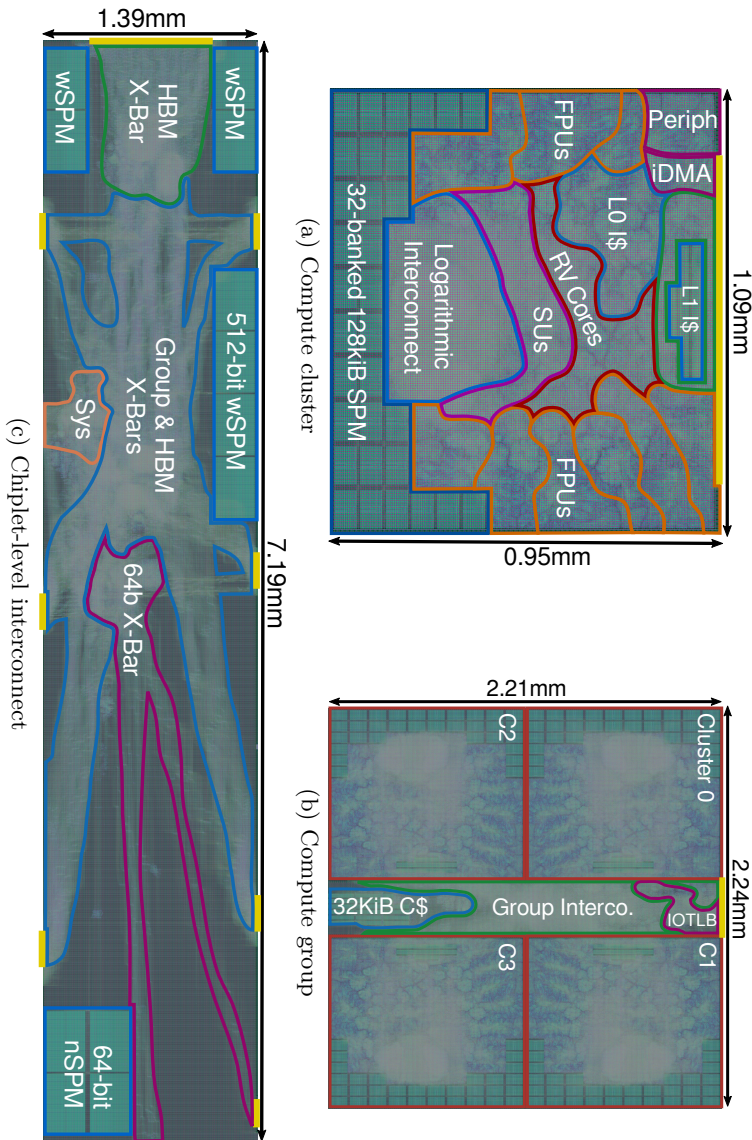


Figure 4.8: Annotated physical layouts of the Occamy chiplet's hierarchical components.



in the  $1.0\text{ mm}^2$  cluster layout shown in Figure 4.8a. The cluster is area-dominated by the nine RISC-V compute cores with extended FPU functionality (44%) and SPM (17%). The group layout, shown in Figure 4.8b, is almost entirely comprised of its four cluster macros (83%) and funnels its shared interconnect ports to a narrow interval on its north edge. The chiplet interconnect is shown in Figure 4.8c; the global SPM SRAMs were placed to avoid obstructing the shortest path for crossbar connections. Further, we implemented the host processor, the eight HBM2E controllers, and the D2D link as hierarchical macros to simplify integration.

The top-level chiplet layout is shown in Figure 4.9; it is area-dominated by the six compute groups (39%), HBM2E interface (25%), and D2D link (11%). In accordance with the interposer arrangement, the west and south chiplet beachfronts are fully reserved for the HBM2E and D2D interfaces, respectively, while the remaining off-interposer IO drivers are kept on the north and west edges. Designing a chiplet for interposers brings additional constraints to the floorplan. First of all, in scaled technologies, complex IP like the HBM2E physical interface are sometimes designed specifically for one orientation (either East-West or North-South). Second is the arrangement of dies on the interposer to satisfy both short signal propagation delays, stay within routing limitations of the interposer structure and consider mechanical stability of the assembled module (bending). Occamy has been designed as a research vehicle, and therefore does not feature high-bandwidth external I/O reducing the constraints on off-module communication. The central chiplet bumps are reserved for power delivery.

#### 4.4.7.1 Hedwig Interposer

The Hedwig interposer is at the center of the 2.5D system, connecting the Occamy chiplets to each other, to their HBM2E stacks, and to the carrier board. On its top side, it exposes  $45\text{ }\mu\text{m}$ -wide *microbump* openings accepting connections from the Occamy chiplets and HBM2E stacks through  $15\text{ }\mu\text{m}$ -wide copper micropillars. On its bottom side, 1399 custom-designed hexagonal *C4 pads* with  $320\text{ }\mu\text{m}$  openings and a  $650\text{ }\mu\text{m}$  pitch allow us to solder the 2.5D assembly onto the carrier PCB using low-temperature bismuth-based *C4 bumps*.

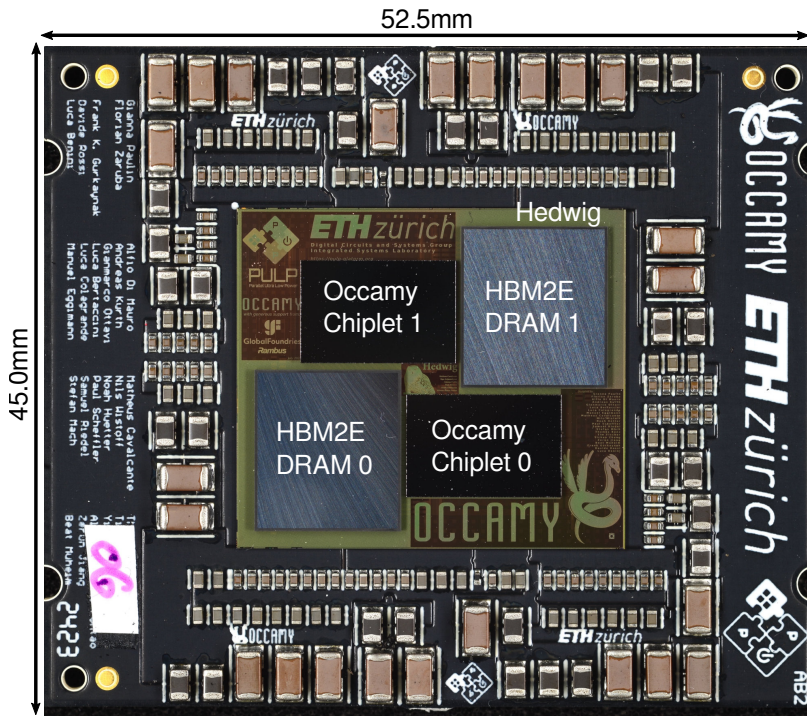


Figure 4.10: 2.5D Occamy assembly mounted on carrier PCB.

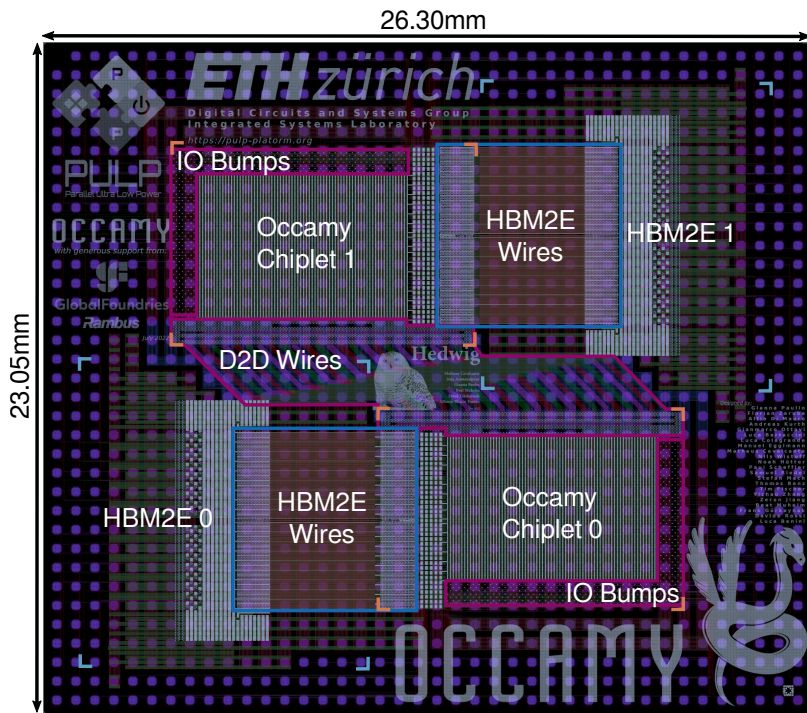


Figure 4.11: Layout of the Hedwig interposer.

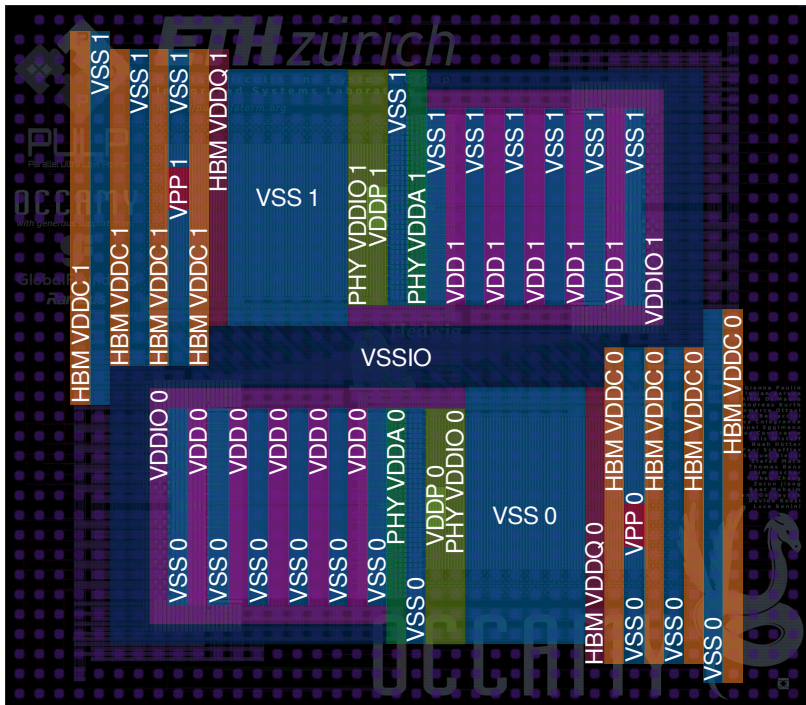


Figure 4.12: C4 bump map of the Hedwig interposer.

The connections between the Occamy chiplets and HBM2E stacks were routed on the odd metal layers with a wire width of  $2.5\text{ }\mu\text{m}$  and a pitch of  $4.1\text{ }\mu\text{m}$ . The HBM2E wire length was kept below  $4.9\text{ mm}$ , and ground shields were introduced on the even layers to ensure signal integrity. Figure 4.11 highlights the HBM2E wires; the routing density inside the rectangles approaches 100%. The 39 D2D link channels were length-matched to  $8.8\text{ mm}$  and combined into 24 wire bundles located at the center of Hedwig as shown in Figure 4.11. The bundles were routed on the three upper metal layers in an alternating pattern, leaving the lowest layer for a shared ground connection. A routing width of  $3.2\text{ }\mu\text{m}$  with a pitch of  $6.4\text{ }\mu\text{m}$  was chosen.

The digital IO of the Occamy chiplets and HBM2E stacks was routed to Hedwig’s edge using  $2.5\text{ }\mu\text{m}$  traces on the three uppermost layers; placing IO-related C4 pads at the edge of Hedwig facilitates the fan-out to the carrier PCB. Figure 4.12 shows Hedwig’s C4 pad map, highlighting the IO-related connections as well as the sixteen power and three ground domains. The ground pads of IO drivers of the two chiplets are connected through the shielding of the D2D link, resulting in a shared IO ground  $VSSIO$ . For the rest of the power domains, each chiplet-HBM2E pair has its own ground  $VSSx$ . The compute fabric, host, and HBM2E controller on each chiplet are supplied through the core power net  $VDDx$ ; the remaining power domains supply the HBM2E PHYs and memory stacks. We designed Hedwig to keep the maximum current below  $540\text{ mA}$  and  $34\text{ mA}$  for each C4 pad and through-silicon via, respectively.

#### 4.4.7.2 Carrier PCB

The carrier PCB completes the Occamy assembly at the lowest level. It serves three main purposes: giving the assembly mechanical stability, implementing the fan-out of the IO signals, and stabilizing the individual power domains. The 12-layer stack-up with  $70\text{ }\mu\text{m}$ -thick copper foil and *ROGERS RO4350B* high-stability, low-CTE laminate ensures high current delivery capabilities while providing sufficient mechanical strength. Decoupling capacitors are placed close to Hedwig on the carrier to comply with the power delivery requirements of the HBM2E stacks.

The carrier PCB implements an industry-standard *LGA 2011-3* CPU socket interface compatible with off-the-shelf mainboard sockets, facilitating the creation of application boards. Most of the 2011 pins are used for power and ground connections, with 877 exposed IOs. The carrier is designed to be strong enough to protect the fragile, 120  $\mu\text{m}$ -thick Hedwig interposer from mechanical stress while being placed into and removed from the test socket.

#### 4.4.8 Bringup and Silicon Measurement Setup

Figure 4.13a shows Occamy's *bringup* board, which consists of a stack of two individual PCBs. The upper PCB holds an LGA 2011 zero insertion force (ZIF) socket for the Occamy system, connectors for the 16 power domains, an interface to a *V93000* automated test equipment (ATE) system, as well as JTAG, UART, and GPIO headers. For standalone operation, the lower PCB provides clocking resources, reset circuitry, configuration headers, and an SD card slot for each chiplet.

To evaluate Occamy, we connect the bringup board to an ATE system, ensuring a stable, low-jitter clock delivery. In all experiments, the temperature of the Occamy system is kept at 25°C through an active temperature forcing system. We use Keysight *E36200* series power supplies for power delivery and current measurements. Two Digilent *JTAG-HS2* programmers are used to program the Occamy system through JTAG, and two FT232 chips relay UART data to a testing workstation using *DUTCTL* (Chapter C).



(a)



(b)

Figure 4.13: (a) Bringup board enabling both testing on an V93000 ATE and standalone operation, and (b) measurement setup.

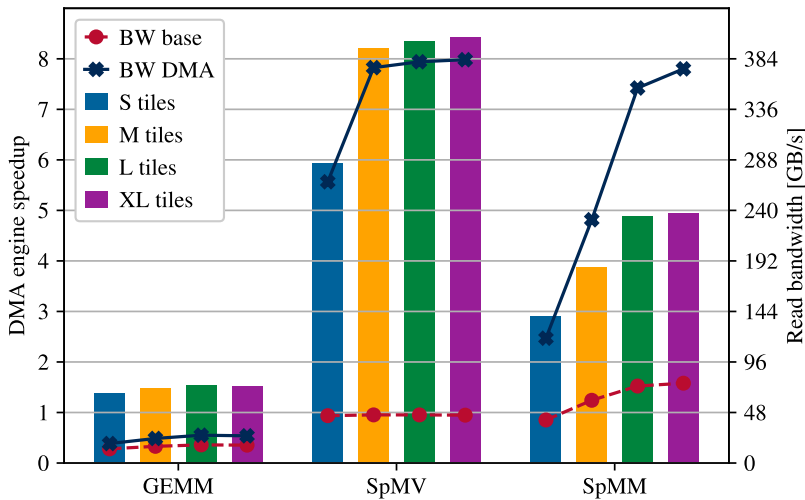


Figure 4.14: Occamy chiplet bandwidths and speedups enabled by iDMA on workloads with varying tile sizes.

## 4.5 Experimental Results

We evaluate GEMM, sparse matrix-vector multiply (SpMV), and sparse matrix-matrix multiply (SpMM) on Occamy with and without the use of cluster DMA engines. We run double-precision tiles and use these results to compute the performance of a single chiplet, taking into account bandwidth bottlenecks and assuming all reused data is ideally cached.

Each workload is evaluated with four cluster tile sizes  $S$ ,  $M$ ,  $L$ , and  $XL$ ; for GEMM, these are square tiles of size 24, 32, 48, and 64, while the two sparse workloads use the matrices of increasing density *diag*, *cz2548*, *bcsstk13*, and *raefsky1* from the SuiteSparse matrix collection [157] as tiles.

As Snitch [139] originally does not include a DMA engine, we compare Occamy to an architecture where the data movement is handled by the worker cores. In this base architecture, we assume the main interconnect to be bandwidth limited to 64 bit per cycle, corresponding to the AXI4 bandwidth of a worker core, but we do

not assume any limitation in the maximum number of outstanding transfers.

Figure 4.14 shows our results. For the highly compute-bound GEMM, our iDMA engines enable moderate, but significant speedups of  $1.37 \times$  to  $1.52 \times$ . Since all tile sizes enable ample cluster-internal data reuse, we see only small benefits as tiles grow. Nevertheless, the cluster engines still increase peak HBM read bandwidth from 17 to 26 GB/s.

SpMV performance, on the other hand, is notoriously data-dependent and memory-bound due to a lack of data reuse. Unable to leverage on-chip caches fed by a wider network, the baseline nearly saturates its narrow interconnect for all tile sizes at 48 GB/s. The iDMA engines only become memory-bound past  $M$ -sized tiles, but then approach the wide interconnect peak throughput of 384 GB/s. Overall, the engines enable significant speedups of  $5.9 \times$  to  $8.4 \times$ .

SpMM is similar to SpMV, but enables on-chip matrix data reuse, becoming compute-bound for both the baseline and iDMA engines. Since data caching is now beneficial, the baseline overcomes the 48 GB/s bottleneck and speedups decrease to  $2.9 \times$  to  $4.9 \times$ . Still, iDMA engines unlock the full compute of clusters on sparse workloads while asymptotically approaching the 384 GB/s peak throughput only for  $XL$  tiles.

## 4.6 Summary and Conclusion

In this chapter, we present tightly coupled instruction-based front-end, called *inst\_64*. Coupled with our 2-D tensor mid-end and iDMA back-end, we create an agile, tightly coupled *data movement accelerator* to be used in Snitch-based systems.

With our *dm* instructions, we define a light-weight RISC-V ISA extension for DMA engines, allowing to launch linear transfers in as few as three instructions and 2-D tensor transfers in as few as 5 instructions. Coupled with our very agile iDMA architecture, we can thus launch DMA jobs in as low as five cycles from the issue of the first *dm* instruction to the first data element issued on the AXI4 interface. We further provide additional instructions for memory initialization and user-defined extensions, including issuing multicast operations.

We integrate our tightly coupled DMA engine into the Snitch cluster by introducing a dedicated *communication processor* to orchestrate the *worker cores* and manage the data movement operations on a high level. We further optimize Snitch’s memory architecture by introducing the concept of wide superbanks and prioritized access via remote units and cluster-local iDMA engines into cluster-local TCDM while still employing a physically implementable single-cycle logarithmic interconnect.

We present the feasibility of our approach by integrating our engine into Occamy, a 2.5D multi-chiplet 432-core RISC-V system featuring HBM memory endpoints. We optimize our iDMA engines and the corresponding wide cluster, group, and chiplet-level interconnect hierarchies to maximize cluster-to-cluster and cluster-to-HBM throughput.

Running both dense and sparse workloads on Occamy, we can report speedups of up to  $8.4 \times$  whilst only increasing cluster area by less than 5%.



# Chapter 5

# Real-time Interconnect Extensions

## 5.1 Introduction

The current trend in industrial domains such as automotive, robotics, and aerospace is towards autonomy, connectivity, and electrification, significantly increasing the demand for onboard computing power and communication infrastructure, thus driving a paradigm shift in their design [3–8].

A clear example is the automotive domain, where the traditional approach — relying on hundreds of embedded real-time ECUs distributed throughout the vehicle — cannot meet the growing compute demands and complicates cable harness management, impacting SWaP-C [8, 18, 19]. This paradigm cannot support the rapid shift toward ACES, which is laying the foundation of ADAS and SDVs [4]. Hence, integrated, interconnected *zonal* and *domain* architectures are becoming the preferred replacements for discrete ECUs, as they deliver the flexibility and compute capability required for ACES mobility and the SWaP-C problem [19, 20].

These architectures are heterogeneous MCSs [21,22]. They comprise general-purpose and domain-specific sub-systems with diverse real-time and specialized computing requirements that execute concurrently on the same silicon die, sharing communication, storage, and micro-architectural resources [23, 24]. Some subsystems handle hard safety- and time-critical workloads, such as engine, brake, and cruise control [8, 25, 26], while others run less time-critical but computationally demanding tasks like perception pipelines, infotainment, and commodity applications [8].

Time- and safety-critical tasks require strict real-time guarantees, ensured through time-predictable run-time mechanisms, composable timing analysis, and safety assessments [158]. However, in heterogeneous MCSs, this process is complicated by the increased interference generated by multiple domains contending for shared hardware resources on the same platform [25]. This additional contention may introduce unpredictable behavior during the system's execution, causing possible deadline misses for time- and safety-critical tasks [159,160]. To preserve the timing behavior of the system under known and predictable bounds, techniques such as spatial and temporal isolation become a prerequisite, as they enhance the *observability* and *controllability* of shared hardware (HW) resources [6,161]. The *interconnect* in modern SoCs is of particular concern; several previous works have highlighted that interference in accessing shared resources regulated by bus arbiters and interconnects is a major source of unpredictability [25,26,159,162].

In this chapter, we present AXI-REALM, an AXI4-based, interconnect extension that improves real-time and predictability behavior of MCSs by monitoring and controlling both the *ingress* and *egress* data streams. The architecture is split into two sub-systems: *irealm*, tasked to guard and regulate the *ingress* stream (requests and data issued by managers) with a *budget and time-slicing* approach; *erealm*, tasked to supervise the *egress* stream (data and responses issued by subordinates) with bandwidth and latency statistics, and eventually protect the system from malfunctioning subordinate devices.

In the following sections, we provide a detailed description of the internal HW components, we include a sequence diagram presenting an example write transaction passing through the various sub-units, combine the ingress [55,56] with the egress units [66] to a unified AXI-REALM system, capable of shaping the ingress traffic and protecting

the interconnect and the system from malfunctioning subordinate devices (Section 5.3), we provide an extensive evaluation at the system-level by integrating AXI-REALM in an open-source MCS characterizing functional, energy, and power performance (Section 5.5), we give an IP-level evaluation (Section 5.4), and we provide a detailed SoA comparison for the unified system (Section 5.6). Finally, Section 5.7 concludes this chapter by summarizing its key contributions and achievements. In more detail, this thesis provides the following contributions to SoA:

- **AXI-REALM:** We present a scheme to enforce predictable behavior compatible with any AXI4-based interconnect which relies on *observing* and *controlling* both its *ingress* and *egress* data streams using ad-hoc HW methodologies. The resulting architecture demands minimal additional hardware resources and no internal modifications to the baseline interconnect, enabling portability across diverse SoC targets.
- **HW-driven traffic controllability:** AXI-REALM’s irealm unit implements a configurable number of subordinate *regions* per manager. Each *region* is runtime-programmable with address range, transfer fragmentation size, transfer budget, and reservation period to control the bus traffic through a *time slicing* approach.
- **HW-driven traffic observability:** AXI-REALM’s irealm and erealm units include modules that observe and track per-manager access and interference statistics, such as transaction latency, bandwidth, and interference with each other manager. With bandwidth-based observability, AXI-REALM can perform per-manager bandwidth throttling, modulating back-pressure.
- **HW-driven safety measures for malfunctioning subordinates:** We include a HW mechanism [66] to isolate and reset malfunctioning subordinates individually, taking advantage of AXI-REALM’s erealm latency tracking capabilities to identify response timeouts, mismatching transactions, and invalid handshakes.

- **IP-level characterization:** We extensively characterize AXI-REALM in a 12 nm technology, presenting an area model as well as timing and latency information.
- **In-system implementation assessment:** We evaluate AXI-REALM in an open-source heterogeneous MCS research platform<sup>1</sup>. We demonstrate the versatility of the proposed approach under interference scenarios between critical and non-critical managers of the system, achieving at least 68% of the single-initiator case (over 95% when distributing the budget in favor of the critical manager). Further, the proposed transfer fragmentation reduces the access latency of the critical manager by 255 cycles from 266 to 11 cycles. AXI-REALM incurs an area overhead of less than 2% in the presented MCS.

The synthesizable and silicon-proven register transfer level description of AXI-REALM and its integration into the presented real-time system are available open-source under a libre Apache-based license<sup>2</sup>.

## 5.2 Background

### 5.2.1 The AMBA AXI4 On-Chip Interconnect

AXI4 is an industry-standard protocol for high-bandwidth, non-coherent, on-chip communication. It defines five separate channels for read and write requests (*AR*, *AW*, *W*) and responses (*R*, *B*). An AXI4 *beat* is the communication in one cycle on an AXI4 channel [38]. An AXI4 *transaction* is the number of beats a manager requires to communicate to a subordinate. The manager initiates a transaction by emitting an *address and control beat* containing the meta information (address, attributes, and length in beats, ...) over either the *AR* or the *AW* channel. The *burst* attribute defines the increment mechanism of the write or read addresses during a transaction.

Each AXI4 transaction carries a *tID*. All beats in a transaction must have the same *tID*. The subordinate completes a transaction by sending a response over the *B* channel in the write case or by returning

---

<sup>1</sup>[github.com/pulp-platform/carfield](https://github.com/pulp-platform/carfield)

<sup>2</sup>[github.com/pulp-platform/axi\\_rt](https://github.com/pulp-platform/axi_rt)

the last read response over the *R* channel read case. The protocol also supports multiple *outstanding* transactions, i.e., initiated by the same manager and simultaneously in progress with the same tID.

Based on tID, the protocol dictates three *ordering rules* for write and read transactions. We recall them in the following: ① for different tIDs, write data on the *W* channel must follow the same order as the address and control beats on the *AW* channel, as *W* beats do not have a tID field; ② transactions with different tIDs can be completed in any order; on the *R* channel, the read data can be interleaved; ③ a manager can have multiple outstanding transactions with the same tID, but they must be performed and completed in the order they were requested, for both writes and reads.

This work uses an open-source and silicon-proven implementation of AXI4 network elements<sup>3</sup>. We refer to a *crossbar* as the main point-to-point network junction between managers and subordinates in the systems (Section 5.3.2 and Section 5.5).

### 5.2.2 MCS Terminology: Essential Insights

*Criticality* designates "*the level of rigor required to develop safety-critical functions so that the risk of failure can be brought to an acceptable level*" [21]. An MCS involves applications with different criticality requirements deployed on the same platform. Safety functions in MCSs are treated as belonging to the highest safety integrity level unless *independence* between them is guaranteed, i.e., applications achieve freedom from interference with each other. This implies demonstrating that (i) independence is achieved in both spatial and temporal domains, and (ii) violation of independence can be controlled (see [163], Sect. 7.4.2.9).

A way to achieve independence is through *isolation*, or partitioning, of HW resources and software (SW) components. Isolation allows the segregation of faults, improves predictability by providing bounds on resource access times [164], and reduces the SW validation and verification (V&V) effort [21]. *Physical* isolation relies on federated HW for each SW component. Hence, resources at all levels are physically decoupled. *Virtual* isolation establishes partitioned HW provisions

---

<sup>3</sup>[github.com/pulp-platform/axi](https://github.com/pulp-platform/axi)

that allow multiple SW components to run on the same HW platform, namely, an MCS [22].

Within *virtual isolation*, we distinguish between *spatial* and *temporal isolation*. Spatial isolation means that an application shall not change data used by another application; it can be achieved with virtualization techniques through a MMU [161]. However, on an integrated HW platform, virtual partitions still share resources such as caches, interconnects, and memory endpoints, making their temporal behavior inter-dependent [22, 164]. Temporal isolation ensures that one application will not cause malfunction of another application by blocking a shared resource over time or consuming another resource execution time. This can be achieved with adequate scheduling methods in SW, or HW/SW time slicing and fencing [21].

Current industrial and academic activities around MCSs do not share a holistic view of fully exploiting HW's potential to isolate executing application layers. However, some initiatives are being developed and studied [165]. A promising direction is that HW can cooperate with SW by enabling fine-grained *observability* and *controllability* of individual application behavior [161]. Proceeding from this premise and terminology background, this work aims to improve the observability and controllability of shared interconnect buses by leveraging time slicing, a temporal isolation technique.

## 5.3 Architecture

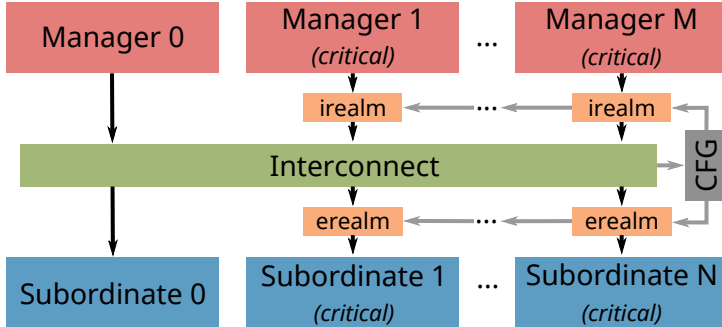


Figure 5.1: Overview of a generic system extended with AXI-REALM. The irealm units monitor and control data from the managers and erealm units guard the subordinate devices.

An overview of a generic system extended with AXI-REALM is provided in Figure 5.1. At the *ingress* of the interconnect, *irealm* units [55, 56] monitor and shape traffic injected by managers, enforcing fairness and reducing congestion within the network as well as at the target devices. The irealm unit tracks the bandwidth and budget on the granularity of a *region*. Each region can encompass a subordinate space, combine multiple subordinates, or only cover a fraction thereof. The number of supported regions can be set through a SV parameter at design time, and the address space covered by each region through SW at runtime. This is explicitly designed to be independent of the addressing of the interconnect.

At the *egress*, *erealm* units [66] guard the subordinate devices. They protect the interconnect and prevent deadline misses of real-time tasks in the case of protocol failures and subordinate regions/devices that extensively delay their responses. Our erealm unit provides two messaging options to inform the core of the unresponsive subordinates: interrupts and AXI4 protocol responses. Moreover, it integrates a framework to isolate, reset, and reinitialize malfunctioning devices within a single cycle [59].

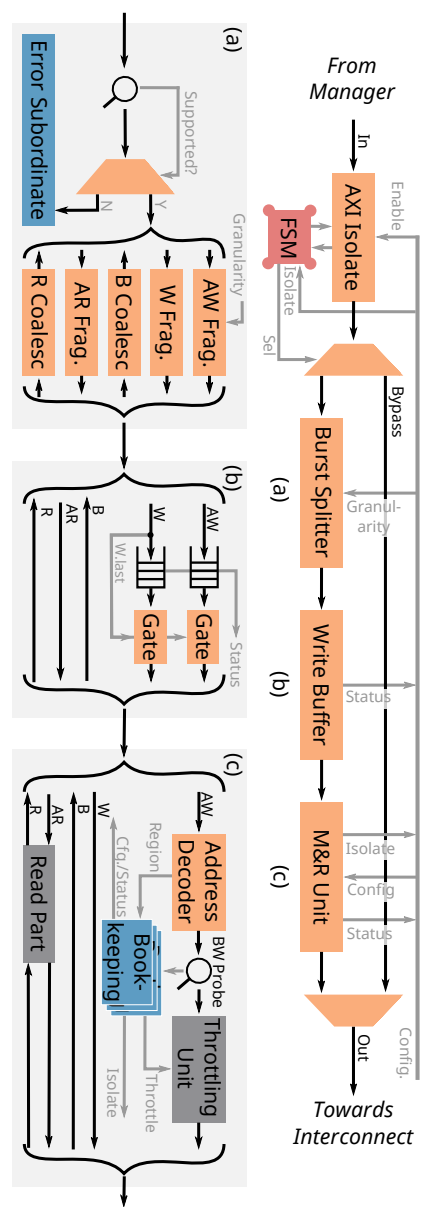


Figure 5.2: Internals of the irealm unit: (a) granular burst splitter, (b) write buffer, and (c) management.

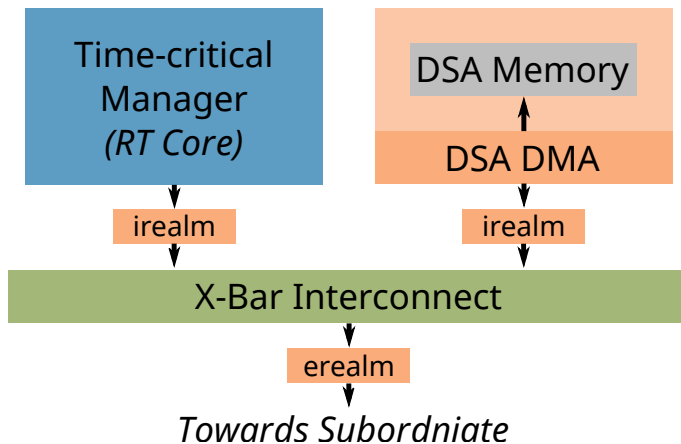


Figure 5.3: Block diagram of an exploratory system featuring two regulated managers, a crossbar-based main interconnect using RR arbitration and a guarded subordinate device. Configuration interfaces are not shown.

### 5.3.1 The irealm Unit and Architecture

The irealm unit comprises three main submodules, shown in Figure 5.2: the *burst splitter* (a), the *write buffer* (b), and monitoring and regulation unit (M&R unit) (c). At the irealm unit's input, an AXI4 isolation block isolates the manager during dynamic reconfiguration of the unit, once the manager's assigned budget expires, or when commanded through SW.

Figure 5.3 shows an exemplary system equipped with AXI-REALM featuring two regulated managers, a crossbar using RR arbitration and a guarded subordinate device. Figure 5.4 shows the function of the irealm and erealm units at two exemplary write transactions; one from a time-critical manager and one from a DMA engine (Figure 5.4a). Only the three write-related channels — see Section 5.2 — of the AXI4 buses are shown. The DMA requires five cycles to read the data from a memory internally to the domain-specific accelerator (DSA) before issuing its first write beat, see Figure 5.4a.

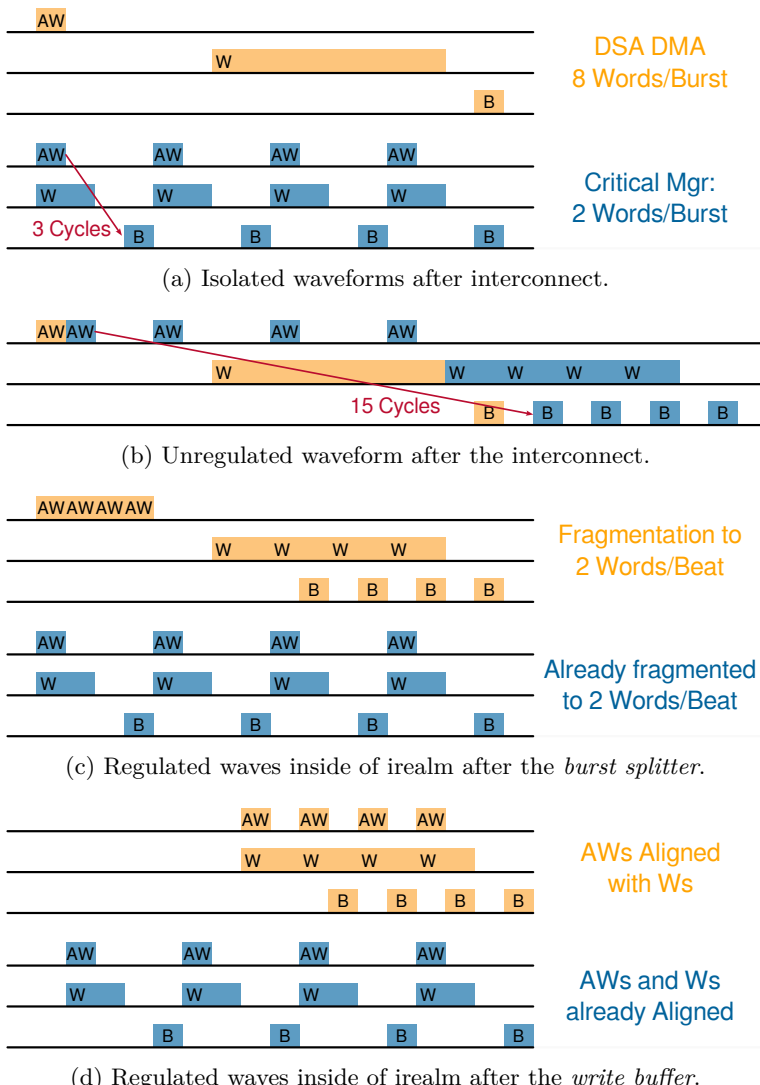


Figure 5.4: Write transaction passing through our irealm unit.  
(continued on next page)

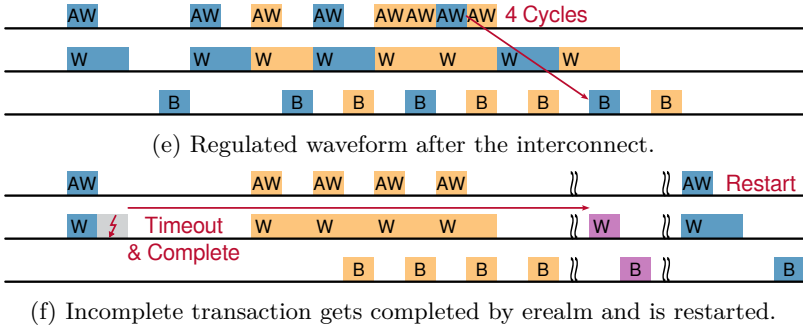


Figure 5.4: Write transaction passing through our irealm unit. (continued from previous page)

In the *unregulated* case, Figure 5.4b, the critical transaction experiences a completion latency of up to fifteen cycles. With our irealm unit activated, the DMA beats are fragmented after the burst splitter, Figure 5.4c, and bandwidth reservation is mitigated, Figure 5.4d, by stalling *AWs* until their corresponding *W* beats arrive. In this *regulated* case, Figure 5.4e, the transaction latency of the critical manager is at most four cycles. Figure 5.4f shows the case of a critical subordinate device timing out and how erealm completes and restarts this pending transaction.

This section explains the architecture and functionality of the irealm unit, detailing how it addresses unfairness from unregulated burst-based communication in RR-arbitrated interconnect systems. It describes how the unit ensures execution predictability using time slicing through static or dynamic budget and period assignments to the managers.

### 5.3.1.1 Granular Burst Splitter

On-chip interconnects can employ burst-based transactions to increase the efficiency of non-coherent interconnect architectures. Such transactions increase bus utilization and decrease the addressing overhead. In heterogeneous SoCs, transactions of different granularities, e.g., short, cache-line-sized transactions issued by a core and a long burst requested by a DSA, are common transaction patterns [159]. Classic

and fair RR arbitration on individual transactions affects bandwidth distribution fairness by increasing the completion latency of short, fine-granular transactions in the presence of long bursts.

As shown in Figure 5.2b, the *burst splitter* accepts incoming burst transactions and splits them to a runtime-configurable granularity, from one to 256 beats, according to the AXI4 specification [38]. Any transaction not supported by the burst-splitter is rejected and handled by an *error subordinate*. For instance, atomic bursts and *non-modifiable* transactions of length sixteen or smaller cannot be fragmented [38]. We store a burst transaction’s meta information (address, transaction size, AXI4 flags), emit the corresponding fragmented transactions, and update the address information. Write responses of the fragmented bursts are coalesced transparently. Read responses are passed through, except for the *R.last* signal, which is gated according to the length of the original transaction. A large granularity requires the write buffer module following the burst-splitter to be large enough to hold a single fragmented write burst. If a manager only emits single-word transactions, the granular burst splitter can be disabled from the irealm unit to reduce the area footprint.

### 5.3.1.2 Write Buffer

The meta information of a transaction is inherently tied to the data being written. AXI4 physically decouples meta information from the payload to increase bus efficiency [38]. However, the write data beats and meta information are not fully decoupled as the write channel does not have a TID field. Most interconnect architectures reserve the bandwidth for an entire write transaction on the *W* channel once the corresponding *AW* is received [38]. Additionally, according to the AXI4 standard, the *W* channel remains indefinitely allocated to the request’s issuer once the request has been propagated through the interconnect. The standard does not specify a maximum delay between the propagation of the request and the provisioning of the corresponding data. A manager device can reserve a large transaction by holding the *W* channel, potentially stalling the interconnect by delaying data injection. In practice, this mechanism is observed with slow manager devices or DMA units copying data from high-latency or bandwidth-limited endpoints, which cause interference in

the downstream memory system, as discussed in [166]. We prevent this behavior by storing the fragmented write burst in a *write buffer*, Figure 5.2b. The buffer forwards the *AW* request and the *W* burst only if the write data is fully contained within the buffer. The transaction buffer is configured to hold two *AWs* and one fragmented write burst.

### 5.3.1.3 Monitoring and Regulation Unit

In contrast to safety- and time-critical tasks executed on general-purpose processors, DSAs often work independently [25] and employ double buffering using their large internal memories; this results in memory-intensive phases followed by compute-intensive phases. The asynchronous nature of DSAs accessing the system’s memory coupled with coarse-grained synchronization results in unpredictable memory access patterns, increasing the timing uncertainty of critical tasks.

The M&R unit, presented in Figure 5.2c, uses a period-based hardware-implemented bandwidth limiting mechanism to prevent managers from injecting more bandwidth for each subordinate region into the network than allowed. The M&R unit is symmetrically designed with identical read and write components. Transactions first pass through the address decoder, which maps them to their respective subordinate region. A *bus probe* measures the transaction bandwidth and latency, providing this data to the *bookkeeping* unit, which is responsible for budget checks and monitoring bandwidth and latency. Each irealm unit can track the data sent to each region.

A different time period and budget can be specified for each irealm unit and each subordinate region. Once activated, this specified budget amount is available and is reduced by every beat passing the unit. Once one subordinate region’s budget exceeds the allocated amount, the number of outstanding transactions is reduced. The corresponding manager is completely isolated once one budget is depleted using the irealm unit’s isolation cell, see Figure 5.2. The budget is automatically renewed once the time period expires.

If the total budget assigned to each manager’s irealm unit is less or equal to what the interconnect and the subordinate devices can handle within a period, the AXI-REALM system ensures each manager can use its assigned budget. The budget distribution should be set according to the real-time task running on the general-purpose cores [25]. The time

period, budget checking, and budget renewal are tracked and handled entirely in hardware, allowing the system to react with clock-cycle accuracy. This allows the irealm unit to set very short periods, ensuring agile regulation and fair bandwidth sharing in the presence of a DSA manager.

Furthermore, we extend this monitor to track the average transaction latency issued through the irealm unit. After a simple profiling run measuring the latency of each manager to each subordinate region in isolation during V&V, average completion latency can be used to reveal inter-manager interference within the network and its subordinate regions or devices. Thus, online performance data can help fine-tune the budget and period settings for each manager and assess how well irealm ensures time-critical tasks meet their deadlines.

### 5.3.2 Interconnect layer

We design AXI-REALM to be independent of the system’s memory architecture, except for fundamental properties. Our approach expects the interconnect to ensure a progress guarantee and route transactions using RR arbitration, which is the most common policy in commercial interconnects [26, 159, 167]. AXI-REALM is primarily intended for mixed-critical systems where DSAs require a high-performance interconnect to satisfy their data demand, and critical actors rely on real-time guarantees. We specifically choose an RR-arbitration mechanism over more classical real-time distribution patterns, like time division multiple access (TDMA) [168], to maintain the high-performance memory access required by the DSAs in today’s emerging heterogeneous systems. We aim to enhance the determinism and fairness of a classic RR-arbitrated interconnect by minimally intruding on its design, using lightweight helper modules at its boundaries.

Thanks to the independence from instance-specific assumptions on the interconnect architecture and to the compliance with the AXI4 specification of our AXI-REALM architecture, verification and maintenance are facilitated by allowing the use of unit-level standalone verification infrastructure.

As mentioned in Section 5.2, the in-system case study and IP-level evaluation presented in this work use a point-to-point-based interconnect constructed from AXI4 crossbars. AXI-REALM can

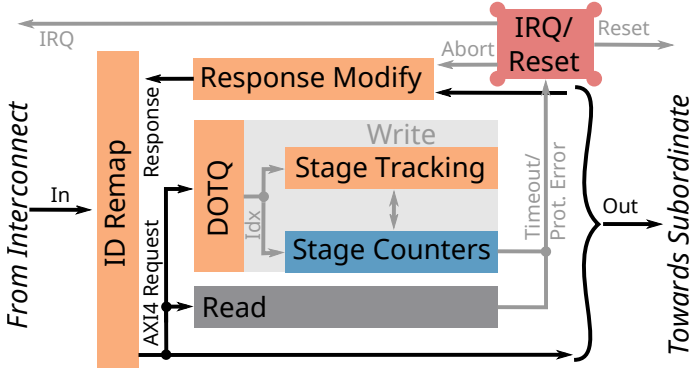


Figure 5.5: The internal architecture of the erealm unit. The read and write parts are constructed equally.

handle hierarchical point-to-point interconnects thanks to the concept of subordinate regions. While outside of the scope of this work, we also ensured compatibility of AXI-REALM with AXI4-based NoC architectures, such as presented in [67].

### 5.3.3 The erealm Unit and Architecture

The erealm unit uses a HW-based approach to monitor the latency of transactions sent to a subordinate device or region, responding promptly to unexpected misbehavior or malfunctions that disrupt the predictability of real-time tasks. This unit is essential because the assumption of perfect behavior by subordinate devices, often made in SoA [159, 162], does not hold in real-world scenarios. Additionally, erealm proactively ensures protocol compliance for all transactions without impacting system throughput or latency.

When responses from a subordinate device exceed user-programmable timeouts or when a protocol violation is detected, erealm completes the outstanding transactions and communicates the cause of the issue with the core either using interrupts or the AXI4 response channel. Error information, including tID, address, and the *specific transaction stage* in which the error occurred, are logged into registers. The unit can reset the connected subordinates through an agile reset controller [59] either

within one clock cycle upon fault detection, or when commanded by the core as part of the fault handling. Overall, erealm guards subordinate devices, guaranteeing responses within user-defined time frames, preventing the interconnect from locking up.

The architecture of erealm is shown in Figure 5.5. An ID remapper at the unit’s input compacts the typically sparsely used tID space, requiring fewer tID bits to track all transactions. The data path is then split into a similarly constructed *Write* and a *Read module*, presented in more detail below.

### 5.3.3.1 Dynamic Outstanding Transaction Queue (DOTQ)

AXI-REALM supports multiple outstanding, multi-id transactions commonly occurring when accessing high-performance subordinate devices; requiring dynamic tracking of multiple data streams, each with several outstanding transactions.

The erealm unit manages this through a dynamic queue consisting of three linked tables: an *ID Head-Tail (HT)* table, a *Transaction Linked Data (LD)* table, and a *Write (W)* or *Read (R)* table present in the write and read path, respectively. The HT table keeps track of active tIDs and enforces ordering for transactions with the same tID and supports efficient tID lookups without scanning through all transactions in the LD table. The LD table stores metadata such as tID, address, state, latency, and timeout, allowing detailed tracking of each outstanding transaction. Finally, the W/R table ensures that write data maintains the correct sequence with address beats, aligning data properly even when tIDs are not explicitly available on the write data channel. The tracking capacity is defined by two design parameters: the maximum number of unique tIDs and the maximum number of transactions each unique tID can support simultaneously.

### 5.3.3.2 Stage-Level Tracking for each Transaction

AXI4 transactions occur in multiple *stages*: address and meta information is sent first, followed by the data beats, and finally, the response stage. As shown in Figure 5.6, the counter-based tracking logic monitors *six* and *four* stages for write and read transactions, respectively. The first stage is the initial handshake transferring

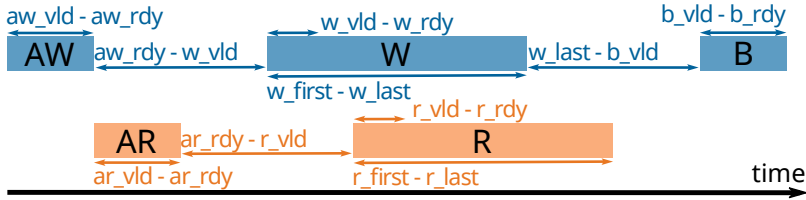


Figure 5.6: Tracked stages in the erealm unit.

address and meta information (*ax\_valid to ax\_ready*) to confirm the transaction acceptance. For the write case, this is followed by the transition from address acceptance to data availability (*aw\_ready to w\_valid*) to ensure that data beats readiness promptly follows. Monitoring continues with the acceptance of the first data beat (*w\_valid to w\_ready*) and in a subsequent stage, the data beat from the first to the last beat (*w\_first to w\_last*) to guarantee continuous and correct data flow. After the last write data beat, the monitoring tracks from (*w\_last to b\_valid*), which is to confirm that the subordinate device sends the write response in time. Finally, the transition from write response valid to response ready (*b\_valid to b\_ready*) checks that the acknowledgment is properly issued by the manager device, which marks the end of the transaction. For read operations, the transition from address acceptance to data availability (*rw\_ready to r\_valid*) is monitored, along with the data beats (*r\_first to r\_last*) and the timely delivery of the read response.

### 5.3.3.3 Stage Budget Allocation

In AXI4 systems, transactions of the same tID are processed sequentially. The stage budget for each transaction is dynamically calculated by multiplying the per-word stage budget, obtained by profiling the system during V&V, with the burst length, granting longer bursts more time to complete.

For write transactions, this impacts the time budget from the *aw\_ready to w\_first* stage, while the time from *w\_first to w\_last* is counted only when the transaction begins servicing, thus excluding prior transaction latency. A similar dynamic stage budgeting method

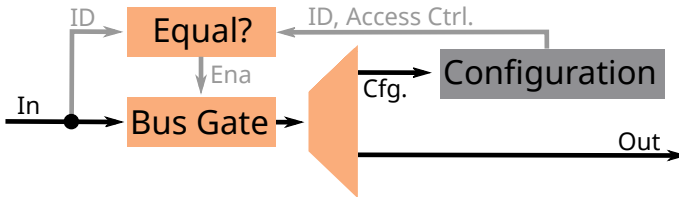


Figure 5.7: The architecture of the *bus guard*.

is applied for read transactions. This ensures that transactions, particularly those with large data beats, have sufficient time to complete.

### 5.3.4 Configuration Interface

In its basic configuration, irealm and erealm units are configured through a shared set of memory-mapped registers, as shown in Figure 5.1. The shared configuration register file can be physically decoupled to increase the scalability of the AXI-REALM architecture in larger designs. Configurations with dedicated configuration register files for each irealm and erealm unit are supported.

The register values are reset to a default configuration on startup, the erealm units are deactivated, and the irealm are bypassed. In this reset state, the AXI-REALM system is inert, interconnect accesses are unregulated, and no additional latency is introduced. One privileged manager, e.g., the booting core from a secure domain, programs the AXI-REALM system. The system's memory protection or AXI-REALM's *bus guard* restricts configuration space access to privileged managers. AXI-REALM can be dynamically reconfigured during the system's runtime.

### 5.3.5 Bus Guard

AXI-REALM's configuration space must be protected against malicious or erroneous accesses. Most systems use physical memory protection units or virtual memory space, e.g., through MMUs, to isolate critical configuration spaces.

Even in systems with no such protection device, our minimal *bus guard* unit, presented in Figure 5.7, restricts unwanted access to the configuration interface. After a system reset, a trusted manager must claim ownership of the configuration space by writing to a *guard register* within the *bus guard*. In the unclaimed state, every access to the configuration space except for the *guard register* returns an error. Once a manager has claimed the address space, it can perform a *handover* operation to transfer the exclusive read/write ownership to any other manager in the system. The *bus guard* differentiates between managers using their unique TID.

Table 5.1: Area contribution *weights* of AXI-REALM’s building blocks as a function of their parameters. All numbers are in GE, at 1 GHz using typical conditions.

		(i) Status	0	0	0	0	0	0	0	24.6
Registers	PUR	(i) Budget/Period	0	0	0	0	0	0	0	1320
		(i) Region Bound.	20.6	0	0	0	0	0	0	0
		(i) Config	0	0	0	0	0	0	0	83.5
Config	PU	(e) Status/Config	0	0	0	0	0	0	0	9.7
		(e) R/W Budget	0	0	0	0	0	770	0	0
		PS Bus Guard	0	0	0	0	0	0	0	261
irealm	PUR	Tracking Cnts.	0	0	0	0	0	0	0	1930
		Region Decoders	20.8	0	0	0	0	0	0	0
	PU	Isolate/Throttle	3.5	2.7	9.0	0	0	0	0	267
		Burst Splitter	49.3	1.5	729	0	0	0	0	4840
		Meta Buffer	38.1	0	0	0	0	0	0	1310
		Write Buffer	0	0	0	0	0	264	0	11.4
errealm	PU	ID Remap.	0	0	0	0	0	0	0	0
		Stage Cnts.	0	0	0	0	0	0	129	735
		HT Table	0	0	201	0	0	0	0	0
		LD Table	0	0	0	51	0	0	0	0
		R/W Table/Ctrl.	0	0	0	0	0	329	0	356
		Reset Ctrl.	0	0	0	0	0	0	0	1270

Addr Width<sup>ab</sup>   Data Width<sup>ab</sup>   Num Pending<sup>c</sup>   Num tIDs<sup>c</sup>   Buffer Depth<sup>c</sup>   Storage Size<sup>ade</sup>   Num Counters<sup>f</sup>   Counter Storage<sup>g</sup>   Constant<sup>h</sup>

<sup>a</sup> in [bit]   <sup>b</sup> evaluated 32 to 64 bit   <sup>c</sup> evaluated 2 to 16 elements   <sup>d</sup> product of *Buffer Depth* and *Data Width*  
<sup>e</sup> evaluated 256 to 8192 bit   <sup>f</sup> product of *Num Pending* and *Num tIDs*   <sup>g</sup> product of *Num Counters* and the  
 counter width (10 to 32 bit)   <sup>h</sup> base area independent of params

## 5.4 Architectural Results

This section provides an extensive area, timing, and latency model to enable quick design-space exploration and promotes fair comparison with other works. For gate-level assessment, we use GlobalFoundries’ GF12LP+ node with a 13-metal stack and 7.5-track standard cell library in the typical corner. We synthesize the designs using Synopsys Design Compiler NXT 2023.12 in topological mode to account for place-and-route constraints, congestion, and physical phenomena. We provide all area results in *gate equivalent (GE)*, a technology-independent circuit complexity metric, allowing comparisons among

technology nodes. A GE represents the area of a two-input, minimum-strength NAND gate.

### 5.4.1 Area Model

Our linear area model, given in Table 5.1, allows us to estimate a system’s AXI-REALM configuration given the number of irealm and erealm units with their respective parameters. We synthesize our AXI-REALM system to construct the model, sweeping the parameter space. The resulting areas are correlated with the input parameters, and a linear model is fitted. The model is divided into three categories: *Configuration Registers*, *irealm*, and *erealm*. Each category is grouped into the sub-categories: *per-system (PS)*, *per-unit (PU)*, and *per unit and region (PUR)*. To estimate the area of an AXI-REALM system or its components, the system’s desired configuration is determined. This includes the number of irealm and erealm units, configuration register files, and regions, as well as the IP’s desired SV parameters. The area of the individual sub-units is given by a linear function of the IP parameters with the coefficient in Table 5.1. The total AXI-REALM area can be obtained by summing over the individual sub-unit’s contributions.

We use the AXI-REALM MCS’s configuration (Table 5.2) presented in Section 5.5 as an example of how to use our model. The *bus guard* is the only PS item with a constant contribution of 261 GE. For each PU and PUR elements we evaluate

$$A_{contrib} = \sum_i param_i * weight_i + constant$$

to obtain their respective area contribution. E.g., for the *write buffer*, we multiply 264 GE with the storage size of 256 and add 11.4 GE. Our example features three irealm units, bringing the total area contribution of all *write buffers* in the AXI-REALM system to 203 kGE. The total modeled area, presented in Table 5.2, is calculated by summing all PS, PU, and PUR contributions together.

Our AXI-REALM architecture does not have inherent limitations in terms of throughput, the supported amount of tIDs, and the number of outstanding transfers as long as the units are tuned to the encompassing system and its use cases.

Table 5.2: Parametrization, the resulting modeled, and actual area of the irealm and erealm units in Carfield (Section 5.5).

Sub-system	Num. Units	Num. Regions	SystemVerilog Parameters						Model Area [kGE]	Design Area [kGE]		
<i>irealm</i>	3	2	48 bit	64 bit	16	-	4	256 bit	-	-	330	328
<i>erealm</i>	1	-	48 bit	64 bit	2	2	-	-	20	200 bit	50	45

Addr Width      Data Width      Num Pending      Num tIDs      Buffer Depth      Storage Size  
 Num Counters      Counter Storage

### 5.4.2 Timing and Latency

The AXI-REALM architecture and its units are designed to achieve clock speeds exceeding 1.5 GHz (corresponding to 25 logic levels) in GF12LP+ when combined with optimized AXI4 IPs for ASICs. The achieved frequency can be further increased at the cost of additional latency by either adding AXI4 cuts around the AXI-REALM units or introducing pipelining into the AXI-REALM units. The irealm unit adds no additional cycle of latency when bypassed and introduces one cycle through the write buffer (Section 5.3.1.2) when active. The erealm unit adds no additional latency, whether bypassed or active.

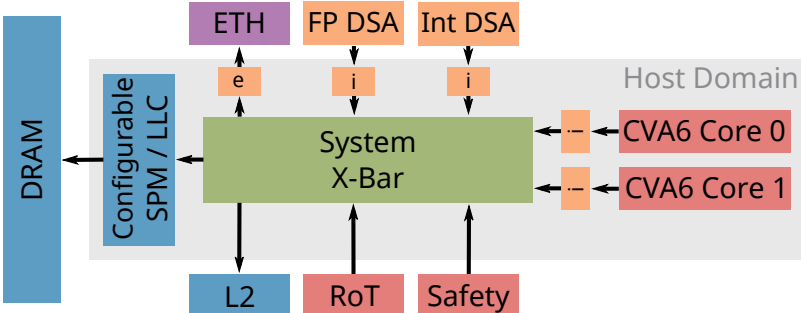


Figure 5.8: Architectural block diagram of the Carfield platform.

## 5.5 Case Study: Automotive MCS

### 5.5.1 Introduction

*Carfield* establishes a heterogeneous platform for mixed-criticality systems and application across domains like automotive, space, and cyber-physical embedded systems. At the core of Carfield, the *host* domain consists of a Linux-capable dual-core *CVA6* system enhanced with virtualization extensions, namely RISC-V's *H-extension* and virtualized fast interrupts. The platform is complemented by a *safety* and a *security* domain, allowing for reliable operation and secure boot, respectively. Carfield computational capabilities are enhanced through general-purpose DSAs. We instantiate two DSAs: one specialized for integer and one for floating-point workloads. Each accelerator features an internal DMA engine to copy data between its private SPM and the MCS's main storage. Carfield features two memory endpoints, a 512 KiB banked L2 memory and an off-chip DRAM accessed through a last-level cache (LLC). Each rank of the platform's LLC can be configured either as software-managed SPM or cache for the DRAM. All five domains are connected through a 64-bit point-to-point AXI4 crossbar.

We integrate AXI-REALM into Carfield by adding four irealm units at the crossbar's ingress of all time-critical managers the two DSAs and the two CVA6 cores. An irealm unit ensures real-time responses from the platform's Ethernet (ETH) controller, which accesses time-critical

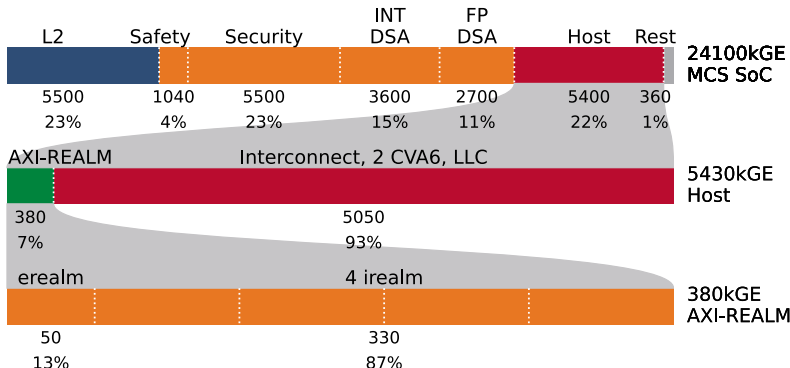


Figure 5.9: Carfield’s hierarchical area including AXI-REALM.

sensor data. Characterization in Carfield shows ETH to be prone to data loss, and it further exhibits strong fluctuations in timing behavior, thus being a representative candidate for a subordinate guarded by irealm. Figure 5.8 shows the enhanced architectural block diagram enhanced with our AXI-REALM units.

### 5.5.2 Area Impact

We synthesize Carfield with the AXI-REALM extensions in Global-Foundries’ 12 nm node using typical timing corners. Figure 5.9 presents the total SoC area of 24 MGE and the hierarchical area contributions of our units introduced. The irealm units incur a total overhead of 330 kGE, contributing 1.4% to the total area. The irealm unit uses 50 kGE (0.21%) of the SoC’s area. The parameterization of the AXI-REALM units implemented in Carfield is given in Table 5.2, Section 5.4.

### 5.5.3 Synthetic Performance Analysis of irealm

We first evaluate the functional performance of the irealm architecture using a memory-bound synthetic benchmark, which emulates the real-time-critical task, to maximize the effects of interconnect and subordinate interference between the processor cores and the platform’s

DSAs. This synthetic benchmark uses CVA6 to copy data between different memory locations while a DMA engine in one of the DSAs performs data transfer operations. The default configuration is to copy 1 KiB of data with the core from Carfield’s hybrid LLC, configured as a SPM, to L2 memory while the DSA causes interference in the SPM using long bursts of 256 beats. Large and equal budget periods as well as a fragmentation size of one are used if nothing else is specified. Results from application benchmarks are presented in Section 5.5.5.

### 5.5.3.1 Controlling Fairness: Burst Fragmentation

We configure the irealm units of CVA6 and one of the DSA to fragment transactions at different granularities without any budget limitation. For this synthetic assessment, the write buffer is disabled, as both managers are under our control, eliminating the possibility of bandwidth stealing. To simulate different DSA workloads, we vary the DMA transaction length in Figure 5.10 from 32 to 256 64-bit words. Fragmenting all beats to single-word granularity results in the best performance independent of the nature of the DMA transfer; in this setting, CVA6 achieves 68% of its isolated performance. The worst slowdown can be observed in the presence of 256-word-long bursts without fragmentation activated, which represents the unregulated case: CVA6 only achieves 1% of the isolated performance. The latency of each core access increases from 11 cycles to 266 cycles, as core transfers are interleaved by the 256-cycle-long DSA transfers.

In a second experiment, Figure 5.11, we copy data between the system’s external DRAM cached by the LLC and the L2 memory. The DSA DMA is configured to emit 256-word-long bursts at varying data set sizes. Due to conflict misses between the DSA and the core, and capacity misses when the DSA transfer size surpasses the LLC capacity, the fraction of isolated performance drops from 80% (16 kB) to 23% (64 kB) at single-word fragmentation. AXI-REALM can help mitigate interference in accessing a shared cached memory location, allowing Carfield to achieve up to 23% of the isolated performance as opposed to 4% without regulation. To improve performance further, complementary regulation strategies must be put in place for the shared LLC. For example, cache coloring or partitioning can mitigate conflict misses or DMA cache bypassing to eliminate capacity misses.

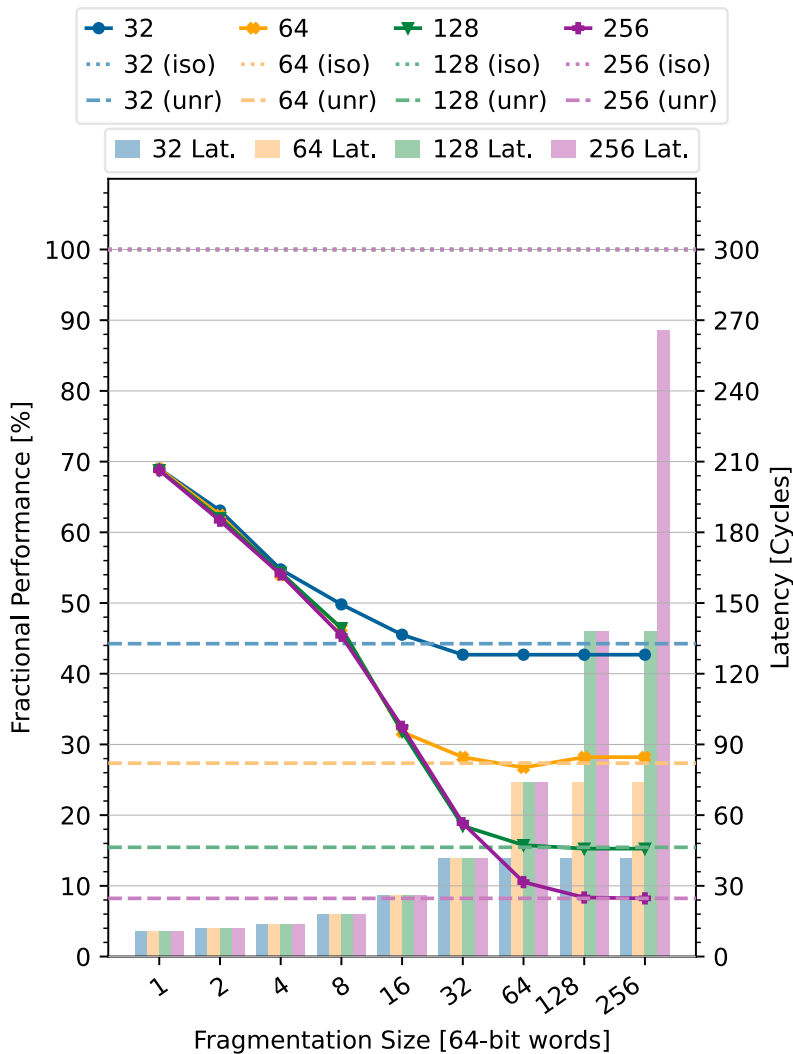


Figure 5.10: Performance results of CVA6 copying data between SPM and L2 with the DSA accessing SPM at various granularities in 64-bit beats. *iso* denotes the isolated — 100% fractional performance, *unr* the unregulated performance.

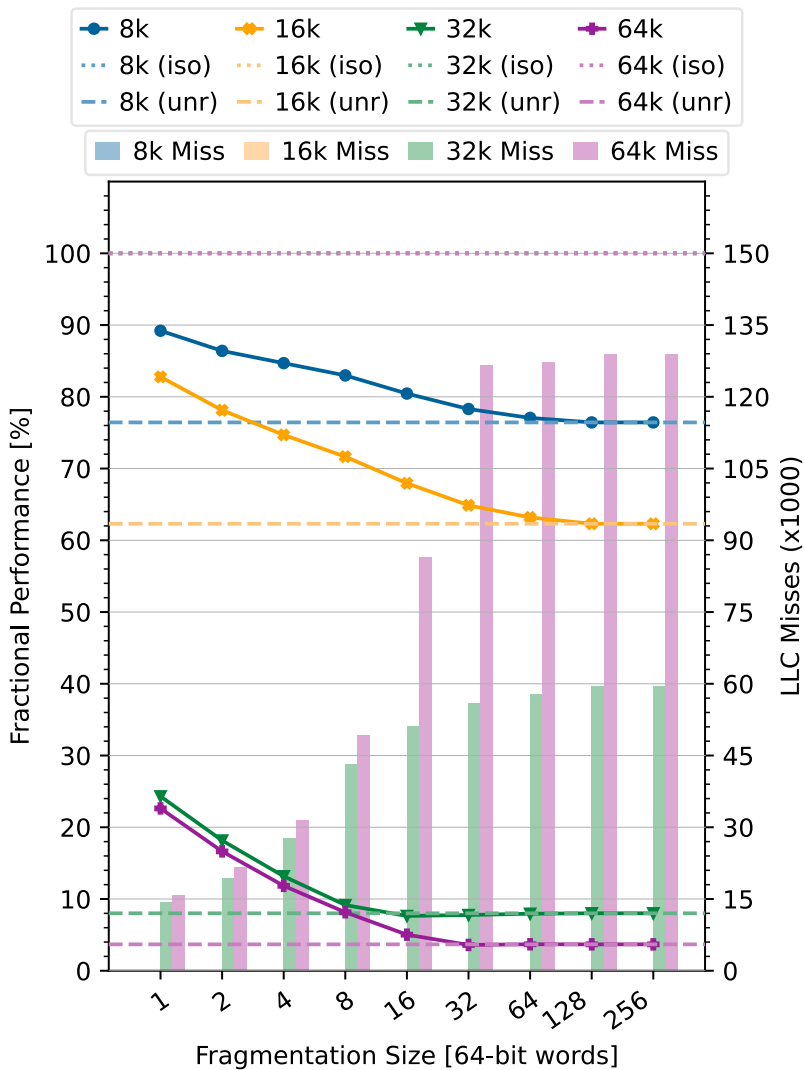
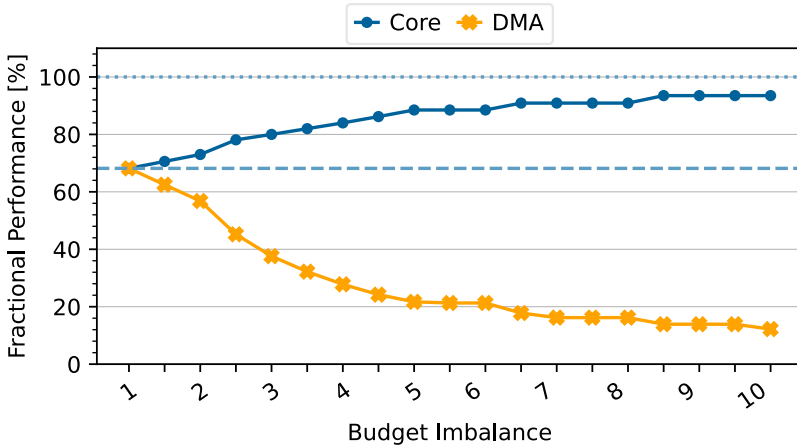
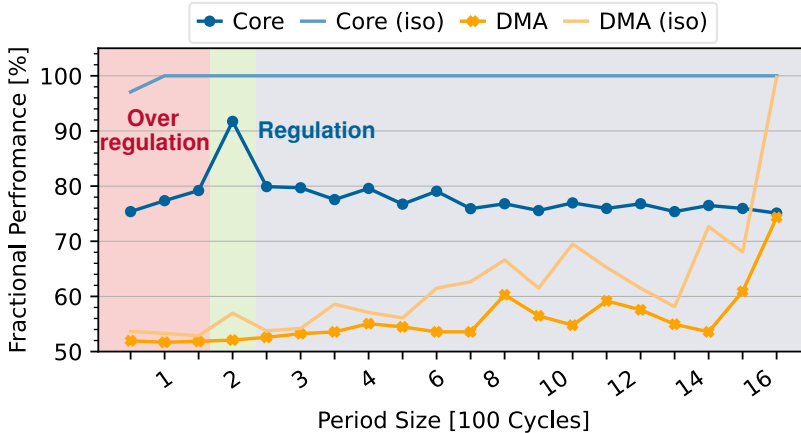


Figure 5.11: DRAM and L2 with the DSA accessing DRAM at various problem sizes in byte. *iso* denotes the isolated — 100% fractional performance, *unr* the unregulated performance.



(a) Fractional performance at different budget imbalances.



(b) Fractional performance at different period sizes.

Figure 5.12: (a) Fractional performance at different budget imbalances favoring the critical manager assuming fragmentation one and (b) fractional performance at different period sizes assuming fragmentation size one and equal budget.

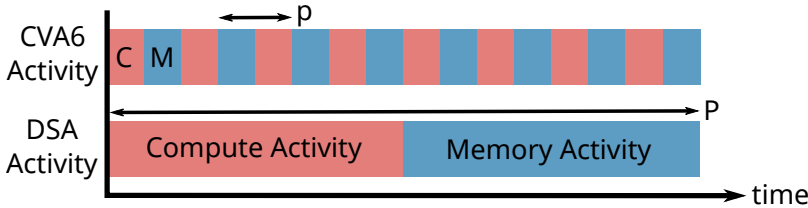


Figure 5.13: Schedule of the periodic ( $p$ ) real-time-critical transactions running on CVA6 and the data copy operation (period  $P$ ) by the DSA DMA.

### 5.5.3.2 Period and Budget Considerations

This section assesses AXI-REALM’s period and budget functionality at fixed fragmentation. In particular, we demonstrate that tuning each manager’s period and budget can prioritize traffic of certain managers over others and even increase fairness [25] further compared to solely acting on the fragmentation size. We observe that the budget imbalance favoring the real-time task restores performance up to 95% of the isolated case, at a performance detriment to the DSA DMA, see Figure 5.12a.

Similarly, the period can be used as a knob for online traffic regulation [25]. AXI-REALM does not limit the managers in how to spend the budget within each period. Larger periods introduce less regulation overhead but allow DSA managers to cause more interference. We assume the periodic execution schedule for the critical manager and the DMA DSA given in Figure 5.13. The first has a period  $p$ , 200 cycles, and the latter a period  $P$ , set to 1600 cycles. Both managers utilize the interconnect 50% within their period; for the critical manager this corresponds to 800 B in 200 cycles, for the DMA 6400 B in 1600 cycles. The corresponding irealm units are configured equally to a fragmentation size of one. The regulation time period is swept from 50 to 1600 cycles with the budget set to half the maximum transfer size possible during the regulation period. E.g., the budget for the critical manager and the DMA are set to 6400 B each when selecting a period of 1600 cycles.

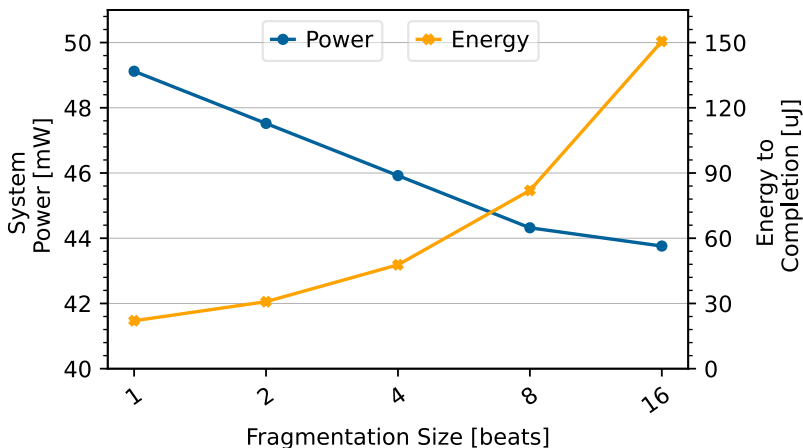


Figure 5.14: Power and energy of CVA6 copying data between SPM and L2 with the DSA accessing SPM given different fragmentation sizes.

Figure 5.12b shows the fractional performance of the DMA and the core given selected period sizes. The performance of the DMA decreases when the irealm period falls below the DMA’s period of  $P$ , regardless of whether the critical manager is active. This happens due to *overregulation* as every DMA transaction no longer fits a period, interrupting it at least once.

The critical manager nearly matches isolated memory performance — over 93% of the isolated case — when the irealm period aligns with the core’s task period of  $p$ . Below this critical period, the core’s transfer is again overregulated.

### 5.5.3.3 Power and Energy Efficiency Analysis

Section 5.5.3.1 establishes full fragmentation as the configuration achieving the best performance in the presence of DSA interference. However, fragmenting transfers to word-level accesses increases the switching activity (e.g., the address changes on every access) and, thus, the power consumed by the interconnect and the subordinate

devices. We evaluate the energy and power consumption of our synthetic benchmark running on Carfield using timing-annotated switching activity on a post-layout netlist using Synopsys PrimeTime 2022.03. We vary the fragmentation size of the irealm units from one to sixteen beats. The peak power consumed by the host domain, which includes the host, the MCS’s main interconnect, and the SPM memory, is linearly increasing with decreasing fragmentation size. When evaluating CVA6’s energy spent to copy 1 KiB of data, the energy required is minimal at a fragmentation size of one. Increasing the burst granularity increases the interference in the memory system prolonging the execution time and thus increasing energy. Even though the activity of fragmenting transactions is increasing the power consumption of the benchmark, the reduction in execution time outweighs the increase in activity, as seen in Figure 5.14.

### 5.5.4 Synthetic Performance Analysis of erealm

To evaluate the functional performance of erealm connected in front of the ETH peripheral in Carfield, we inject AXI4 transaction faults within the ETH peripheral by either delaying to accept requests or stalling responses. This behavior may occur due to a full transmission buffer or the ETH device failing to send the requested data.

We define the worst-case detection time (WCDT) as the time between the occurrence of a fault and the erealm unit detecting it. Most protocol errors, e.g., a wrong tID or a superfluous handshake, are detected instantaneously. To derive the WCDT, we thus consider a timeout event. As explained in Section 5.3.3, an AXI4 transaction is tracked in different stages, each having a dedicated time budget assigned. The WCDT is equal to the time of the largest budget configured for all stages. For most transactions, the longest stage monitors the read or write data beats (*r/w\_first to r/w\_last*), see Figure 5.6. A timeout happens when a peripheral sends the first read or write *r/w\_first* but never continues to issue any more beats; the erealm unit detects this after the stage’s budget is depleted.

In Carfield, we set the budgets for all stages, but the *r/w\_first to r/w\_last* to 20 cycles. As the ETH IP supports bursts up to 256 beats in length, we set the budget for the read and write monitoring to

300 cycles, corresponding to the WCDT of the ETH IP. Carfield implements fast virtualized interrupt support through a core-local interrupt controller, enabling best-in-class interrupt responses of 100 cycles on the CVA6 host core, ensuring quick and agile system reactions to disturbances. The worst-case latency, from the fault occurring to the core reacting, is thus at most 400 cycles. The erealm unit can be configured to automatically reset the faulty subordinate device within two cycles from fault detection, preparing it to resume operation immediately once the core is informed.

Thanks to the stage-level tracking of erealm and the fast interrupt support of Carfield, we can inform the core and reset the subordinate in as low as 100 cycles with a WCDT of 400 cycles for the ETH IP in Carfield. This response time is substantially lower than waiting for a deadline miss or a system-wide watchdog reset due to an interconnect stall from a faulty subordinate.

### 5.5.5 Case Study on Carfield

We evaluate the performance of AXI-REALM using heterogeneous benchmark applications on Carfield, as synthetic benchmarks alone do not suffice to fully characterize memory interference [30]. We combine a ML inference application running on either one or both of Carfield’s machine-learning-optimized DSAs while executing time-critical applications from *TACLeBench* [169] on the platform’s host RISC-V cores. To simulate a truly heterogeneous application including communication and coarse-grained synchronization, both the DSA and the time-critical tasks access Carfield’s shared L2 SPM memory. TACLeBench provides two real-world applications: *lift* and *powerwindow*; the first mimics the controller of an industrial elevator, the latter one of the four car windows controlled by the driver and the passenger [169].

We use AXI-REALM to control and monitor the data streams injected by the DSAs and the RISC-V cores to restore the performance of the TACLeBench applications. We keep the budget between the actors equal and large enough to restrict neither the accelerator’s DMAs nor the cores from accessing L2. We chose a reasonably small period of 100 cycles to mitigate any imbalance issues presented in Section 5.5.3.2. The fragmentation is swept between *one*, *fairest*, and *255* (no fragmentation).

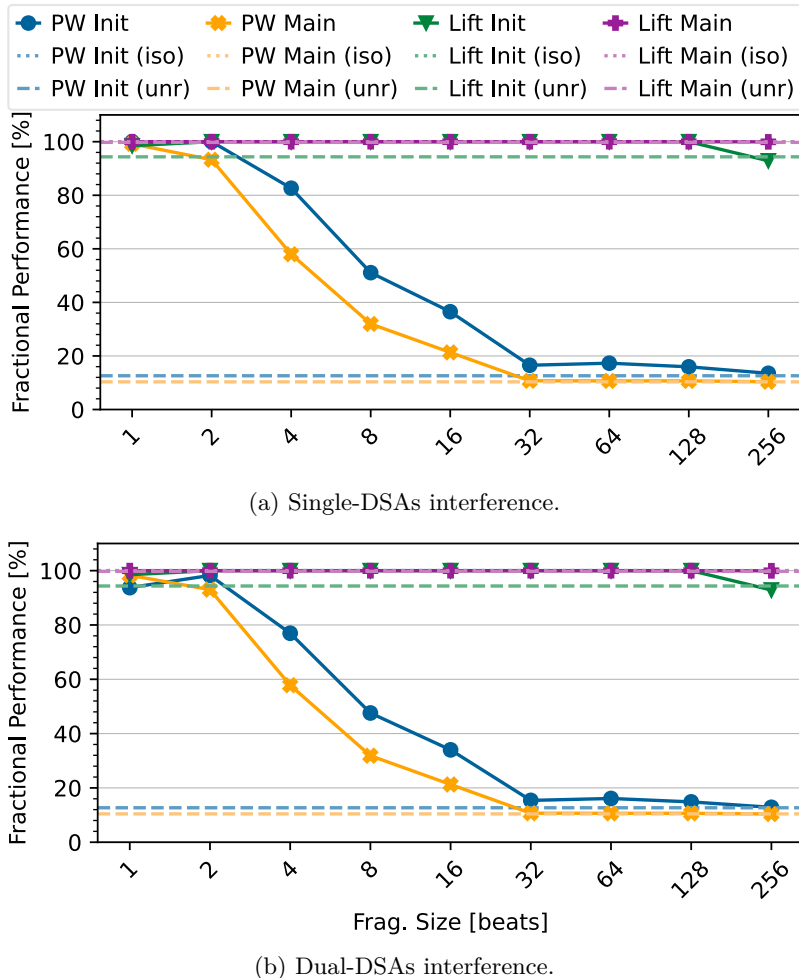


Figure 5.15: TACLeBench [169] performance of CVA6 with (a) one and (b) two DSAs interfering. A budget imbalance of 1:1 and a period longer than the application’s runtime is selected. We vary the fragmentation granularity. The applications contain an initialization, *init*, and a *main* phase. *iso* denotes the isolated, *unr* the unregulated performance.

For compute-bound applications (*lift*), we observe no interference of the DSAs with the execution of the critical program. AXI-REALM does not introduce any measurable overheads in these cases. If security is not a main concern, AXI-REALM can be rapidly disabled by the OS, see Section 5.3.4, should a non-memory-intensive task be executed on the platform, fully eliminating any dynamic power overhead of the AXI-REALM units. The *powerwindow* task faces up to  $9.7 \times$  interference from the DSAs in shared memory. (Figure 5.15). AXI-REALM reduces this delay by achieving in both cases up to 99% of isolated performance with full fragmentation.

## 5.6 Related Work

We structure AXI-REALM’s related work into two parts: Section 5.6.1 compares the irealm unit to real-time interconnects and regulation modules and Section 5.6.2 compares the erealm unit to SoA transaction monitoring units.

### 5.6.1 Real-time Extensions: irealm

The SoA of real-time interconnect extensions can be divided into two fundamental design strategies: *drop-in regulation modules*, which are integrated between the managers and the interconnect itself, or intrusive *interconnect architecture customizations*. The latter strategy profoundly changes the interconnect’s internal structure, intertwining the enhancements with a given memory system architecture and, thus, with a given system [26, 159, 167].

#### 5.6.1.1 Drop-in Regulation Modules

Credit-based mechanisms are commonly introduced at the boundary of existing interconnect configurations to impose spatial and temporal bounds on non-coherent, on-chip interconnect networks.

Pagani *et al.* and Restuccia *et al.* analyze and address the problem of multiple DSAs either competing for bandwidth or causing interference in heterogeneous, AXI4-based FPGA SoCs. They propose three units to mitigate contention. The *AXI4 budgeting unit* (ABU) [25] extends the concept of inter-core memory reservation established in multi-processor systems on chip (MPSoCs) to heterogeneous SoCs. The ABU uses counter-based budgets and periods assigned for each manager in the system, reserving a given bandwidth to each manager. The *AXI4 burst equalizer* (ABE) [162] tackles unfair arbitration by limiting the nominal burst size and a maximum number of outstanding transactions for each manager. The *Cut and Forward* (C&F) [166] unit prevents ahead-of-time bandwidth reservations by holding back transactions until they can certainly be issued. Our AXI-REALM architecture tackles these challenges while optimizing the design to be suitable for high-performance systems and use cases. AXI-REALM

adds only one cycle of latency (Section 5.3) and extremely low area overhead (Section 5.4).

Similarly to ABU, Valente et al. [170] present *Runtime Bandwidth Regulator* (RBR) implementing a bandwidth equalization mechanism using counter-based budgets and periods, targeting primarily FPGA accelerators. Our AXI-REALM provides a similar functionality, whilst additionally preventing bandwidth reservations and automatically equalizing burst lengths among all memory actors.

Farshchi et al. [171] propose the *Bandwidth Regulation Unit* (BRU), a HW module aimed at reducing the regulation overheads of SW approaches. Designed for coherent multicore SoCs, BRU manages memory traffic per core. Akin to AXI-REALM, it employs a time-slicing approach, albeit with one global period shared by all domains. The design can only regulate the maximum bandwidth, whose size is fixed to the dimension of a cache line, while the number of memory access transactions is user-configurable. Implemented in a 7 nm node, BRU adds minimal logic overhead (<0.3%) and reduces the maximum achievable frequency by <2%. Furthermore, BRU can independently control the write-back traffic to the main memory, mitigating write-read imbalances. Unlike SW techniques [172], this functionality requires significant HW modifications to the cache hierarchy. We argue that it would favor a cache-centric partitioning strategy over an auxiliary module for the system bus.

A key aspect of achieving temporal isolation for shared resources involves extracting significant data from functional units during V&V. This step is essential for determining an optimal upper limit for resource usage during operation. Cabo et al. [173, 174] propose *SafeSU*, a minimally invasive statistics unit. SafeSU tracks inter-core interference in MPSoCs using dedicated counters. Instead of limiting the number of transferred bytes, the maximum-contention control unit (MCCU) allocates timing interference quotas to each manager core in clock cycles. Whenever the allocated quota is exceeded, an interrupt is raised. SafeSU uses temporal information, including contention, request duration, and interference quota, as knobs to enhance traffic observability and enforce controllability. Furthermore, the mechanism addresses interference exclusively in symmetric, general-purpose, multicore systems. AXI-REALM leverages spatial and temporal information for traffic regulation (i.e., bandwidth reservation and time

slicing) and extends the monitoring capabilities to heterogeneous MCSSs comprising of real-time-critical, general-purpose, and high-performance domain-specific managers.

#### 5.6.1.2 Interconnect Customization

Restuccia *et al.* [159] propose *HyperConnect*, a custom AXI4-based functional unit block for virtualized FPGA-SoCs. While being the closest SoA to AXI-REALM, HyperConnect does not tackle ahead-of-time bandwidth reservation issues caused by a slow manager stalling the interconnect (Section 5.3.1.2).

Recently, Jiang *et al.* introduced *AXI-IC<sup>RT</sup>* [26], one of the first end-to-end AXI4 microarchitectures tailored for real-time use cases. AXI-IC<sup>RT</sup> leverages the AXI4 user signal to assign priorities and introduces a dual-layer scheduling algorithm for the dynamic allocation of budget and period to each manager during runtime. To prevent request starvation on low-priority managers, AXI-REALM does not depend on the concept of priority, but rather on a credit-based mechanism and a *burst splitter* to distribute the bandwidth according to the real-time guarantee of the SoC. While AXI-IC<sup>RT</sup> supports several budget reservation strategies, it limits the assessment to managers with equal credit (bandwidth). Finally, from an implementation angle, the design strategy followed by AXI-IC<sup>RT</sup> adds extensive buffering to the microarchitecture to create an observation window for early service of incoming transactions based on priorities. Overall, HyperConnect and AXI-IC<sup>RT</sup> lack monitoring capabilities to track traffic statistics.

In industry, Arm’s *CoreLink QoS-400* is widely integrated into modern FPGA-SoCs to manage contention using the QoS signal defined in the AXI4 and AXI5 specifications. However, QoS-400 has several limitations, as analyzed in [167]. One significant drawback is its intrusiveness; for instance, in a Zynq Ultrascale+ FPGA, the authors report the need to coordinate over 30 QoS points to effectively control traffic [167].

#### 5.6.2 Subordinate Guarding: erealm

All the works described in Section 5.6.1 assume *perfect* subordinate behavior, providing a response within a bounded time, and focus on

the manager side without considering malfunctioning or misbehaving subordinates. Our erealm unit tackles these challenges by monitoring and guarding subordinate devices. Transaction monitoring and guarding are crucial in studying security, performance analysis, fault detection, and system reliability. With the erealm unit, we use these established concepts in real-time memory interconnect systems.

Arm’s *SP805 Watchdog* [175] is primarily designed for fault detection and system protection by safeguarding the SoCs against SW malfunctions due to unresponsive or runaway processes. The operating system has to reset an internal counter regularly; if it becomes unresponsive, SP805 can either emit an interrupt or reset the entire system. In contrast, erealm provides a HW solution that monitors every subordinate access, reducing fault detection latency. We allow dynamic time budgeting of each subordinate device’s transaction phases and thus support tight latency bounds for each device individually. Unlike SP805, our approach allows the selective reset of the non-responsive subordinate device within a single cycle, leaving the rest of the system operational.

We identify multiple units specialized in monitoring subordinate devices. With Synopsys’ *Smart Monitor* [176] and AMD’s *AXI4 Performance Monitor* [177], industry provides performance monitoring solutions for AXI4 buses and subordinate devices. These units monitor bus traffic and compute key performance metrics, such as data byte count, throughput, and latency. In academia, Ravi *et al.* present a *Bus Monitor* [178] and Kyung *et al.* describe their *Performance Monitoring Unit (PMU)* [179] to capture key performance metrics such as transaction count, transfer size, and latency distributions for AXI4 transactions through HW counters. Compared to erealm, neither support multiple outstanding transactions nor provide detailed, *stage-specific* transaction insights. This limits their use in heterogeneous SoCs, where high-performance DSAs emit complex transactions, and detailed performance reports of individual transactions are required.

Delayed or missing responses are not the only critical fault a subordinate device can experience. Lee *et al.* [180] describe a *Reconfigurable Bus Monitor Tool Suite* for on-chip monitoring of SoCs. The suite offers a *Bus Monitor IP* designed to monitor the device’s performance and check key protocol properties. For the latter, it verifies simple specification-compliance, but unlike erealm, it does not offer any

Table 5.3: SoA comparison of AXI-REALM.

	Budget/ Time Slicing	Granularity	Fair Arbitration	Bandwidth Reservation Prevention	Manager Isolation	Statistics	Protocol Checking	Fault Handling	Multiple Outstanding Transactions	Target Technology	Area Overhead
ABU [25]	Period- Based <sup>a</sup>	One Subordinate Only	X	X	X	X	N.A.	Ideal	X	Xilinx FPGA	715 LUT <sup>b</sup> 908 FF
ABE [102]	X	N.A.	Transfer Fragmentation	X	X	X	N.A.	Subordinate Assumed	✓	Xilinx FPGA	1130 LUT <sup>b</sup> 582 FF
C&F [166]	X	N.A.	X	Write Buffering	X	X	N.A.	Ideal Assumed	N.A.	Xilinx FPGA	3088 LUT <sup>c,d</sup> 1467 FF
RBR [170]	Period- Based <sup>a</sup>	FPGA Accelerator	X	X	X	X	N.A.	Subordinate Assumed	X	Xilinx FPGA	6541 LUT <sup>e</sup> 607 FF
SaIoT [173, 174]	SW	N.A.	X	X	Bandwidth, Latency, Interference	N.A.	X	Ideal	X	Tech- Independent	83.1 kGE <sup>f,g</sup> 223 kGE <sup>h</sup>
BRU [171]	Global Period- Based <sup>a</sup>	Shared Memory	X	X	X	X	N.A.	Subordinate Assumed	✓	Tech- Independent	57.2 kGE <sup>i</sup>
Hyperconnect [159]	Period- Based <sup>a</sup>	Per Subordinate	Transfer Fragmentation	X	X	X	N.A.	Ideal Assumed	✓	Xilinx FPGA	3020 LUT <sup>j</sup> 1289 FF
AXIICar <sup>j</sup> [26]	Period- Based <sup>a</sup>	Per Subordinate	Transfer Buffering	X	X	X	N.A.	X	✓	FFGA	4745 LUT <sup>j</sup> 4184 FF
QoS-400 [167]	Proto- Based <sup>a</sup>	Subordinate	X	X	X	N.A.	N.A.	✓	✓	Tech- Independent	N.A.
SPI805 [175]	N.A.	Entire System	N.A.	X	X	X	X	IRQ, Global Reset	X	Tech- Independent	N.A.
Synopsis [176]	N.A.	Subordinate	N.A.	X	X	X	X	N.A.	X	Tech- Independent	N.A.
AMD [177]	N.A.	Subordinate	N.A.	X	X	X	X	N.A.	X	Tech- Independent	N.A.
Ravi <i>et al.</i> [178]	N.A.	Subordinate	N.A.	X	X	X	X	N.A.	X	Tech- Independent	8.86 kGE <sup>k</sup>
Kyung <i>et al.</i> [179]	N.A.	Subordinate	N.A.	X	X	X	X	N.A.	X	FFGA Platform	N.A.
Lee <i>et al.</i> [180]	N.A.	Subordinate	N.A.	X	X	✓	✓	Longing- Only	X	Tech- Independent	70.7 kGE
AXIChecker [181]	N.A.	Configurable Subordinate Regions	Transfer Fragmentation	Write Buffering	Per Manager	Per- Region Bandwidth, Latency	N.A.	Per-Subordinate Reset	✓	Tech- Independent	As Low As 5 kGE
realm AXI-REALM / Ours <sup>l</sup>	Period- Based <sup>a</sup>	Subordinate Per	N.A.	N.A.	X	Performance	X	Reset	✓	assuming 0.087 48 $\mu\text{m}^2$ for 1 GE assuming 0.718 $\mu\text{m}^2$ for 1 GE	As Low As 15 kGE
realm										bSafeSU-2	assuming 0.087 48 $\mu\text{m}^2$ for 1 GE (bSafeSU-1, bSafePT-75k-N)

<sup>a</sup> in hardware<sup>b</sup> Xilinx Zynq-7020<sup>c</sup> Xilinx ZCU102<sup>d</sup> C=4<sup>e</sup> assuming 0.718  $\mu\text{m}^2$  for 1 GE<sup>f</sup> assuming 1.28  $\mu\text{m}^2$  for 1 GE<sup>g</sup> Xilinx XCZ109EG<sup>h</sup> assuming 0.087 48  $\mu\text{m}^2$  for 1 GE<sup>i</sup> assuming 0.087 48  $\mu\text{m}^2$  for 1 GE<sup>j</sup> Xilinx VC709

protection in multi-ID scenarios with multiple outstanding transactions, e.g., tID mismatch. Chen *et al.* developed *AXIChecker* [181], a rule-based, synthesizable protocol checker enforcing 44 rules ensuring managers and subordinates operate protocol-compliant. Compared to *realm*, it can log protocol issues but lacks performance monitoring and reaction capabilities.

### 5.6.3 Final Remarks: AXI-REALM

A distinctive aspect of *AXI-REALM* is in its modular design. It seamlessly combines ingress monitoring and throttling to ensure real-time behavior across managers with egress monitoring and guarding to guarantee timely responses from subordinate devices. Its transparent and modular design requires minimal changes to the system, and its compatibility with many well-tested, silicon-proven crossbars and interconnects eases integration and verification. Most SoA solutions explicitly restrict the design and evaluation on FPGA platforms, lacking support for ASICs. Our technology-independent approach provides in-system and IP-level gate-level characterization in a modern technology node, facilitating SoA comparisons.

## 5.7 Conclusion and Summary

In this chapter, we present AXI-REALM a lightweight, minimally invasive, architecture-independent, open-source interconnect extension to enable real-time behavior in high-performance interconnects used in heterogeneous systems.

The irealm unit offers an effective solution for monitoring and moderating manager traffic during interference scenarios on a shared interconnect. It provisions isolation and enforces real-time guarantees to managers executing critical tasks in heterogeneous systems. Integrated into Carfield, an open-source MCS research platform, we achieve 68% of the ideal performance in memory-bound applications, massively reducing the memory access latency by  $24 \times$ , while incurring less than 2% of additional area. When distributing the budget in favor of the core, we achieve over 95% of the isolated performance. Running applications from TACLeBench, we achieve over 98% of the isolated performance.

With the irealm unit, we include an effective HW-based solution to gracefully handle malfunctioning subordinates individually without stalling or locking the rest of the interconnect or the system. The unit monitors the transaction latency and protocol correctness of each guarded subordinate, being able to inform the application-class core in as low as 100 cycles, handshake open transaction, and reset the device should a transaction be overly delayed or the subordinate malfunctioning ensuring timely responses and real-time guarantees.



# Chapter 6

# Conclusions and Future Directions

## 6.1 Summary and Main Results

In my thesis titled *Development of an Energy-Efficient and Real-Time Data Movement Strategy for Next-Generation Heterogeneous Mixed-Criticality Systems*, we firstly tackle efficient, agile, and high-performance data movement in heterogeneous systems by presenting a modular and highly customizable DMA architecture, *iDMA*, applicable across the entire compute continuum and serving the diverse needs of today’s heterogeneous platforms. Secondly, we elaborate how we integrate our DMA architecture in a wide range of systems and how we enhance our architecture with multiple extensions, further accelerating DMA transfers and increasing their efficiency. In multiple case studies, we show the applicability and the benefits of *iDMA* in silicon-implemented systems and across the entire compute continuum, including an application-grade Linux-capable SoC, an energy-efficient multicore compute cluster, and an automotive-grade MCS, each introducing its own *iDMA* extension tailored to the system’s use case. We then explored the integration and use of *iDMA* as an agile, tightly coupled data movement accelerator in a scaled-out manycore system optimized for massive floating-point compute. Finally, we

introduce *AXI-REALM*, a modular interconnect extension, tackling the predictability problem arising in heterogeneous MCS running real-time-critical applications in the presence of DMA transfers originating from domain-specific accelerators.

We summarize the key achievements below:

**Modular DMA Architecture** We first design a modular and highly versatile DMA architecture, called iDMA, which can be used in applications ranging from simple and dedicated I/O-DMAs controlling autonomous data transfer for peripherals to high-performance multi-channel engines providing massive throughput at near-ideal bus utilization with minimal latency overheads of only one to two cycles. With the key insight in mind, that most commonly used on-chip interconnect protocols share a byte-addressed data stream, iDMA is designed to support five industry-grade protocols, translating seamlessly between them, facilitating iDMA’s integration in heterogeneous SoCs. Our architecture enables the creation of both ultra-small iDMA engines incurring less than 2 kGE, as well as large high-performance iDMA engines running at over 1 GHz on a 12 nm node. Flexibility and parameterization allow us to create configurations that achieve asymptotically full bus utilization and can fully hide latency in arbitrary deep memory systems while incurring less than 400 GE per trackable outstanding transfer. In a 32-bit system, our iDMA engines achieve almost perfect bus utilization for 16 B-long transfers when accessing an endpoint with 100 cycles of latency.

**Architectural DMA Extensions** We integrate iDMA in a wide range of systems, ranging from ULP to HPC use cases, covering a large set of application scenarios and proving the applicability of the architecture. As part of these integration efforts, we develop three different system bindings for iDMA: a simple configuration-register-based interface, a Linux-capable transfer-descriptor-based scheme, and an agile RISC-V-compliant instruction-based front-end. Integrated in Cheshire, our Linux-capable SoC platform [60], we achieve  $1.66 \times$  less latency, increasing bus utilization by up to  $2.5 \times$  in an ideal memory system with 64-B transfers, overall requiring 11% fewer LUT and 23% fewer FF without requiring any block RAMs compared to Arm’s

LogiCore DMA IP [102]. In deep memory systems, we show an even more significant increase in the utilization of  $3.6 \times$  with 64-B transfers.

To accelerate commonly occurring transfer patterns, we develop a set of DMA extensions facilitating data orchestration by handling N-D tensor transfers, and scheduling of real-time transfers directly in hardware. We further include a standardized interface in iDMA’s data path to integrate in-stream operations. Finally, we develop a stream-optimized MMU to be integrated into iDMA, allowing the DMA to autonomously handle VM in conjunction with an application-grade host. Equipped with our N-D tensor mid-end and our light-weight register-based front-end, our iDMA engine almost fully utilizes the bandwidth to the L2 and TCDM in both directions in PULP-open: measuring with the on-board timer, a transfer of 8 KiB from the cluster’s TCDM to L2 requires 1107 cycles, of which 1024 cycles are required to transfer the data using a 64-bit data bus. Our multi-channel extensions show performance improvements in memory-bound kernels like vector addition and the dot product, which are dominated by the data transfers and reach speedups of  $15.7 \times$  and  $15.8 \times$ . From FPGA profiling runs, we find that our real-time sensor DMA (sDMA) engine saves about 2200 execution cycles every scheduling period, thus increasing the slack of the PVCT task. In the case of eight events and sixteen outstanding transactions, our sDMA unit is about 11 kGE in size, accounting for an area increase of only 0.001% of the original ControlPULP’s area. Enhancing our DMA architecture with VM support with our sMMU requires 8.1 kFF and 9.0 kLUT whilst not impacting the critical path of the SoC. Copying transfers of varying length, sMMU can achieve in excess of 99% of the non-translated performance when issuing 4-kB-sized transfers.

**Communication Processor** We combine iDMA with a tiny 20 kGE RISC-V processor tightly coupled through our instruction-based system binding, creating an agile communication processor capable of complex data scheduling and orchestration. We integrate this communication processor into a compute-cluster-based accelerator architecture with a focus on an optimal connection between the DMA engine and the cluster-local scratchpad memory. This cluster architecture is then scaled out to a 432-core dual-chiplet manycore system featuring

fourteen iDMA engines and 16 GiB of HBM2E memory connected through a hierarchical crossbar-based point-to-point interconnect. For the highly compute-bound GEMM, our iDMA engines enable moderate, but significant speedups of  $1.37 \times$  to  $1.52 \times$  increasing peak HBM read bandwidth from 17 to 26 GB/s. For SpMV performance, our cluster-level iDMA engines approach the wide interconnect peak throughput of 384 GB/s, overall enabling significant speedups of  $5.9 \times$  to  $8.4 \times$ . SpMM is similar to SpMV, but enables on-chip matrix data reuse, becoming compute-bound for both the baseline and iDMA engines, still achieving speedups of  $2.9 \times$  to  $4.9 \times$ .

**Real-time Interconnect Extensions** With an efficient DMA engine developed and its integration into multiple systems studied, we shift focus towards the host by investigating real-time data transfers in heterogeneous MCSs, which become increasingly important with the advent of AI-driven applications in automotive and aeronautical use cases. We develop AXI-REALM, a lightweight and interconnect-agnostic helper-module-based architecture to modulate the amount of data managers can inject into the shared interconnect. This is especially important, as iDMA-equipped accelerators are tuned for maximal bandwidth efficiency through long data bursts, which can, if kept unregulated, lead to adverse performance of time-critical applications running on the host cores. Integrated into Carfield, an open-source MCS research platform, we achieve 68% of the ideal performance in memory-bound applications, massively reducing the memory access latency by  $24 \times$ , while incurring less than 2% of additional area. When distributing the budget in favor of the core, we achieve over 95% of the isolated performance. Running applications from TACLeBench, we achieve over 98% of the isolated performance. introducing the erealm units to monitor the transaction latency and protocol correctness of each guarded subordinate, being able to inform the application-class core in as low as 100 cycles, handshake open transaction, and reset the device should a transaction be overly delayed or the subordinate malfunctioning, we can ensure timely responses and real-time guarantees.

These contributions address pressing challenges in designing energy-efficient and high-performance real-time memory systems for heterogeneous MCSs required to carry the next generation of cyber-physical systems.

A large portion of this work has been contributed to the European Processor Initiative (EPI) project<sup>1</sup>. An even larger portion of this work has been silicon-proven in a wide range of tapeouts, see Chapter A, providing an energy-efficient and high-performance data movement solution. To allow anyone to make use of this work, all design files and many ASIC implementations are freely available under a libre license<sup>2</sup>.

---

<sup>1</sup><https://www.european-processor-initiative.eu>

<sup>2</sup><https://github.com/pulp-platform>

## 6.2 Outlook

This thesis lays the groundwork for multiple future research directions. Thanks to the open-source nature of this work and our detailed OOC models of our architectural components, we provide a strong baseline for broader adaptations of our ideas.

**Reliable Data Movement** With Chapter 5, we present a light-weight interconnect extension to enable high-performance real-time interconnect architectures in MCSs, which is a fundamental requirement to adopt zonal and domain architectures in next-generation ACES-enabled SDVs. To expand our systems to include aerospace applications, tackling reliable transfer becomes a core necessity. Our iDMA architecture can be expanded to not only feature error handling, but also complete data integrity checks and perform, if required, retransmission of erroneous data transfers. With our ability to support multiple read and write ports with iDMA, we could read data from multiple sources, and add an in-stream accelerator to check the data's integrity and add redundant data before sending it over our high-performance, real-time-enabled interconnect.

**Extend the Concept of an Intelligent DMA Engine** Integrated in our Snitch cluster and coupled with our data movement core, our iDMA engine becomes a data movement accelerator allowing us to efficiently perform complex and even data-dependent transfer patterns. Still coupled to a Snitch core, but outside a compute-cluster, iDMA could truly become an intelligent data mover. Coupled with in-stream accelerators, e.g., matrix transposition units, such a unit could be programmed using high-level API calls and complete complex DMA transfers autonomously as a service.

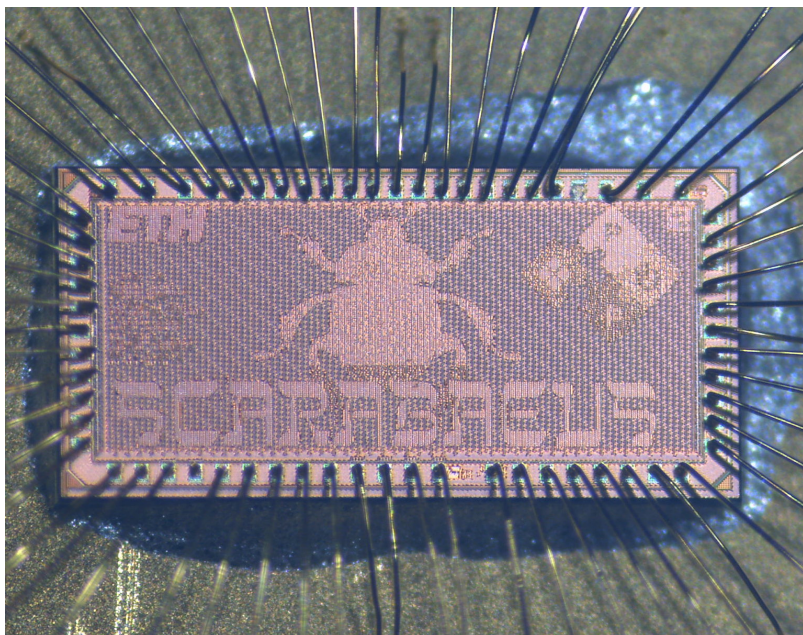
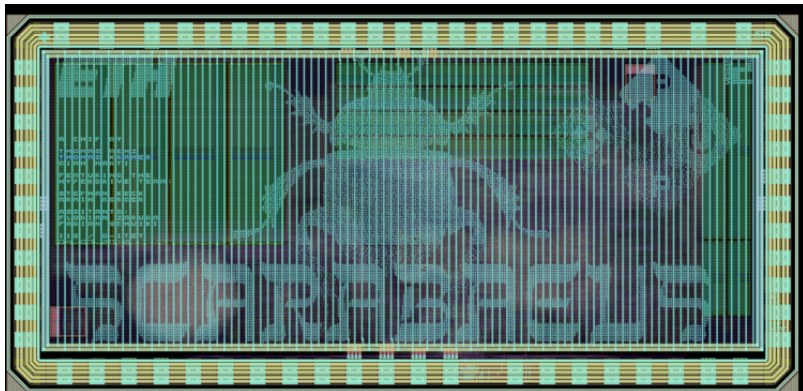
**Scaling-out of an AXI-REALM System** Chapter 5 focuses enhancing high-performance on crossbar-based point-to-point interconnects with real-time guarantees. Future work could tackle a fully scaled-out MCS using a NoC-based interconnect. AXI-REALM is designed to fundamentally be compatible with AXI4-based NoCs, but work is needed to evaluate our ideas in such distributed contexts.

# Appendix A

## Chip Gallery

This appendix lists all fabricated chips the author has contributed to, in both the form of technical work or supervision. A complete, up-to-date list can be found online at: [http://asic.ethz.ch/authors/Thomas\\_Benz.html](http://asic.ethz.ch/authors/Thomas_Benz.html).

## A.1 Scarabaeus



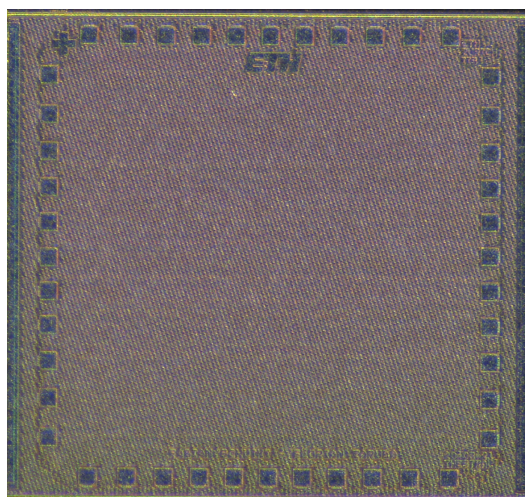
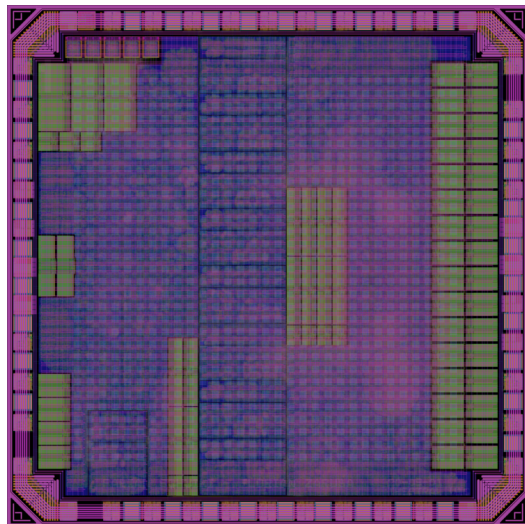
Name	Scarabaeus
Designers	<b>Thomas Benz</b> , Thomas Krammer, Gian Marti, Stephan Keck, Armin Berger, Fabian Schuiki, Florian Zaruba
Application / Publication	PULP Student MCU
Technology / Package	UMC65 / QFN56
Dimensions	2.626 mm $\times$ 1.252 mm
Circuit Complexity	1200 kGE
Voltage	1.2 V
Power	45.97 mW @ 1.2 V and 200 MHz
Clock Frequency	200 MHz

Specifically Crafted Acronym Referencing an Ariane in a Brilliantly and Artistically Engineered Unprecedented SoC (Scarabaeus), affectionately named after a *Dung Beetle*, implements an Ariane-based [182] RISC-V (RV64IMC) SoC including a 64 KiB L2 memory, and a 4 KiB data and instruction cache. In this project, we extend the existing PULP modules by a PLIC as specified by the RISC-V standard, and by a DMA controller that is capable of transferring arbitrarily shaped, aligned and strided data of up to 4-D on a 64-bit AXI4 bus.

The chip also includes a *HyperBus* controller, rewritten from scratch, and supporting *Cypress HyperRAM* [128] chips. This interface contains thirteen I/O pads occupies the lower side of the chip. The control logic has been placed between the pads and occupies less than 10 kGE including clock synchronization between two independent clock domains (*HyperBus* runs at 166 MHz and the SoC at 200 MHz). When operating with long data bursts, we achieve an effective bandwidth of 327 MB/s.

The chip further includes several peripherals, a JTAG debug module for programming, eight GPIOs, and an UART. Finally the chip contains an 8-bit RISC processor called fiercely immature, risky, empirically obscure, radical eastereg (Fireore). Fireore uses the AetherOre eXecutable version 01 (AOX-01) instruction set architecture, which specifies a four-class reduced instruction set with three 8-bit special-purpose registers.

## A.2 Thestral



Name	Thestral
Designers	Fabian Schuiki, Florian Zaruba, <b>Thomas Benz</b> , Paul Scheffler, Wolfgang Roenninger
Application / Publication	PULP SoC / Benz <i>et al.</i> [59]
Technology / Package	GF22 / QFN40
Dimensions	1.25 mm × 1.25 mm
Circuit Complexity	6 MGE
Voltage	0.8 V
Clock Frequency	650 MHz

Thestral is a small test chip implementing our Snitch compute cluster architecture [139]. Snitch is centered around a small 32-bit RISC-V (RV32IMAF) core coupled to a capable 64-bit FPU subsystem optimized for stream processing.

The chip contains our next *Snitcholution (Snitch evolution)* with architectural improvements and fine-grain power gating infrastructure. Notable changes compared to the system in *Baikonur* [183] are:

- Thestral features 20 different power domains. Each FPU/integer processing unit (IPU), as well as the cluster, can be individually power gated.
- Double-pumped FPUs and IPUs. The compute units (and the TCDM) can be operated at twice the integer core speed, allowing for higher peak throughput.
- SV32 VM support
- More accurate L1 instruction cache prefetching
- Thestral is the first silicon demonstrator including iDMA

Thestral's architecture features one governor core with its private FPU, IPU, TCDM, and L1 instruction cache. The governor manages the SoC, by controlling the system iDMA and the chip's fine-grain power management.

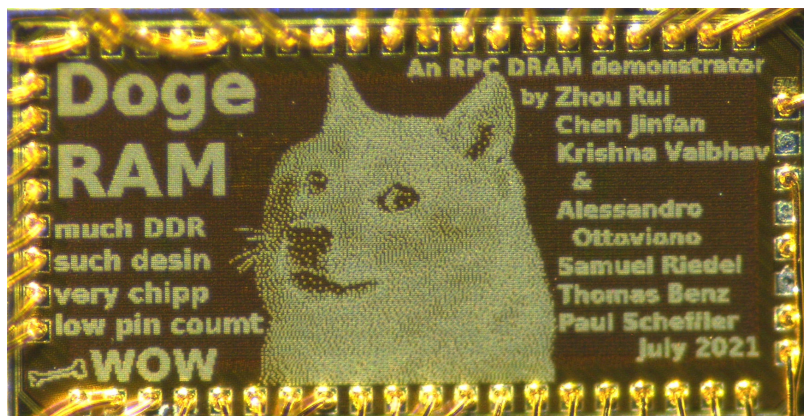
The primary compute is provided by a Snitch cluster consisting of eight cores, each coupled to a FPU and a IPU subsystem accessing a 64 KiB TCDM.

Additional peripherals such as *HyperBus*, a fully digital serial link, *USB device*, and *I<sup>2</sup>C* provide enough infrastructure to operate the chip stand-alone. 24 KiB LLC are used to reduce expensive off-chip accesses to the *HyperBus* device.

Thestral is the third chip in our Snitch-based systems, following *Billywig* and *Baikonur* [183], the latter includes three clusters and one governor. The naming continues our tradition naming chips after beasts from the *Harry Potter* universe. As described in the *Harry Potter Fandom wiki*, a *Thestral* can only be seen by people who've seen death, or in our case, dead chips.



### A.3 Dogeram



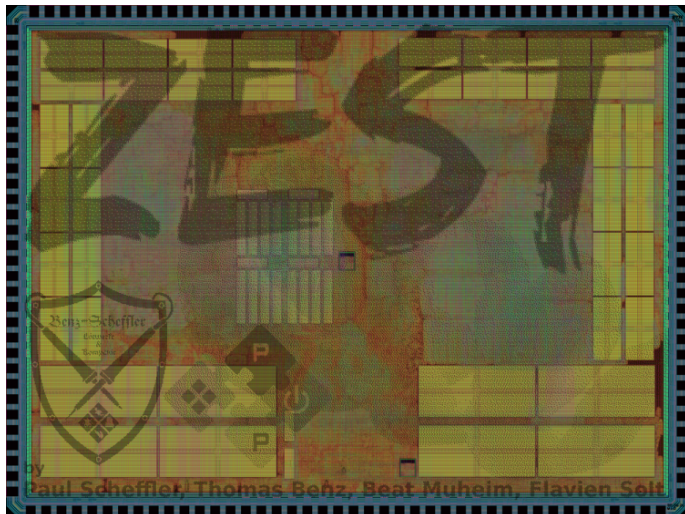
---

Name	Dogeram
Designers	Rui Zhou, Jinfan Chan, Vaibhav Krishna, Alessandro Ottaviano, Samuel Riedel, <b>Thomas Benz</b> , Paul Scheffler
Application / Publication	PULP Student MCU / Ottaviano <i>et al.</i> [60]
Technology / Package	TMSC65 / QFN56
Dimensions	2 mm × 1 mm
Voltage	1.2 V
Clock Frequency	200 MHz

---

DogeRAM is a chip to test our newly developed RPC DRAM interface, which is connected over the system’s AXI4 crossbar to a minimal two-core Snitch-based PULP SoC. At 200 MHz (at worst case conditions), the chip achieves up to 751.5 MB/s throughput over the RPC DRAM interface. The name captures a bit the Zeitgeist and is a play on the meme culture.

## A.4 Zest



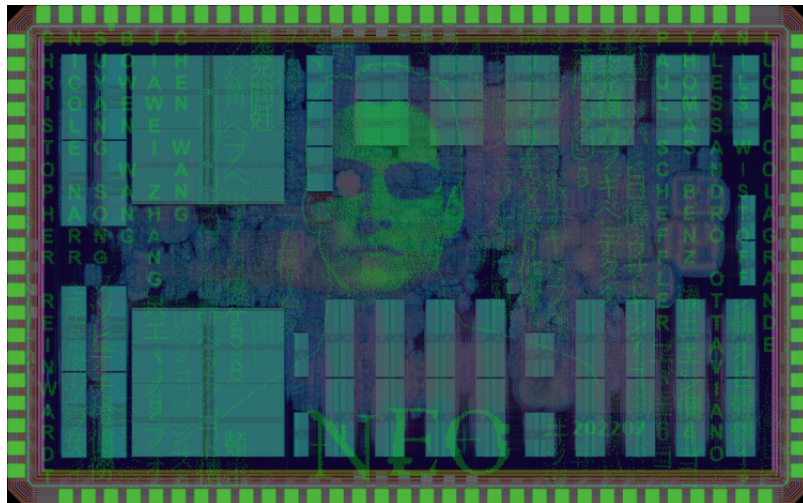
Name	Zest
Designers	Flavien Solt, <b>Thomas Benz</b> , Paul Scheffler, Beat Muheim
Application / Publication	PULP Student SoC
Technology / Package	TMSC65 / QFN88
Dimensions	4 mm × 3 mm
Circuit Complexity	6 MGE
Voltage	1.2 V
Clock Frequency	230 MHz

Zest is the first SoC of our group featuring a Snitch and a PULP clusters in one SoC. It also demonstrates the *Fenrir peripheral system*, a predecessor to the I/O-DMA, presented in Section 3.6, supporting *UART*, *I2C*, *QSPI*, *Camera interface*, and *DVSI event camera link*. Zest additionally features a *HyperBus* controller and a custom double data rate serial link. As a result of all these additions, it uses a rather large QFN88 package.

In total Zest has eight *RI5CY* cores connected to a 128 KiB TCDM memory, *4+1* Snitch cores in their own cluster with 128 KiB TCDM, and an additional 256 KiB of shared memory for both clusters.

There is an orange peel on the logo as a play on the name Zest.

## A.5 Neo



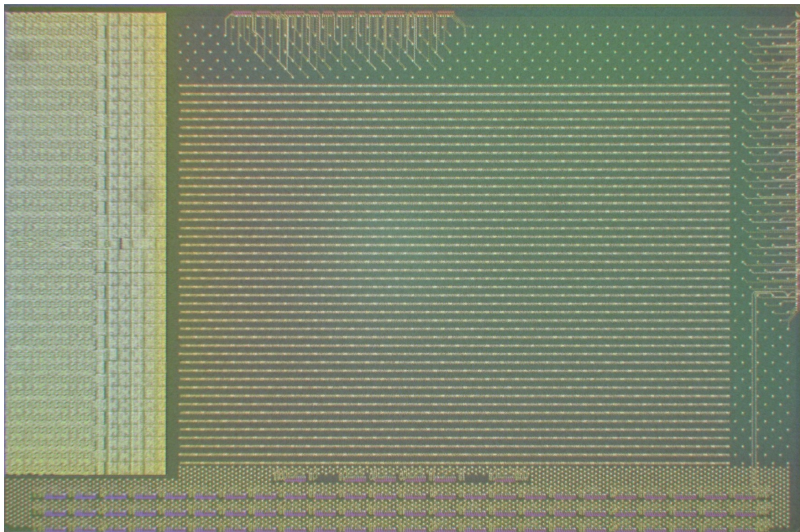
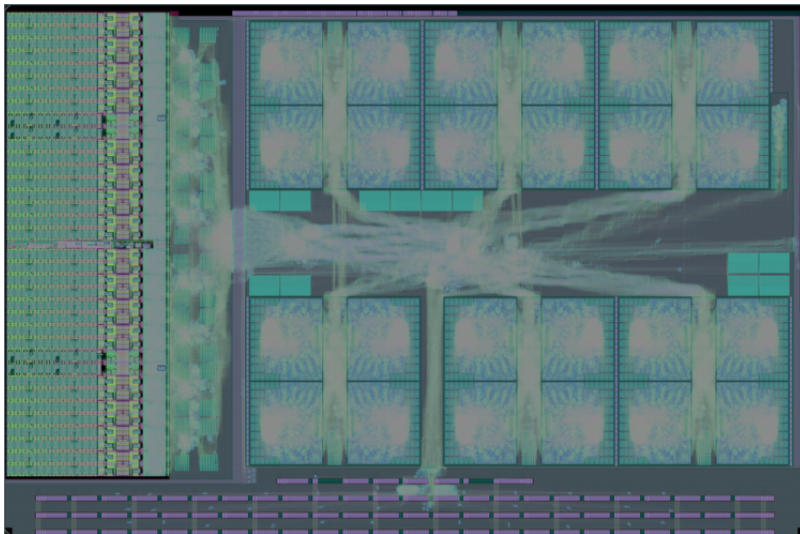
Name	Neo
Designers	Christopher Reinwardt, Nicole Narr, Suyong Song, Bowen Wang, Jiawei Zhang, Chen Wang, Paul Scheffler, <b>Thomas Benz</b> , Alessandro Ottaviano, Nils Wistoff, Luca Colagrande
Application / Publication	PULP Student SoC / Ottaviano <i>et al.</i> [60]
Technology / Package	TMSC65 / QFN64
Dimensions	3.2 mm × 2 mm
Circuit Complexity	2500 kGE
Voltage	1.2 V
Power	65 mW @ 1.2 V and 200 MHz
Clock Frequency	200 MHz

Neo is the first design that integrates a Linux-capable RISC-V core - the well-known Ariane (CVA6) - with an enhanced RPC DRAM memory controller for off-chip communication and peripherals to form an SoC capable of booting Linux.

In addition, a new VGA controller allows to drive VGA displays, and its functionality has been proven by emulating the design on an FPGA before chip tapeout. The RPC controller is fully AXI4-compliant, which makes it stand as a reusable IP, that allows off-chip communication with 700 MiB/s bandwidth while preventing an explosion in the number of off-chip memory pins.

The name of the chip was supposed to be *Neo-Scarabaeus* as a follow up chip to *Scarabaeus* which had a similar goal. The name was just a bit too long, and we ended up keeping the Neo part. Once the name stuck like that, the logo followed as well.

## A.6 Occamy



Name	Occamy
Designers	Gianna Paulin, Florian Zaruba, Fabian Schuiki, Stefan Mach, Manuel Eggimann, Matheus Cavalcante, Paul Scheffler, Yichao Zhang, Tim Fischer, Nils Wistoff, Luca Bertaccini, <b>Thomas Benz</b> , Luca Colagrande, Alfio Di Mauro, Andreas Kurth, Samuel Riedel, Noah Huetter, Gianmarco Ottavi, Zerun Jiang, Beat Muheim, Frank K. Gurkaynak, Davide Rossi, Luca Benini
Application / Publication	PULP HPC / Scheffler <i>et al.</i> [69]
Technology / Package	GF12 / LGA2011
Dimensions	10.5 mm × 6.95 mm
Circuit Complexity	600 MGE
Voltage	0.8 V
Power	10 W @ 0.8 V and 1 GHz
Clock Frequency	1 GHz

Occamy is a research prototype to demonstrate and explore the scalability, performance, and efficiency of our RISC-V-based architecture in a 2.5D- integrated chiplet system showcasing GlobalFoundries' technologies and their IP ecosystem, as well as Rambus' and Micron's HBM2E IPs.

The Occamy project started as a serendipitous outcome of the *Manticore* [183] high-performance architecture concept we presented at the Hot Chips symposium in 2020. After Hot Chips 2020, the PULP platform team was approached by GlobalFoundries with an exciting proposal to turn a concept architecture into a real silicon design. The project was made possible by the generous contribution and strong support of GlobalFoundries (technology access, expert advice, ecosystem enablement, and silicon budget), Rambus (HBM2E controller IP and integration support), Micron (HBM2E DRAM supply and integration support), Synopsys (electronic design automation (EDA) tool licenses

and support) and Avery (HBM2E DRAM verification model). We kick-started the Occamy project on the 20th of April 2021 and taped out the compute chiplet in GlobalFoundries’ 12 nm FinFet technology in July 2022 after less than 15 months of hard work with a team of less than 25 people.

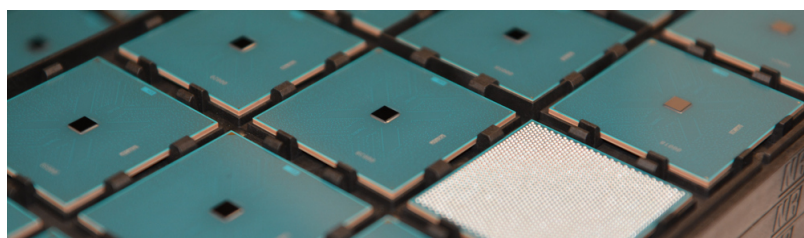
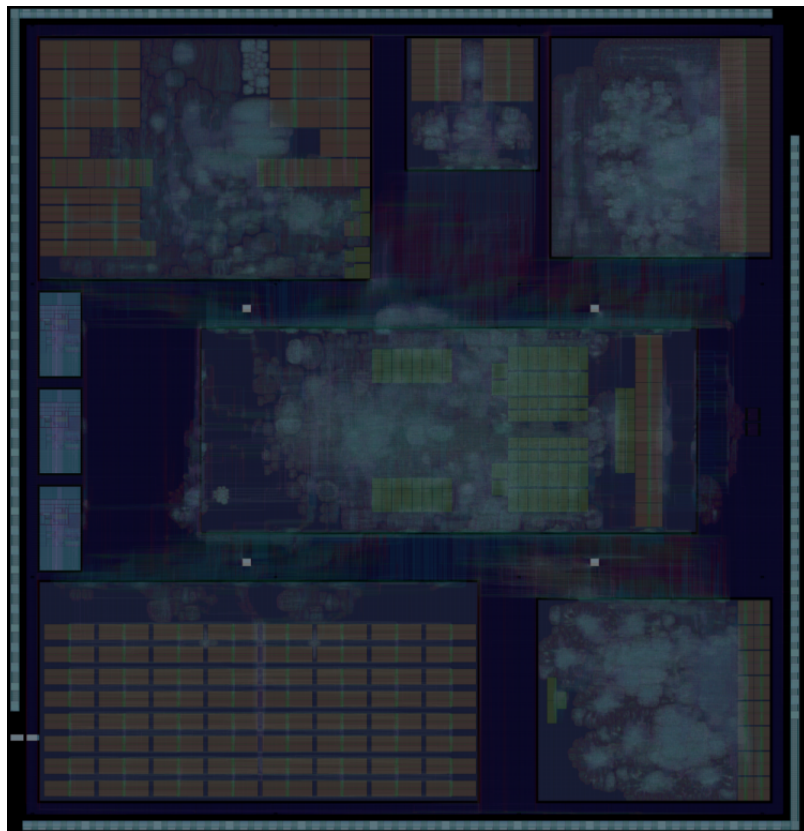
In this work, we combine a small and super-efficient, in-order, 32-bit RISC-V integer core called Snitch with a large multi-precision-capable FPU subsystem enhanced with SIMD capabilities. In addition to the standard RISC-V FMA instructions, the two 8-bit and two 16-bit floating-point (FP) formats have the new expanding sum-dot-product and three-addend summation (*exsdotp*, *exvsum*, and *vsum*) instructions.

To achieve ultra-efficient computation on data-parallel *FP* workloads, two architectural extensions are exploited: data-prefetchable register file entries and repetition buffers. The corresponding RISC-V ISA extensions stream semantic registers (SSRs) and floating-point repetition (FREP) enable the Snitch core to achieve FPU utilization higher than 90% for compute-bound kernels.

Each Occamy chiplet contains 216 Snitch cores organized in six groups of four compute clusters. Each cluster shares a TCDM among eight compute cores and a high-bandwidth (512-bit) DMA-enhanced core orchestrating the data flow, see Chapter 4. An AXI4-based wide, multi-stage interconnect and dedicated iDMA engines help manage the massive on-chip bandwidth. A CVA6 Linux-capable RISC-V core manages all compute clusters and system peripherals. Each chiplet has a private 16 GiB HBM2E and can communicate with a neighboring chiplet over a 8 GB/s wide, source-synchronous technology-independent die-to-die DDR link. The dual-chiplet Occamy system achieves a peak performances of 0.768 TFLOP/s for FP64, 1.536 TFLOP/s for FP32, 3.072 TFLOP/s for FP16/FP16alt, and 6.144 TFLOP/s for FP8/FP8alt.



## A.7 Carfield



Name	Carfield
Designers	Angelo Garofalo, Alessandro Ottaviano, Matteo Perotti, Robert Balas, Yvan Tortorella, Michael Rogenmoser, Chi Zhang, Luca Bertaccini, Nils Wistoff, Maicol Ciani, Thomas Benz, Cyril Koenig, Luca Valente, Mattia Sinigaglia, Paul Scheffler, Manuel Eggimann, Matheus Cavalcante, Beat Muheim, Zerun Jiang, Davide Rossi, Frank K. Gurkaynak, Luca Benini
Application / Publication	PULP MCS / Garofalo <i>et al.</i> [68]
Technology / Package	Intel16 / BGA1733
Dimensions	4.085 mm × 3.922 mm
Circuit Complexity	70 MGE
Voltage	0.8 V
Power	450 mW @ 0.8 V and 600 MHz
Clock Frequency	600 MHz

Carfield is our first prototype in Intel’s 16 nm FinFet technology of our open-research platform for safety, resilient and time-predictable systems.

The rapid evolution of AI algorithms, the massive amount of sensed data and the pervasive influence of AI-enhanced applications across application-domains like automotive, space and cyber-physical embedded systems, call for a paradigm shift from simple micro-controllers towards powerful and heterogeneous edge computers for the design of next-generation mixed-criticality systems. These must not only deliver outstanding performance and energy efficiency but also ensure steadfast safety, resilience, and security.

The Carfield SoC aims to tackle these architectural challenges establishing itself as a pre-competitive heterogeneous research platform for mixed-criticality systems, underpinned by fully open-source IPs. The SoC showcases pioneering hardware solutions, addressing challenges related to time-predictable on/off-chip communication, robust fault

recovery mechanisms, secure boot processes, cryptographic acceleration services, hardware-assisted virtualization, and accelerated computation for both floating-point and integer workloads. Carfield’s architecture features three domains and two DSAs.

The host domain integrates two memory-consistent 64-bit CVA6 cores with support for virtualization at different levels. Leveraging H-extensions within the RISC-V ISA, the system can accommodate the execution of multiple OSs, including rich, Unix-like OSs and real-time OSs, via an intermediate Hypervisor layer. The host domain provides a flexible interrupt subsystem, allowing for fast and virtualized interrupts through the RISC-V core-local interrupt controller (CLIC), and ensures hardware-based spatial isolation of cache resources to comply with freedom from interference requirements in modern MCS. Carfield’s host domain builds on top of *Cheshire* by enhancing it with fully configurable real-time features in HW.

The safety island [61], a simple MCU-like domain, comprises three 32-bit physically isolated cores operating in triple-lockstep mode. These cores, enhanced with the CLIC and optimized for fast interrupt handling and context switch, run real-time OS (RTOS) and safety-critical applications, embodying a core tenet of the platform reliability.

The secure domain, based on the *OpenTitan* project, serves as the hardware root of trust (HWRoT), handling secure boot procedures, system integrity monitoring, and cryptographic acceleration services.

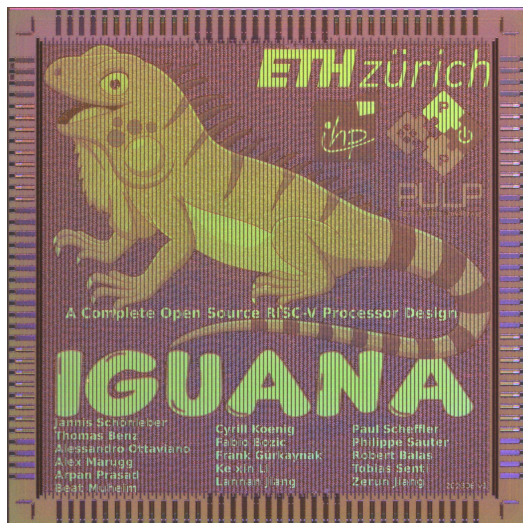
To augment computational capabilities, Carfield incorporates two general-purpose accelerators: the *Spatz* cluster, which handles vectorizable multi-format floating-point workloads (down to FP8), and the *HMR* 12-core integer cluster, specialized in executing quantized neural networks (QNN) operations, exploiting the *HMR* technique for rapid fault recovery and integer arithmetic support in the ISA of the RISC-V cores from 32-bit down to 2-bit.

The system’s interconnect relies upon a 64-bit AXI4 crossbar, enriched with AXI-REALM, see Chapter 5.

A full set of peripherals, including *SPI*, *I2C*, *Serial Link*, *CAN FD*, *HyperBUS*, and timers, including watchdogs, complete the features of the SoC.



## A.8 Iguana



Name	Iguana
Designers	Jannis Schoenleber, <b>Thomas Benz</b> , Alessandro Ottaviano, Alex Marugg, Arpan Prasad, Beat Muheim, Cyril Koenig, Fabio Bozic, Frank K. Gurkaynak, Kexin Li, Lannan Jiang, Paul Scheffler, Philippe Sauter, Robert Balas, Tobias Senti, Zerun Jiang
Application / Publication	PULP SoC-130-o / Benz <i>et al.</i> [74]
Technology / Package	IHP130 / QFN88
Dimensions	6.264 mm × 6.264 mm
Circuit Complexity	3 MGE
Voltage	1.2 V
Clock Frequency	60 MHz

Iguana is our first attempt at using IHP’s 130 nm open PDK. The chip’s architecture connects our Cheshire SoC platform to a HyperBus memory controller for off-chip data storage.

The design was completed using only open-source standard cell libraries, and although an almost complete backend run was made with OpenROAD, a last minute issue resulted in a backup design, made with commercial EDA tools, to be taped.

We introduce the terminology of *SoC-130-o* to describe an end-to-end open-source (SW, RTL, EDA, PDK, PHYs) SoC.

## A.9 Basilisk



---

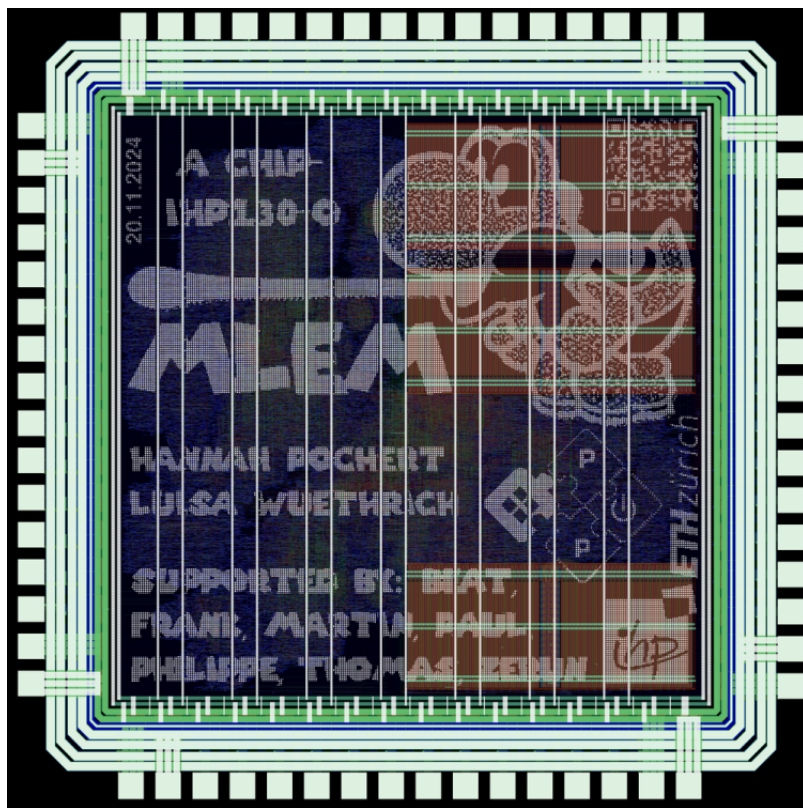
Name	Basilisk
Designers	Philippe Sauter, <b>Thomas Benz</b> , Paul Scheffler, Beat Muheim, Zerun Jiang, Frank K. Gurkaynak, Luca Benini
Application / Publication	PULP SoC-130-o / Sauter <i>et al.</i> [83]
Technology / Package	IHP130 / QFN88
Dimensions	6.264 mm × 5.498 mm
Circuit Complexity	3 MGE
Voltage	1.2 V
Clock Frequency	60 MHz

---

Following *Iguana*, Basilisk is our second attempt at using the IHP's 130 nm open PDK. Basilisk features the same architecture as Iguana with some minor tweaks and improvements.

This time around, a completely open flow, using Yosys for synthesis and OpenROAD for implementation, was successfully used. Iguana also includes novel aging sensors developed by IHP. Basilisk successfully boots Linux.

## A.10 MLEM



---

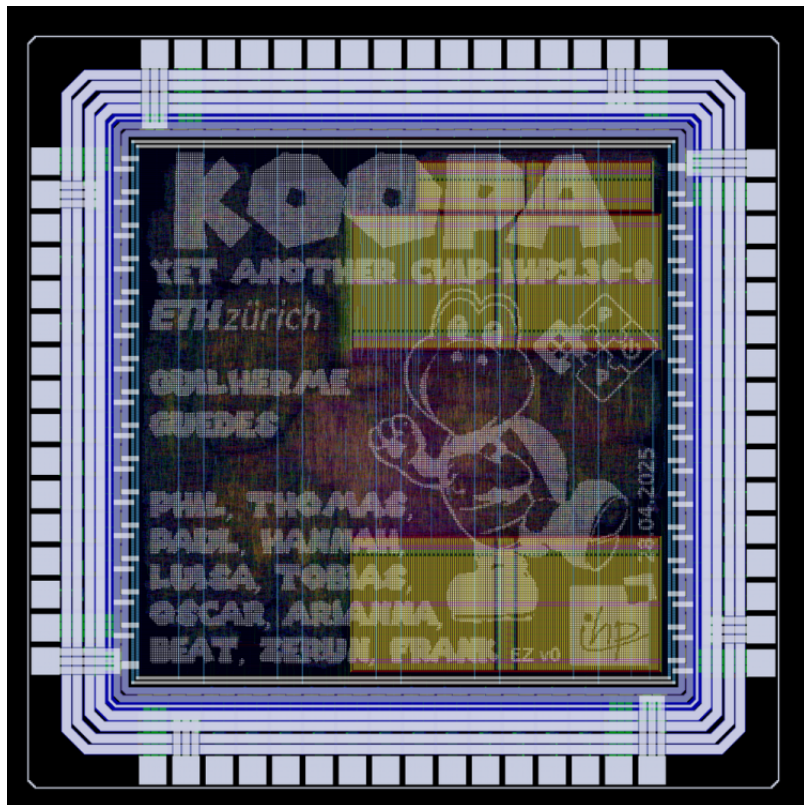
Name	MLEM
Designers	Hannah Pochert, Luisa Wuethrich, Philippe Sauter, Paul Scheffler, <b>Thomas Benz</b>
Application / Publication	PULP Student MCU-130-o / Sauter <i>et al.</i> [82]
Technology / Package	IHP130 / QFN56
Dimensions	2.235 mm × 2.235 mm
Circuit Complexity	350 kGE
Voltage	1.2 V
Clock Frequency	80 MHz

---

MLEM, named after the sound *Yoshi* (from *Super Mario*) makes when eating a tasty fruit, is the first tapeout based on the *Croc* MCU platform [82]. MLEM was designed and prepared for tapeout by students using a complete open-source tool flow, including a new SV frontend for Yosys developed by Martin Povišer. This chip serves as a pilot for the new open VLSI II lecture starting in 2025, where students get the opportunity to prepare a Croc-based tapeout with any custom addition in IHP’s 130 nm open PDK.

For MLEM, students contributed a SV *UART* peripheral to replace the existing VHDL version, a *GPIO* peripheral, and a *Neopixel* controller to drive RGB LEDs.

## A.11 Koopa



Name	Koopa
Designers	Guilherme Guedes, Philippe Sauter <b>Thomas Benz</b> , Paul Scheffler, Hannah Pochert, Luisa Wuethrich, Tobias Senti, Oscar Castaneda, Arianna Rubino, Beat Muheim, Zerun Jiang, Frank K. Gurkaynak
Application / Publication	PULP MCU-130-o
Technology / Package	IHP130 / QFN56
Dimensions	2.235 mm $\times$ 2.235 mm
Circuit Complexity	250 kGE
Voltage	1.2 V
Clock Frequency	74 MHz

Following *MLEM*, Koopa is our second Croc-based MCU. Next to various minor updates to the IPs compared to *MLEM*, Koopa features a newly designed QSPI interface. Koopa further uses a first version of *EZ130*, a new open-source standard-cell library developed by and for the VLSI 5 course at ETH Zurich, led by Oscar Castañeda and Christoph Studer.

### A.12 Fluffy



---

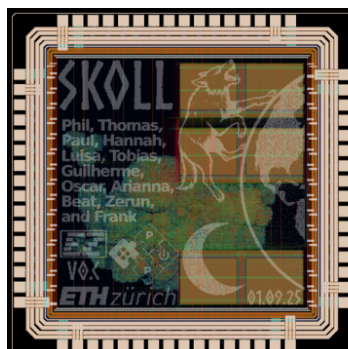
Name	Fluffy
Designers	Konrad Roth, Ludwig Itschner <b>Thomas Benz</b> , Lorenzo Leone,
Application / Publication	PULP Student MCU-130-o
Technology / Package	IHP130 / QFN56
Dimensions	2.235 mm × 2.235 mm
Circuit Complexity	470 kGE
Voltage	1.2 V
Power	45 mW @ 1.2 V and 51 MHz
Clock Frequency	51 MHz

---

Fluffy integrates a multi-head-capable iDMA engine into a Croc-based MCU. This newly developed engine can copy two data streams simultaneously from Croc's SRAM banks, perform an element-wise arithmetic operation on them, and store the resulting vector back in SRAM. Executing a vector add using our multi-head iDMA engine results in a speedup of  $9.14 \times$  compared to the baseline execution on Croc's CVE2 core.

Fluffy was designed as part of a mini project alongside our new VLSI II course. It is one of five student designs chosen for a tapeout in 2025 thanks to its novel results, well-executed implementation, and outstanding report.

### A.13 Skoll



---

Name	Skoll
Designers	Philippe Sauter, <b>Thomas Benz</b> Paul Scheffler, Hannah Pochert Luisa Wuethrich, Tobias Senti, Guilherme Guedes, Oscar Castaneda, Arianna Rubino, Beat Muheim, Zerun Jiang, Frank K. Gurkaynak
Application / Publication	PULP MCU-130-o
Technology / Package	IHP130 / QFN56
Dimensions	2.235 mm × 2.235 mm
Circuit Complexity	250 kGE
Voltage	1.2 V
Clock Frequency	80 MHz

---

Hati and Skoll are two Croc-based MCU featuring an identical RTL code based on the architecture of Koopa. They serve to silicon-harden v1.2.0 of Croc, evaluate the improvements of the open-source EDA tools since the tapeout of *MLEM*, and to evaluate and compare the newest versions of the two standard cell libraries in IHP's 130 nm open PDK.

Skoll implements the MCU using *v0.c* of the EZ130 standard cells.

## A.14 Hati



---

Name	Hati
Designers	<b>Thomas Benz</b> , Philippe Sauter Paul Scheffler, Hannah Pochert Luisa Wuethrich, Tobias Senti, Guilherme Guedes, Oscar Castaneda, Arianna Rubino, Beat Muheim, Zerun Jiang, Frank K. Gurkaynak
Application / Publication	PULP MCU-130-o
Technology / Package	IHP130 / QFN56
Dimensions	2.235 mm × 2.235 mm
Circuit Complexity	250 kGE
Voltage	1.2 V
Clock Frequency	90 MHz

---

Hati and Skoll are two Croc-based MCU featuring an identical RTL code based on the architecture of Koopa. They serve to silicon-harden v1.2.0 of Croc, evaluate the improvements of the open-source EDA tools since the tapeout of *MLEM*, and to evaluate and compare the newest versions of the two standard cell libraries in IHP's 130 nm open PDK.

Hati implements the MCU using *r0.1.3* of IHP's standard cells.

## A.15 Flamingo





# Appendix B

## ArtistIC

### B.1 Introduction

Recent advances in open-source electronic design automation (OSEDA) spawned countless ASIC projects developed by industry, research, and hobbyists. Even though the content and organization of these projects could not be more diverse, they share a common requirement to present their project using outreach material to gain attention, share resources and results, and secure funding. Especially in the early design phases of projects, sharing the ASIC under design can prove very difficult as no running prototype can be shown.

Methodologies have been established to render and visualize layout (GDSII) files, but they are limited either in scope or fidelity. The *TinyTapeout* project [184] uses a 3D-GDSII viewer to visualize their layouts directly within a web browser [185]. Proving an excellent tool to visualize tiny designs on the standard-cell level in 3D, it is not suited to render research or industry-grade chips on a poster scale. KLayout [186] has established itself as the default open-source GDSII viewer featuring a powerful scripting API, which can be used to export high-resolution ( $\lesssim 250$  Mpx) renders of the current view [187]. Our experiments show that a much higher resolution is required to capture the intricate details of the lower-level metalization layers of research-scale [69, 76] chips. Furthermore, KLayout does not provide

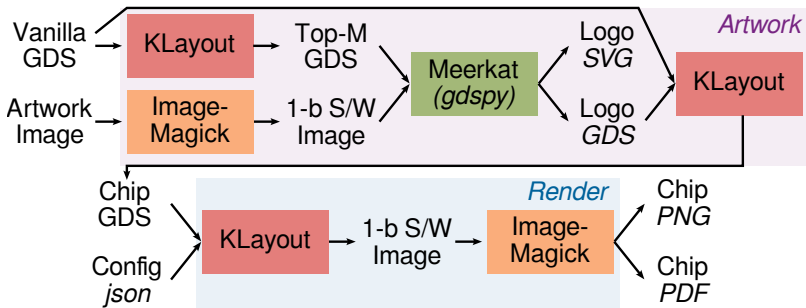


Figure B.1: The ArtistIC toolflow.

a transparency option for individual layers, leading to upper metal levels covering up lower-level details.

Adding top-metal artwork is a well-established way of branding the design files and the fabricated silicon [188]. To our knowledge, no open-source tool exists to translate and embed artwork into GDSII layouts.

To tackle these points, we propose ArtistIC, an open-source framework to translate and insert top-metal ASIC art into GDSII layout files and create artistic ultra-high-fidelity renders thereof. In particular, we present the following contributions:

- A *Gdsp*-based [189] script translating and inserting DRC-clean top-metal artworks into GDSII files.
- A tile-based image rendering methodology supporting arbitrary high resolutions through tiling and capable of individual layer transparencies.
- A case study presenting insights from analyzing the layout renders of two RISC-V ASICs [69, 76].

## B.2 Toolflow

ArtistIC's toolflow, presented in Figure B.1, accepts a DRC-clean *vanilla* GDSII file and a lossless artwork image as primary inputs. In

Table B.1: ArtistIC runtime of open-source RISC-V ASICs.

Chip	Chip Size	Render Res.	Print Res.	Print Size	Runtime
<i>Mlem/Croc</i> [133, 134, 190]	5 mm <sup>2</sup>	25 nm/px	2 Gpx	A1 <sup>a</sup>	0.9 h <sup>b</sup>
<i>Basilisk</i> [76]	35 mm <sup>2</sup>	25 nm/px	55 Gpx	2x2 m <sup>a</sup>	6.1 h <sup>b</sup>

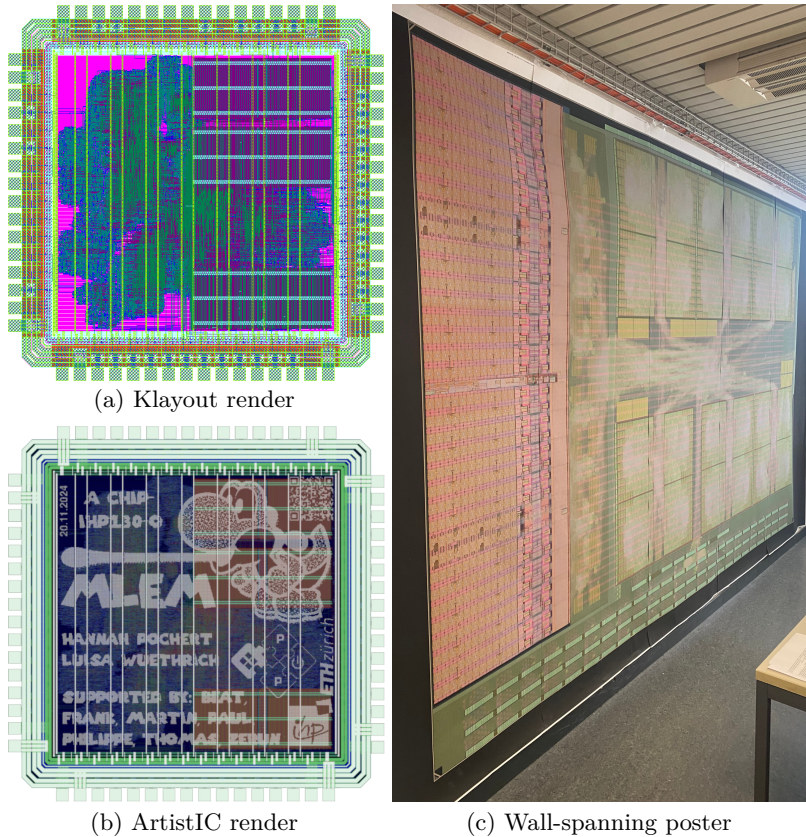
<sup>a</sup> target: 2400 dpi    <sup>b</sup> 2.5 GHz Xeon E5-2670

the first step, KLayout is used to export the top-metal layer from the GDSII file and the logo is translated into a 1-bit *b/w* image. *Meerkat*, a *Gdspy*-based script, converts the *b/w* image to *tetromino*-like shapes following DRC and density rules as well as flowing them around existing top-metal structures. *Meerkat* exports a vector graphic image and a GDSII file containing the logo only; KLayout is then used to merge the vanilla and logo GDSII files.

A *json* configuration file specifies the resulting image size, render resolution, layer colors and transparencies, and the used layer stack. Using a maximum individual tile size of around 250 Mpx, we use KLayout to export each layer of the ASIC as *b/w* image tiles. The tiles can be rendered at a higher resolution than the final image size to keep fine layout details while ensuring a manageable image file size. In the last step, *ImageMagick* is used to color the layer tiles, merge the colored layers using the specified transparencies, and resize and merge the tiles to a complete image, which is then embedded into a *PDF* container for printing.

## B.3 Results

Figure B.2a shows the *vanilla* GDSII file [133, 134, 190] rendered with KLayout [186, 187] and Figure B.2b with ArtistIC including a generated top-level metal artwork. Table B.1 presents ArtistIC’s runtimes for two open-source ASICs. Figure B.2c displays a 2.3 by 4.2 m poster of one Occamy die [69] rendered at 57 Gpx (44 nm/px) and printed at 1600 dpi demonstrating the scalability of ArtistIC.



## B.4 Case Study: RISC-V SoCs

ArtistIC can directly be used in scientific publications to analyze, evaluate, and compare ASIC layouts. Figure B.3 presents three high-fidelity layout renders with annotations of exemplary insights gained; for a more detailed analysis, we refer to our peer-reviewed works on these systems [69, 76]. In Figure B.3a, we see ❶ the bootrom, which is closely interconnected and thus densely packed, ❷ empty space, and ❸ an area of high connectivity; the routing uses higher top metals (rendered in red). In Figure B.3b, ❹ highlights the high routing effort of the *logarithmic interconnect* and ❺ the *pipeline stages* of one of the computing units. In Figure B.3c, ❻ annotates one of the top-level interconnect buses with individual pipeline stages visible.

## B.5 Conclusion & Outlook

With ArtistIC, we present a framework to embed images as top-metal ASIC art into existing GDSII layouts and to render them artistically with ultra-high fidelity. ArtistIC cannot only be used to generate outreach material for ASIC projects to gain attention, share results, and secure funding, but also to build the foundation for scientific discussions concerning chip layouts. With ArtistIC available open source<sup>1</sup>, we hope to see many high-resolution ASIC renders and posters emerging.

---

<sup>1</sup>[github.com/pulp-platform/artistic](https://github.com/pulp-platform/artistic)

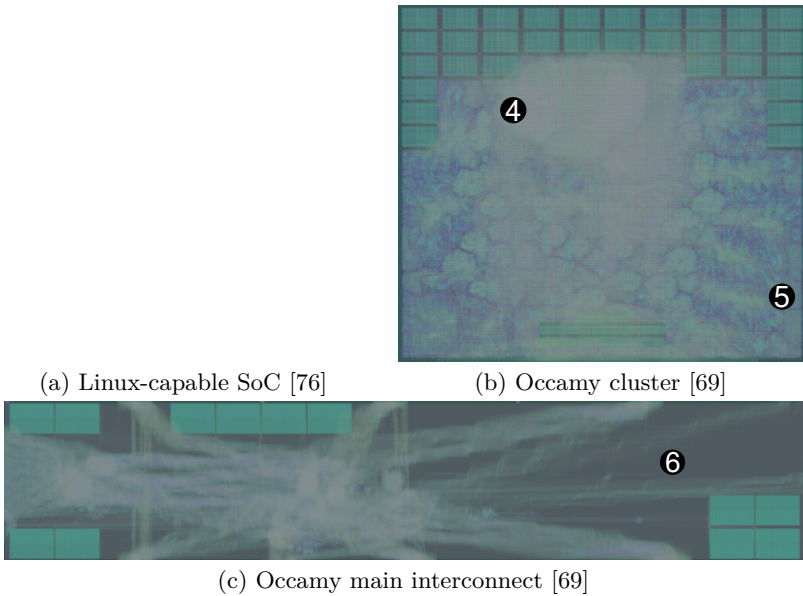


Figure B.3: Insights gained through ArtistIC.

# Appendix C

# DUTCTL

## C.1 Introduction

Silicon testing and characterization, driven in industry by ATE [191], is an essential part of ASIC production. Modern ATE systems enable comprehensive, calibrated, and high-resolution functional and physical evaluation of ASICs; however, they are expensive to purchase and maintain and require specialized training to program and operate.

With open-source hardware initiatives like RISC-V on the rise, small organizations and research groups increasingly design their own prototype SoCs. In such low-volume settings, purchasing and operating ATE usually cannot be justified.

Luckily, the bring-up and basic characterization of prototype SoCs can also be accomplished with commodity hardware. Unlike generic ASICs, SoCs are designed to be highly software-controllable; RISC-V debug modules (DBGMs) [192] enable full external control of on-chip harts through standard interfaces like JTAG. Power and clocks can be provided by bench-top supplies and signal generators, respectively. Most SoC I/Os (e.g., UART, SPI, DRAM) adhere to established protocols and can be connected to off-the-shelf devices or adapters; debugging is possible with oscilloscopes and logic analyzers.

Nevertheless, this approach inherently lacks coordination and automation. To match ATE systems, a solution to externally control

and coordinate power delivery, clocking, reset, and debugging is required. This, in turn, is what enables the sequencing, sweeping, and reproduction of tests that is required for automated, in-depth characterization across production runs.

We thus present DUTCTL [80, 193], an open-source framework automating the rapid, ATE-less bring-up and characterization of RISC-V-based SoCs by controlling and coordinating the necessary external devices. DUTCTL provides the following features:

- It configures and controls any number of network-attached supplies, clock sources, and reset generators described in a customizable configuration.
- It coordinates a full reset-and-power cycle, ensuring statelessness and reproducibility, and provides a fully scriptable GDB [194] debugging session.
- It monitors and stores the SoC’s serial output; through control sequences, the SoC can communicate internal measurements (e.g. computed results, cycle counts) or trigger external measurements (e.g. supply power) with precise timing.
- Through iterated sessions with different parameters and debugging payloads, it enables the design of full test flows and characterization sweeps.
- It enables easy *shared* and *remote* access to limited engineering samples for time-efficient testing and software exploration.

## C.2 Architecture

Figure C.1 shows a generic DUTCTL setup composed of a software part running on a workstation and instruments and adapters connecting to the DUT. Instruments are interfaced through an extensible Python library with generic bindings; in our case, they are controlled using standard commands for programmable instruments (SCPI) [195] over Ethernet. Adapters connect directly to the test workstation and

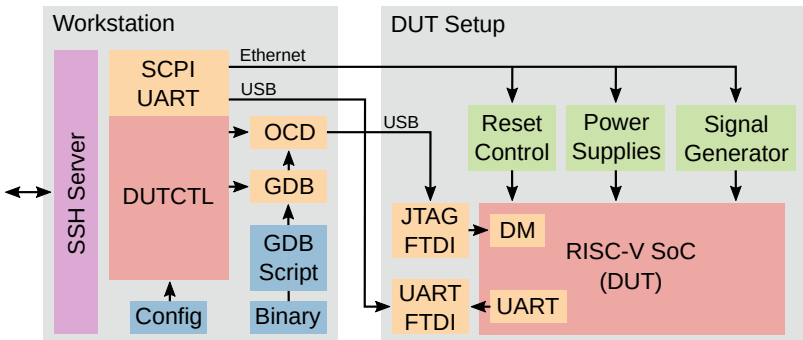


Figure C.1: A generic DUTCTL setup. Software running on a workstation orchestrates equipment around the device under test (DUT).

leverage existing drivers and software; we currently support JTAG adapters for RISC-V debugging and UART adapters for serial IO.

A DUTCTL session is launched using a single command specifying an instrument configuration, a GDB script, and optionally a serial port. DUTCTL first connects to all instruments and configures them; this includes voltages and current limits for supply channels or frequencies and waveforms for signal generators. After configuration, instrument outputs are enabled and any configured resets issued through instrument GPIOs. DUTCTL then launches a GDB session sourcing the passed script, which may preload, execute, and debug RISC-V binaries. In parallel, it monitors the DUT's serial output for control sequences communicating internal results or triggering external instrument measurements with precise timing relative to binary execution. The session ends when GDB exits, which may be triggered by the DUT using `ebreak`. Test failures are communicated through nonzero return codes. Instrument outputs are disabled to purge non-resettable state (e.g. SRAMs) within the DUT.

Launching multiple consecutive sessions with different parameters enables full test flows and characterization sweeps. For example, a *Schmoo* plot [196] may be created by sweeping clock frequency and

supply voltage and recording for each session whether a workload terminates with correct results. With DUTCTL, we can easily enhance this binary *pass-or-fail* plot with execution times and power measurements. By customizing instrument configurations and scripts, arbitrary test flows and sweeps may be assembled from DUTCTL sessions, allowing custom SoCs to be extensively tested, characterized, and binned.

### C.3 Results and Conclusion

As shown in Figure C.2, we successfully used DUTCTL to bring up, test, and characterize an open-source RISC-V SoC using a testflow composed of a series of functional and sweep tests. Clock speed is an important figure of merit even for small-scale runs. To create the enhanced Schmoo plot shown in Figure C.3, hundreds of DUTCTL sessions must be executed sequentially. We found the test runtime to be dominated by the payload’s execution time, which requires a minimum duration to allow precise steady-state current measurements.

With DUTCTL, we present and release an open-source framework automating the ATE-less bring-up and characterization of RISC-V-based SoCs. DUTCTL’s modularity allows easy replacement of individual components and addition of test equipment.

Figure C.2: Photograph of a running DUTCTL setup.

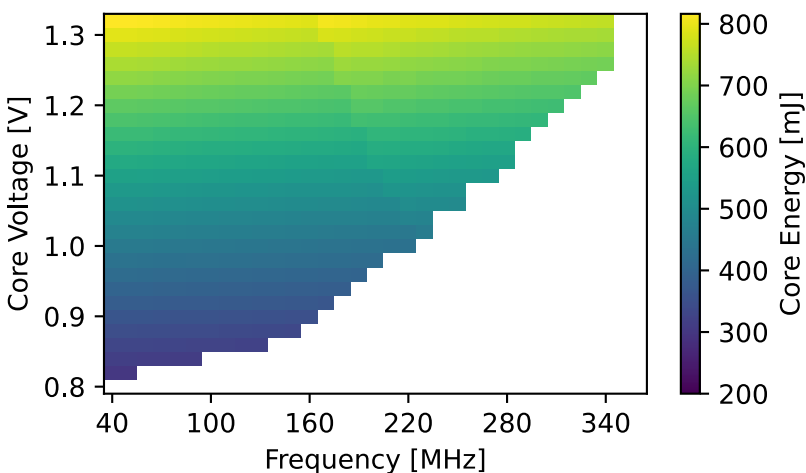


Figure C.3: Voltage-frequency sweep running a matrix multiplication; failing operating points are denoted in *white*, passing according to total core energy to completion.

## Appendix D

# Student Theses Supervised

During my Ph.D. studies, I had the chance to supervise the following student theses. I am very grateful for the opportunity to work with so many students, the chance to grow on the challenges tackled together, and to be able to improve my teaching and supervision skills.

### D.1 2020

N. Huetter, “A Snitch-based compute accelerator for HERO,” Semester [197] Thesis, ETH Zurich, 2020

F. Solt, “A flexible peripheral system for high-performance systems on chips,” [131] Master’s Thesis, ETH Zurich, 2020

### D.2 2021

F. Bucheli, “A Snitch-based SoC on iCE40 FPGAs,” Bachelor’s Thesis, ETH [198] Zurich, 2021

R. Zhou, V. Krishna, and J. Chen, “An RPC DRAM implementation for [199] energy-efficient ASICs,” Semester Thesis, ETH Zurich, 2021

J. Eudine, L. Meier, and T. Mettler, “Bringup and evaluation of an energy- [200] efficient heterogeneous manycore compute platform,” Semester Thesis, ETH Zurich, 2021

W. Ho, Kin, “Investigation of the high-performance multi-threaded out-of-order IBM A2O core,” Semester Thesis, ETH Zurich, 2021

L. Hauser, “Lcore: A minimal RISC-V core designed for teaching,” Bachelor’s Thesis, ETH Zurich, 2021

C. Zhang, “Extending AXI4 with common stream semantics,” Semester Thesis, ETH Zurich, 2021

### D.3 2022

K. Schaeerer, “Enhancing our DMA engine with vector processing capabilities,” Bachelor’s Thesis, ETH Zurich, 2022

T. Senti, “Extension and evaluation of the iDMA architecture for multiple on-chip communication protocols,” Bachelor’s Thesis, ETH Zurich, 2022

N. Narr and C. Reinwardt, “A 64-bit Linux-capable RISC-V system-on-chip in 65nm CMOS,” Semester Thesis, ETH Zurich, 2022

S. Song, B. Wang, C. Wang, and Z. Jiawei, “An AXI4 slave interface and digital memory controller for RPC DRAM,” Semester Thesis, ETH Zurich, 2022

A. Vanoni, “Linux support for DMA engine,” Bachelor’s Thesis, ETH Zurich, 2022

A. Brandl, “A power measurement ASIC for evaluating the iDMA architecture,” Semester Thesis, ETH Zurich, 2022

M. Raeber, “Developing an energy-efficient transposition unit supporting a wide range of data widths,” Semester Thesis, ETH Zurich, 2022

F. Svelto, “Towards a technology-independent and synthesizable AXI4 performance monitoring unit,” Semester Thesis, ETH Zurich, 2022

C. Zhang, “AXI-PACK: Near-memory bus packing for bandwidth-efficient spare workloads,” Master’s Thesis, ETH Zurich, 2022

### D.4 2023

E. Werner, “A flexible FPGA-based peripheral platform extending Linux-capable systems on chip,” Bachelor’s Thesis, ETH Zurich, 2023

J. Holborn, “Towards an affordable SoC characterization platform for automated voltage-frequency sweeps,” Bachelor’s Thesis, ETH Zurich, 2023

F. Bozic, "Verifying Iguana using open-source simulation and FPGA emulation," Bachelor's Thesis, ETH Zurich, 2023

V. Kuenzli, "Implementing virtual memory support for our DMA engine," Semester Thesis, ETH Zurich, 2023

T. Senti, "The OpenRoad towards Iguana - a fully open-source Linux-capable ASIC," Semester Thesis, ETH Zurich, 2023

L. Jiang and K. Li, "Towards open-source ASICs: Physical implementation gap-analysis of a Linux-Capable SoC vehicle in 130nm CMOS," Semester Thesis, ETH Zurich, 2023

P. Sauter, "Towards SystemVerilog support for open-source tools," Semester Thesis, ETH Zurich, 2023

L. Guzenko, "Implementing USB support in Cheshire," Semester Thesis, ETH Zurich, 2023

L. Leone, "A reduction-capable AXI XBAR for fast M-to-1 communication," Master's Thesis, ETH Zurich, 2023

P. Sauter, "Basilisk: Open-source IC design," Master's Thesis, ETH Zurich, 2023

## D.5 2024

M. Gedik, "A video output peripheral for Cheshire-based SoCs," Bachelor's Thesis, ETH Zurich, 2024

G. Frehner, "JTAG generator," Bachelor's Thesis, ETH Zurich, 2024

F. Hauser, "Integrating the Snitch cluster into a PULPissimo microcontroller for a GF22 SoC," Bachelor's Thesis, ETH Zurich, 2024

T. Dubochet, "FPGA verification and debugging enhancements for the Monoceros GF22 SoC," Bachelor's Thesis, ETH Zurich, 2024

M. Hirs, "Fixing bring-up related design flaws in the Snitch cluster with an implementation for GF22," Bachelor's Thesis, ETH Zurich, 2024

I. Gruenberg, "Optimizing the performance and bandwidth of a 64-bit Linux-capable RISC-V SoC," Bachelor's Thesis, ETH Zurich, 2024

L. Braun, "Towards a full verification framework for iDMA - comparing open and closed approaches," Bachelor's Thesis, ETH Zurich, 2024

A. Dumik, "Bufferless transposition engine," Semester Thesis, ETH Zurich, 2024

T. Hung, Ho and C. Wang, “Designing a scalable miniature ioDMA,”  
[231] Semester Thesis, ETH Zurich, 2024

L. Wuethrich, “MLEM: A PULP SoC for education with an end-to-end  
[133] open-source flow for a physical design - NeoPixel edition,” Bachelor’s Thesis,  
ETH Zurich, 2024

H. Pochert, “MLEM: A PULP SoC for education with an end-to-end open-  
[190] source flow for a physical design - UART edition,” Bachelor’s Thesis, ETH  
Zurich, 2024

F. Hauser, “Creating a SystemVerilog USB1.1 host controller for Linux-  
[232] capable SoCs,” Semester Thesis, ETH Zurich, 2024

J. Sommerhaeuser, “Enabling Linux DMA support in our Linux-capable  
[233] Cheshire SoC,” Semester Thesis, ETH Zurich, 2024

R. Roth, “Towards a virtual-memory-enhanced DMA for Linux-capable  
[234] SoCs,” Semester Thesis, ETH Zurich, 2024

L. Luzi, “Multi-channel memory transfers in huge manycore systems with  
[235] multiple HBM channels,” Master’s Thesis, ETH Zurich, 2024

## D.6 2025

A. Buchner and M. Wehrli, “Towards an SDIO peripheral for Linux-capable  
[236] SoCs,” Bachelor’s Thesis, ETH Zurich, 2025

L. Itschner, “Adding multi-head capabilities to our DMA infrastructure,”  
[237] Bachelor’s Thesis, ETH Zurich, 2025

B. Koellbl, “Commercial versus open-source: A comprehensive survey of  
[238] power simulation flows for digital ICs,” Bachelor’s Thesis, ETH Zurich, 2025

K. Schaeerer, “Exploring virtual memory architectures for linux-capable  
[239] heterogeneous systems,” Master’s Thesis, ETH Zurich, 2025

A. Rosetti, “Performance-oriented improvements to Cheshire SoC,” Semester  
[240] Thesis, ETH Zurich, 2025

A. Vanoni, “Accelerating MMC performance to enable persistent boot on  
[241] open-source RISC-V,” Semester Thesis, ETH Zurich, 2025

# Appendix E

## Acronyms

This document is incomplete. The external file associated with the glossary ‘main’ (which should be called `main.gls`) hasn’t been created.

Check the contents of the file `main.glo`. If it’s empty, that means you haven’t indexed any of your entries in this glossary (using commands like `\gls` or `\glsadd`) so this list can’t be generated. If the file isn’t empty, the document build process hasn’t been completed.

If you don’t want this glossary, add `nomain` to your package option list when you load `glossaries-extra.sty`. For example:

```
\usepackage[nomain]{glossaries-extra}
```

Try one of the following:

- Add `automake` to your package option list when you load `glossaries-extra.sty`. For example:

```
\usepackage[automake]{glossaries-extra}
```

- Run the external (Lua) application:

```
makeglossaries-lite.lua "main"
```

- Run the external (Perl) application:

```
makeglossaries "main"
```

Then rerun `LATEX` on this document.

This message will be removed once the problem has been fixed.



# List of Figures

1.1	Training compute and thus number of parameters of ML models and their trends. Image taken from [11]. .	2
1.2	Transition from a flat or distributed ECU architecture to a structured domain and finally a zonal architecture with MCS nodes. . . . .	4
1.3	Abstract representation of a computing system; a PE including an ALU sits at the center accessing both the physical world through I/O and memory. . . . .	6
1.4	Abstract representation on a computing system extended with DMA units. A I/O DMA accelerates accesses to the physical world, whereas a memory DMA can be used to copy and reorganize data in memory. .	7
1.5	Abstract view of the internals of a DMA unit. <i>Control</i> and <i>data planes</i> can be differentiated; the former includes a system binding allowing the PE to interface the unit, the latter includes the interconnect binding over which the unit accesses memory and/or I/O. At the center, an address generator enumerates the memory region to be copied. . . . .	8
1.6	Overview of this thesis's chapters. Chapter 2 with iDMA builds the <i>foundation</i> of this thesis. Chapter 3 defines important DMA extension which are developed into a communication processor in Chapter 4, supporting our goal of a energy-efficient real-time data movement strategy presented in Chapter 5. . . . .	13

2.1	Schematic of iDMA: Our engines are split into three parts: at least one front-end, one or multiple optional mid-ends, and at least one back-end. . . . .	27
2.2	Outline of the <i>1-D transfer descriptor</i> (exchanged between mid- and back-end). The <i>options</i> field contains protocol-specific configuration independently of the chosen configuration to keep the back-end's interface interchangeable. . . . .	27
2.3	The internal architecture of the back-end. The <i>transport layer</i> handles the actual copying of the data on the on-chip protocol, supported by the optional <i>transfer legalizer</i> and the <i>error handler</i> . . . . .	28
2.4	The internal architecture of the <i>transfer legalizer</i> . Any given transfer can be legalized except for zero-length transactions: They may optionally be rejected. . . . .	29
2.5	The architecture of the <i>transport layer</i> . One or multiple <i>read manager(s)</i> feed a stream of bytes into the <i>source shifter</i> , the <i>data flow element</i> , the <i>destination shifter</i> , and finally, into one or multiple <i>write manager(s)</i> .  denotes the <i>in-stream accelerator</i> . . . . .	30
2.6	Simple system containing an iDMA; the subordinate device can either handle one read or write burst at the same time. Should the endpoint accept the write burst first and the back-end-internal dataflow buffer is not large enough to hold the full burst, a deadlock occurs as the data cannot be read from the endpoint concurrently. . . . .	34
2.7	Our script, <i>Mario</i> , customizes and properly connects the SV template files of iDMA to adapt it to specified protocol configurations. . . . .	36
2.8	Internal architecture of iDMA's <i>error handler</i> . A <i>buffer</i> holds the emitted transfer information to be reported or replayed in the case of an error. . . . .	38
2.9	Area scaling of a back-end base configuration ( <i>32-bit</i> address and data width, <i>two</i> outstanding transactions). Markers represent the measurement points and lines the fitted model. . . . .	41

2.10	Clock period scaling of a back-end base configuration (32-bit address and data width, <i>two</i> outstanding transactions). Lower is better. <i>AXI4L</i> denotes AXI4 Lite, <i>AXI4S</i> , AXI4 Stream. . . . .	44
2.11	Bus utilization of our iDMA engine in the base configuration (32-bit address and data width) with varying amounts of outstanding transactions in three different memory systems; <i>SRAM</i> , <i>RPC DRAM</i> [93], <i>HBM</i> [94]. . . . .	46
3.1	Overview of the DMAC, containing request logic with internal registers for configuration and read logic to fetch the descriptor, and feedback logic to update the system once the iDMA back-end completes the transfer. . . . .	59
3.2	Integration of our DMAC into the Cheshire [60]. The two manager interfaces, after arbitration, as well as the subordinate configuration port of the DMAC, are connected to the SoC's interconnect. The IRQ line is connected to the platform's PLIC. . . . .	62
3.3	The OOC testbench setup; the DMAC has its two AXI4 manager interfaces connected to a fair round-robin arbiter (RR), which in turn is connected to a latency-configurable memory system. Contention between DMA data transfers and reading descriptors is thus modeled. Descriptors are loaded into the memory using backdoor access and are launched via the DMAC's subordinate configuration interface. . . . .	64
3.4	DMAC <i>steady-state</i> bus utilization given a prefetch hit rate of 100% in memory systems featuring various latencies. <i>Ideal</i> , <i>DDR3</i> , <i>Ultra-deep</i> memory systems featuring 1, 13, 100 cycles of latency, respectively. . . . .	66
3.5	DMAC steady-state bus utilization in the case of the DDR3 main memory with speculation misses; <i>speculation</i> configuration. . . . .	67
3.6	Architecture of our sMMU implemented as a mid-end. It is placed between a 1-D front-end and an iDMA back-end. . . . .	73
3.7	Our sMMU integrated into Cheshire's SoC-level iDMA engine. . . . .	74

3.8	Architecture of the register-based front-end and its connection to our tensor mid-end. Each PE has its private register file containing the transfer shape. . . . .	76
3.9	Architecture of our tensor mid-end. Each stage is activated by the previous; the strides of the highest stage are added to the base address. . . . .	77
3.10	(a) Block diagram of the PULP-open system. (b) Configuration of the cluster iDMA engine. . . . .	78
3.11	The architecture of our multichannel <i>MemPool</i> ( <i>mp</i> ) mid-ends. . . . .	81
3.12	Our distributed iDMA engine is implemented in MemPool. <i>Mp_split</i> splits the transfers along their L1 boundaries, and a tree of <i>mp_dist</i> mid-ends distribute the transfer. . . . .	82
3.13	I/O-DMA template. . . . .	85
3.14	Top-level architecture of MLEM, including our Neopixel host controller. . . . .	86
3.15	Architecture of our Neopixel host controller including an iDMA back-end. . . . .	87
3.16	Architecture of the real-time mid-end. The event state, holding the frequency and the shape of the transfer, can be part of the front-end. . . . .	89
4.1	Architecture of the tightly coupled <i>Snitch</i> DMA engine. It combines the <i>inst_64</i> front-end with a configurable number of <i>tensor_ND</i> mid-ends and iDMA back-ends. . . . .	98
4.2	Our iDMA integration into a Snitch compute cluster. . . . .	102
4.3	Architecture of the Occamy compute clutser, the worker core, and the compute group. . . . .	106
4.4	Architecture and interconnection of the three cooperating sparsity-capable SUs in each worker core. . . . .	107
4.5	Architecture of the two Occamy chiplets. Occamy features only one address region; narrow managers can access wide subordinates and vice versa through the <i>system</i> crossbar. . . . .	109
4.6	Architecture of the wide D2D segment with its 38 source-synchronous double-data-rate PHYs, carrying up to 2 GiB/s of raw data at a clock speed of 125 MHz. . . . .	110

4.7	Hierarchical area breakdown of the Occamy system. . . . .	113
4.8	Annotated physical layouts of the Occamy chiplet’s hierarchical components. . . . .	114
4.9	Annotated physical layouts of the Occamy chiplet (block IO is shown in yellow). . . . .	115
4.10	2.5D Occamy assembly mounted on carrier PCB. . . . .	117
4.11	Layout of the Hedwig interposer. . . . .	118
4.12	C4 bump map of the Hedwig interposer. . . . .	119
4.13	(a) Bringup board enabling both testing on an V93000 ATE and standalone operation, and (b) measurement setup. . . . .	122
4.14	Occamy chiplet bandwidths and speedups enabled by iDMA on workloads with varying tile sizes. . . . .	123
5.1	Overview of a generic system extended with AXI-REALM. The irealm units monitor and control data from the managers and erealm units guard the subordinate devices. . . . .	133
5.2	Internals of the irealm unit: (a) <i>granular burst splitter</i> , (b) <i>write buffer</i> , and (c) <i>management and regulation unit</i> . . . . .	134
5.3	Block diagram of an exploratory system featuring two regulated managers, a crossbar-based main interconnect using RR arbitration and a guarded subordinate device. Configuration interfaces are not shown. . . . .	135
5.4	Write transaction passing through our irealm unit. (continued on next page) . . . . .	136
5.4	Write transaction passing through our irealm unit. (continued from previous page) . . . . .	137
5.5	The internal architecture of the erealm unit. The read and write parts are constructed equally. . . . .	141
5.6	Tracked stages in the erealm unit. . . . .	143
5.7	The architecture of the <i>bus guard</i> . . . . .	144
5.8	Architectural block diagram of the Carfield platform. . . . .	149
5.9	Carfield’s hierarchical area including AXI-REALM. . . . .	150

5.10 Performance results of CVA6 copying data between SPM and L2 with the DSA accessing SPM at various granularities in 64-bit beats. <i>iso</i> denotes the isolated — 100% fractional performance, <i>unr</i> the unregulated performance. . . . .	152
5.11 DRAM and L2 with the DSA accessing DRAM at various problem sizes in byte. <i>iso</i> denotes the isolated — 100% fractional performance, <i>unr</i> the unregulated performance. . . . .	153
5.12 (a) Fractional performance at different budget imbalances favoring the critical manager assuming fragmentation one and (b) fractional performance at different period sizes assuming fragmentation size one and equal budget. . . . .	154
5.13 Schedule of the periodic ( $p$ ) real-time-critical transactions running on CVA6 and the data copy operation (period $P$ ) by the DSA DMA. . . . .	155
5.14 Power and energy of CVA6 copying data between SPM and L2 with the DSA accessing SPM given different fragmentation sizes. . . . .	156
5.15 TACLeBench [169] performance of CVA6 with (a) one and (b) two DSAs interfering. A budget imbalance of 1:1 and a period longer than the application's runtime is selected. We vary the fragmentation granularity. The applications contain an initialization, <i>init</i> , and a <i>main</i> phase. <i>iso</i> denotes the isolated, <i>unr</i> the unregulated performance. . . . .	159
B.1 The ArtistIC toolflow. . . . .	214
B.2 GDSII renders . . . . .	216
B.3 Insights gained through ArtistIC. . . . .	218
C.1 A generic DUTCTL setup. Software running on a workstation orchestrates equipment around the DUT. . . . .	221
C.2 Photograph of a running DUTCTL setup. . . . .	223
C.3 Voltage-frequency sweep running a matrix multiplication; failing operating points are denoted in <i>white</i> , passing according to total core energy to completion. . . . .	224

# List of Tables

1.1	Common non-coherent on-chip protocols and their key characteristics. All protocols share <i>byte addressability</i> and a <i>ready-valid</i> handshake. . . . .	11
2.1	Available on-chip protocols and their key characteristics. All protocols share <i>byte addressability</i> and a <i>ready-valid</i> handshake. . . . .	32
2.2	Area decomposition of the DMA engine configuration used in the PULP-open cluster, see Section 3.4.3. The <i>base</i> area is always required, the contribution of each protocol added is shown. If the area contribution is non-zero, the parameter influencing the value is provided using the <i>big-O</i> notation. The area contribution scales linearly with the data width ( <i>DW</i> ) if no scaling is provided. . . . .	43
2.3	Comparison of iDMA to the SoA. . . . .	50
3.1	Identifiers and descriptions of front-ends employed in the use cases. Front-ends in gray are available but not further discussed in this thesis. . . . .	54
3.2	The compile-time parameters used in our OOC experiments. . . . .	63
3.3	Area requirements at the maximum clock frequency of the DMAC and its main sub-components; desc_64 and the iDMA back-end. Clock frequencies are achieved in typical conditions. . . . .	65

3.4	FPGA resource requirements of the DMAC at 200 MHz.	68
3.5	DMAC latencies between various events and memory systems for the <i>scaled</i> configuration . . . . .	69
4.1	Events emitted by the tightly coupled Snitch DMA. .	99
4.2	Our RISC-V <i>dm</i> instructions introduced by <i>inst_64</i> . .	101
5.1	Area contribution <i>weights</i> of AXI-REALM’s building blocks as a function of their parameters. All numbers are in GE, at 1 GHz using typical conditions. . . . .	146
5.2	Parametrization, the resulting modeled, and actual area of the irealm and erealm units in Carfield (Section 5.5).	148
5.3	SoA comparison of AXI-REALM. . . . .	165
B.1	ArtistIC runtime of open-source RISC-V ASICs. . . .	215

# Bibliography

- [1] OpenAI, “Introducing OpenAI o3 and o4-mini,” 2025, <https://openai.com/index/introducing-o3-and-o4-mini>, Accessed: 06/03/2025.
- [2] M. T. Bennett and E. Perrier, “An AI system has reached human level on a test for general intelligence. Here’s what that means,” 2024, <https://theconversation.com/an-ai-system-has-reached-human-level-on-a-test-for-general-intelligence-heres-what-that-means-246529>, Accessed: 06/03/2025.
- [3] Semiconductor Research Corporation (SRC), “MAPT microelectronics and advanced packaging technologies roadmap,” <https://srcmapt.org/wp-content/uploads/2024/03/SRC-MAPT-Roadmap-2023-v4.pdf>, Accessed: 12/20/2024.
- [4] O. Burkacky, F. Steiner, M. Kellner, J. Deichmann, and J. Werra, “Getting ready for next-generation E/E architecture with zonal compute,” <https://mckinsey.com/industries/semiconductors/our-insights/getting-ready-for-next-generation-ee-architecture-with-zonal-compute#>, Accessed: 12/20/2024.
- [5] A. Mutschler, “Automotive OEMs focus on SDVs, zonal architectures,” <https://semiengineering.com/automotive-oems-focus-on-sdvs-zonal-architectures/>, Accessed: 12/20/2024.
- [6] Z. Jiang, K. Yang, Y. Ma, N. Fisher, N. Audsley, and Z. Dong, “Towards hard real-time and energy-efficient virtualization for many-core embedded systems,” *IEEE Transactions on Computers*, vol. 72, no. 1, pp. 111–126, 2023.

- [7] S. Kasarapu and S. M. P. Dinakarao, “Performance and environment-aware advanced driving assistance systems,” *IEEE Transactions on Computers*, vol. 74, no. 1, pp. 131–142, 2025.
- [8] R. Fletcher, A. Mahindroo, N. Santhanam, and A. Tschesner, “The case for an end-to-end automotive-software platform,” <https://mckinsey.com/industries/automotive-and-assembly/our-insights/the-case-for-an-end-to-end-automotive-software-platform>, Accessed: 12/20/2024.
- [9] IEA, “AI is set to drive surging electricity demand from data centres while offering the potential to transform how the energy sector works.” 2025, <https://iea.org/news/ai-is-set-to-drive-surging-electricity-demand-from-data-centres-while-offering-the-potential-to-transform-how-the-energy-sector-works>, Accessed: 07/03/2025.
- [10] U. Ntabeni, B. Basutli, H. Alves, and J. Chuma, “Device-level energy efficient strategies in machine type communications: Power, processing, sensing, and RF perspectives,” *IEEE Open Journal of the Communications Society*, vol. 5, pp. 5054–5087, 2024.
- [11] J. Sevilla and E. Roldán, “Training compute of frontier AI models grows by 4-5x per year,” 2024, <https://epoch.ai/blog/training-compute-of-frontier-ai-models-grows-by-4-5x-per-year>.
- [12] P. Villalobos and A. Ho, “Trends in training dataset sizes,” 2022, <https://epoch.ai/blog/trends-in-training-dataset-sizes>, Accessed: 06/04/2025.
- [13] P. Villalobos, A. Ho, J. Sevilla, T. Besiroglu, L. Heim, and M. Hobbhahn, “Will we run out of data? Limits of LLM scaling based on human-generated data,” 2024, <https://epoch.ai/blog/will-we-run-out-of-data-limits-of-lm-scaling-based-on-human-generated-data>, Accessed: 06/04/2025.
- [14] P. Villalobos, J. Sevilla, T. Besiroglu, L. Heim, A. Ho, and M. Hobbhahn, “Machine learning model sizes and the parameter gap,” 2022.

- [15] A. Pandharipande, C.-H. Cheng, J. Dauwels, S. Z. Gurbuz, J. Ibanez-Guzman, G. Li, A. Piazzoni, P. Wang, and A. Santra, "Sensing and machine learning for automotive perception: A review," *IEEE Sensors Journal*, vol. 23, no. 11, pp. 11 097–11 115, 2023.
- [16] D. Lee, L. Subramanian, R. Ausavarungnirun, J. Choi, and O. Mutlu, "Decoupled direct memory access: Isolating CPU and IO traffic by leveraging a dual-data-port DRAM," in *2015 International Conference on Parallel Architecture and Compilation (PACT)*, Oct. 2015, pp. 174–187, iSSN: 1089-795X.
- [17] P. McLellan, "What is zonal architecture? And why is it upending the automotive supply chain?" 2023, [https://community.cadence.com/cadence\\_blogs\\_8/b/breakfast-bytes/posts/zonal](https://community.cadence.com/cadence_blogs_8/b/breakfast-bytes/posts/zonal), Accessed: 06/08/2025.
- [18] J. Lim, J. Lee, Y. S. Hong, and C. Kang, "A framework for designing zonal architectures for in-vehicle networks: Balancing communication load and wiring length," *IEEE Transactions on Vehicular Technology*, vol. 74, no. 5, pp. 7940–7952, 2025.
- [19] S. Pinto, H. Araujo, D. Oliveira, J. Martins, and A. Tavares, "Virtualization on trustzone-enabled microcontrollers? Voilà!" in *2019 IEEE Real-Time and Embedded Technology and Applications Symposium (RTAS)*, 2019, pp. 293–304.
- [20] H. Jang, C. Park, S. Goh, and S. Park, "Design of a hybrid in-vehicle network architecture combining zonal and domain architectures for future vehicles," in *2023 IEEE 6th International Conference on Knowledge Innovation and Invention (ICKII)*, 2023, pp. 33–37.
- [21] A. Esper, G. Nelissen, V. Nelis, and E. Tovar, "An industrial view on the common academic understanding of mixed-criticality systems," *Real-Time Systems*, vol. 54, no. 3, p. 745–795, Jul. 2018.
- [22] A. Burns and R. I. Davis, "A survey of research into mixed criticality systems," *ACM Computing Surveys*, vol. 50, no. 6, Nov. 2017.

- [23] S. Majumder, J. F. D. Nielsen, and T. Bak, “Partaa: A real-time multiprocessor for mixed-criticality airborne systems,” *IEEE Transactions on Computers*, vol. 69, no. 8, pp. 1221–1232, 2020.
- [24] B. Sá, J. Martins, and S. Pinto, “A first look at RISC-V virtualization from an embedded systems perspective,” *IEEE Transactions on Computers*, vol. 71, no. 9, pp. 2177–2190, 2022.
- [25] M. Pagani, E. Rossi, A. Biondi, M. Marinoni, G. Lipari, and G. Buttazzo, “A bandwidth reservation mechanism for AXI-based hardware accelerators on FPGAs,” in *31st Euromicro Conference on Real-Time Systems (ECRTS 2019)*, ser. Leibniz International Proceedings in Informatics (LIPIcs), S. Quinton, Ed., vol. 133. Dagstuhl, Germany: Schloss Dagstuhl – Leibniz-Zentrum für Informatik, 2019, pp. 24:1–24:24.
- [26] I. Gray, Z. Jiang, K. Yang, N. Fisher, N. Audsley, and Z. Dong, “AXI-IC<sup>RT</sup>: Towards a real-time AXI-interconnect for highly integrated SoCs,” *IEEE Transactions on Computers*, vol. 72, no. 3, pp. 786–799, 2023.
- [27] M. Ditty, “NVIDIA ORIN system-on-chip,” in *2022 IEEE Hot Chips 34 Symposium (HCS)*. IEEE Computer Society, 2022, pp. 1–17.
- [28] E. Talpes, D. D. Sarma, G. Venkataramanan, P. Bannon, B. McGee, B. Floering, A. Jalote, C. Hsiong, S. Arora, A. Gorti, and G. S. Sachdev, “Compute solution for tesla’s full self-driving computer,” *IEEE Micro*, vol. 40, no. 2, pp. 25–35, 2020.
- [29] WikiChip Contributors, “FSD chip - Tesla,” [https://en.wikichip.org/wiki/tesla\\_\(car\\_company\)/fsd\\_chip](https://en.wikichip.org/wiki/tesla_(car_company)/fsd_chip).
- [30] L. Carletti, A. Serafini, G. Brilli, A. Capotondi, A. Biasci, P. Valente, and A. Marongiu, “Taking a closer look at memory interference effects in commercial-off-the-shelf multicore SoCs,” *Journal of Systems Architecture*, vol. 167, p. 103487, 2025.
- [31] L. F. Menabrea and A. Lovelace, “Sketch of the analytical engine invented by Charles Babbage,” *Sci Mem*, vol. 3, pp. 666–731, 1843.

- [32] A. W. Burks, H. H. Goldstine, and J. Von Neumann, “Preliminary discussion of the logical design of an electronic computing instrument,” in *The origins of digital computers: Selected papers*. Springer, 1946, pp. 399–413.
- [33] S. Ma, Y. Lei, L. Huang, and Z. Wang, “MT-DMA: A DMA controller supporting efficient matrix transposition for digital signal processing,” *IEEE Access*, vol. 7, pp. 5808–5818, 2019.
- [34] A. Pullini, D. Rossi, I. Loi, G. Tagliavini, and L. Benini, “Mr.Wolf: An energy-precision scalable parallel ultra low power SoC for IoT edge processing,” *IEEE Journal of Solid-State Circuits*, vol. 54, no. 7, pp. 1970–1981, 2019.
- [35] A. Pullini, D. Rossi, G. Haugou, and L. Benini, “μDMA: An autonomous I/O subsystem for IoT end-nodes,” in *2017 27th International Symposium on Power and Timing Modeling, Optimization and Simulation (PATMOS)*, Sep. 2017, pp. 1–8.
- [36] D. Rossi, I. Loi, G. Haugou, and L. Benini, “Ultra-low-latency lightweight DMA for tightly coupled multi-core clusters,” in *Proceedings of the 11th ACM Conference on Computing Frontiers*, ser. CF ’14. New York, NY, USA: Association for Computing Machinery, 2014.
- [37] J. Fjeldtvædt and M. Orlandić, “CubeDMA - Optimizing three-dimensional DMA transfers for hyperspectral imaging applications,” *Microprocessors and Microsystems*, vol. 65, pp. 23–36, Mar. 2019.
- [38] ARM, “AMBA AXI and ACE Protocol Specification AXI3, AXI4, and AXI4-Lite ACE and ACE-Lite,” 2023, <https://developer.arm.com/documentation/ih0022/k>, Version K, Accessed: 12/20/2024.
- [39] ——, “AMBA AXI-Stream protocol specification,” <https://developer.arm.com/documentation/ih0051/b/?lang=en>, 2021, version B, Accessed: 12/20/2024.
- [40] Silicon Labs, Inc., “OBI 1,” <https://github.com/openhwgroup/programs/blob/master/TGs/cores-task-group/obi/OBI-v1.5.0.pdf>, 2020, version 1.5.0, Accessed: 12/20/2024.

- [41] SiFive, “SiFive TileLink specification,” [https://starfivetech.com/uploads/tilelink\\_spec\\_1.8.1.pdf](https://starfivetech.com/uploads/tilelink_spec_1.8.1.pdf), version 1.8.1, Accessed: 12/20/2024.
- [42] OpenCores, “WISHBONE System-on-Chip (SoC) interconnection architecture for portable IP cores,” [https://cdn.opencores.org/downloads/wbspec\\_b3.pdf](https://cdn.opencores.org/downloads/wbspec_b3.pdf), version B.3, Accessed: 12/20/2024.
- [43] M. Dubois and F. A. Briggs, “Effects of cache coherency in multiprocessors,” *SIGARCH Computer Architecture News*, vol. 10, no. 3, p. 299–308, Apr. 1982.
- [44] D. Burger, J. R. Goodman, and A. Kägi, “Memory bandwidth limitations of future microprocessors,” *SIGARCH Computer Architecture News*, vol. 24, no. 2, p. 78–89, May 1996.
- [45] M. V. Wilkes, “The memory gap and the future of high performance memories,” *ACM SIGARCH Computer Architecture News*, vol. 29, no. 1, pp. 2–7, 2001.
- [46] J. L. Hennessy and D. A. Patterson, *Computer architecture: a quantitative approach*. Elsevier, 2011.
- [47] M. Cavalcante, A. Kurth, F. Schuiki, and L. Benini, “Design of an open-source bridge between non-coherent burst-based and coherent cache-line-based memory systems,” in *Proceedings of the 17th ACM International Conference on Computing Frontiers*, ser. CF ’20. New York, NY, USA: Association for Computing Machinery, 2020, p. 81–88.
- [48] D. Molka, D. Hackenberg, R. Schone, and M. S. Muller, “Memory performance and cache coherency effects on an Intel Nehalem multiprocessor system,” in *2009 18th International Conference on Parallel Architectures and Compilation Techniques*. IEEE, 2009, pp. 261–270.
- [49] A. Kurth, W. Rönninger, T. Benz, M. Cavalcante, F. Schuiki, F. Zaruba, and L. Benini, “An open-source platform for high-performance non-coherent on-chip communication,” *IEEE Transactions on Computers*, vol. 71, no. 8, pp. 1794–1809, 2022.

- [50] A. Ottaviano, “Design of heterogeneous architectures for mixed-critical autonomous embedded systems,” PhD Thesis, ETH Zurich, Jun. 2025.
- [51] P. Scheffler, “Acceleration of sparse and irregular workloads through energy-efficient stream extensions,” PhD Thesis, ETH Zurich, 2025, unpublished.
- [52] T. Benz, “Snitch scale-out on Amazon F1 instances,” Master’s Thesis, ETH Zurich, 2020.
- [53] T. Benz, M. Rogenmoser, P. Scheffler, S. Riedel, A. Ottaviano, A. Kurth, T. Hoefer, and L. Benini, “A high-performance, energy-efficient modular DMA engine architecture,” *IEEE Transactions on Computers*, vol. 73, no. 1, pp. 263–277, 2024.
- [54] T. Benz, A. Vanoni, M. Rogenmoser, and L. Benini, “A direct memory access controller (DMAC) for irregular data transfers on RISC-V Linux systems,” 2025.
- [55] T. Benz, A. Ottaviano, R. Balas, A. Garofalo, F. Restuccia, A. Biondi, and L. Benini, “AXI-REALM: A lightweight and modular interconnect extension for traffic regulation and monitoring of heterogeneous real-time SoCs,” in *2024 Design, Automation & Test in Europe Conference & Exhibition (DATE)*, 2024, pp. 1–6.
- [56] T. Benz, A. Ottaviano, C. Liang, R. Balas, A. Garofalo, F. Restuccia, A. Biondi, D. Rossi, and L. Benini, “AXI-REALM: Safe, modular and lightweight traffic monitoring and regulation for heterogeneous mixed-criticality systems,” *IEEE Transactions on Computers*, vol. 74, no. 9, pp. 3072–3086, 2025.
- [57] S. Di Girolamo, A. Kurth, A. Calotoiu, T. Benz, T. Schneider, J. Beránek, L. Benini, and T. Hoefer, “PsPIN: A high-performance low-power architecture for flexible in-network compute,” 2021.
- [58] ———, “A RISC-V in-network accelerator for flexible high-performance low-power packet processing,” in *2021 ACM/IEEE*

*48th Annual International Symposium on Computer Architecture (ISCA)*, 2021, pp. 958–971.

- [59] T. Benz, L. Bertaccini, F. Zaruba, F. Schuiki, F. K. Gürkaynak, and L. Benini, “A 10-core SoC with 20 fine-grain power domains for energy-proportional data-parallel processing over a wide voltage and temperature range,” in *ESSCIRC 2021 - IEEE 47th European Solid State Circuits Conference (ESSCIRC)*, 2021, pp. 263–266.
- [60] A. Ottaviano, T. Benz, P. Scheffler, and L. Benini, “Cheshire: A lightweight, Linux-capable RISC-V host platform for domain-specific accelerator plug-in,” *IEEE Transactions on Circuits and Systems II: Express Briefs*, vol. 70, no. 10, pp. 3777–3781, 2023.
- [61] M. Rogenmoser, A. Ottaviano, T. Benz, R. Balas, M. Perotti, A. Garofalo, and L. Benini, “SentryCore: A RISC-V co-processor system for safe, real-time control applications,” *RISC-V Summit Europe*, 2024.
- [62] A. Ottaviano, R. Balas, T. Fischer, T. Benz, A. Bartolini, and L. Benini, “ControlPULPlet: A flexible real-time multicore RISC-V controller for 2.5-D systems-in-package,” *IEEE Transactions on Very Large Scale Integration (VLSI) Systems*, vol. 33, no. 11, pp. 3057–3070, 2025.
- [63] M. Khalilov, M. Chrapek, S. Shen, A. Vezzu, T. Benz, S. Di Girolamo, T. Schneider, D. De Sensi, L. Benini, and T. Hoefler, “OSMOSIS: Enabling Multi-Tenancy in datacenter SmartNICs,” in *2024 USENIX Annual Technical Conference (USENIX ATC 24)*. Santa Clara, CA: USENIX Association, Jul. 2024, pp. 247–263.
- [64] G. Paulin, P. Scheffler, T. Benz, M. Cavalcante, T. Fischer, M. Eggimann, Y. Zhang, N. Wistoff, L. Bertaccini, L. Colagrande, G. Ottavi, F. K. Gürkaynak, D. Rossi, and L. Benini, “Occamy: A 432-core 28.1 DP-GFLOP/s/W 83% FPU utilization dual-chiplet, dual-HBM2E RISC-V-based accelerator for stencil and sparse linear algebra computations with 8-to-64-bit floating-point support in 12nm FinFET,” in *2024 IEEE Symposium on VLSI*

*Technology and Circuits (VLSI Technology and Circuits)*, 2024, pp. 1–2.

- [65] C. Liang, A. Ottaviano, T. Benz, M. Sinigaglia, L. Benini, A. Garofalo, and D. Rossi, “A gigabit, DMA-enhanced open-source Ethernet controller for mixed-criticality systems,” in *Proceedings of the 21st ACM International Conference on Computing Frontiers: Workshops and Special Sessions*, ser. CF '24 Companion. New York, NY, USA: Association for Computing Machinery, 2024, p. 55–58.
- [66] C. Liang, T. Benz, A. Ottaviano, A. Garofalo, L. Benini, and D. Rossi, “Towards reliable systems: A scalable approach to AXI4 transaction monitoring,” in *2025 Design, Automation & Test in Europe Conference (DATE)*, 2025, pp. 1–7.
- [67] T. Fischer, M. Rogenmoser, T. Benz, F. K. Gürkaynak, and L. Benini, “FlooNoC: A 645-Gb/s/link 0.15-pJ/B/hop open-source NoC with wide physical links and end-to-end AXI4 parallel multistream support,” *IEEE Transactions on Very Large Scale Integration (VLSI) Systems*, vol. 33, no. 4, pp. 1094–1107, 2025.
- [68] A. Garofalo, A. Ottaviano, M. Perotti, T. Benz, Y. Tortorella, R. Balas, M. Rogenmoser, C. Zhang, L. Bertaccini, N. Wistoff, M. Ciani, C. Koenig, M. Sinigaglia, L. Valente, P. Scheffler, M. Eggimann, M. Cavalcante, F. Restuccia, A. Biondi, F. Conti, F. K. Gurkaynak, D. Rossi, and L. Benini, “A reliable, time-predictable heterogeneous SoC for AI-enhanced mixed-criticality edge applications,” *IEEE Transactions on Circuits and Systems II: Express Briefs*, vol. 72, no. 11, pp. 1625–1629, 2025.
- [69] P. Scheffler, T. Benz, V. Potocnik, T. Fischer, L. Colagrande, N. Wistoff, Y. Zhang, L. Bertaccini, G. Ottavi, M. Eggimann *et al.*, “Occamy: A 432-core dual-chiplet dual-HBM2E 768-DP-GFLOP/s RISC-V system for 8-to-64-bit dense and sparse computing in 12-nm FinFET,” *IEEE Journal of Solid-State Circuits (JSSC)*, vol. 60, no. 4, pp. 1324–1338, 2025.
- [70] Alessandro Ottaviano et al., “Carfield: An open-source mixed-criticality heterogeneous RISC-V platform for next-generation autonomous systems,” 2025, unpublished.

- [71] S. Mazzola, T. Benz, B. Forsberg, and L. Benini, “A data-driven approach to lightweight DVFS-aware counter-based power modeling for heterogeneous platforms,” in *Embedded Computer Systems: Architectures, Modeling, and Simulation*. Cham: Springer International Publishing, 2022, pp. 346–361.
- [72] V. Jain, M. Cavalcante, N. Bruschi, M. Rogenmoser, T. Benz, A. Kurth, D. Rossi, L. Benini, and M. Verhelst, “PATRONoC: Parallel AXI transport reducing overhead for networks-on-chip targeting multi-accelerator DNN platforms at the edge,” in *2023 60th ACM/IEEE Design Automation Conference (DAC)*, 2023, pp. 1–6.
- [73] C. Zhang, P. Scheffler, T. Benz, M. Perotti, and L. Benini, “AXI-Pack: Near-memory bus packing for bandwidth-efficient irregular workloads,” in *2023 Design, Automation & Test in Europe Conference & Exhibition (DATE)*, 2023, pp. 1–6.
- [74] T. Benz, P. Scheffler, Schönleber, and L. Benini, “Iguana: An end-to-end open-source Linux-capable RISC-V SoC in 130nm CMOS,” *RISC-V Summit Europe*, 2023.
- [75] P. Sauter, T. Benz, P. Scheffler, Z. Jiang, B. Muheim, F. K. Gürkaynak, and L. Benini, “Basilisk: Achieving competitive performance with open EDA tools on an open-source Linux-capable RISC-V SoC,” *RISC-V Summit Europe*, 2024.
- [76] P. Sauter, T. Benz, P. Scheffler, F. K. Gürkaynak, and L. Benini, “Insights from Basilisk: Are open-source EDA tools ready for a multi-million-gate, Linux-booting RV64 SoC design?” *33rd International Workshop on Logic & Synthesis (IWLS)*, 2024.
- [77] P. Scheffler, P. Sauter, T. Benz, F. K. Gürkaynak, and L. Benini, “Basilisk: An end-to-end open-source Linux-capable RISC-V SoC in 130nm CMOS,” *2nd Safety and Security in Heterogeneous Open System-on-Chip Platforms Workshop (SSH-SoC 2024)*, 2024.
- [78] C. Zhang, P. Scheffler, T. Benz, M. Perotti, and L. Benini, “Near-memory parallel indexing and coalescing: Enabling highly

efficient indirect access for SpMV,” in *2024 Design, Automation & Test in Europe Conference & Exhibition (DATE)*, 2024, pp. 1–6.

- [79] S. Mazzola, G. Ara, T. Benz, B. Forsberg, T. Cucinotta, and L. Benini, “Data-driven power modeling and monitoring via hardware performance counter tracking,” *Journal of Systems Architecture*, vol. 167, p. 103504, 2025.
- [80] T. Benz, P. Scheffler, J. Holborn, and L. Benini, “DUTCTL: A flexible open-source framework for rapid bring-up, characterization, and remote operation of custom-silicon RISC-V SoCs,” *RISC-V Summit Europe*, 2024.
- [81] T. Benz, P. Scheffler, N. Wistoff, P. Sauter, B. Muheim, and L. Benini, “ArtistIC: An open-source toolchain for top-metal IC art and ultra-high-fidelity GDSII renders,” *Free Silicon Conference (FSiC)*, 2025.
- [82] P. Sauter, T. Benz, P. Scheffler, H. Pochert, L. Wüthrich, M. Povišer, B. Muheim, F. K. Gürkaynak, and L. Benini, “Croc: An end-to-end open-source extensible RISC-V MCU platform to democratize silicon,” *RISC-V Summit Europe*, 2025.
- [83] P. Sauter, T. Benz, P. Scheffler, M. Povišer, F. K. Gurkaynak, and L. Benini, “Basilisk: A 34mm<sup>2</sup> end-to-end open-source 64-bit Linux-capable RISC-V SoC in 130nm BiCMOS,” in *2025 IEEE Hot Chips 37 Symposium (HCS)*. IEEE Computer Society, 2025, pp. 1–14.
- [84] C. Zhang, L. Colagrande, R. Andri, T. Benz, G. Islamoglu, A. Nadalini, F. Conti, Y. Li, and L. Benini, “FlatAttention: Dataflow and fabric collectives co-optimization for efficient multi-head attention on tile-based many-PE accelerators,” *2025 IEEE Computer Society Annual Symposium on VLSI (ISVLSI)*, vol. 1, pp. 1–6, 2025.
- [85] J. Choquette, W. Gandhi, O. Giroux, N. Stam, and R. Krashinsky, “NVIDIA A100 tensor core GPU: Performance and innovation,” *IEEE Micro*, vol. 41, no. 2, pp. 29–35, 2021.

- [86] S. Lee, S. Hwang, M. J. Kim, J. Choi, and J. H. Ahn, “Future scaling of memory hierarchy for tensor cores and eliminating redundant shared memory traffic using inter-warp multicasting,” *IEEE Transactions on Computers*, vol. 71, no. 12, pp. 3115–3126, 2022.
- [87] D. Blythe, “XeHPC Ponte Vecchio,” in *2021 IEEE Hot Chips 33 Symposium (HCS)*. IEEE Computer Society, 2021, pp. 1–34.
- [88] X. Wang, A. Tumeo, J. D. Leidel, J. Li, and Y. Chen, “HAM: Hotspot-aware manager for improving communications with 3D-stacked memory,” *IEEE Transactions on Computers*, vol. 70, no. 6, pp. 833–848, 2021.
- [89] R. Branco and B. Lee, “Cache-related hardware capabilities and their impact on information security,” *ACM Computing Surveys*, vol. 55, no. 6, Dec. 2022.
- [90] V. Nagarajan, D. J. Sorin, M. D. Hill, and D. A. Wood, “A primer on memory consistency and cache coherence,” *Synthesis Lectures on Computer Architecture*, vol. 15, no. 1, pp. 1–294, 2020.
- [91] A. Jain and C. Lin, “Cache replacement policies,” *Synthesis Lectures on Computer Architecture*, vol. 14, no. 1, pp. 1–87, 2019.
- [92] R. Balasubramonian, N. P. Jouppi, and N. Muralimanohar, “Multi-core cache hierarchies,” *Synthesis Lectures on Computer Architecture*, vol. 6, no. 3, pp. 1–153, 2011.
- [93] Etron Technology, Inc., “256Mb high bandwidth RPC DRAM,” [https://etron.com/wp-content/uploads/2022/04/EM6GA16LGDBXCAEA-RPC1-DRAM-Induatrial\\_Rev.-1.4.pdf](https://etron.com/wp-content/uploads/2022/04/EM6GA16LGDBXCAEA-RPC1-DRAM-Induatrial_Rev.-1.4.pdf), 2024, Revision 1.4.
- [94] F. Zaruba, F. Schuiki, and L. Benini, “A 4096-core RISC-V chiplet architecture for ultra-efficient floating-point computing,” in *2020 IEEE Hot Chips 32 Symposium (HCS)*. IEEE Computer Society, 2020, pp. 1–24.

- [95] Etron Technology, Inc., “Reduced pin count (RPC®) DRAM,” <https://etron.com/wp-content/uploads/2022/06/RPC-DRAM-Overview-Flyer-v20202605.pdf>, 2022, v20052605.0.
- [96] K. Paraskevas, N. Chrysos, V. Papaefstathiou, P. Xirouchakis, P. Peristerakis, M. Giannioudis, and M. Katevenis, “Virtualized multi-channel RDMA with software-defined scheduling,” *Procedia Computer Science*, vol. 136, pp. 82–90, 2018.
- [97] H. Morales, C. Duran, and E. Roa, “A low-area direct memory access controller architecture for a RISC-V based low-power microcontroller,” in *2019 IEEE 10th Latin American Symposium on Circuits & Systems (LASCAS)*, Feb. 2019, pp. 97–100, iSSN: 2473-4667.
- [98] Synopsys, “DesignWare IP Solutions for AMBA - AXI DMA Controller,” [https://www.synopsys.com/dw/ipdir.php?ds=amba\\_axi\\_dma](https://www.synopsys.com/dw/ipdir.php?ds=amba_axi_dma), Accessed: 09/06/2022.
- [99] ARM, “CoreLink™ DMA-330 DMA controller,” <https://developer.arm.com/documentation/ddi0424/d/?lang=en>, 2012, version r1p2, Accessed: 09/06/2022.
- [100] “Antmicro releases FastVDMA open-source resource-light DMA controller,” <https://abopen.com/news/antmicro-releases-fastvdma-open-source-resource-light-dma-controller>, Sep. 2019.
- [101] M. Rhu, M. O’Connor, N. Chatterjee, J. Pool, Y. Kwon, and S. W. Keckler, “Compressing DMA engine: Leveraging activation sparsity for training deep neural networks,” in *2018 IEEE International Symposium on High Performance Computer Architecture (HPCA)*, Feb. 2018, pp. 78–91, iSSN: 2378-203X.
- [102] AMD Xilinx, “AXI DMA v7.1 LogiCORE IP Product Guide,” 2022, [https://docs.amd.com/r/en-US/pg021\\_axi\\_dma](https://docs.amd.com/r/en-US/pg021_axi_dma), Accessed: 09/06/2022.
- [103] PLDA (Rambus), “DMA AXI IP controller,” <https://www.plda.com/products/vdma-axi>, Accessed: 09/06/2022.

- [104] STMicroelectronics, “Dmaengine overview - STM32 MPU,” [https://wiki.st.com/stm32mpu/wiki/Dmaengine\\_overview](https://wiki.st.com/stm32mpu/wiki/Dmaengine_overview), Accessed: 09/06/2022.
- [105] Design and Reuse, “DDMA, multi-channel DMA controller IP core from DCD-SEMI,” <https://www.design-reuse.com/news/53210/multi-channel-dma-controller-ip-core-dcd-semi.html>, Accessed: 09/06/2022.
- [106] W. Su, L. Wang, M. Su, and S. Liu, “A processor-DMA-based memory copy hardware accelerator,” in *2011 IEEE Sixth International Conference on Networking, Architecture, and Storage*, Jul. 2011, pp. 225–229.
- [107] N. Nandan, “High performance DMA controller for ultra HDTV video codecs,” in *2014 IEEE International Conference on Consumer Electronics (ICCE)*, Jan. 2014, pp. 65–66, iSSN: 2158-4001.
- [108] D. Comisky, S. Agarwala, and C. Fuoco, “A scalable high-performance DMA architecture for DSP applications,” in *Proceedings 2000 International Conference on Computer Design*, Sep. 2000, pp. 414–419.
- [109] J. Frazelle, “Chip measuring contest: The benefits of purpose-built chips,” *Queue*, vol. 19, no. 5, pp. 5–21, Oct. 2021.
- [110] M. Kumar, M. Serrano, J. Moreira, P. Pattnaik, W. P. Horn, J. Jann, and G. Tanase, “Efficient implementation of scatter-gather operations for large scale graph analytics,” in *2016 IEEE High Performance Extreme Computing Conference (HPEC)*, Sep. 2016, pp. 1–7.
- [111] G. Ma and H. He, “Design and implementation of an advanced DMA controller on AMBA-based SoC,” in *2009 IEEE 8th International Conference on ASIC*, Oct. 2009, pp. 419–422, iSSN: 2162-755X.
- [112] D. Chen, A. G. Gara, M. E. Giampapa, P. Heidelberger, B. Steinmacher-Burow, and P. Vranas, “DMA engine for

repeating communication patterns,” US Patent US7 802 025B2, Sep., 2010.

- [113] M. Jang, J. Kim, J. Kim, and S. Kim, “ENCORE compression: Exploiting narrow-width values for quantized deep neural networks,” in *2022 Design, Automation & Test in Europe Conference & Exhibition (DATE)*, Mar. 2022, pp. 1503–1508, iSSN: 1558-1101.
- [114] S. Ma, L. Huang, Y. Lei, Y. Guo, and Z. Wang, “An efficient direct memory access (DMA) controller for scientific computing accelerators,” in *2019 IEEE International Symposium on Circuits and Systems (ISCAS)*, May 2019, pp. 1–5, iSSN: 2158-1525.
- [115] “The Linux kernel documentation - The Linux kernel documentation,” <https://www.kernel.org/doc/html/latest/index.html>, Accessed: 09/20/2022.
- [116] “Genesys 2 reference manual - Digilent Reference,” <https://digilent.com/reference/programmable-logic/genesys-2/reference-manual>, Accessed: 09/06/2022.
- [117] P. J. Denning, “Virtual memory,” *ACM Computing Surveys*, vol. 2, no. 3, p. 153–189, Sep. 1970.
- [118] M. Rodríguez, F. Costa, B. V. Sá, and S. Pinto, “Open-source RISC-V Input/Output memory management unit (IOMMU) IP,” *RISC-V Summit Europe*, 2023.
- [119] C. Koenig, E. Zelioli, and L. Benini, “Evaluating IOMMU-based shared virtual addressing for RISC-V embedded heterogeneous SoCs,” in *2025 Design, Automation & Test in Europe Conference (DATE)*, 2025, pp. 1–7.
- [120] A. Kurth, P. Vogel, A. Capotondi, A. Marongiu, and L. Benini, “HERO: Heterogeneous embedded research platform for exploring RISC-V manycore accelerators on FPGA,” 2017.
- [121] A. Kurth, B. Forsberg, and L. Benini, “HEROv2: Full-stack open-source research platform for heterogeneous computing,” *IEEE Transactions on Parallel and Distributed Systems*, vol. 33, no. 12, pp. 4368–4382, 2022.

- [122] A. Kurth, P. Vogel, A. Marongiu, and L. Benini, “Scalable and efficient virtual memory sharing in heterogeneous SoCs with TLB prefetching and MMU-aware DMA engine,” in *2018 IEEE 36th International Conference on Computer Design (ICCD)*, Oct. 2018, pp. 292–300, iSSN: 2576-6996.
- [123] E. Zelioli, A. Ottaviano, R. Balas, N. Wistoff, A. Garofalo, and L. Benini, “vCLIC: Towards fast interrupt handling in virtualized RISC-V mixed-criticality systems,” in *2024 IEEE 42nd International Conference on Computer Design (ICCD)*, Los Alamitos, CA, USA, Nov. 2024, pp. 288–291.
- [124] RISC-V, “The RISC-V instruction set manual: Volume II - Privileged architecture,” [https://drive.google.com/file/d/17GeetSnT5wW3xNuAHI95-SI1gPGd5sJ\\_/view?pli=1](https://drive.google.com/file/d/17GeetSnT5wW3xNuAHI95-SI1gPGd5sJ_/view?pli=1), 2025, v20250508.
- [125] G. H. Golub and J. M. Ortega, *Scientific computing: an introduction with parallel computing*. Elsevier, 2014.
- [126] G. H. Golub and C. F. Van Loan, *Matrix computations*. JHU press, 2013.
- [127] M. Gates, “BLAS quick reference guide,” 2024, <https://www.netlib.org/blas/>, Accessed: 12/10/2024.
- [128] Cypress Semiconductor, “HyperBus<sup>TM</sup> spec.” 2019, revision H.
- [129] A. Burrello, A. Garofalo, N. Bruschi, G. Tagliavini, D. Rossi, and F. Conti, “DORY: Automatic end-to-end deployment of real-world DNNs on low-cost IoT MCUs,” *IEEE Transactions on Computers*, vol. 70, no. 8, pp. 1253–1268, 2021.
- [130] S. Riedel, M. Cavalcante, R. Andri, and L. Benini, “MemPool: A scalable manycore architecture with a low-latency shared L1 memory,” *IEEE Transactions on Computers*, vol. 72, no. 12, pp. 3561–3575, 2023.
- [131] F. Solt, “A flexible peripheral system for high-performance systems on chips,” Master’s Thesis, ETH Zurich, 2020.

- [132] P. Burgess, “Adafruit neopixel überguide, adafruit,” <https://learn.adafruit.com/adafruit-neopixel-uberguide/the-magic-of-neopixels>, Accessed: 12/10/2024, 2013.
- [133] L. Wuethrich, “MLEM: A PULP SoC for education with an end-to-end open-source flow for a physical design - NeoPixel edition,” Bachelor’s Thesis, ETH Zurich, 2024.
- [134] PULP-Platform Contributors, “Croc,” <https://github.com/pulp-platform/croc>, 2024.
- [135] A. Ottaviano, R. Balas, G. Bambini, A. Del Vecchio, M. Ciani, D. Rossi, L. Benini, and A. Bartolini, “ControlPULP: A RISC-V on-chip parallel power controller for many-core HPC processors with FPGA-based hardware-in-the-loop power and thermal emulation,” *International Journal of Parallel Programming*, vol. 52, no. 1, pp. 93–123, 2024.
- [136] A. Ottaviano, R. Balas, G. Bambini, C. Bonfanti, S. Benatti, D. Rossi, L. Benini, and A. Bartolini, “ControlPULP: A RISC-V power controller for HPC processors with parallel control-law computation acceleration,” in *Embedded Computer Systems: Architectures, Modeling, and Simulation: 22nd International Conference, SAMOS 2022*, 2024, pp. 120–135.
- [137] T. Rosedahl, M. Broyles, C. Lefurgy, B. Christensen, and W. Feng, “Power/performance controlling techniques in Open-POWER,” in *High Performance Computing*. Cham: Springer International Publishing, 2017, pp. 275–289.
- [138] I. Ripoll and R. Ballester-Ripoll, “Period selection for minimal hyperperiod in periodic task systems,” *IEEE Transactions on Computers*, vol. 62, no. 9, pp. 1813–1822, 2013.
- [139] F. Zaruba, F. Schuiki, T. Hoefer, and L. Benini, “Snitch: A tiny pseudo dual-issue processor for area and energy efficient execution of floating-point intensive workloads,” *IEEE Transactions on Computers*, vol. 70, no. 11, pp. 1845–1860, 2021.

- [140] H. Jun, J. Cho, K. Lee, H.-Y. Son, K. Kim, H. Jin, and K. Kim, “HBM (high bandwidth memory) DRAM technology and architecture,” in *2017 IEEE International Memory Workshop (IMW)*, 2017, pp. 1–4.
- [141] Nvidia Corporation, “NVIDIA H100 tensor core GPU architecture,” <https://resources.nvidia.com/en-us-tensor-core/gtc22-whitepaper-hopper>, 2024, v1.04.
- [142] N. Nassif, A. O. Munch, C. L. Molnar, G. Pasdast, S. V. Lyer, Z. Yang, O. Mendoza, M. Huddart, S. Venkataraman, S. Kandula, R. Marom, A. M. Kern, B. Bowhill, D. R. Mulvihill, S. Nimmagadda, V. Kalidindi, J. Krause, M. M. Haq, R. Sharma, and K. Duda, “Sapphire Rapids: The next-generation Intel Xeon scalable processor,” in *2022 IEEE International Solid-State Circuits Conference (ISSCC)*, vol. 65, 2022, pp. 44–46.
- [143] A. Biswas, “Sapphire Rapids,” in *2021 IEEE Hot Chips 33 Symposium (HCS)*. IEEE Computer Society, 2021, pp. 1–22.
- [144] S. Dave, R. Baghdadi, T. Nowatzki, S. Avancha, A. Shrivastava, and B. Li, “Hardware acceleration of sparse and irregular tensor computations of ML models: A survey and insights,” *Proceedings of the IEEE*, vol. 109, no. 10, pp. 1706–1752, 2021.
- [145] Z. Zhang, Y. Xu, J. Yang, X. Li, and D. Zhang, “A survey of sparse representation: Algorithms and applications,” *IEEE Access*, vol. 3, pp. 490–530, 2015.
- [146] Z. Qureshi, V. S. Mailthody, S. W. Min, I. Chung, J. Xiong, W.-m. Hwu *et al.*, “Tearing down the memory wall,” *arXiv preprint arXiv:2008.10169*, 2020.
- [147] L. Colagrande and L. Benini, “Taming offload overheads in a massively parallel open-source RISC-V MPSoC: Analysis and optimization,” *IEEE Transactions on Parallel and Distributed Systems*, vol. 36, no. 6, pp. 1193–1205, 2025.
- [148] O. Goldreich and R. Ostrovsky, “Software protection and simulation on oblivious RAMs,” *J. ACM*, vol. 43, no. 3, p. 431–473, May 1996.

- [149] P. Scheffler, L. Colagrande, and L. Benini, “SARIS: Accelerating stencil computations on energy-efficient RISC-V compute clusters with indirect stream registers,” in *Proceedings of the 61st ACM/IEEE Design Automation Conference*, ser. DAC ’24. New York, NY, USA: Association for Computing Machinery, 2024.
- [150] P. Scheffler, F. Zaruba, F. Schuiki, T. Hoefer, and L. Benini, “Sparse stream semantic registers: A lightweight ISA extension accelerating general sparse linear algebra,” *IEEE Transactions on Parallel and Distributed Systems*, vol. 34, no. 12, pp. 3147–3161, 2023.
- [151] C. Alappat, J. Laukemann, T. Gruber, G. Hager, G. Wellein, N. Meyer, and T. Wettig, “Performance modeling of streaming kernels and sparse matrix-vector multiplication on A64FX,” in *2020 IEEE/ACM Performance Modeling, Benchmarking and Simulation of High Performance Computer Systems (PMBS)*, 2020, pp. 1–7.
- [152] C. Alappat, G. Hager, O. Schenk, and G. Wellein, “Level-based blocking for sparse matrices: Sparse matrix-power-vector multiplication,” *IEEE Transactions on Parallel and Distributed Systems*, vol. 34, no. 2, pp. 581–597, 2023.
- [153] Y. Niu, Z. Lu, M. Dong, Z. Jin, W. Liu, and G. Tan, “TileSpMV: A tiled algorithm for sparse matrix-vector multiplication on GPUs,” in *2021 IEEE International Parallel and Distributed Processing Symposium (IPDPS)*, 2021, pp. 68–78.
- [154] L. Bertaccini, G. Paulin, M. Cavalcante, T. Fischer, S. Mach, and L. Benini, “MiniFloats on RISC-V cores: ISA extensions with mixed-precision short dot products,” *IEEE Transactions on Emerging Topics in Computing*, vol. 12, no. 4, pp. 1040–1055, 2024.
- [155] S. Naffziger, K. Lepak, M. Paraschou, and M. Subramony, “2.2 AMD chiplet architecture for high-performance server and desktop products,” in *2020 IEEE International Solid-State Circuits Conference - (ISSCC)*, vol. 63, 2020, pp. 44–45.

- [156] G. Paulin, M. Cavalcante, P. Scheffler, L. Bertaccini, Y. Zhang, F. Gürkaynak, and L. Benini, “Soft tiles: Capturing physical implementation flexibility for tightly-coupled parallel processing clusters,” in *2022 IEEE Computer Society Annual Symposium on VLSI (ISVLSI)*, 2022, pp. 44–49.
- [157] T. A. Davis and Y. Hu, “The university of Florida sparse matrix collection,” *ACM Transactions on Mathematical Software*, vol. 38, no. 1, 2011, art. no. 1.
- [158] R. Wilhelm, J. Engblom, A. Ermedahl, N. Holsti, S. Thesing, D. Whalley, G. Bernat, C. Ferdinand, R. Heckmann, T. Mitra, F. Mueller, I. Puaut, P. Puschner, J. Staschulat, and P. Stenström, “The worst-case execution-time problem—overview of methods and survey of tools,” *ACM Transactions on Embedded Computing Systems*, vol. 7, no. 3, May 2008.
- [159] F. Restuccia, A. Biondi, M. Marinoni, G. Cicero, and G. Buttazzo, “AXI HyperConnect: A predictable, hypervisor-level interconnect for hardware accelerators in FPGA SoCs,” in *2020 57th ACM/IEEE Design Automation Conference (DAC)*, 2020, pp. 1–6.
- [160] Certification Authorities Software Team (CAST), FAA: Washington, DC, USA, “Position paper, CAST-32A, multi-core processors, rev 0,” [https://faa.gov/aircraft/air\\_cert/design\\_approvals/air\\_software/cast/cast-32a.pdf](https://faa.gov/aircraft/air_cert/design_approvals/air_software/cast/cast-32a.pdf), Accessed: 12/20/2024.
- [161] F. Rehm, J. Seitter, J.-P. Larsson, S. Saidi, G. Stea, R. Zippo, D. Ziegenbein, M. Andreozzi, and A. Hamann, “The road towards predictable automotive high - performance platforms,” in *2021 Design, Automation & Test in Europe Conference & Exhibition (DATE)*, 2021, pp. 1915–1924.
- [162] F. Restuccia, M. Pagani, A. Biondi, M. Marinoni, and G. Buttazzo, “Is your bus arbiter really fair? Restoring fairness in AXI interconnects for FPGA SoCs,” *ACM Transactions on Embedded Computing Systems*, vol. 18, no. 5s, Oct. 2019.

- [163] “IEC 61508-3: Functional safety of electrical/electronic/programmable electronic safety-related systems - Part 3: Software requirements,” International Electrotechnical Commission, <https://webstore.iec.ch/en/publication/5517>, Accessed: 12/20/2024.
- [164] B. Cilku and P. Puschner, “Towards temporal and spatial isolation in memory hierarchies for mixed-criticality systems with hypervisors,” *In Proceedings of the 19th IEEE International Conference on Embedded and Real-Time Computing Systems and Applications (RTCSA), 1st workshop on Real-Time Mixed Criticality Systems (ReTiMiCS)*, pp. 25–28, 2013.
- [165] ARM, “Arm architecture reference manual supplement memory system resource partitioning and monitoring (MPAM) for Armv8-A,” 2023, <https://developer.arm.com/documentation/ddi0598/db>, Version D.b, Accessed: 12/20/2024.
- [166] F. Restuccia and R. Kastner, “Cut and forward: Safe and secure communication for FPGA system on chips,” *IEEE Transactions on Computer-Aided Design of Integrated Circuits and Systems*, vol. 41, no. 11, pp. 4052–4063, 2022.
- [167] A. Serrano-Cases, J. M. Reina, J. Abella, E. Mezzetti, and F. J. Cazorla, “Leveraging hardware QoS to control contention in the Xilinx Zynq UltraScale+ MPSoC,” in *33rd Euromicro Conference on Real-Time Systems (ECRTS 2021)*, ser. LIPIcs, B. B. Brandenburg, Ed., vol. 196. Dagstuhl, Germany: Schloss Dagstuhl – Leibniz-Zentrum für Informatik, 2021, pp. 3:1–3:26.
- [168] F. Poletti, D. Bertozzi, L. Benini, and A. Bogliolo, “Performance analysis of arbitration policies for SoC communication architectures,” *Design Automation for Embedded Systems*, vol. 8, no. 2–3, p. 189–210, Jun. 2003.
- [169] H. Falk, S. Altmeyer, P. Hellinckx, B. Lisper, W. Puffitsch, C. Rochange, M. Schoeberl, R. B. Sørensen, P. Wägemann, and S. Wegener, “TACLeBench: A benchmark collection to support worst-case execution time research,” in *16th International Workshop on Worst-Case Execution Time Analysis (WCET 2016)*, ser. OpenAccess Series in Informatics (OASIcs),

M. Schoeberl, Ed., vol. 55. Dagstuhl, Germany: Schloss Dagstuhl – Leibniz-Zentrum für Informatik, 2016, pp. 2:1–2:10.

- [170] G. Valente, G. Brilli, T. Di Mascio, A. Capotondi, P. Burgio, P. Valente, and A. Marongiu, “Fine-grained QoS control via tightly-coupled bandwidth monitoring and regulation for FPGA-based heterogeneous SoCs,” *IEEE Transactions on Parallel and Distributed Systems*, vol. 36, no. 2, pp. 326–340, 2025.
- [171] F. Farshchi, Q. Huang, and H. Yun, “BRU: Bandwidth regulation unit for real-time multicore processors,” in *2020 IEEE Real-Time and Embedded Technology and Applications Symposium (RTAS)*, 2020, pp. 364–375.
- [172] M. G. Bechtel and H. Yun, “Denial-of-service attacks on shared cache in multicore: Analysis and prevention,” *2019 IEEE Real-Time and Embedded Technology and Applications Symposium (RTAS)*, pp. 357–367, 2019.
- [173] G. Cabo, S. Alcaide, C. Hernández, P. Benedicte, F. Bas, F. Mazzocchetti, and J. Abella, “SafeSU-2: a safe statistics unit for space MPSoCs,” in *2022 Design, Automation & Test in Europe Conference & Exhibition (DATE)*, 2022, pp. 1085–1086.
- [174] P. Andreu, S. Alcaide, P. Lopez, J. Abella, and C. Hernandez, “Expanding SafeSU capabilities by leveraging security frameworks for contention monitoring in complex SoCs,” *Future Generation Computer Systems*, vol. 163, p. 107518, 2025.
- [175] ARM, “ARM watchdog module (SP805) technical reference manual,” 2024, <https://developer.arm.com/documentation/ddi0270/b>, Version r1p0, Accessed: 12/20/2024.
- [176] Synopsys, “Enhancing Arm SoCs performance with smart monitors,” 2023, <https://synopsys.com/blogs/chip-design/smart-monitors-improve-arm-socs-performance.html>, Accessed: 12/20/2024.
- [177] AMD, “AXI performance monitor v5.0,” 2017, [https://docs.amd.com/v/u/en-US/pg037\\_axi\\_perf\\_mon](https://docs.amd.com/v/u/en-US/pg037_axi_perf_mon), PG037, Accessed: 12/20/2024.

- [178] S. Ravi, K. Ezra, and K. H. Mallikarjun, “Design of a bus monitor for performance analysis of AXI protocol based SoC systems,” *International Journal for Research in Applied Science and Engineering Technology (IJRASET)*, vol. 9, no. 19, pp. 6313–6324, 2014.
- [179] H.-m. Kyung, G.-h. Park, J. W. Kwak, W. Jeong, T.-J. Kim, and S.-B. Park, “Performance monitor unit design for an AXI-based multi-core SoC platform,” in *Proceedings of the 2007 ACM Symposium on Applied Computing*, ser. SAC ’07. New York, NY, USA: Association for Computing Machinery, 2007, pp. 1565–1572.
- [180] P.-C. Lee and J. Huang, “Reconfigurable bus monitor tool suite for on-chip SoC for performance and protocol monitoring,” in *2014 9th International Symposium on Reconfigurable and Communication-Centric Systems-on-Chip (ReCoSoC)*, 2014, pp. 1–6.
- [181] C.-H. Chen, J.-C. Ju, and J. Huang, “A synthesizable AXI protocol checker for SoC integration,” in *2010 International SoC Design Conference (ISOCC)*, 2010, pp. 103–106.
- [182] F. Zaruba and L. Benini, “The cost of application-class processing: Energy and performance analysis of a Linux-ready 1.7-GHz 64-bit RISC-V core in 22-nm FDSOI technology,” *IEEE Transactions on Very Large Scale Integration (VLSI) Systems*, vol. 27, no. 11, pp. 2629–2640, 2019.
- [183] F. Zaruba, F. Schuiki, and L. Benini, “Manticore: A 4096-core RISC-V chiplet architecture for ultraefficient floating-point computing,” *IEEE Micro*, vol. 41, no. 2, pp. 36–42, 2021.
- [184] M. Venn, “Tiny Tapeout: A shared silicon tapeout platform accessible to everyone,” *Authorea Preprints*, 2024.
- [185] mbalestrini, “TinyTapeout GDS Viewer,” [https://github.com/mbalestrini/tinytapeout\\_gds\\_viewer](https://github.com/mbalestrini/tinytapeout_gds_viewer), 2022.
- [186] M. Köfferlein, “Klayout,” [https://largo.lip6.fr/fileadmin/user\\_upload/soc/events/klayout\\_20180404.pdf](https://largo.lip6.fr/fileadmin/user_upload/soc/events/klayout_20180404.pdf), 2020.

- [187] ——, “Screenshot with options,” <https://klayout.org/svn-public/klayout-resources/trunk/scripts/screenshot.lym>.
- [188] H. Goldstein, “The secret art of chip graffiti,” *IEEE Spectrum*, vol. 39, no. 3, pp. 50–55, 2002.
- [189] “Gdsp’s documentation,” <https://gdspy.readthedocs.io/en/stable/>, Accessed: 03/07/2024.
- [190] H. Pochert, “MLEM: A PULP SoC for education with an end-to-end open-source flow for a physical design - UART edition,” Bachelor’s Thesis, ETH Zurich, 2024.
- [191] M. Bushnell and V. Agrawal, *Essentials of Electronic Testing for Digital, Memory and Mixed-Signal VLSI Circuits*. Springer Publishing Company, Incorporated, 2013.
- [192] RISC-V International, “RISC-V external debug support version 0.13.2,” <https://riscv.org/wp-content/uploads/2019/03/riscv-debug-release.pdf>, Accessed: 03/07/2024.
- [193] PULP-Platform Contributors, “DUTCTL,” <https://github.com/pulp-platform/dutctl>.
- [194] Free Software Foundation, Inc, “GDB: The GNU project debugger,” <https://www.sourceware.org/gdb/>, Accessed: 03/07/2024.
- [195] National Instruments, “Documentation about the SCPI specification,” <https://knowledge.ni.com/KnowledgeArticleDetails?id=kA00Z0000019S48SAE>, Accessed: 03/07/2024.
- [196] C. P. Womack, “Schmoo plot analysis of coincident-current memory systems,” *IEEE Transactions on Electronic Computers*, vol. EC-14, no. 1, pp. 36–44, 1965.
- [197] N. Huetter, “A Snitch-based compute accelerator for HERO,” Semester Thesis, ETH Zurich, 2020.
- [198] F. Bucheli, “A Snitch-based SoC on iCE40 FPGAs,” Bachelor’s Thesis, ETH Zurich, 2021.

- [199] R. Zhou, V. Krishna, and J. Chen, “An RPC DRAM implementation for energy-efficient ASICs,” Semester Thesis, ETH Zurich, 2021.
- [200] J. Eudine, L. Meier, and T. Mettler, “Bringup and evaluation of an energy-efficient heterogeneous manycore compute platform,” Semester Thesis, ETH Zurich, 2021.
- [201] W. Ho, Kin, “Investigation of the high-performance multi-threaded out-of-order IBM A2O core,” Semester Thesis, ETH Zurich, 2021.
- [202] L. Hauser, “Lcore: A minimal RISC-V core designed for teaching,” Bachelor’s Thesis, ETH Zurich, 2021.
- [203] C. Zhang, “Extending AXI4 with common stream semantics,” Semester Thesis, ETH Zurich, 2021.
- [204] K. Schaeerer, “Enhancing our DMA engine with vector processing capabilities,” Bachelor’s Thesis, ETH Zurich, 2022.
- [205] T. Senti, “Extension and evaluation of the iDMA architecture for multiple on-chip communication protocols,” Bachelor’s Thesis, ETH Zurich, 2022.
- [206] N. Narr and C. Reinwardt, “A 64-bit Linux-capable RISC-V system-on-chip in 65nm CMOS,” Semester Thesis, ETH Zurich, 2022.
- [207] S. Song, B. Wang, C. Wang, and Z. Jiawei, “An AXI4 slave interface and digital memory controller for RPC DRAM,” Semester Thesis, ETH Zurich, 2022.
- [208] A. Vanoni, “Linux support for DMA engine,” Bachelor’s Thesis, ETH Zurich, 2022.
- [209] A. Brandl, “A power measurement ASIC for evaluating the iDMA architecture,” Semester Thesis, ETH Zurich, 2022.
- [210] M. Raeber, “Developing an energy-efficient transposition unit supporting a wide range of data widths,” Semester Thesis, ETH Zurich, 2022.

- [211] F. Svelto, “Towards a technology-independent and synthesizable AXI4 performance monitoring unit,” Semester Thesis, ETH Zurich, 2022.
- [212] C. Zhang, “AXI-PACK: Near-memory bus packing for bandwidth-efficient spare workloads,” Master’s Thesis, ETH Zurich, 2022.
- [213] E. Werner, “A flexible FPGA-based peripheral platform extending Linux-capable systems on chip,” Bachelor’s Thesis, ETH Zurich, 2023.
- [214] J. Holborn, “Towards an affordable SoC characterization platform for automated voltage-frequency sweeps,” Bachelor’s Thesis, ETH Zurich, 2023.
- [215] F. Bozic, “Verifying Iguana using open-source simulation and FPGA emulation,” Bachelor’s Thesis, ETH Zurich, 2023.
- [216] V. Kuenzli, “Implementing virtual memory support for our DMA engine,” Semester Thesis, ETH Zurich, 2023.
- [217] T. Senti, “The OpenRoad towards Iguana - a fully open-source Linux-capable ASIC,” Semester Thesis, ETH Zurich, 2023.
- [218] L. Jiang and K. Li, “Towards open-source ASICs: Physical implementation gap-analysis of a Linux-Capable SoC vehicle in 130nm CMOS,” Semester Thesis, ETH Zurich, 2023.
- [219] P. Sauter, “Towards SystemVerilog support for open-source tools,” Semester Thesis, ETH Zurich, 2023.
- [220] L. Guzenko, “Implementing USB support in Cheshire,” Semester Thesis, ETH Zurich, 2023.
- [221] L. Leone, “A reduction-capable AXI XBAR for fast M-to-1 communication,” Master’s Thesis, ETH Zurich, 2023.
- [222] P. Sauter, “Basilisk: Open-source IC design,” Master’s Thesis, ETH Zurich, 2023.

- [223] M. Gedik, “A video output peripheral for Cheshire-based SoCs,” Bachelor’s Thesis, ETH Zurich, 2024.
- [224] G. Frehner, “JTAG generator,” Bachelor’s Thesis, ETH Zurich, 2024.
- [225] F. Hauser, “Integrating the Snitch cluster into a PULPissimo microcontroller for a GF22 SoC,” Bachelor’s Thesis, ETH Zurich, 2024.
- [226] T. Dubochet, “FPGA verification and debugging enhancements for the Monoceros GF22 SoC,” Bachelor’s Thesis, ETH Zurich, 2024.
- [227] M. Hirs, “Fixing bring-up related design flaws in the Snitch cluster with an implementation for GF22,” Bachelor’s Thesis, ETH Zurich, 2024.
- [228] I. Gruenberg, “Optimizing the performance and bandwidth of a 64-bit Linux-capable RISC-V SoC,” Bachelor’s Thesis, ETH Zurich, 2024.
- [229] L. Braun, “Towards a full verification framework for iDMA - comparing open and closed approaches,” Bachelor’s Thesis, ETH Zurich, 2024.
- [230] A. Dumik, “Bufferless transposition engine,” Semester Thesis, ETH Zurich, 2024.
- [231] T. Hung, Ho and C. Wang, “Designing a scalable miniature ioDMA,” Semester Thesis, ETH Zurich, 2024.
- [232] F. Hauser, “Creating a SystemVerilog USB1.1 host controller for Linux-capable SoCs,” Semester Thesis, ETH Zurich, 2024.
- [233] J. Sommerhaeuser, “Enabling Linux DMA support in our Linux-capable Cheshire SoC,” Semester Thesis, ETH Zurich, 2024.
- [234] R. Roth, “Towards a virtual-memory-enhanced DMA for Linux-capable SoCs,” Semester Thesis, ETH Zurich, 2024.

- [235] L. Luzi, “Multi-channel memory transfers in huge manycore systems with multiple HBM channels,” Master’s Thesis, ETH Zurich, 2024.
- [236] A. Buchner and M. Wehrli, “Towards an SDIO peripheral for Linux-capable SoCs,” Bachelor’s Thesis, ETH Zurich, 2025.
- [237] L. Itschner, “Adding multi-head capabilities to our DMA infrastructure,” Bachelor’s Thesis, ETH Zurich, 2025.
- [238] B. Koelbli, “Commercial versus open-source: A comprehensive survey of power simulation flows for digital ICs,” Bachelor’s Thesis, ETH Zurich, 2025.
- [239] K. Schaeerer, “Exploring virtual memory architectures for linux-capable heterogeneous systems,” Master’s Thesis, ETH Zurich, 2025.
- [240] A. Rosetti, “Performance-oriented improvements to Cheshire SoC,” Semester Thesis, ETH Zurich, 2025.
- [241] A. Vanoni, “Accelerating MMC performance to enable persistent boot on open-source RISC-V,” Semester Thesis, ETH Zurich, 2025.

# Curriculum Vitae



Thomas Benz was born in Zürich, Switzerland, in April 1994. He received his B.Sc. and M.Sc. degrees in electrical engineering and information technology from ETH Zurich in 2018 and 2020, respectively. He completed his Ph.D. degree in the Digital Circuits and Systems group of Prof. Benini in 2025. His research interests include energy-efficient high-performance computer architectures, memory interconnects, data movement, heterogeneous mixed-criticality systems, and the design of ASICs. He received the ETH Medal for outstanding Master's Theses in 2021 and won Best Student Poster at HotChips Symposium in 2025. He has published more than 20 research articles in peer-reviewed journals and conference proceedings and contributed to over 15 ASIC tapeouts. He has advised over 40 Bachelor's/Semester Theses and 6 Master's Theses.





